

Deposit & Copying of Dissertation Declaration



UNIVERSITY OF
CAMBRIDGE

Board of Graduate Studies

Please note that you will also need to bind a copy of this Declaration into your final, hardbound copy of thesis - this has to be the very first page of the hardbound thesis.

| | | | |
|---|--|---------------------|--------------|
| 1 | Surname (Family Name) | Forenames(s) | Title |
| | Jermyn | Adam Sean | Mr |
| 2 | Title of Dissertation as approved by the Degree Committee | | |
| | Turbulence and Transport in Stars and Planets | | |

In accordance with the University Regulations in *Statutes and Ordinances* for the PhD, MSc and MLitt Degrees, I agree to deposit one print copy of my dissertation entitled above and one print copy of the summary with the Secretary of the Board of Graduate Studies who shall deposit the dissertation and summary in the University Library under the following terms and conditions:

1. Dissertation Author Declaration

I am the author of this dissertation and hereby give the University the right to make my dissertation available in print form as described in 2. below.

My dissertation is my original work and a product of my own research endeavours and includes nothing which is the outcome of work done in collaboration with others except as declared in the Preface and specified in the text. I hereby assert my moral right to be identified as the author of the dissertation.

The deposit and dissemination of my dissertation by the University does not constitute a breach of any other agreement, publishing or otherwise, including any confidentiality or publication restriction provisions in sponsorship or collaboration agreements governing my research or work at the University or elsewhere.

2. Access to Dissertation

I understand that one print copy of my dissertation will be deposited in the University Library for archival and preservation purposes, and that, unless upon my application restricted access to my dissertation for a specified period of time has been granted by the Board of Graduate Studies prior to this deposit, the dissertation will be made available by the University Library for consultation by readers in accordance with University Library Regulations and copies of my dissertation may be provided to readers in accordance with applicable legislation.

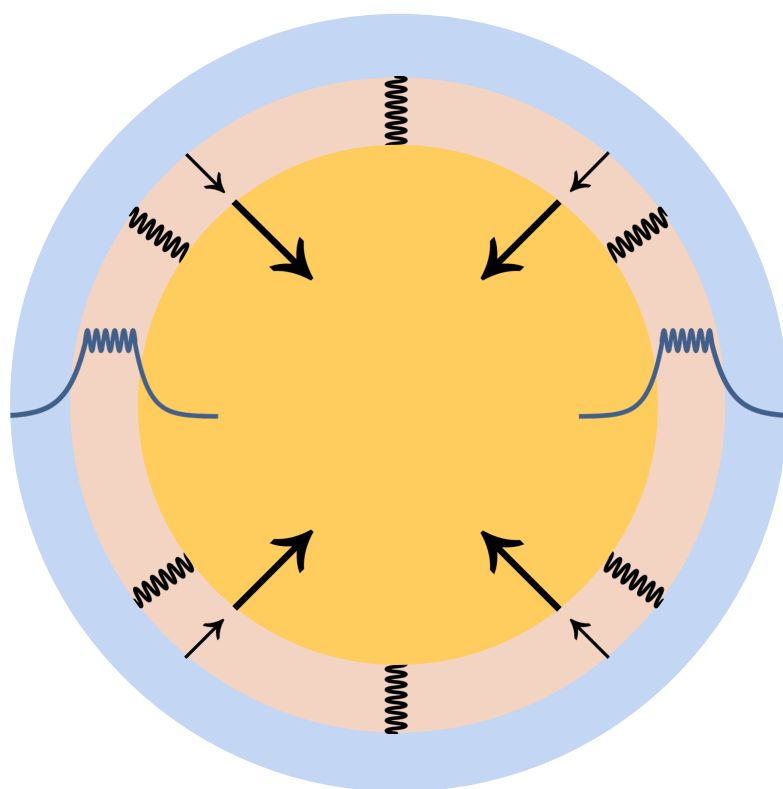
| | | |
|---|------------------|---------------|
| 3 | Signature | Date |
| | | July 10, 2018 |

Corresponding Regulation

Before being admitted to a degree, a student shall deposit with the Secretary of the Board one copy of his or her hard-bound dissertation and one copy of the summary (bearing student's name and thesis title), both the dissertation and the summary in a form approved by the Board. The Secretary shall deposit the copy of the dissertation together with the copy of the summary in the University Library where, subject to restricted access to the dissertation for a specified period of time having been granted by the Board of Graduate Studies, they shall be made available for consultation by readers in accordance with University Library Regulations and copies of the dissertation provided to readers in accordance with applicable legislation.

Adam Sean Jermyn

Turbulence and Transport in Stars and Planets



This dissertation is submitted for the degree of Doctor of Philosophy.

CHURCHILL COLLEGE · UNIVERSITY OF CAMBRIDGE · JULY 10, 2018

Turbulence and Transport in Stars and Planets

Adam Sean Jermyn

In this dissertation I have argued that the study of stars and gaseous planets has relied too heavily on simplifying assumptions. In particular, I have demonstrated that the assumptions of spherical symmetry, thermal equilibrium, dynamical equilibrium and turbulent anisotropy all hide interesting phenomena which make a true difference to the structure and evolution of these bodies.

To begin I developed new theoretical tools for probing these phenomena, starting with a new model of turbulent motion which accounts for many different sources of anisotropy. Building on this I studied rotating convection zones and determined scaling relations for the magnitude of differential rotation. In slowly-rotating systems the differential rotation is characterised by a power law with exponent of order unity, while in rapidly-rotating systems this exponent is strongly suppressed by the rotation. This provides a full characterisation of the magnitude of differential rotation in gaseous convection zones, and is in reasonable agreement with a wide array of simulations and observations.

I then focused on the convection zones of rotating massive stars and found them to exhibit significantly anisotropic heat fluxes. This results in significant deviations from spherical symmetry and ultimately in qualitatively enhanced circulation currents in their envelopes. Accordingly, these stars ought to live much longer and have a different surface temperature. This potentially resolves several outstanding questions such as the anomalously slow evolution of stars on the giant branch, the dispersion in the observed properties of giant stars and the difficulty stellar modelling has to form massive binary black holes.

In the same vein I examined the convection zones of bloated hot Jupiters and discovered a novel feedback mechanism between non-equilibrium tidal dissipation and the thermal structure of their upper envelopes. This mechanism stabilises shallow radiative zones against the convective instability, which would otherwise take over early on in the planet's formation as it proceeds to thermal equilibrium. Hence tidal dissipation is dramatically enhanced, which serves to inject significant quantities of heat into the upper layers of the planet and causes it to inflate. This mechanism can explain most of the observed population of inflated planets.

Finally, I studied material mixing in the outer layers of accreting stars and developed a method for relating the observed surface chemistry to the bulk and accreting chemistries. This enables the direct inference of properties of circumstellar material and accretion rates for a wide variety of systems.

Copyright © 2018 Adam S. Jermyn

This dissertation was typeset with the `tufte-book` L^AT_EXclass.

Title image: Schematic of a thermomechanical feedback mechanism. The upper convective layer (blue), radiative layer (beige) and inner convective layer (yellow) are shown as concentric shells. The boundaries of the radiative layer are moving inward at different rates, allowing the zone to resize. Profiles of g-modes (dark blue) are shown along the equator and schematically depicted at other latitudes.

Submitted April 2018

*To those who always had time for my questions,
To those who helped me find my own answers,
And to my parents.*

Turbulence and Transport in Stars and Planets

Adam Sean Jermyn

The Universe is a place of unimaginable scales, both large and small. The challenge in astronomy is to tame these scales, to bridge the gap between the fundamental laws of Nature and the incredible variety of phenomena that result from their application to the countless constituents of the heavens. Nowhere is this challenge as evident as in the study of stars and planets. These bodies exhibit physics ranging in energy from the radio all the way to the nuclear. They evolve on timescales of billions of years, yet they oscillate in hours, flare in minutes and explode in seconds. Their features span the gamut from hurricanes the size of Earth to prominences and winds many times the size of the Sun. And most importantly, all of these phenomena interact with one another across great swaths of space and time.

Broadly speaking there are two tools that theoretical physics has to meet this challenge. The first is to impose assumptions on Nature. This often serves to make questions more tractable, but at the cost that the answers one finds are only as good as the assumptions one uses. The second is to climb up the ladder of complexity, using the laws of physics on one rung to formulate effective laws on the next. This is more physically justified but also considerably more difficult. In this dissertation I have argued that in the study of stars and gaseous planets astronomy has relied too heavily on the former and perhaps not enough on the latter. In particular, I have demonstrated that the assumptions of spherical symmetry, thermal equilibrium, dynamical equilibrium and turbulent anisotropy all hide interesting phenomena which make a true difference to the structure and evolution of these bodies.

To begin I developed new theoretical tools for probing these phenomena, starting with a new model of turbulent motion which accounts for many different sources of anisotropy. Building on this I studied rotating convection zones in stars and gaseous planets and determined scaling relations for the magnitude of differential rotation across all possible mean rotation rates. In slowly-rotating systems the differential rotation is characterised by a power law with exponent of order unity, while in rapidly-rotating systems this exponent is strongly suppressed by the rotation. This provides a full characterisation of the magnitude of differential rotation

in gaseous convection zones, and is in reasonable agreement with a wide array of simulations and observations.

I then focused on the convection zones of rotating massive stars and found them to exhibit significantly anisotropic heat fluxes. This results in significant deviations from spherical symmetry and ultimately in qualitatively enhanced circulation currents in their envelopes. Accordingly, these stars ought to live much longer and have a different surface temperature. This potentially resolves several outstanding questions such as the anomalously slow evolution of stars on the giant branch, the dispersion in the observed properties of giant stars and the difficulty stellar modelling has to form massive binary black holes.

In the same vein I examined the convection zones of bloated hot Jupiters and discovered a novel feedback mechanism between non-equilibrium tidal dissipation and the thermal structure of their upper envelopes. This mechanism stabilises shallow radiative zones against the convective instability, which would otherwise take over early on in the planet's formation as it proceeds to thermal equilibrium. As a result there is a hysteresis effect whereby radiative zones, present when the planet forms, may be preserved for most of the lifetime of the host star. This dramatically enhances tidal dissipation and can inject significant quantities of heat into the upper layers of the planet, causing it to inflate. This mechanism can explain most of the observed population of inflated planets.

Finally, I studied material mixing in the outer layers of accreting stars and developed a method for relating the observed surface chemistry to the bulk and accreting chemistries. This enables the direct inference of properties of circumstellar material and accretion rates for a wide variety of systems.

My work suggests a new landscape of complex feedback between heat and momentum transport processes and turbulence which is only apparent when overly-simple assumptions are replaced by a picture which better reflects the true complexity of Nature.

Contents

| | | |
|----------|---|-----------|
| I | <i>Introduction</i> | 17 |
| 1.1 | <i>Overview</i> | 17 |
| 1.2 | <i>Constituents</i> | 20 |
| 1.3 | <i>Thermodynamics</i> | 22 |
| 1.4 | <i>Diffusion</i> | 24 |
| 1.5 | <i>Advection</i> | 32 |
| 1.6 | <i>Turbulence</i> | 37 |
| 1.7 | <i>Geometry and Symmetry</i> | 41 |
| | | |
| 2 | <i>Turbulence Closure</i> | 45 |
| 2.1 | <i>Introduction</i> | 46 |
| 2.2 | <i>Closure Formalism</i> | 48 |
| 2.3 | <i>Perturbative Corrections</i> | 52 |
| 2.4 | <i>Equations of Motion</i> | 54 |
| 2.5 | <i>Stresses and Transport</i> | 57 |
| 2.6 | <i>Software Details</i> | 57 |
| 2.7 | <i>Results</i> | 59 |
| 2.8 | <i>Discussion and Outlook</i> | 82 |
| | | |
| 3 | <i>The Magnitude of Convective Differential Rotation</i> | 83 |
| 3.1 | <i>Introduction</i> | 84 |

| | | |
|------|--|-----|
| 3.2 | <i>Assumptions</i> | 87 |
| 3.3 | <i>Vorticity</i> | 89 |
| 3.4 | <i>Magnetic Fields</i> | 92 |
| 3.5 | <i>Thermal Equilibrium</i> | 94 |
| 3.6 | <i>Thermal Wind</i> | 98 |
| 3.7 | <i>Stiffness</i> | 99 |
| 3.8 | <i>Slow Rotation</i> | 100 |
| 3.9 | <i>Advective Terms</i> | 106 |
| 3.10 | <i>Rapid Rotation</i> | 118 |
| 3.11 | <i>Inverse Cascade</i> | 133 |
| 3.12 | <i>Breakup Rotation</i> | 135 |
| 3.13 | <i>Tests</i> | 138 |
| 3.14 | <i>Limitations</i> | 143 |
| 3.15 | <i>Discussion and Outlook</i> | 146 |
| 3.16 | <i>Data Processing</i> | 149 |
| 4 | <i>Rotational Mixing in Massive Stars</i> | 161 |
| 4.1 | <i>Introduction</i> | 162 |
| 4.2 | <i>Origins of Meridional Flow</i> | 163 |
| 4.3 | <i>Differential Rotation</i> | 167 |
| 4.4 | <i>Anisotropic Convection</i> | 174 |
| 4.5 | <i>Centrifugal Effects</i> | 179 |
| 4.6 | <i>Meridional Circulation in the Convection Zone</i> | 179 |
| 4.7 | <i>Effects in Massive Stars</i> | 183 |
| 4.8 | <i>Chemical Composition Gradients</i> | 195 |
| 4.9 | <i>Convective Overshooting</i> | 195 |
| 4.10 | <i>Implementation in Stellar Models</i> | 200 |
| 4.11 | <i>Interpretation</i> | 202 |
| 4.12 | <i>Dicsussion and Outlook</i> | 203 |

| | | |
|------|--|-----|
| 5 | <i>Tidal heating of Hot Jupiters</i> | 205 |
| 5.1 | <i>Introduction</i> | 206 |
| 5.2 | <i>Isotropic Planetary Structure</i> | 207 |
| 5.3 | <i>Angular Temperature Distribution</i> | 213 |
| 5.4 | <i>Heated Thermal Structure</i> | 217 |
| 5.5 | <i>Expansion</i> | 221 |
| 5.6 | <i>G-Modes</i> | 223 |
| 5.7 | <i>Equilibrium Radius</i> | 237 |
| 5.8 | <i>Energetic Timescales</i> | 241 |
| 5.9 | <i>Comparison</i> | 241 |
| 5.10 | <i>Discussion and Outlook</i> | 242 |
| 6 | <i>Stellar Photospheric Abundances as a Probe of Disks and Planets</i> | 243 |
| 6.1 | <i>Introduction</i> | 244 |
| 6.2 | <i>Theory</i> | 245 |
| 6.3 | <i>Mixing Depth</i> | 250 |
| 6.4 | <i>Mixing Processes</i> | 259 |
| 6.5 | <i>Application to observations</i> | 266 |
| 6.6 | <i>Discussion and Outlook</i> | 281 |
| 7 | <i>Conclusions</i> | 283 |
| | <i>Bibliography</i> | 289 |

Preface

This dissertation is the result of my work at the Institute of Astronomy at the University of Cambridge between September 2015 and April 2018 with the guidance of Christopher Tout. All of the text is mine, though some of it is based on work for which he, Pierre Lesaffre, Shashikumar Chitre, Gordon Ogilvie, Mihkel Kama, Rob Izzard, Anna Żytkow, Sterl Phinney, Jim Fuller, Matteo Cantiello and anonymous referees have provided advice and/or editing. All figures are mine except where noted; all external sources of data and ideas are referenced in the text; and any errors or omissions are mine.

Parts of this dissertation have been previously published or submitted for publication and parts will be submitted for publication in the near future. Chapter 2 is based on work which has been published ¹. Chapter 3 will soon be submitted for publication in the *Monthly Notices of the Royal Astronomical Society* under the title “The Magnitude of Differential Rotation in Convection Zones”². Chapter 4 is in review at the same under the title “Enhanced Rotational Mixing in the Radiative Zones of Massive Stars”³. Chapter 5 is based on work which has been published ⁴. Chapter 6 is based on work which has been published ⁵.

I hereby declare that this dissertation entitled “Turbulence and Transport in Stars and Planets” is the result of my own work and includes nothing which is the outcome of work done in collaboration except as declared in this Preface and specified in the text. It is not substantially the same as any that I have submitted or is being concurrently submitted for a degree or diploma or other qualification at the University of Cambridge or any other University or similar institution. I further state that no substantial part of my dissertation has already been submitted or is being concurrently submitted for any such degree, diploma or other qualification at the University of Cambridge or any other University or similar institution. This dissertation does not exceed 60,000 words.

¹ Jermyn, Lesaffre, Tout & Chitre 2018

² This work was done in collaboration with Shashikumar Chitre, Pierre Lesaffre and Christopher Tout.

³ This work was done in collaboration with Christopher Tout and Shashikumar Chitre.

⁴ Jermyn, Tout & Ogilvie 2017

⁵ Jermyn & Kama 2018

I Introduction

There's such a lot in the world. There's so much distance between the fundamental rules and the final phenomenon that it's almost unbelievable that the final variety of phenomena can come from such a steady operation of such simple rules.

Richard P. Feynman

1.1 Overview

The theoretical study of stars has proceeded in earnest for over a century, from early investigations of their thermal structure ¹ to the discovery of nuclear processes ² to detailed modelling ³. These efforts have been met with success beyond any reasonable hope and mark some of the great triumphs of physics, including the origin of the chemical elements ⁴, the age of the solar system, the compositions of the stars and the origins of their heat and light.

Along the way a persistent theme that emerged was the need to understand the role fluid dynamics and turbulence play in transporting heat, momentum and chemistry within stars. Early on significant attention was paid to the details of these processes ⁵ but over time the field has accreted more and more simplifying assumptions, many of which are now used well beyond the regimes in which they are justified. This has caused a great deal of confusion and gives the mistaken impression that fundamental problems are few and far between.

In fact nothing could be further from the truth. In the regimes where they fail, many simplifying assumptions hide a rich variety of fascinating and exciting phenomena⁶. Some of these have come to light with new numerical simulations and observations, but it is usually quite difficult to decompose the results into distinct physical processes which can then be understood and used predictively. Thus there is a great deal still to be

¹ Jeans 1902, 1917; Eddington 1917, 1918; Chandrasekhar 1931

² Becquerel 1896; Rutherford 1919; Chadwick 1932

³ Paczyński 1969; Eggleton 1971; Pols et al. 1995; Paxton et al. 2015

⁴ Holloway & Bethe 1940; Wagoner et al. 1967; Hoyle & Fowler 1973

⁵ Eddington 1929; Chandrasekhar 1961

⁶ A fun example is provided by Lecoanet & Quataert (2013), who find that while convectively-excited internal gravity waves are essentially always negligible in terms of the total energy budget of a star, under the right conditions they can come to dominate the radiative luminosity which escapes from its surface.

learned by starting from the full set of physical equations and evaluating them with pen on paper.

This is doubly true in light of the vast array of extra-solar planets that have recently been discovered ⁷. These worlds, which in many ways are quite similar to stars in their structure and evolution ⁸, exhibit a striking diversity that cannot be explained without invoking a wide range of complex physical interactions.

⁷ Rein 2012

⁸ Stevenson 1991; Guillot et al. 2004

The purpose of this dissertation is then twofold. First, I have developed several theoretical tools for understanding the structure and evolution of stars and gaseous planets which make fewer simplifying assumptions. These are principally analytic methods though I have employed numerical methods where advantageous. Secondly, I have applied these tools in various specific instances to learn more about astrophysical systems.

In the remainder of this introduction I review the basic physics which enters into the study of stellar structure and evolution, with a focus on those aspects which arise in this work. This is largely the same physics as enters into the study of gaseous planets though I note where differences arise. A key point of this overview is that convection is critically important to heat, momentum and material transport in a wide variety of circumstances.

Following this, in Chapter 2 I develop a new turbulence closure model which provides access to turbulent correlation functions without imposing any significant assumptions apart from axisymmetry. I include rotation, magnetism, shear and baroclinicity. Attempts have been made to include and analyze some of these complications ⁹, but now is the first time that such a breadth of effects have been incorporated without invoking many free parameters¹⁰ and in a way that can be rapidly incorporated into existing computational models of stellar and planetary structure. In particular my approach, which covers all of the effects that are likely to be relevant for stars and planets, requires just one free parameter¹¹ and is computationally efficient. Using this model I also extracted scaling laws to understand turbulence analytically and explained them in intuitive physical terms. Several of these laws were already known but many are brand new.

⁹ Canuto 1997; Lesaffre et al. 2013

¹⁰ Many models perform extremely well by virtue of having many fitted parameters. This makes them good for engineering applications where they serve as effective interpolations but poor as predictive models.

¹¹ This makes it both predictive and readily testable.

Using results obtained from this turbulence closure model I then turn to the question of differential rotation in Chapter 3, where I derive general scaling relations for differential rotation in convection zones of stars and planets. The results suggest that the order-unity differential rotation observed in the Sun is actually a generic feature of slowly rotating convection zones, regardless of the mean rate of rotation. Beyond a certain point the shear continues to grow with the rotation rate but the *relative* shear declines.

This is driven by the increasing importance of the Taylor–Proudman term in the vorticity equation, which couples the shear to the rotation axis. Along the way I also derive previously-known scaling relations for the turbulent magnetic field and use these to highlight the additional suppression of differential rotation owing to magnetism.

In Chapter 4 I then build on that analysis to study the effects of rotation on massive stars. I have found that because convection in their cores is quite slow, even relatively modest rotation suffices to make it substantially anisotropic. This causes the flux distribution in the core to be far from spherical. At the core–envelope interface heat transport transitions from convective to radiative, which translates this flux anisotropy into a thermal anisotropy. In effect the envelope becomes strongly baroclinic. This drives a circulation current in the radiative envelopes of massive rotating stars which is qualitatively enhanced relative to what was previously expected. As a result these stars ought to live longer, because more fuel is mixed from the envelope into the core, and ought to be redder, because the metallicity of the envelope is enhanced by fusion ashes from the core. This potentially resolves several outstanding questions such as the anomalously slow evolution of stars on the giant branch, the dispersion in the observed properties of giant stars and the difficulty stellar modelling has in forming massive binary black holes such as those discovered by the LIGO collaboration recently ¹². These are large effects which were entirely missed because of one simple assumption: that convection is isotropic. Ordinarily this assumption is fine because either the corrections are not so great or the consequences of those corrections are not so significant, but in this case both the corrections and the consequences are large.

¹² Abbott et al. 2016

Turning to the question of planetary structure, in Chapter 5 I examine the common assumptions of mechanical and thermal equilibrium. I found that in hot Jupiter systems both can fail. In particular, I discovered a form of feedback between the thermal and mechanical structures of the outer envelopes of these planets. If there is a region with a shallow temperature gradient in the envelope, so that heat is transported by radiation rather than convection, that region acts as a resonant cavity for tides. In effect the tidal pull from the host star has an enhanced impact in such zones.

Ordinarily this phenomenon is of little interest because radiative zones disappear early on in the thermal evolution of gaseous planets. What I found however is that the non-equilibrium tides inject heat into such zones and this sustains them out of thermal equilibrium. Thus they are allowed to survive throughout the planet’s evolution and so tidal dissipation

is significantly enhanced over a long period of time. The tides inject additional energy into the regions above the radiative zone and causes such planets to expand. This mechanism explains most of the observed population of inflated hot Jupiters, potentially resolving one of the great mysteries of the field.

Finally in Chapter 6 I study the manner in which material accreting onto a star mixes into its outer layers. I developed a tool, the Contamination by Accretion Method (CAM), to link the observed chemistry of the photosphere to those of the stellar bulk and circumstellar material. This provides an independent means to infer the accretion rate onto a star from its assumed bulk chemistry and observed surface chemistry. Likewise the method may be used in reverse to infer the chemistry of either the accretion or bulk material from the accretion rate and observed surface chemistry. This provides an important cross-check of existing measurements of stellar accretion rates, which are often highly uncertain, and allows for previously-impossible inferences of circumstellar disk chemistry.

I close in Chapter 7 with a summary of these results and a discussion of future prospects. This work emphasizes that stars and gaseous planets are vastly richer than one-dimensional equilibrium models give them credit for. More than anything that is the result I wish to convey.

1.2 Constituents

Stars and gaseous planets are composed principally of protons, neutrons and electrons¹³. Except for brief intervals of freedom between fission and fusion events, neutrons are generally bound together with protons by the nuclear forces in atomic nuclei¹⁴. This is a result of the immense energy scales involved in the nuclear forces, which generally exceed the kinetic energy per particle that may be found in these systems.

By contrast electrons may or may not be bound together with atomic nuclei to form atoms¹⁵. This is because the force which binds them, namely the electromagnetic interaction, is characterised by much smaller energy scales than the nuclear forces. There is thus much more opportunity for free motion of electrons. Indeed as we shall note further on, whether electrons are free or bound is often a key determinant of the properties of matter, and has significant consequences for stellar and planetary structure.

It is not generally practical to calculate the motions of all of the particles in a bacterium, let alone in a star or planet. There are simply too many particles to give any a meaningful amount of attention. Furthermore particles may influence one another at arbitrary distances¹⁶, making the

¹³ Neutrinos are generally also present but usually negligible owing to their weak interactions, which allow them to easily pass through a star or planet. Dark matter may or may not be present but if present its effects on stellar and planetary structure have yet to be observed. There are also, of course, the force-carrying bosons, but these are so different in behaviour that we consider them separately.

¹⁴ The exceptions to this are in compact stellar remnants, such as neutron stars.

¹⁵ In some cases these atoms even bind to form molecules!

¹⁶ This is a consequence of the photon and graviton being massless, and is also why seeing is possible and why the large-scale structure of the Universe is so complex.

task appear even less tractable. In order for us to proceed then it must be the case that in some fashion the small-scale interactions of individual particles give rise to behaviours which may be understood on larger scales. Fortunately this is a common theme in physics¹⁷. Whilst the resulting behaviours may look very unlike those from which they emerge¹⁸, it appears that in a great many cases we may construct useful and intuitive descriptions of the behaviour of the unimaginably-numerous particles which make up macroscopic matter.

In general the approach that is taken is to create a description of the physics which emerges at a slightly larger scale than that of the current description, making approximations as needed, and to then iterate on this procedure until the desired scale is reached. Indeed we have already taken one step in that direction by discussing the bound states of protons and neutrons, and have implicitly taken another by not beginning with quarks and gluons. The next significant step is one which carries us a great deal further, and that is to divide the motions of these constituent particles into two categories, namely random and structured. The former encompasses thermal motions, and is relevant whenever particles scatter frequently¹⁹ and thereby ergodically explore the available phase space²⁰. A defining feature of these random motions is that they are readily summarised at larger scales by local thermally-averaged quantities. Thus, for instance, the flux of momentum carried by particles is renormalized and becomes the pressure. Similarly the energy of the particles is summarised by the temperature, and their numbers by the density.

By contrast structured motion is not so easily summarised. This encompasses phenomena such as waves, shocks, and flows. In each case there is some large-scale structure which is imposed on the small-scale motions of particles. Unlike the case of random motions there is very little which can be said generically of structured motions. Sometimes they obey the principal of superposition, in which different structures may coexist and linearly superimpose, but sometimes not. This is usually determined by the amplitude of the motion. Sometimes they interact with small-scale random motions, as in the case of waves in a fluid, but sometimes not, as in the case of magnetic prominences.

Of course there are also motions which are difficult to classify, of which turbulence is the most notorious example²¹. The chief difficulty posed by turbulence is that it is structured. Depending on the circumstances it can exhibit granules²², bands²³ and eddies of all scales²⁴. On the other hand turbulence is undeniably random, at least in the sense in which

¹⁷ This is best known as the Renormalization Group, which was introduced in its modern form by Wilson (1971) and later expanded by Fisher (1974).

¹⁸ This was perhaps best expressed by Anderson (1972) with the phrase “More is different.”

¹⁹ Whenever a scale is large or small, or a phenomenon is frequent or rare, the crucial question is with respect to what? In this case frequently means relative to the time-scale over which the boundary conditions on the region of interest change.

²⁰ Kardar 2006

²¹ To highlight this, Horace Lamb was quoted by Goldstein (1969) as saying “I am an old man now, and when I die and go to Heaven there are two matters on which I hope for enlightenment. One is quantum electrodynamics, and the other is the turbulent motion of fluids. And about the former I am really rather optimistic.”

²² Bahng & Schwarzschild 1961

²³ Rhines 1973

²⁴ Richardson 1922

thermal motion is random. Turbulent motion is fluctuating and chaotic in nature ²⁵. The resolution of this apparent conflict is that turbulence exhibits structure in its statistical correlations, but is effectively random in its instantiation. This is also the reason that turbulence has proven so difficult a problem: it is structured yet it does not suffice to examine a specific instance. For our purposes therefore we shall use theories which make statistical predictions about turbulence and other such in-between phenomena.

²⁵ Deissler 1986

Broadly speaking then there are three classes of phenomena we shall consider, namely thermal, turbulent and structured. We now proceed to discuss descriptions of specific physical phenomena which arise in stars and planets.

1.3 Thermodynamics

It is a general rule that systems of identical featureless particles in a translationally-invariant thermal ensemble may be described by two state variables ²⁶. Intuitively this is because once one specifies the temperature the mean energy of particles is fixed. The mean momentum is therefore also fixed, and because momentum determines velocity this combined with the density also determines the pressure. This relationship is often summarised in terms of the equation of state, which may be written as

²⁶ Kardar 2006

$$f(\rho, p, T) = 0,$$

where ρ is the density, p is the pressure and T is the temperature.

When the particles are not featureless the system may require more variables to be fully specified. For example when particles have spin then one might specify the magnetisation of the ensemble, which plays a role in determining thermal averages which couple to magnetism. While this is a commonly considered case in the realm of condensed matter, it is rarely of interest in stars and planets because the temperatures involved are typically much greater than the energy which couples individual spins to the overall magnetic field. Hence for the purposes of this work we neglect spin as a thermodynamic variable.

Of more interest, in cases in which there are multiple kinds of particles present the density may be broken out into a per-species density, such that

$$f(\{\rho_i\}, p, T) = 0,$$

where ρ_i is the density of species i . In particular, for an ideal gas the

existence of multiple species only matters in determining the relationship between the number density n of particles and their mass density ρ . Hence the equation of state is often written as

$$f(\mu, \rho, p, T) = 0,$$

where μ is the mean molecular weight. For historical reasons this is expressed as a multiple of the proton mass m_p .

While a great deal of work has gone into characterising the equation of state in stellar and planetary matter ²⁷, the effects which are caused by complications in the equation of state are quite well-captured in modern one-dimensional stellar evolution simulations ²⁸ and are not our focus. Even in places where significant mysteries remain as to *what* the equation of state is, as in neutron stars ²⁹, the consequences of different such equations of state are well-understood. The main exception to this arises in the case of turbulence in radiatively-dominated optically-thin regions where the impact of the equation of state is not particularly well-understood and is under active investigation ³⁰. Exciting as those questions are, however, such considerations are not relevant in any of the cases which we shall consider and so we neglect them. Hence we use the ideal gas equation of state, which is written as

$$m_p \mu p = \rho k_B T, \quad (1.1)$$

where k_B is the Boltzmann constant.

A straightforward consequence of equation (1.1) and the first law of thermodynamics is that the entropy of matter is given by ³¹

$$s = \ln p - \gamma \ln \rho + g \left(\left\{ \frac{\rho_i}{\rho} \right\} \right) + c,$$

where γ is the adiabatic index, g is a function only of the mass fractions of the various species and c is a constant which serves to non-dimensionalise p and ρ . In cases in which the composition of the material is held fixed the third term is constant and so we may write

$$s = \ln p - \gamma \ln \rho, \quad (1.2)$$

where we have neglected the constant because only differences in entropy are physically meaningful. As one final simplification we often take $\gamma = 5/3$, which is appropriate for a monotomic gas which is not undergoing ionization ³². This is changed by ionization and radiation pressure but

²⁷ Rogers et al. 1996; Timmes & Swesty 2000; Guillot et al. 2004

²⁸ Eggleton 1971

²⁹ Lattimer 2012

³⁰ Shaviv 2001, 2005

³¹ Kardar 2006

³² Hansen & Kawaler 1994

such changes are not important in our analysis and so we neglect them.

Finally it is useful to note that the specific³³ internal energy of an ideal gas is

$$U = \left(\frac{1}{\gamma - 1} \right) \frac{k_B T}{\mu m_p},$$

which with $\gamma = 5/3$ produces

$$U = \frac{3}{2} \frac{k_B T}{\mu m_p}. \quad (1.3)$$

1.4 Diffusion

An assumption we made in the previous section was that the thermal ensemble was translationally invariant. When properties of the system vary in space this fails. For instance in the Earth's atmosphere translational symmetry is broken by the gravitational field, causing particles to preferentially group near the surface of the planet. So long as the scale over which this symmetry-breaking occurs is large relative to the mean free path λ particles take between thermalising collisions this is not a problem. There is still a nearly-thermal ensemble in each region larger than λ , so we may simply promote each of pressure, temperature and density to be a function of position.

If the ensemble in each region were independent of all of the others there would be nothing more to say. This is not the case, however. Particles may flow freely, subject to scattering, between neighbouring regions. As they do so they carry energy and momentum and mass, and so generate fluxes of these quantities. On length-scales larger than λ these fluxes are characterised by Fick's law of diffusion³⁴, which states that the flux of a quantity ψ which is carried by particles in random motion is given by

$$\mathbf{F}_\psi = -\mathbf{D}_\psi \cdot \nabla \psi, \quad (1.4)$$

where \mathbf{D}_ψ is the diffusivity tensor associated with ψ . Note that ψ may be vector- or tensor-valued, in which case the diffusivity tensor must carry and sum over indices associated with these additional properties³⁵. For instance the diffusivity of spin, which is a vector, must incorporate the fact that in scattering events particles may change their spins, such that the components of ψ mix in the process of diffusion. Further note that equation (1.4) holds even if $\nabla \psi$ is quite large, though under such circumstances the diffusivity tensor may become dependent on $\nabla \psi$ and

³³ By specific we always mean per unit mass.

³⁴ Fick 1855

³⁵ In particular the diffusivity of a rank- n object requires $2n + 2$ components. These are broken down as one to match the gradient, one to give the flux a direction and $2n$ to mix the n indices of ψ into the n corresponding indices of the flux.

the flux may cease to be linear in this gradient.

An important consequence of equation (1.4) is that the diffusivity has dimensions of length squared per unit time. That is, material diffuses a distance l in time proportional to l^2 . Fundamentally this arises because the particles in our system are undergoing random walks, but from a practical perspective it means that the scale of a diffusivity is best judged by a combination of two lengths, which may be the same, and one time.

A crucial simplification of equation (1.4) comes about when the random motion of particles is locally rotationally symmetric. That is there must be no preferred directions apart from that of $\nabla\psi$. When this is the case \mathbf{D}_ψ must be isotropic. Furthermore when the quantity ψ is a scalar such as energy density the diffusivity must be a rank-2 tensor because there are no additional indices to sum over. The only rank-2 isotropic tensors are multiples of the identity, so

$$\mathbf{F}_\psi = -D_\psi \nabla\psi,$$

where D_ψ is a scalar.

Even when ψ is not a scalar the assumption of rotational invariance³⁶ significantly simplifies the diffusivity tensor. For instance momentum is a vector so its diffusivity tensor is rank-4. All isotropic rank-4 tensors may be written as linear combinations of³⁷ $\delta_{ij}\delta_{kl}$, $\delta_{ik}\delta_{jl}$ and $\delta_{il}\delta_{jk}$, where δ_{ij} is the Kronecker delta and equals one when $i = j$ and zero otherwise. In this case the diffusivity may be written as

$$F_{ij} = -(D_1\delta_{ij}\delta_{kl} + D_2\delta_{ik}\delta_{jl} + D_3\delta_{il}\delta_{jk}) \frac{\partial\psi_l}{\partial x_k}, \quad (1.5)$$

where D_1 , D_2 and D_3 are scalars, F_{ij} is the flux of ψ_j along the direction \mathbf{e}_i , x_k are spatial coordinates and summation is implied over repeated indices.

The assumption of isotropy is very often satisfied in stars and planets. Random thermal motions are often very nearly rotationally symmetric. This is because the energy scale involved in thermal motions is usually much greater than that involved in the various symmetry-breaking forces such as gravity acting over the mean free path³⁸. We therefore proceed on the assumption that these diffusivities associated with random motion, hereinafter referred to as microscopic diffusivities, are isotropic. In the remainder of this section we examine the typical forms and magnitudes of several important microscopic diffusivities.

³⁶ e.g. isotropy

³⁷ Landau & Lifshitz 1959

³⁸ A notable exception to this is in highly-magnetised compact stellar remnants such as white dwarfs and neutron stars. Intense magnetic fields in those systems make the motion of electrons highly anisotropic and cause the charge diffusivity tensor to be similarly anisotropic. See e.g. Yakovlev & Shalybkov (1991).

1.4.1 Viscosity

The viscosity is the diffusivity of momentum. Because momentum is a vector this must be a rank-4 tensor. On the assumption of isotropy we follow equation (1.5) and write

$$D_{ijkl} = D_1 \delta_{ij} \delta_{kl} + D_2 \delta_{ik} \delta_{jl} + D_3 \delta_{il} \delta_{jk}.$$

In the case of momentum diffusion though there is another constraint, namely that the flux F_{ij} must be symmetric³⁹. To see this note that the torque on a piece of material is given by the flux of angular momentum through its boundary. Hence

$$\tau_j = \int_S \mathcal{J}_{ij} dA_i, \quad (1.6)$$

where A_i is the area element of the closed surface S over which the integral runs and \mathcal{J}_{ij} is the flux of angular momentum. The angular momentum flux is related to the momentum flux by

$$\mathcal{J}_{ij} = \epsilon_{jlm} x_l F_{im},$$

where ϵ_{jlm} is the Levi-Civita symbol, which equal to zero when any of its indices are equal, +1 when its indices represent an even permutation of the sequence $\{1, 2, 3\}$ and -1 when they represent an odd permutation of the same. Inserting this into equation (1.6) we find

$$\tau_j = \epsilon_{jlm} \int x_l F_{im} dA_i,$$

This is related to the rate of change of the mean angular velocity Ω of the piece of material by its moment of inertia I , so that

$$I_s \frac{d\Omega_s}{dt} = \epsilon_{jlm} \int x_l F_{im} dA_i. \quad (1.7)$$

Now the moment of inertia scales linearly with the mass m of the material and the square of its linear size l . Using $m \propto \rho l^3$ we find $I \propto \rho l^5$. The right-hand side, on the other hand, scales as l^3 because it contains the coordinate \mathbf{x} once and is an integral over a surface. It follows that

$$\frac{d\Omega_s}{dt} \propto l^{-2}.$$

This, which diverges as the element of interest becomes smaller, is not physical⁴⁰. It follows that the flux of angular momentum into the element must vanish as $l \rightarrow 0$.

³⁹ Landau & Lifshitz 1959

⁴⁰ An exception arises when the mean free path λ is not small. This is because the $l \rightarrow 0$ limit is actually not physical: the most we can do is proceed to $l \approx \lambda$, at which point our description of the system in terms of locally averaged quantities breaks down. Hence if the behaviour of the angular acceleration is reasonable when $l = \lambda$ then the stress need not be symmetric. This only arises in the astrophysical context in very low-density systems and so is not of interest for stars or planets.

The resolution to this contradiction is symmetry. Using the divergence theorem we write equation (1.7) as

$$\tau_j = \epsilon_{jlm} \int \frac{\partial}{\partial x_i} (x_l F_{im}) d^3 \mathbf{x},$$

where now the integral runs over the volume of interest rather than its bounding surface. Expanding the derivative yields

$$\tau_j = \epsilon_{jlm} \int F_{lm} + x_l \frac{\partial F_{lm}}{\partial x_i} d^3 \mathbf{x}.$$

The second term in the integral counts the angular momentum flux which arises from the flux of linear momentum into the volume and may be eliminated in the limit as $l \rightarrow 0$ by centering the coordinate system on the mean point of the volume⁴¹. The first term vanishes if either F_{lm} vanishes or else if it is symmetric. The former is not generally possible so we find the latter to be true.

The constraint of symmetry further restricts the form of the diffusivity, so we write

$$D_{ijkl} = D_1 \delta_{ij} \delta_{kl} + D_2 (\delta_{ik} \delta_{jl} + \delta_{il} \delta_{jk}). \quad (1.8)$$

This is the most general form of the microscopic viscosity tensor. An important consequence of this form relating to the symmetry of F_{ij} is that rigid rotational motion does not couple to the viscosity, so a rigidly-rotating state does not exhibit diffusive transport of angular momentum.

The viscosity is generally quite small in magnitude relative to the momentum scales of interest. The fluids of interest are typically ionized hydrogen-dominated plasmas, so the diffusivity has magnitude⁴²

$$|\mathbf{D}| \approx 5.2 \times 10^{-15} (\ln \Lambda)^{-1} \left(\frac{T}{\text{K}} \right)^{5/2} \left(\frac{\rho}{\text{g cm}^{-3}} \right)^{-1} \text{cm}^2 \text{s}^{-1} \quad (1.9)$$

(Spitzer, 1956), where $|\dots|$ denotes the maximum value of any entry in the tensor,

$$\ln \Lambda = \begin{cases} -17.4 + 1.5 \ln T - 0.5 \ln \rho & T < 1.1 \times 10^5 \text{K} \\ -12.7 + \ln T - 0.5 \ln \rho & T > 1.1 \times 10^5 \text{K} \end{cases}$$

and T and ρ are implicitly divided by C.G.S.K. units when they appear in a logarithm. Putting in typical numbers for the interiors of stars and gaseous planets we see that typical magnitudes of the viscosity are $10^0 - 10^5 \text{cm}^2 \text{s}^{-1}$. To put this number in context we define the Reynolds number⁴³

⁴¹ For a small enough volume the gradient of F_{lm} may be treated as constant. If x_l is centered on the mean point of the volume then the integral of x_l over the volume vanishes by definition. The next-order term is non-vanishing but scales as l^5 and so does not cause a divergence in the angular acceleration as $l \rightarrow 0$.

⁴² We have neglected the radiative viscosity because it is often, though not always, similarly small. Because it scales as T^4 while the particle viscosity scales as $T^{5/2}$ this becomes more relevant at high temperatures and may dominate in the deep interiors of massive stars. This becomes relevant in Chapter 4 and we discuss the radiative viscosity there.

⁴³ Stokes 1851

$$\text{Re} \equiv \frac{vl}{|\mathbf{D}|},$$

where v is the characteristic velocity scale of a shear and l is the characteristic length scale. This number is responsible for determining the importance of the viscosity in a fluid flow. In the slow convective cells of planets and stellar cores⁴⁴ $v \approx 100\text{cm s}^{-1}$ and $l \approx 10^7 - 10^{11}\text{cm}$ so the Reynolds number is in excess of 10^4 . Likewise in regions which are differentially rotating typically $v \approx \Delta\Omega l$, where $\Delta\Omega$ is the differential rotation rate and $l \approx 10^{11}\text{cm}$ is of order the radius of the system. Typical differential rotation rates⁴⁵ are at least of order 10^{-6}s^{-1} so $vl \approx 10^{16}\text{cm}^2\text{s}^{-1}$, which again produces an enormous Reynolds number. These numbers are quite approximate, but they are at the very low end of what is seen in stars and gaseous planets. The full question of stability is somewhat more complicated than a simple Reynolds number calculation, but this strongly suggests that stellar and planetary systems readily develop turbulence. Under such circumstances the microscopic viscosity may usually be neglected, and unless explicitly noted we do so from now on.

⁴⁴ See Chapters 4 and 5 for examples.

⁴⁵ See Chapter 3 for details.

1.4.2 Electrical Diffusivity

The electrical diffusivity is the diffusivity associated with electric charge. When electrons and protons are strongly bound in individual atoms this vanishes because charge carriers are unable to move without a carrier of the opposite charge moving in the same manner. Hence in non-ionized gaseous regions like the outer parts of Jupiter this conductivity is small, typically vanishingly so⁴⁶. As a result we ignore the electrical conductivity of atomic and molecular matter. This effectively decouples the matter from the effects of electromagnetic fields. In particular, this also means that the diffusivity of electromagnetic fields through the material is infinite because the two are non-interacting.

⁴⁶ Liu et al. 2008

There are two ways in which a significant electrical diffusivity may be achieved. First, material may be ionized⁴⁷. In this case electrons are unbound and charge diffuses easily. Secondly, atoms may bind together in a metallic state⁴⁸. Electrons are then bound but have wavefunctions which are spread out over many atomic sites, and so may easily hop from nucleus to nucleus in the metal. In both cases for simplicity we take the electrical diffusivity to be so large as to be effectively infinite. There are two consequences of this. First, electric fields cannot penetrate the material because it instantaneously adjusts its charge distribution to repel them⁴⁹. Secondly, magnetic fields cannot move through the material because in

⁴⁷ Spitzer 1956

⁴⁸ Ashcroft & Mermin 1976

⁴⁹ Feynman 1964

doing so they set up infinitely large currents which oppose the change according to Lenz's law ⁵⁰. In most cases the infinite charge-diffusivity zero field-diffusivity limit is an excellent approximation for metallic or ionized systems ⁵¹ so we proceed with this approximation.

There is, as usual, an intermediate regime. This arises most often in the context of accretion disks, where the ionization fraction may be low yet produce a non-negligible conductivity ⁵². Our focus here is never on such systems, however. This regime also arises in some low-mass stars and many gaseous planets in their ionization zones, but these are typically small enough relative to either the atomic or ionized regions that they may safely be neglected in the cases we examine. Hence we ignore this regime completely and take systems to be in one or the other extreme.

Before moving on there is one subtlety worth noting, which is that whether the electrical diffusivity is physically relevant really depends on what one is interested in. When the question is one of charge transport the diffusivity is relevant whenever it is large, whereas when the question is one of electromagnetic field transport it is relevant when small. In general we are much more concerned with field transport than with charge transport, as we expect systems to do a good job of remaining neutral ⁵³. For the same reason magnetic fields are generally of much more interest than electric fields, except to the extent that electric fields arise from time-varying magnetic fields.

1.4.3 Thermal Diffusivity

The thermal diffusivity is just the diffusion coefficient associated with heat. This generally arises from two sources, namely material conduction and radiative transfer.

Material conduction just refers to the diffusion of particles between regions of different temperatures. This motion carries energy from hot regions to cold ones⁵⁴ and so transports heat. This occurs even when there are collisions or interactions which transfer momentum between particles because these on average serve to transfer energy from hot to cold⁵⁵. While the thermal diffusivity of solids is rather complicated ⁵⁶ and not particularly of interest, that in gaseous systems is well approximated by the viscosity. That is, the particle diffusivity of heat is similar to that of momentum. The reason for this is that both heat and momentum are carried by particles, so both diffusivities are to leading order just given by the particle diffusivity. There are of course corrections to this arising from the microscopic details of particle interactions⁵⁷. These serve to modify

⁵⁰ Feynman 1964

⁵¹ Liu et al. 2008

⁵² Ilgner & Nelson 2006

⁵³ Spitzer 1956

⁵⁴ More formally heat is carried from regions of high free energy density to those of low free energy density.

⁵⁵ While there are physical justifications for this for any given kind of microscopic interaction, the fundamental reason for this is the second law of thermodynamics, which among other things precludes heat from diffusing from cold to hot without an input of free energy. See Kardar (2006) for more details.

⁵⁶ Ashcroft & Mermin 1976

⁵⁷ For instance, the more collisions preserve the directions of the incident momenta the more the momentum is carried along the direction of motion. This may be viewed as a modification to the mean free path, but different modifications are required for the diffusion of other quantities such as spin, which depends on the probability of spin flips in collisions, and heat, which depends on the extent to which collisions exchange energy.

the mobility⁵⁸ of the diffusing quantity. The mobility \mathcal{X} then sets the diffusivity via the Einstein relation ⁵⁹

$$D = \mathcal{X}k_{\text{B}}T.$$

These considerations typically correct the mobility by a dimensionless factor of order unity, so as a first approximation they may be neglected.

Radiative transfer, similarly, refers to the diffusion of photons between regions of different temperatures. This diffusion occurs because the photon density scales as T^4 and hence gradients in temperature result in gradients in photon density ⁶⁰. This mode of thermal diffusion has two key advantages over material conduction. First, photons travel at the speed of light rather than at the necessarily subluminal speeds of matter. Secondly, photons often have much smaller collisional cross-sections than electrons and nuclear matter. The chief disadvantage of photons in this race is that their share of the thermal energy scales much more strongly with temperature, going as T^4 rather than as T for the matter component. At high temperatures this favours optical conduction, but at low temperatures there may be insufficient thermal energy in photons for them to provide any significant heat transport. Needless to say these calculations have been done, with the conclusion that radiative transfer is the dominant source of thermal diffusivity in all gaseous phases of stellar and planetary matter ⁶¹. In degenerate matter such as that found in white dwarfs, neutron stars and giant planetary cores material conduction is the dominant effect, but these regions are not of interest here and so we only need to consider radiative effects moving forward.

Radiative transfer is often parameterised in terms of the opacity κ , which is a measure of the cross-section for photon-matter interactions per unit mass. This is generally a function of frequency as well as of thermodynamic state. When the mean free paths of photons are short, however, the frequency dependence becomes irrelevant because the photons are well approximated as being in local thermal equilibrium and so follow a black-body distribution ⁶². This is the limit of interest so we use the resulting frequency-averaged opacity, known as the Rosseland mean opacity ⁶³, which is appropriate for calculating the heat flux associated with radiative transfer.

Where detailed opacities are needed, as in Chapter 6, we use the OPAL (Iglesias & Rogers, 1996) and Ferguson (Ferguson et al., 2005) tables for solar composition and metallicity. This is not quite right when the composition is different from solar, but is a good enough approxi-

⁵⁸ The ratio of drift velocity to applied force

⁵⁹ Einstein 1905

⁶⁰ Kardar 2006

⁶¹ Hansen & Kawaler 1994

⁶² Planck 1914

⁶³ Hansen & Kawaler 1994

mation for our purposes. The Ferguson tables are more accurate at low temperatures while OPAL extends to much higher temperatures, so we choose the Ferguson opacities where available and the OPAL otherwise. The result is shown as a function of temperature and density in Fig. 1.1. White regions are those not covered by the tables or with opacities falling outside the range from $10^{-2} - 10^5 \text{ cm}^2 \text{ g}^{-1}$.

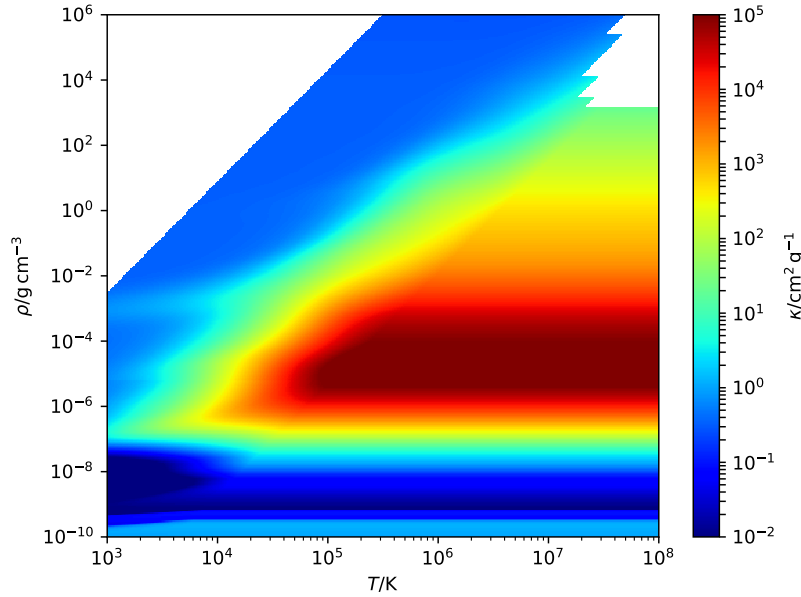


Figure 1.1: The opacity for solar composition is shown in colour on a logarithmic scale as a function of density and temperature. The top-right region is most representative of the deep interiors of stars, the bottom-left of their atmospheres, and the top-left of the interiors of gaseous planets.

Where detailed opacities are not needed we approximate them as appropriate to the regime of interest, using electron-scattering calculations in the high-temperature limit⁶⁴ and molecular/dust calculations in the low-temperature limit⁶⁵. These limits have opacities of order $10 \text{ cm}^2 \text{ g}^{-1}$ and $10^{-2} \text{ cm}^2 \text{ g}^{-1}$ respectively. Additionally in intermediate temperatures at the densities typical of stellar interiors we sometimes use Kramers' opacity law, which states that ⁶⁶

$$\kappa \propto \rho T^{-7/2},$$

where the proportionality constant depends on both metallicity and composition and is omitted because in all cases where we use this law we are only concerned with the scaling of the opacity and not with its overall magnitude. The regime in which this scaling is applicable is readily seen in Fig. 1.1 as beginning at a density of $10^{-6} \text{ g cm}^{-3}$ and at temperatures between 10^3 K and 10^5 K . This window extends with $T \propto \rho^{2/7}$ up to densities of order 1 g cm^{-3} , at which point free electron scattering sets a lower bound on the opacity.

⁶⁴ See Chapter 4.

⁶⁵ See Chapter 5.

⁶⁶ Kramers 1923

1.5 Advection

In the previous section we saw that random thermal motions result in diffusion, and before that we saw that thermal systems may be summarised by just a few local variables. This represents a dramatic reduction in complexity and so it is not too steep a price to pay that in the process we picked up diffusivities which vary with temperature and pressure in complicated ways.

The next step is to determine an equivalent large-scale description for ordered motions. To do so we let the momentum density be \mathbf{p} and the mean velocity be \mathbf{v} . Both are defined as averages over a distance somewhat greater than the mean free path of particles in the system.

Next consider some small volume \mathcal{V} with bounding surface $\partial\mathcal{V}$. The rate of change of some locally conserved quantity ψ in this volume is related to its flux through the volume by⁶⁷

$$\frac{d}{dt} \int_{\mathcal{V}} \psi d^3\mathbf{x} = - \int_{\partial\mathcal{V}} F_{\psi,i} dA_i, \quad (1.10)$$

where F_{ψ} is the flux of ψ and dA_i is the outward-oriented area element. If ψ is carried by particles in the system then

$$F_{\psi} = \mathbf{v}\psi.$$

That is, the flux of ψ is given by the rate at which particles move times the density of ψ among them⁶⁸. Inserting this into equation (1.10) and employing the divergence theorem we find⁶⁹

$$\frac{\partial\psi}{\partial t} = -\nabla \cdot (\mathbf{v}\psi).$$

A special instance of this is given when $\psi = \rho$, in which case we find that local conservation of mass requires

$$\frac{\partial\rho}{\partial t} = -\nabla \cdot (\mathbf{v}\rho). \quad (1.11)$$

It is usually the case that conserved quantities carried by particles are proportional to the mass density. This is because they are proportional to the particle density, which is related to the mass density by the mean molecular weight μ . Letting

$$\psi \equiv \rho\bar{\psi},$$

where $\bar{\psi}$ is a conserved quantity per unit mass rather than per unit volume,

⁶⁷ When defined in this manner ψ must be a volumetric density of some quantity which is carried by individual particles.

⁶⁸ It is interesting to note that this statement holds even for thermal motions, it is just not terribly useful in that case because on average particles move in one direction just as much as they move in any other so one immediately has to consider the statistics of the motion rather than the motion itself.

⁶⁹ Note that the derivatives in time become partial derivatives because our volume has become a point with spatial coordinates which may also vary.

we find

$$\frac{\partial(\rho\bar{\psi})}{\partial t} = -\nabla \cdot (\mathbf{v}\rho\bar{\psi}).$$

Expanding the derivatives on both sides produces

$$\rho \frac{\partial \bar{\psi}}{\partial t} + \bar{\psi} \frac{\partial \rho}{\partial t} = -\rho \mathbf{v} \cdot \nabla \bar{\psi} - \nabla \cdot (\mathbf{v}\rho) \bar{\psi}.$$

Inserting equation (1.11) the second term on the left-hand side cancels the second term on the right-hand side and we find

$$\frac{\partial \bar{\psi}}{\partial t} = -\mathbf{v} \cdot \nabla \bar{\psi}. \quad (1.12)$$

This expression of the conservation of specific⁷⁰ quantities is so important that it is often simplified using the so-called material derivative, defined as

⁷⁰ e.g. per unit mass

$$D \equiv \frac{\partial}{\partial t} + \mathbf{v} \cdot \nabla. \quad (1.13)$$

With this, equation (1.12) becomes

$$\frac{D\bar{\psi}}{Dt} = 0. \quad (1.14)$$

An immediate application of equation (1.14) may be made to the velocity, which is just the specific momentum density. In the absence of accelerating forces,

$$\rho \frac{D\mathbf{v}}{Dt} = 0,$$

where by convention we have left in a prefactor of density. This is not quite right, however, because there is also a flux of momentum owing to the viscosity. Incorporating this we find

$$\rho \frac{D\mathbf{v}}{Dt} = \nabla \cdot \mathbf{T}_v, \quad (1.15)$$

where, following equation (1.8),

$$\mathbf{T}_{v,ij} \equiv \rho \left(D_1 \frac{\partial v_k}{\partial x_k} + D_2 \left(\frac{\partial v_i}{\partial x_j} + \frac{\partial v_j}{\partial x_i} \right) \right)$$

is the viscous stress tensor. The form of this tensor is fixed by the arguments in Section 1.4.1. Notably because the tensor is symmetric with respect to interchange of indices it does not couple to rigid rotation, and so can only act on rotational motion when it is differential.

A key point to note is that this seemingly-linear equation hides a non-linearity. Expanding the material derivative we find

$$\rho \frac{\partial \mathbf{v}}{\partial t} + \rho \mathbf{v} \cdot \nabla \mathbf{v} = \nabla \cdot \mathbf{T}_v.$$

The second term depends quadratically on velocity. This non-linearity is the source of turbulence and the many other varied and complicated phenomena which fluids are known to exhibit. Without it the velocity would evolve linearly in time and be unable to exhibit chaos.

In addition to producing diffusion, random thermal motions may also contribute to the ordered motion of the flow. When the pressure is uniform these motions carry no net momentum and so do not couple to the velocity. When this condition is removed the random thermal motions pick up an ordered component associated with the fact that particles preferentially flow along the pressure gradient⁷¹. Hence equation (1.15) becomes⁷²

$$\rho \frac{D\mathbf{v}}{Dt} = -\nabla p + \nabla \cdot \mathbf{T}_v.$$

In the presence of accelerating forces, which we summarize with the term \mathbf{f} , this becomes

$$\rho \frac{D\mathbf{v}}{Dt} = \mathbf{f} - \nabla p + \nabla \cdot \mathbf{T}_v. \quad (1.16)$$

This is the famous Navier-Stokes equation⁷³. While its formal closure remains an open question we shall proceed in the normal tradition of physics by assuming that it fully determines the evolution of velocity given equations specifying \mathbf{f} , p and ρ everywhere.

There are two further complications which we must introduce to equation (1.16). The first is to note that pressure and density do not evolve independently. In particular they are related to each other and to the temperature by the equation of state. When the temperature is specified this is not a problem, but when it is not this requires a further equation for closure. This is supplied by the first law of thermodynamics, which states that the change in the internal energy of a system is equal to sum of the heat it receives and the work done upon it⁷⁴. That is⁷⁵,

$$dU = dQ + dW,$$

where U is the specific internal energy, Q is the specific heat⁷⁶ and W is

⁷¹ Imagine a box containing vacuum on one side of a divider and a gas on the other. Upon removing the dividing barrier the gas flows into the vacuum side because motions which were previously turned around by collisions with the wall simply carry onwards, whereas those oriented away from the vacuum side continue to experience collisions. In this way particles orient towards the vacuum and random motion becomes ordered. The second law of thermodynamics is satisfied because what we gain in knowledge of the momenta of the particles we more than lose in ignorance of their positions in the now-expanded volume.

⁷² The precise form, with no prefactor multiplying ∇p , arises because the pressure is by definition a flux of momentum, so its gradient specifies how much more momentum flows in one direction than in its reverse.

⁷³ Landau & Lifshitz 1959

⁷⁴ This is assuming that there is no significant entropy of mixing and that there are no chemical or nuclear reactions.

⁷⁵ Kardar 2006

⁷⁶ This is related to the entropy via $dQ = (k_B/\mu)Tds$, see e.g. Kardar (2006).

the specific work. The work done upon a fluid is

$$dW = -pdV = p \frac{d\rho}{\rho^2},$$

where $V \equiv \rho^{-1}$ is the specific volume. Using equation (1.3) we find

$$\frac{3}{2}k_B dT = dQ + \frac{p}{\rho^2} d\rho.$$

Because this relation applies to a specific piece of material the derivatives may be promoted to materials derivatives. This yields

$$\frac{3}{2}k_B \frac{DT}{Dt} = \frac{DQ}{Dt} + \frac{p}{\rho^2} \frac{D\rho}{Dt}.$$

The heating term is usually split into a component associated with local heat input and one associated with the heat flux. The former is generally written in terms of the specific heating rate ϵ while the latter is $-\rho^{-1} \nabla \cdot \mathbf{F}$, where \mathbf{F} is the heat flux. Hence we find

$$\rho c_V \frac{DT}{Dt} = \rho \epsilon - \nabla \cdot \mathbf{F} + \frac{p}{\rho} \frac{D\rho}{Dt}, \quad (1.17)$$

where

$$c_V \equiv \frac{3}{2} \left(\frac{k_B}{\mu m_p} \right)$$

is the specific heat capacity at constant volume.

Two special limits of equation (1.17) are commonly used. First suppose that the fluid is nearly incompressible. Then ρ does not vary along the flow and

$$\rho c_V \frac{DT}{Dt} = \rho \epsilon - \nabla \cdot \mathbf{F}.$$

On the other hand suppose that p does not vary along the flow and neglect variations in μ . Then using equation (1.1) we find

$$\rho (c_V + 1) \frac{DT}{Dt} = \rho \epsilon - \nabla \cdot \mathbf{F}.$$

This is more commonly written as

$$\rho c_P \frac{DT}{Dt} = \rho \epsilon - \nabla \cdot \mathbf{F}, \quad (1.18)$$

where

$$c_P \equiv \frac{5}{2} \left(\frac{k_B}{\mu m_p} \right) \quad (1.19)$$

is the specific heat capacity at constant pressure. For our purposes this is the one which is most often of interest because the pressure gradients in stars and gaseous planets are large and so flows typically proceed primarily along isobars. There are exceptions to this but the difference between the two equations is a factor of γ which does not make a significant difference in any of our analyses.

The second complication is magnetism. In the limit of vanishing charge diffusivity⁷⁷ magnetism is completely decoupled from matter and so there is nothing further to be done. In the opposing limit the magnetic field is pinned to the matter. This statement has the pleasingly-simple expression

$$\frac{D}{Dt} \left(\frac{\mathbf{B}}{\rho} \right) = 0, \quad (1.20)$$

so that the magnetic flux through the material is conserved and advected along as it flows. This may be seen intuitively by noting that if a conducting material is stretched perpendicular to \mathbf{B} the field lines must dilute in proportion to preserve the magnetic flux, while if it stretched along the field no dilution is required.

Assuming that there are no magnetic monopoles⁷⁸ the magnetic field also obeys

$$\nabla \cdot \mathbf{B} = 0. \quad (1.21)$$

Furthermore in this limit there is no charge accumulation, such that the electric field is fully determined by the magnetic field. When the flow is non-relativistic⁷⁹ the magnetic field is much greater than the electric. In this case the electromagnetic force on the fluid is given by the divergence of the magnetic stress tensor⁸⁰

$$\Pi_{B,ij} \equiv -\frac{1}{4\pi} (B_i B_j - B^2 \delta_{ij}). \quad (1.22)$$

Hence equation (1.16) becomes

$$\rho \frac{D\mathbf{v}}{Dt} = \mathbf{f} - \nabla p - \nabla \cdot \Pi_B + \nabla \cdot \mathbf{T}_v, \quad (1.23)$$

where \mathbf{f} now excludes electromagnetic forces. This may also be written as

$$\rho \frac{D\mathbf{v}}{Dt} = \mathbf{f} - \nabla \cdot \Pi + \nabla \cdot \mathbf{T}_v, \quad (1.24)$$

where

$$\Pi_{ij} \equiv -\frac{1}{4\pi} (B_i B_j - (4\pi p + B^2) \delta_{ij}) \quad (1.25)$$

⁷⁷ This is the non-ionized non-metallic limit.

⁷⁸ These are expected to exist as per arguments by Dirac (1931) but upper bounds on their density and lower bounds on their mass suggest that they may be neglected for our purposes. See e.g. Cabrera (1982).

⁷⁹ That is, much slower than the speed of light.

⁸⁰ Here we have used the C.G.S.K. unit system in which $\mu_0 = 4\pi$.

is the combined magnetic and thermal stress tensor.

When velocities are small⁸¹ equations (1.16) and (1.24) both support waves. These are oscillatory modes which appear in the linear expansion of the equations which satisfy

$$\mathbf{v}(\mathbf{x}, t) = \mathbf{h} \left(\mathbf{x} - \int \mathbf{c} dt \right)$$

for some function h and some velocity \mathbf{c} . In other words wave solutions *propagate*. This makes them almost uniquely tractable to study amongst solutions for the motions of fluids and forms the basis for the seismic study of stars⁸².

Waves, along with shocks⁸³, together describe the bulk of structured fluid motions. In the next section we shall examine turbulence, which straddles the line between structure and randomness.

1.6 Turbulence

Turbulence is the motion which arises when the non-linearities inherent in equation (1.16) dominate. The full behaviour of turbulence is far from fully-characterised and so here we shall just give an overview of its known characteristics.

To begin we neglect pressure, assume incompressibility⁸⁴ and neglect D_1 relative to D_2 in the viscosity⁸⁵. Equation (1.16) then becomes

$$\frac{D\mathbf{v}}{Dt} = \rho^{-1} \mathbf{f} + 2\nabla \cdot (D_2 \nabla \mathbf{v}).$$

We further take D_2 to be spatially invariant and write it instead with the symbol $\nu/2$, so that

$$\frac{D\mathbf{v}}{Dt} = \rho^{-1} \mathbf{f} + \nu \nabla^2 \mathbf{v}.$$

Expanding the material derivative we find

$$\frac{\partial \mathbf{v}}{\partial t} + \mathbf{v} \cdot \nabla \mathbf{v} = \rho^{-1} \mathbf{f} + \nu \nabla^2 \mathbf{v}. \quad (1.26)$$

Now let

$$g(\mathbf{x}) \equiv \frac{1}{(2\pi)^{3/2}} \int \tilde{g}(\mathbf{k}) e^{i\mathbf{k} \cdot \mathbf{x}} d^3 \mathbf{k}$$

define the inverse Fourier transform of any variable \tilde{g} . The forward trans-

⁸¹ In this case they must be small relative to the scale $\sqrt{f l / \rho}$, where f is a characteristic force-scale and l is the length-scale over which it acts.

⁸² Gough & Thompson 1991

⁸³ We do not discuss shocks here because they are rarely relevant in the interiors of stars and gaseous planets, though as always there are exceptions. These include planetary systems with jet-streams and the explosions stars may suffer towards the ends of their lives.

⁸⁴ Hence $\nabla \cdot \mathbf{v} = 0$.

⁸⁵ None of these are particularly physical assumptions but they serve to illustrate the character of the problem.

formation is

$$\tilde{g}(\mathbf{k}) \equiv \frac{1}{(2\pi)^{3/2}} \int g(\mathbf{x}) e^{-i\mathbf{k} \cdot \mathbf{x}} d^3\mathbf{x}.$$

With these we may take the Fourier transform of equation (1.26) to find⁸⁶

$$\frac{\partial \tilde{\mathbf{v}}(\mathbf{k})}{\partial t} + \frac{1}{(2\pi)^{3/2}} \int i\mathbf{k}' \cdot \tilde{\mathbf{v}}(\mathbf{k} - \mathbf{k}') \tilde{\mathbf{v}}(\mathbf{k}') d^3\mathbf{k}' = \rho^{-1} \tilde{\mathbf{f}}(\mathbf{k}) - \nu k^2 \tilde{\mathbf{v}}(\mathbf{k}).$$

When the velocity is small the second term on the left-hand side may be ignored. In this case there is some forcing \mathbf{f} which causes the fluid to move. This motion evolves independently for each different \mathbf{k} and decays owing to the viscosity.

On the other hand when the velocity is not small the second term in equation (1.26) cannot be ignored. This term may exceed the damping⁸⁷, in which case it serves to move energy between different points in \mathbf{k} -space. This allows energy to build up at longer length-scales and grows the importance of the non-linear term. Eventually the system may reach a statistical steady state where the expected amount of energy at each k is no longer changing. When this occurs there must be a pathway which flows from the scales on which \mathbf{f} injects energy to those which are principally responsible for removing it through the damping. In the limit as $\nu \rightarrow 0$ this must constitute a flow from large to small scales because otherwise there is no damping.

The flow of energy from large scales to small is known as the turbulent or energy cascade⁸⁸. When the system is isotropic and incompressible the analysis becomes particularly straightforward because the flow must be purely unidirectional⁸⁹. This special case results in the so-called Kolmogorov Cascade, with the celebrated scaling relation⁹⁰

$$E(k) \propto k^{-5/3},$$

where $E(k)$ is the specific energy per unit $\ln k$. Under more realistic conditions the cascade is less straightforward⁹¹, but such a flow must nevertheless be present in the limit of vanishing viscosity⁹²

A more general framework has since emerged in the form of the Renormalization Group⁹³. In this framework one defines the correlation functions of interest and then studies how they vary with length-scale. More specifically, in analogy to what one does in statistical mechanics and high energy field theory one might define a partition functional \mathcal{Z} with the

⁸⁶ This can be accomplished using the Convolution Theorem. Equivalently it suffices to note that $\int e^{i\mathbf{k} \cdot \mathbf{x}} d^3\mathbf{x} = (2\pi)^3 \delta^3(\mathbf{k})$, where δ is the Dirac delta distribution.

⁸⁷ This is particularly the case for small k because the non-linear term scales as k whereas the damping scales as k^2 .

⁸⁸ Richardson 1922

⁸⁹ That is, with these constraints all orientations at fixed k hold the same amount of energy and so the flow is just in the scalar k , and the only one-dimensional flow with no accumulation at intermediate scales is a unidirectional one.

⁹⁰ Kolmogorov 1941b

⁹¹ There are even cases where the flow is reversed and proceeds for a while to larger scales before turning around and heading for smaller ones. See e.g. Sukoriansky et al. (2006); Danilov & Gurarie (2002).

⁹² i.e. infinite Reynolds number.

⁹³ Wilson 1971

property that

$$\frac{\delta^n \ln \mathcal{Z}}{\delta \mathbf{w}(\mathbf{r}_1) \dots \delta \mathbf{w}(\mathbf{r}_n)} = \langle \mathbf{v}(\mathbf{r}_1) \dots \mathbf{v}(\mathbf{r}_n) \rangle,$$

where n is the order of the correlation function, \mathbf{w} is an auxiliary field which couples to the velocity and δ denotes a functional derivative. One further defines an upper length scale L_0 characteristic of the large-scale structure of the system as well as a lower length-scale λ characteristic of the viscosity⁹⁴. The idea is then to study the behaviour of \mathcal{Z} as one varies L_0 and λ . Frequently this allows one to define a set of differential equations relating the effective fluid properties such as viscosity to the length scales of interest⁹⁵. The net result is a set of equations of motion, the form and scaling of which capture the correlations of turbulence but produce an effective laminar flow. This is a very powerful method and has found great success in reproducing the statistics of turbulence⁹⁶. Unfortunately unlike in solid state systems, astrophysical fluids rarely enjoy many symmetries or convenient boundary conditions and so the algebraic manipulations involved in this analysis rapidly become extremely unwieldy. This does not appear to be an insurmountable barrier but has thus far discouraged this approach which otherwise has so many appealing properties.

A key insight of the renormalization approach to turbulence is that the Reynolds-averaged turbulent stress

$$\mathbf{T} \equiv \langle v^2 \rangle - \langle v \rangle^2$$

plays the same role as the viscous stress and indeed originates in the viscous stress⁹⁷. That is, the viscous stress \mathbf{T}_v flows under the renormalization group procedure into the turbulent stress \mathbf{T} . This provides a formal justification for the use of equations (I.16) and (I.24) with effective turbulent stresses and has proven to be a powerful technique to calculate the effects of turbulence on large-scale structures within a purely laminar framework⁹⁸.

Finally a discussion of turbulence would not be complete without comment on numerical simulations. These are methods in which space and time are discretised. The equations of motion are then likewise discretised. In this way one arrives at an equation of the form

$$\psi_i(t + \Delta t) - \psi_i(t) = \Delta t \mathcal{H}(\{\psi_j(t)\}),$$

where \mathcal{H} is a non-linear operator⁹⁹. The clear advantage of this method is that it provides solutions to the equations of motion in whatever instances one desires, subject to the convergence properties of the numerical methods

⁹⁴ The system must be laminar on scales of order λ and must not possess features on scales larger than L_0 . These are often called the dissipative or Kolmogorov scale [Kolmogorov \(1941b\)](#) and the outer scale respectively.

⁹⁵ [Yakhot & Orszag 1986](#)

⁹⁶ [Carati 1990](#); [Zhou et al. 1997](#)

⁹⁷ [Yakhot & Orszag 1986](#)

⁹⁸ For an example of this in action see [Kitchatinov \(2013\)](#).

⁹⁹ For simplicity we have written the equation using an explicit time-stepping scheme, though generally one instead relates several consecutive time-steps and solves for $\psi_i(t)$ self-consistently across them. This often provides more rapid numerical convergence to the true solution.

used. This has led to great success in studying convection and dynamos and a host of other turbulent phenomena¹⁰⁰.

Unfortunately there are three significant challenges posed by simulations. First, they introduce an artificial length scale, namely that of the discretisation. In astrophysical systems this is never even close to the scale on which the fluid is laminar¹⁰¹ and so the simulation intrinsically misses turbulent dynamics on all scales in between this and the dissipative scale. Fortunately analyses performed with both the renormalization group and simulations have found that correlations between motions on different scales frequently decay as the separation between the scales increases¹⁰². With the former this may be shown formally in certain cases¹⁰³, while the latter demonstrates it by exhibiting invariant results with respect to the discretisation scale once this scale is sufficiently small. There is still room for error in this regard, but these results suggest that it suffices to resolve a few orders of magnitude around the scales of interest and hence that it is not necessary to resolve down to the dissipation scale¹⁰⁴.

A related point is that for computational reasons one must often pick and choose what physics to employ in a simulation. The simulation does not indicate whether the choice of physics is appropriate, so there is a danger of significant error arising from the choice of physics. For instance simulations of the solar convection zone which omit magnetic fields are known to be significantly in error yet remain commonplace¹⁰⁵.

The second challenge is that any given simulation only provides a single instance of the turbulent flow. Because turbulence is chaotic¹⁰⁶ what is of interest is not the particular flow achieved by one set of initial conditions but rather the statistics of the flow averaged over initial conditions. These simulations are generally very expensive and so one usually averages the quantities of interest over time¹⁰⁷ rather than over multiple runs in the hope that the simulation ergodically explores the space of possible configurations. There is reason to believe that this is a justified approach¹⁰⁸, but the time-scales available remain relatively short and so the uncertainties in the averaging process remain large. Furthermore this limits the study of time-dependent processes, which intrinsically cannot use such an averaging process and must instead employ multiple simulations.

The third challenge posed by simulations is more philosophical in nature. Even when they definitely provide the correct answer this does not come with an explanation. A very productive route around this problem is to develop intuition from a broader study of the output of a simulation and use that to construct explanations, but this makes simulations very different

¹⁰⁰ See e.g. [Brown et al. \(2007\)](#).

¹⁰¹ Stars are often discretized on scales of 30km or larger, which is vastly larger than the 10^2 cm or smaller scales on which viscosity dominates. See e.g. [Brown et al. \(2007\)](#).

¹⁰² This may be understood as saying that the turbulent stress \mathbf{T} depends only weakly on the smallest length-scale in the system.

¹⁰³ [Yakhot & Orszag 1986](#)

¹⁰⁴ The former is within reach on modern supercomputers while the latter requires of order 10^{20} times more computational power. The latter was estimated using the fact that the dissipation scale is typically 10^5 times smaller than the scales currently reached and computation cost scales proportional to resolution to the power of dimension. The dimension is four because the temporal discretisation must scale with the spatial one in accordance with the Courant condition. See [Courant et al. \(1929\)](#) for details.

¹⁰⁵ [Browning et al. 2003](#)

¹⁰⁶ [Deissler 1986](#)

¹⁰⁷ [Brown et al. 2007](#)

¹⁰⁸ The chaotic nature of turbulence means that configurations which are initially similar diverge exponentially in time. Numerical error therefore rapidly compounds and so may provide something akin to an ensemble average over initial conditions. Unfortunately this averaging has not been characterised in any formal way and so this remains an assumption, albeit one which empirically seems to hold. This may be understood intuitively by noting that the energy input rapidly reaches the dissipation scale, which sets an effective upper bound on the autocorrelation time.

in kind from other *a priori* methods.

In short, simulations provide a valuable tool in the study of turbulence but, like many other theoretical tools, their application carries significant caveats. For the kind of analyses in this dissertation they are useful as a means of empirical validation and motivation but not as a substitute for theoretical reasoning. We therefore compare our results with simulations wherever possible and appropriate but avoid leaning too heavily on their results for justification. Furthermore as a precaution we refer to simulations from as many different groups and codes as possible and practical because these likely exhibit different averaging properties and different forms of numerical error. This approach is justified in Chapters 2 and 3, where we find significant scatter amongst different simulations of the same underlying phenomenon.

1.7 Geometry and Symmetry

The final aspect of stellar and planetary structure we must discuss is geometry. A defining property of these bodies is that they are gravitationally bound¹⁰⁹. When the system is rotationally symmetric and in steady state the velocity must vanish. This is because the only spherically symmetric vector field up to rescaling is radial and this cannot satisfy equation (1.11) in steady state. Likewise the magnetic field vanishes because a non-vanishing radial field cannot satisfy equation (1.21). Hence the only possible bound configuration is one in which

$$\nabla p = -\rho \mathbf{g}, \quad (1.27)$$

where \mathbf{g} is the acceleration owing to gravity. It is straightforward to show that¹¹⁰

$$\mathbf{g} = -\frac{GM\mathbf{e}_r}{r^2},$$

where \mathbf{e}_r is the radial unit vector, G is Newton's gravitational constant and M is the mass in a spherical shell of radius r .

The assumption that the system is in steady state was crucial in deriving equation (1.27). This is because this assumption in its most basic form precludes turbulence, in which case there is no spontaneous symmetry breaking¹¹¹. When this assumption is relaxed to one of statistical steady state, such that turbulence is allowed, spontaneous symmetry breaking becomes possible¹¹². This is a consequence of the Mermin-Wagner theorem, which states that spontaneous symmetry breaking is possible in

¹⁰⁹ This is meant in the thermodynamic sense rather than in the purely dynamical sense. That is, it may be the case that the net energy of the system is positive, but so long as the free energy is negative they are statistically and in all practical senses bound. The distinction is relevant in, for instance, red giants, where the net energy is often positive owing to the energy of ionization yet the system remains bound because it is entropically disfavoured for all of the electrons to bind to nuclei and release their energy kinetically. Likewise in common envelope systems there are indications that the unbinding process takes advantage of the energy input from the central stellar cores to overcome this entropy barrier.

¹¹⁰ This was first done by Newton (1687). For a more modern version of the same approach see Schmid (2011).

¹¹¹ The analysis proceeds by supposing a perturbation which breaks the system away from spherical symmetry and showing that the resulting perturbations to the velocity field scale as a positive power-law with the perturbation. This has not been shown in full generality but has been demonstrated for many different classes of perturbations. In particular it was shown for rotation by Zahn (1992) and for magnetism is a result of the conservation of magnetic flux. It has likewise been shown for gravitational perturbations in analyses of tides such as that of Ogilvie (2013) and for thermal perturbations in analyses of asymmetrically heated systems such as that of Jermyn (2015).

¹¹² This was pointed out to me by the late Donald Lynden-Bell.

statistical ensembles with local interactions only when the dimension is at least two ¹¹³. Despite this possibility, spontaneous symmetry breaking has not been observed or seen in any simulations of turbulence, though it has been suggested in several instances ¹¹⁴. A case which comes close is the turbulent dynamo, which amplifies seed magnetic fields to magnitudes independent of that of the seed ¹¹⁵. For slowly rotating systems, however, the resulting field is generally not structured and so likely does not break spherical symmetry on expectation. Given this we proceed on the assumption that there is no spontaneous symmetry breaking, so that turbulent phenomena at most modify equation (1.27) with an additional pressure term ¹¹⁶.

The geometry of equation (1.27) may be used in conjunction with the mechanisms of heat transport to infer the thermal structure of the system. In particular, we show that the temperature decreases or is constant as one moves radially outwards. To see this first note that in a convection zone the entropy is constant or decreasing along \mathbf{e}_r . Hence equation (1.2) gives

$$\frac{\partial \ln p}{\partial r} \leq \gamma \frac{\partial \ln \rho}{\partial r}.$$

Inserting equation (1.1) and neglecting variations of μ we find

$$\frac{\partial \ln p}{\partial r} \leq \gamma \left(\frac{\partial \ln p}{\partial r} - \frac{\partial \ln T}{\partial r} \right).$$

Hence

$$\frac{\partial \ln T}{\partial r} \leq \frac{\gamma - 1}{\gamma} \frac{\partial \ln p}{\partial r}.$$

Because $\gamma > 1$ and $\partial \ln p / \partial r < 0$ it follows that the temperature and pressure gradients are in the same direction, so the body is hotter at the centre.

When the system is radiative rather than convective the direction of the temperature gradient may instead be inferred with the steady state assumption and the assumption that there are no heat sinks. That is, nowhere in the body is heat converted into other forms of energy in significant quantities ¹¹⁷. With this we see that

$$\nabla \cdot \mathbf{F} \geq 0.$$

This, combined with spherical symmetry, implies that \mathbf{F} points radially outward. Because in radiative zones the temperature gradient is antiparallel to the radiative heat flux this means that ∇T is pointed radially

¹¹³ Mermin & Wagner 1966

¹¹⁴ See Chapter 2 for examples.

¹¹⁵ Christensen & Aubert 2006

¹¹⁶ Gough 1977

¹¹⁷ Because the system is assumed to be in steady state, except perhaps in the composition of regions responsible for energy generation, this amounts to precluding net-endothermic reactions. Such reactions do occur in some stars, for instance when temperatures are high enough for electron-positron pair creation, but in all known cases these endothermic reactions lead to violent instabilities and so strongly violate the steady state assumption.

inward, along ∇p .

In stars energy is generated by nuclear fusion. Because fusion rates are generally increasing in both pressure and temperature^{118 119} and because both temperature and pressure increase with depth these processes are largely confined to the centres of stars. Hence to first approximation heat is generated at a point in the centre of a star and must then be transported outwards to the surface in order for the system to remain in equilibrium. When this does not happen heat accumulates in the star and causes the pressure to rise and the star to expand. This causes the central temperature to fall, which reduces the luminosity, and provides the luminosity with more area over which to spread. Hence thermal equilibrium is usually restored by this process. In the event that this does not prove sufficient the system continues to expand, either exploding or asymptotically stabilising. Fascinating though stellar explosions are, we do not consider them here. Likewise the latter case may prove of interest in other contexts but is not in any of the situations considered here. As a result we generally assume that stars gradually adjust in size to carry the available luminosity.

By contrast in planets there is little internal heat generation. Heat may be generated centrally if there is radioactive material present, but this is not expected to contribute much to the overall energy budget of the system. Hence to leading order we approximate planets as having no internal heat source unless some other effect such as tidal dissipation gives us reason to believe otherwise. Over time they cool, and in the process heat flows out of the interior to the surface where it is radiated away¹²⁰. When the system is spherically symmetric this produces a heat flux which is actually quite similar to that found in stars, with the main component being radially outwards and, because the bulk of the thermal mass is in the core where the material is densest, central in origin. In Chapter 5 we discuss the question of when planets may be approximated as spherically symmetric and so we leave that question for now, only noting that it is generally very accurate at even modest depths.

In summary then, in both planets and stars, our expectation is of an approximately radial heat flux which originates from a small region near the centre of the object. Outside of the centre this flux is related to the temperature by

$$\rho c_p \frac{\partial T}{\partial t} = -\nabla \cdot \mathbf{F}.$$

¹¹⁸ The rates depend most strongly on temperature because this enters exponentially by virtue of the Coulomb barrier. The separate dependence on pressure is really a dependence on density, which enters because of the multibody nature of fusion reactions.

¹¹⁹ Burbidge et al. 1957

¹²⁰ In principle this means we must give up the steady state assumption, though in practice the cooling time is so long that the violation is negligible.

In equilibrium this reduces to

$$\nabla \cdot \mathbf{F} = 0.$$

In nearly every case we will assume the systems of interest to be in thermal equilibrium, with the exception of the scenario in Chapter 5, where the violation of this assumption is of central importance.

While both the assumption of spherical symmetry and that of a statistical steady state are generally violated they provide a useful starting point from which to study more general scenarios. Moreover certain broad statements remain true despite this. In particular stars and planets are usually hottest in their centres. Furthermore the heat flow and pressure and temperature gradients are usually at least approximately radial. Because this is a special and highly-symmetric state we are principally interested in its response to symmetry-breaking perturbations. Hence Chapters 2, 5 and 6 study deviations from a steady state, both in the strict sense and in the statistical. Likewise Chapters 2, 3, 4 and 5 examine magnetic, tidal and rotational effects, which introduce a preferred direction and so break spherical symmetry.

2 *Turbulence Closure*

Big whirls have little whirls,
That feed on their velocity;
And little whirls have lesser whirls,
And so on to viscosity.

Lewis Fry Richardson

Abstract

We present an approach to turbulence closure based on mixing length theory with three-dimensional fluctuations against a two-dimensional background. This model is intended to be rapidly computable for implementation in stellar evolution software and to capture a wide range of relevant phenomena with just a single free parameter, namely the mixing length. We incorporate magnetic, rotational, baroclinic and buoyancy effects exactly within the formalism of linear growth theories with non-linear decay. We treat differential rotation effects perturbatively in the corotating frame using a novel controlled approximation which matches the time evolution of the reference frame to arbitrary order in the shear. We then implement this model in an efficient open source code and discuss the resulting turbulent stresses and transport coefficients. We demonstrate that this model exhibits convective, baroclinic and shear instabilities as well as the magnetorotational instability (MRI). It also exhibits non-linear saturation behaviour, and we use this to extract the asymptotic scaling of various transport coefficients in physically interesting limits.

2.1 Introduction

An understanding of turbulent transport and stresses remains one of the major outstanding problems in the astrophysics of fluids. While many pieces of this puzzle are understood in broad strokes, the nature of this problem is such that the details are almost as important as the big picture. The magnetorotational instability (MRI), for instance, is understood conceptually but making predictions which match observed accretion discs is a persistent problem ¹. Similarly the solar differential rotation is understood to arise from turbulent stresses but precisely how this works and in balance with what other forces remains uncertain ².

Significant progress has indeed been made with three-dimensional turbulence simulations ³ but these are generally relevant only on short timescales and in small volumes. Performing so-called global simulations over large times and distances requires a turbulence closure model to substitute for resolution at small scales ⁴.

At the other extreme models of stellar evolution generally assume extremely simple analytical transport coefficients to overcome the tremendous gap between turbulent timescales of minutes and nuclear timescales of millions of years ⁵. A variety of such approaches have been developed. For instance the mixing length theory of Böhm-Vitense (1958) provided a closure of convection. This was then put on firmer theoretical ground by Gough (1977, 2012) and extended to include additional phenomena ⁶. Kichatinov (1986) introduced an entirely different closure formalism, arriving at an expression for the so-called Λ -effect ⁷, and later incorporating it under the $\alpha - \Lambda$ formalism with Rudiger ⁸. What these formalisms have in common is a minimal set of free parameters: the mixing length formalism has just the mixing length, and the formalism of Kichatinov & Rudiger (1993) has just the anisotropy parameter.

Another set of models has arisen which aims to reproduce higher-order moments of the turbulent fields. This increases the number of free parameters and a number of approaches have been developed to deal with this. For instance Garaud et al. (2017) and Garaud et al. (2010) fit their free parameters against small-scale simulations while Canuto (1997) fits his against experimental results. In addition there are models, such as that of Canuto (1994), which fix at least some free parameters by introducing new assumptions, in that case regarding the various relevant time-scales. Regardless of the details of how they close the equations of turbulent moments, models of this sort generally take the form of physically motivated

¹ Murphy & Pessah 2015

² Schou et al. 1998

³ Lee 2013; McKinney et al. 2014; Salvesen et al. 2016

⁴ Launder & Spalding 1974; Canuto 1994

⁵ Maeder 1995

⁶ Smolec et al. 2011; Lesaffre et al. 2013

⁷ Kichatinov 1987

⁸ Kichatinov & Rudiger 1993

analytic expressions which provide ready access to scaling laws. Their free parameters then serve to better their agreement with data, at the cost of being less straightforwardly interpreted and extended.

The availability of growing computational resources in recent years has provided a new niche in this landscape in the form of computational closure models. These are models which do not seek analytic solutions but which are nonetheless distinct from attempts to simulate turbulence in all its detail. Some may introduce new dynamical fields, as in the $k - \epsilon$ model ⁹, while others invoke effective theories of small-scale motion ¹⁰. The latter kind are theories which accept the cost of having to numerically accommodate complex behaviour in exchange for more precision over a wider variety of phenomena. Combined with perturbation theory this approach represents a tunable middle-ground between expensive simulations and simple analytic models, allowing the computational cost to be traded off against fidelity to suit the problem at hand. The model we present here is in this spirit.

⁹ Launder & Spalding 1974

¹⁰ Canuto & Hartke 1986

We construct a mixing-length theory which incorporates a spectrum of three-dimensional fluctuations against a two-dimensional axisymmetric background. This is done by treating each mode as growing with its linear growth rate before saturating at an amplitude set by the turbulent cascade ¹¹. The motion in each mode is taken to be uncorrelated with that in each other mode. We treat the geometry of the flow in full generality, allowing for baroclinic effects as well as magnetism and rotational shears. To incorporate differential rotation we use a time-dependent sheared coordinate system ¹². In this frame there is a continual flow of modes across Fourier space, lending a time dependence to growth rates. Corrections to saturation amplitudes owing to this flow are incorporated perturbatively with the time derivatives of the growth rate.

¹¹ Lesaffre et al. 2013

¹² Balbus & Scharf 2012

In Section 2.2 we describe our closure framework in more detail, paying particular attention to the choice of mixing length. We then develop a perturbative approach for correcting the saturation amplitude in Section 2.3. In Section 2.4 we introduce the sheared coordinate system and the linearised equations of motion. Finally in Section 2.7 we show results from our theory, including calculations for the solar convection zone and accretion discs.

The software implementing our model is open source and available under a GPLv3 license. Details of the implementation are given in Section 2.6. Tabulated transport coefficients produced by the code are also available under the same license and both may be found at github.com/

adamjermyn/Mixer.

2.2 Closure Formalism

Turbulent phenomena generically exhibit a cascade of energy between large and small scales ¹³. With some notable exceptions ¹⁴ this cascade begins at a large scale L_0 set by the overall structure of the fluid flow and ends at an extremely small scale λ related to the microscopic viscosity¹⁵. Between these scales, yet far from each of them, lies the so-called inertial range where the fluid flow is scale-free ¹⁶. In this range all correlations of the turbulent motion obey simple power laws.

This statement was originally proved by Kolmogorov (1941b) for isotropic turbulence. It was later found to be a broader consequence of the renormalizability of the Navier–Stokes equation ¹⁷ and consequently holds quite generally. This means that there is a single relevant scale L_0 for a given turbulent flow which fully characterises the turbulence as seen by measurements performed over length scales $L \gg L_0$. This is the modern interpretation and justification of the original mixing length hypothesis, which asserts that turbulent fluctuations on scales $L \ll L_0$ are not dynamically coupled to the large-scale ($L \gg L_0$) flow properties ¹⁸.

The scale-free nature of turbulence in the inertial range means that modes of significantly different wavevectors are uncorrelated. A natural extension of this is to assume that all modes of distinct wavevectors are at least approximately uncorrelated. That is, we assume that

$$\langle \tilde{v}_{\mathbf{k}} \otimes \tilde{v}_{\mathbf{k}'}^* \rangle = (2\pi)^3 \delta^3(\mathbf{k} - \mathbf{k}') \mathbf{V}_{\mathbf{k}}, \quad (2.1)$$

where v is the velocity, \otimes denotes the outer product, $\langle \dots \rangle$ denotes the time-averaged expectation, $\tilde{v}_{\mathbf{k}}$ is the amplitude of the Fourier mode with wavevector \mathbf{k} and $\mathbf{V}_{\mathbf{k}}$ is the tensor specifying how different components of the same mode are correlated with one another. It is crucial to notice that the quantity $\mathbf{V}_{\mathbf{k}}$ is also the Reynolds stress of mode \mathbf{k} . This, and several other closely related quantities, are ultimately what we seek. These two-point correlation functions suffice to characterise not only the stresses but also all higher-order correlations through Wick’s theorem and perturbation theory ¹⁹ ²⁰.

To determine $\mathbf{V}_{\mathbf{k}}$ we begin by writing the linearised equations of motion as

$$\partial_t \mathbf{v}(\mathbf{r}) = \mathcal{L} [\mathbf{v}(\mathbf{r}), \partial_i \mathbf{v}, \partial_i \partial_j \mathbf{v}, \dots, \mathbf{r}, t],$$

¹³ Zhou et al. 1997; Lohse & Xia 2010

¹⁴ Galperin et al. 2007

¹⁵ This is what we have previously called the dissipative scale.

¹⁶ Kolmogorov 1941b

¹⁷ Yakhot & Orszag 1986; Carati 1990

¹⁸ Böhm-Vitense 1958

¹⁹ Wick 1950; Isserlis 1918

²⁰ This is, of course, subject to the existence of a Gaussian fixed point. Should this not exist the two-point functions suffice to characterise the stress but not the higher-order moments.

where \mathcal{L} is a linear operator of its first argument and \mathbf{v} is the fluctuating part of the velocity field. In principle we can work with this operator, though the derivatives of the velocity field make it highly inconvenient. Fortunately at short length scales the operator \mathcal{L} may be treated as translation-invariant and so we may compute a Fourier transform in \mathbf{r} without coupling different modes. This gives

$$\frac{d\tilde{\mathbf{v}}_{\mathbf{k}}}{dt} = \tilde{\mathcal{L}}[\tilde{\mathbf{v}}_{\mathbf{k}}, \mathbf{k}, t].$$

The modes are decoupled in this regime so $\tilde{\mathcal{L}}$ can be represented by a matrix \mathbf{L} , and we write

$$\frac{d\tilde{\mathbf{v}}_{\mathbf{k}}}{dt} = \mathbf{L}(\mathbf{k}, t)\mathbf{v}_{\mathbf{k}}. \quad (2.2)$$

When \mathbf{L} is independent of t equation (2.2) is straightforward to solve and gives us

$$\frac{d\tilde{\mathbf{v}}_{\mathbf{k}}}{dt} = \sum_i v_{0,i} \hat{\mathbf{v}}_{\mathbf{k},i} e^{\lambda_i t}, \quad (2.3)$$

where $v_{0,i}$ are the initial mode amplitudes and $\hat{\mathbf{v}}_{\mathbf{k},i}$ and λ_i are respectively the normalised right eigenvectors and eigenvalues of \mathbf{L} . The vectors $\hat{\mathbf{v}}_{\mathbf{k},i}$ then specify the modes of the system at a given wavevector.

If the eigenvalues are not precisely degenerate then modes which begin in phase rapidly become uncorrelated and we may extend equation (2.1) to the modes at each wavevector and write

$$\langle \tilde{\mathbf{v}}_{\mathbf{k},i} \otimes \tilde{\mathbf{v}}_{\mathbf{k}',j}^* \rangle = (2\pi)^3 \delta^3(\mathbf{k} - \mathbf{k}') \delta_{ij} \mathbf{V}_{\mathbf{k},i}. \quad (2.4)$$

This result holds even when modes are degenerate. Because evolution under \mathbf{L} is deterministic, the expectation $\langle \dots \rangle$ represents a sum over initial conditions. In this sum all relative phases between the modes are explored, so even degenerate modes become uncorrelated.

Inserting equation (2.3) into equation (2.4) and summing over j and integrating over \mathbf{k}' gives us

$$\mathbf{V}_{\mathbf{k},i} = \hat{\mathbf{v}}_{\mathbf{k},i} \otimes \hat{\mathbf{v}}_{\mathbf{k},i} \langle |v_{0,i}|^2 \exp[2t\Re[\lambda_i]] \rangle. \quad (2.5)$$

Generally some λ_i have positive real parts and so in a long-term expectation this exponential diverges. Indeed it turns out that these growing modes are precisely those which matter! What happens of course is just that these modes eventually reach amplitudes where the linear approximation fails. By assumption the system is stable over long times relative to the

turbulent scale so this must result in these modes saturating. This has been variously described as mode crashing or the action of parasitic modes ²¹ but, regardless of the mechanism, it simply means that these modes exit the linear regime and find their growth impeded.

To complete the closure we must find the saturation amplitude. Relying again on the scale-free nature of turbulence we note that this must be a power law in k . That is,

$$\langle \tilde{v}_{k,i}^2 \rangle = \text{Tr} [V_{k,i}] = \frac{A}{M} \left(\frac{k_0}{k} \right)^{2n}, \quad (2.6)$$

where A depends on the large scale properties of the flow but is independent of k , M is the number of modes per wavevector and n is the index of the turbulence.

The general question of which turbulent index to use and under what circumstances remains open though many specific cases are well understood. In the case of isotropic incompressible turbulence the Kolmogorov index is well-known to be $n = 11/6$ ²². There is more debate over the index to use for convection, with answers ranging from $n = 5/2$ ²³ to $n = 21/10$ ²⁴ and $n = 2.4 \pm 0.2$ ²⁵. There has also been work attempting to determine the spectrum in a context-sensitive manner through energy balance arguments ²⁶. In the magnetised case sources differ even more, with some suggesting that this range still applies ²⁷, some arguing for a Kolmogorov-like spectrum ²⁸ and others giving a range of indices depending on geometry and the direction of the wavevector ²⁹.

From numerical experiments with our closure model we have found that the magnetic stress scales sufficiently rapidly with k that it is divergent for $n = 11/6$ and not for ³⁰ $n = 8/3$. This favours the scenario of Goldreich & Sridhar (1995), who argue that in the strongly-magnetised limit the index ought to be $n = 8/3$.

In order to consistently treat both the non-magnetic and the strongly-magnetised limits, we choose a simple prescription in which $n = 11/6$ when one of $|N|$, or $|R\nabla\Omega|$ exceeds kv_A , where v_A is the Alfvén speed, and use $n = 8/3$ otherwise. This means that there is a critical wavenumber

$$k_c \equiv \frac{\max(|N|, |R\nabla\Omega|)}{v_A}$$

at which the spectrum changes. In the non-magnetic case the evolution matrix is independent of the magnitude of the wavevector and so altering the index just alters the correlation coefficients by a multiplicative factor. In the magnetic case the potential for error is larger because the magnitude

²¹ Pessah & Goodman 2009; Lesaffre et al. 2009

²² Kolmogorov 1941a

²³ Benzi et al. 1994

²⁴ Procaccia & Zeitak 1989

²⁵ Ashkenazi & Steinberg 1999

²⁶ Yakhot & Orszag 1986

²⁷ Dobrowolny et al. 1980

²⁸ Goldreich & Sridhar 1995

²⁹ Sridhar & Goldreich 1994

³⁰ As we shall discuss later, the turbulent magnetic field scales with k so its contribution to the stress scales with k^2 . In order for this to converge when integrated against k^{-2n} over all k above some cutoff it must be that $5 - 2n < 0$. Hence $n = 11/6$ is not suitable but $n = 8/3$ is.

of the wavevector is relevant but there appears to be no consensus on the best prescription and so we make do with what is available.

The wavenumber k_0 is just that of the characteristic length-scale, and is given by

$$k_0 = \frac{2\pi}{L_0}. \quad (2.7)$$

Replacing the divergent expression in equation (2.5) with this amplitude we find

$$\mathbf{v}_{\mathbf{k},i} = \frac{A}{M} \left(\frac{k_0}{k} \right)^{2n} \hat{v}_{\mathbf{k},i} \otimes \hat{v}_{\mathbf{k},i}.$$

It only remains to determine A . To do this we note that there is one characteristic length scale L_0 and one characteristic timescale, the growth rate $\Re[\lambda_i]$ of the mode. Because A has dimensions of velocity squared we find

$$\mathbf{v}_{\mathbf{k},i} = \frac{c}{M} L_0^2 \Re[\lambda_i]^2 \left(\frac{k_0}{k} \right)^{2n} \hat{v}_{\mathbf{k},i} \otimes \hat{v}_{\mathbf{k},i}, \quad (2.8)$$

where c is a dimensionless constant of order unity. This constant, known as the mixing length parameter, varies from theory to theory, so for clarity we set $c = 1$ in this work but this degree of freedom is important to note when comparing between models. In effect what we have done is incorporate the non-linearity of turbulence by means of the spectrum while using linear growth rates to set the characteristic scale. In practice the spectrum only acts to provide a convergent measure over modes, and it is the growth rate and the modes themselves that yield the anisotropies and other phenomena of interest. This is closely related to the approaches of [Lesaffre et al. \(2013\)](#) and [Canuto & Hartke \(1986\)](#).

This prescription is easily extended in cases where there are additional dynamical fields, such as the turbulent displacement or a fluctuating magnetic field. The additional fields are simply incorporated into the vector describing the state and M is increased accordingly. We can continue to use equation (2.6) to fix the amplitude of the entire mode against that of the velocity as long as we know the turbulent index n . Note, however, that if the addition fields have their own characteristic length-scales those must be considered in choosing L_0 , as the Kolmogorov hypothesis is only valid in the inertial range.

Up to this point this prescription is mathematically identical to that of [Lesaffre et al. \(2013\)](#), with the exception that we define the mixing wave vector as in equation (2.7) while they use π/L_0 instead. In the next section

we introduce perturbative corrections to this model to capture a wider variety of phenomena.

2.3 *Perturbative Corrections*

Now consider the case where the matrix \mathbf{L} is time-dependent. Most of our reasoning about the behaviour of modes from the previous section still holds but, because the eigenvectors are time-dependent, we no longer have a well-defined notion of a mode as a long-running solution to the equations of motion. When the time dependence is periodic Floquet theory applies, but in the cases of interest the time dependence is aperiodic. To recover modes when the time evolution matrix itself evolves and does so aperiodically we begin by expanding as

$$\mathbf{L}(t) = \mathbf{L}(0) + t \frac{d\mathbf{L}}{dt} + \frac{1}{2} t^2 \frac{d^2\mathbf{L}}{dt^2} + \dots \quad (2.9)$$

This series can be truncated to produce an approximation of \mathbf{L} which is accurate in a certain window around $t = 0$.

We may likewise write the velocity at a given wavevector as

$$\tilde{\mathbf{v}}_{\mathbf{k}}(t) = \tilde{\mathbf{v}}_{\mathbf{k}}(0) + t \left. \frac{d\tilde{\mathbf{v}}_{\mathbf{k}}}{dt} \right|_0 + \frac{1}{2} t^2 \left. \frac{d^2\tilde{\mathbf{v}}_{\mathbf{k}}(t)}{dt^2} \right|_0 + \dots$$

This suggests defining a new vector

$$\Phi_{\mathbf{k}}(t) \equiv \left\{ \tilde{\mathbf{v}}_{\mathbf{k}}, \frac{d\tilde{\mathbf{v}}_{\mathbf{k}}}{dt}, \frac{d^2\tilde{\mathbf{v}}_{\mathbf{k}}}{dt^2}, \dots \right\},$$

which, in principle, encodes the full time evolution of the velocity field.

This vector evolves according to

$$\frac{d\Phi_{\mathbf{k}}}{dt} = \mathbf{A}\Phi_{\mathbf{k}} \quad (2.10)$$

where \mathbf{A} is formed of blocks given by

$$\mathbf{A}_{ij} = \binom{i}{j} \frac{d^{i-j}}{dt^{i-j}} \mathbf{L}.$$

By definition though we also have

$$\frac{d\Phi_{\mathbf{k},i}}{dt} = \Phi_{\mathbf{k},i+1}, \quad (2.11)$$

where $\Phi_{\mathbf{k},0} = \tilde{\mathbf{v}}_{\mathbf{k}}$, $\Phi_{\mathbf{k},1} = d\tilde{\mathbf{v}}_{\mathbf{k}}/dt$ and so on. Thus we are searching for a simultaneous solution of equations (2.10) and (2.11).

In order to close the system we must truncate it at some finite order

N . Doing so makes the assumption that the behaviour of the system at all greater N is known. Inspired by the solution for time-independent \mathbf{L} , we try an exponential behaviour. This truncates equation (2.11) such that it applies only to $i < N - 1$ and means that we are searching for vectors with

$$(\mathbf{A}\Phi_{\mathbf{k}})_{N-1} = \lambda\Phi_{\mathbf{k},N-1}$$

and

$$\Phi_{\mathbf{k},i+1} = (\mathbf{A}\Phi_{\mathbf{k}})_i, i < N - 1.$$

These equations are most straightforwardly written as a general eigensystem and this has the advantage of restricting the dimension of the linear space to just those states obeying the constraint of equation (2.11). This is possible because both \mathbf{A} and the constraint are lower-triangular in the same basis, and so each row may be substituted into the next, leading to an eigenproblem of the form

$$\mathbf{Q}\Phi_{\mathbf{k},0} = \lambda\mathbf{W}\Phi_{\mathbf{k},0}, \quad (2.12)$$

where \mathbf{Q} and \mathbf{W} are matrices acting only on the 0-block. For example, in the case where $N = 2$, our equations are

$$\Phi_{\mathbf{k},1} = \mathbf{M}\Phi_{\mathbf{k},0}$$

and

$$\mathbf{M}\Phi_{\mathbf{k},1} + \dot{\mathbf{M}}\Phi_{\mathbf{k},0} = \lambda\Phi_{\mathbf{k},1},$$

which may be put in the form of equation (2.12) with

$$\mathbf{Q} = \mathbf{M}^2 + \dot{\mathbf{M}}$$

and

$$\mathbf{W} = \mathbf{M}.$$

The eigenvectors of this system are solutions of the original equation (2.2) because if $\psi_{\mathbf{k}}^i$ is such an eigenvector then

$$\tilde{\mathbf{v}}_{\mathbf{k},i}(t) \equiv \sum_{j=0}^N \frac{t^j}{j!} \psi_{\mathbf{k}}^i$$

solves

$$\frac{d\tilde{v}_{k,i}}{dt} = \mathbf{L}(t)\tilde{v}_{k,i}(t)$$

over the time window for which \mathbf{L} is well-approximated at N -th order. As a result we say that $\phi_i(t)$ are the instantaneous modes of the system at N -th order and use them and in equation (2.8). In place of the eigenvalue we use the instantaneous growth rate of the velocity, which is given by

$$g \equiv \frac{1}{2} \frac{dv^2}{dt} = \frac{\Re(\Phi_{k,0} \cdot \Phi_{k,1})}{|\Phi_{k,0}|^2}.$$

This approximation is controlled in the sense that so long as $\mathbf{L}(t)$ converges as N grows, so does the inferred velocity history. In this work we present results with $N = 2$ so that \mathbf{A} involves both \mathbf{L} and $\dot{\mathbf{L}}$. We leave the exploration of larger N to later work.

2.4 Equations of Motion

We now specialise to the case of an ideal gas obeying the ideal MHD equations. This section largely follows the derivation of Balbus & Schaan (2012) so we present only the pieces necessary to understand later parts of this work as well as the few places where our derivation diverges from theirs.

We take the background to be axisymmetric, the fluctuations to be adiabatic and we work in cylindrical coordinates. We neglect both the microscopic viscosity and the microscopic thermal diffusivity because these are both negligible in most circumstances in stellar physics³¹. For simplicity we also ignore the meridional circulation³². Because our closure model treats turbulent properties as local, we compute all background quantities at a reference point \mathbf{r}_0 . Relative to this point we define the Lagrangian separation $\delta\mathbf{r}$ and velocity $\delta\mathbf{v}$ equivalent to ξ and $D\xi/Dt$ of Balbus & Schaan (2012). In addition we take the Boussinesq approximation that density variations are ignored except in terms involving gravitational acceleration. With the above definitions the continuity equation may be written as³³

$$\nabla \cdot \delta\mathbf{r} = 0. \quad (2.13)$$

In a fixed coordinate system differential rotation is difficult to analyze so we make two reference frame changes. First we switch from an inertial frame to one rotating at

$$\Omega_0 \equiv \Omega(\mathbf{r}_0).$$

³¹ It would not be difficult, however, to incorporate them into this framework at a later date.

³² In convecting systems this is a good approximation because, as we shall discuss in the next two chapters, this flow is usually small relative to the convection speed and in any case obeys the same symmetries as the convection. In stably stratified systems this approximation is worse and we intend to explore the consequences of this in the future.

³³ In Fourier space this is

$$\mathbf{q} \cdot \delta\tilde{\mathbf{r}} = 0.$$

Taking the time derivative of both sides we see that

$$\partial_t(\mathbf{q} \cdot \delta\tilde{\mathbf{r}}) = \mathbf{q} \cdot \delta\tilde{\mathbf{v}} + \delta\tilde{\mathbf{r}} \cdot \partial_t\mathbf{q} = 0.$$

As a result

$$\delta\tilde{\mathbf{v}} \cdot \mathbf{q} = -\delta\tilde{\mathbf{r}} \cdot \partial_t\mathbf{q} \neq 0.$$

This is quite peculiar, but is just an artefact of our coordinate system. Because the wavevectors are time-dependent, maintaining the volume of a fluid parcel requires that the displacement be orthogonal to the wavevector, which actually means that the velocity is generally not orthogonal to the wavevector.

Secondly we make a formal change of coordinates

$$\phi \rightarrow \phi - t\delta\mathbf{r} \cdot \nabla\Omega$$

without altering the corresponding unit vectors. Under this last change the gradient transforms as

$$\nabla \rightarrow \nabla - t(\nabla\Omega)\partial_\phi.$$

Because the operator \mathcal{L} is most easily expressed in Fourier space we define the transformed wavevector as

$$\mathbf{q} \equiv \mathbf{k} - tk_\phi R\nabla\Omega.$$

With this the transformed equations (1.20) and (1.24) may be linearised and written as

$$\delta\tilde{\mathbf{B}} = \mathbf{B} \cdot \mathbf{q}\delta\tilde{\mathbf{r}} \quad (2.14)$$

and

$$\partial_t\delta\tilde{\mathbf{v}} + 2\Omega \times \delta\tilde{\mathbf{v}} + \hat{R}R\delta\tilde{\mathbf{r}} \cdot \nabla\Omega^2 - \frac{1}{\gamma\rho}(\delta\tilde{\mathbf{r}} \cdot \nabla_s)\nabla \cdot \Pi + \frac{i}{\rho}\mathbf{q} \cdot \delta\tilde{\Pi} = 0, \quad (2.15)$$

where s is the specific entropy given by equation (1.2) and Π is the stress tensor given by equation (1.25) as

$$\Pi \equiv p\mathbf{I} - \frac{1}{\mu_0} \left(\mathbf{B} \otimes \mathbf{B} - \frac{1}{2}B^2\mathbf{I} \right).$$

All quantities prefixed with δ are fluctuating, a tilde denotes the Fourier transformed function, and all other quantities are background fields evaluated at \mathbf{r}_0 . It is straightforward to see that this is the same equation as that derived by Balbus & Scharf (2012) once the appropriate relations for the pressure and magnetic force are substituted. Note that the second term describes the Coriolis effect ³⁴ and the third is a restoring force related to the centrifugal acceleration. Both arise from our choice of reference frame and not from the underlying dynamics, though their effects are quite real³⁵.

The fluctuation in the pressure tensor may be written as

$$\delta\Pi = \delta p\mathbf{I} - \frac{1}{\mu_0} (\mathbf{B} \otimes \delta\mathbf{B} + \delta\mathbf{B} \otimes \mathbf{B} - \mathbf{I}\mathbf{B} \cdot \delta\mathbf{B}),$$

so in Fourier space

$$\delta\tilde{\Pi} = \delta\tilde{p}\mathbf{I} - \frac{1}{\mu_0} (\mathbf{B} \otimes \delta\tilde{\mathbf{B}} + \delta\tilde{\mathbf{B}} \otimes \mathbf{B} - \mathbf{I}\mathbf{B} \cdot \delta\tilde{\mathbf{B}}).$$

³⁴ Coriolis 1835

³⁵ Had we chosen an inertial reference frame these terms would disappear but other terms related to the background azimuthal motion would arise and play a similar role.

Combining this with equation (2.14) and the Boussinesq approximation we find

$$\mathbf{q} \cdot \delta \tilde{\Pi} = \mathbf{q} \delta p - \frac{i}{\mu_0} (\mathbf{B} \cdot \mathbf{q})^2 \delta \tilde{\mathbf{r}}.$$

Note that as did Balbus & Schaan (2012) we take $\mathbf{B} \cdot \mathbf{q}$ to be constant in time as implied by the Boussinesq and ideal-MHD conditions. We now depart from prior work and use this equation along with equation (2.15) taking the component perpendicular to \mathbf{q} to eliminate δp and find

$$0 = \left(\partial_t \delta \tilde{\mathbf{v}} + 2\Omega \times \delta \tilde{\mathbf{v}} + \hat{R} R \delta \tilde{\mathbf{r}} \cdot \nabla \Omega^2 - \frac{1}{\gamma \rho} (\delta \tilde{\mathbf{r}} \cdot \nabla_s) \nabla \cdot \Pi + \frac{1}{\mu_0 \rho} (\mathbf{B} \cdot \mathbf{q})^2 \delta \tilde{\mathbf{r}} \right)_{\perp \mathbf{q}}, \quad (2.16)$$

where the notation $(\dots)_{\perp \mathbf{q}}$ denotes the component perpendicular to \mathbf{q} .

Equation (2.16) is the linear equation which we aim to solve. To do this we construct the matrix version \mathbf{L} of this equation. In the process we must choose a coordinate system. Both because of the constraint (2.13) and because equation (2.16) is written in the plane perpendicular to \mathbf{q} we choose the unit vectors

$$\hat{\mathbf{a}} \equiv \frac{\hat{\mathbf{q}} \times \hat{\mathbf{w}}}{\sqrt{1 - (\hat{\mathbf{q}} \cdot \hat{\mathbf{w}})^2}}$$

and

$$\hat{\mathbf{b}} \equiv \hat{\mathbf{q}} \times \hat{\mathbf{a}},$$

where $\hat{\mathbf{w}}$ is any unit vector with $\hat{\mathbf{w}} \cdot \hat{\mathbf{q}} \neq 1$. This choice of basis ensures that our vectors are perpendicular to the wavevector.

A choice of particular convenience for $\hat{\mathbf{w}}$ is³⁶

$$\hat{\mathbf{w}} = \frac{\nabla \Omega}{|\nabla \Omega|}.$$

With this choice $\hat{\mathbf{a}}$ is time-independent, because the component of \mathbf{q} perpendicular to \mathbf{w} is time-independent, and so we may write

$$\delta \tilde{\mathbf{r}} = \alpha \hat{\mathbf{a}} + \beta \hat{\mathbf{b}}$$

and

$$\delta \tilde{\mathbf{v}} = \dot{\alpha} \hat{\mathbf{a}} + \dot{\beta} \hat{\mathbf{b}} + \beta \partial_t \hat{\mathbf{b}}.$$

Note that there is a removeable singularity when $\hat{\mathbf{w}} \parallel \hat{\mathbf{q}}$. The matrix \mathbf{L} is then given by computing the relation between $\partial_t \{\alpha, \beta, \dot{\alpha}, \dot{\beta}\}$ and $\{\alpha, \beta, \dot{\alpha}, \dot{\beta}\}$. The result is quite unwieldy so we do not present it here but

³⁶ In the limit as $\nabla \Omega$ vanishes this vector becomes meaningless, but in that case there is no differential rotation and our motivation for this choice similarly disappears. In that limit we choose $\hat{\mathbf{w}}$ arbitrarily.

note that it is fully documented in the software in which we implement these equations.

2.5 Stresses and Transport

The equations of motion contain the position and the velocity, so our expanded vector space is

$$\Phi = \{\delta \mathbf{r}, \delta \mathbf{v}, \partial_t \delta \mathbf{v}, \dots\}.$$

Combining the linearised equations of motion with our closure scheme we can compute the correlation function

$$\langle \Phi \otimes \Phi \rangle = \int \frac{d^3 \mathbf{k}}{(2\pi)^3} \sum_i \langle \Phi_{\mathbf{k}}^i \otimes \Phi_{\mathbf{k}}^{i*} \rangle,$$

where the index i ranges over eigenvectors. This function contains all of the usual stresses and transport functions. For instance, the Reynolds stress is

$$R \equiv \langle \delta \mathbf{v} \otimes \delta \mathbf{v} \rangle = \langle \Phi_1 \otimes \Phi_1 \rangle.$$

Likewise up to a dimensionless constant of order unity the turbulent diffusivity is

$$d \equiv \langle \delta \mathbf{v} \otimes \delta \mathbf{r} \rangle = \langle \Phi_1 \otimes \Phi_0 \rangle.$$

and the turbulent viscosity is

$$Q \equiv \langle \delta \mathbf{v} \otimes \delta \mathbf{r} \rangle + \langle \delta \mathbf{r} \otimes \delta \mathbf{v} \rangle = \langle \Phi_1 \otimes \Phi_0 \rangle + \langle \Phi_0 \otimes \Phi_1 \rangle.$$

Similar expressions hold for the dynamo effect, the transport of magnetic fields, and material diffusion.

2.6 Software Details

The software used for this work is Mixer version 1, which we have released under a GPLv3 license at github.com/adamjermyn/Mixer. This solves equation (2.12) with the time evolution given by equation (2.16) and, by integrating over wave-vectors, produces the correlation functions given in Section 2.5. All data produced for this work are available at the same location as HDF5 tables with attributes documenting the physical inputs. Post-processing and visualisation of the data was done with the Python modules Numpy ³⁷ and Matplotlib ³⁸ and the relevant scripts for this are included with Mixer.

The core of Mixer is written in C++, for performance reasons, and

³⁷ van der Walt et al. 2011

³⁸ Hunter 2007

the code is supplied with a Makefile which supports compilation on both Linux and MacOS. Mixer makes use of the Eigen library ³⁹ for linear algebra. Mixer also uses the Cubature library for numerical integration. This library is an implementation of the algorithms by [Genz & Malik \(1980\)](#) and [Berntsen et al. \(1991\)](#). These integration routines are supplemented by a Python integration routine tailored for integrands with small support regions. The details will be explored in later work. In addition, many routines provide a Python interface. Currently Mixer only supports single-threaded operation, though it may be used inside parallelised scripts through the Python wrapper. The version of Mixer used to generate the data in this work was compiled against Cubature version 1.0.2 and Eigen version 3.3.3, though the code does not use any features which require recent versions, so many likely suffice.

³⁹ [Guennebaud et al. 2010](#)

Mixer is optimised for convecting systems for which achieving accuracy better than 10^{-5} relative and absolute typically requires between 1ms and 1s on a single core of a 2016 Intel CPU. This is further improved when the differential rotation is minimal, in which case the perturbative expansion may be turned off to save a factor of several in runtime. In stably stratified zones and those with magnetic fields up to 10^3 s may be required to achieve good convergence.

In cases where the code has more difficulty it is quite likely that Mixer becomes the bottleneck in simulations and so, under these circumstances, we recommend tabulating results in advance. This is still considerably more performant than direct numerical simulation, and the results can generally be guaranteed to converge at much higher precision, so that derivatives may be extracted as well.

At various points in the software we must divide by the magnitude of the velocity of an eigenmode. This may approach zero in some cases. To avoid dividing by zero in these cases we place a lower bound on this magnitude, such that

$$|\delta v|^2 \geq \epsilon,$$

where $\epsilon = 10^{-20} L_0^2 |N|^2$ in the calculations presented in this work and N is the Brunt-Väisälä frequency. This corresponds to setting an upper bound on the length scale d of the displacements $\delta \mathbf{r}$, namely

$$|\delta \mathbf{r}|^2 \leq L_0^3 |N| \epsilon^{-1/2},$$

which means that $d = 10^{10} L_0$ in this work.

To verify that this numerical fix does not impact our results we have examined the correlation functions in several scenarios as a function of this numerical cutoff L . For example, figure 2.1 shows the $r - \theta$ and $r - \phi$ correlations as a function of d for a stably stratified differentially rotating system. The results are constant over many orders of magnitude so long as $d > 10^5 L_0$, which is easily satisfied by our default choice.

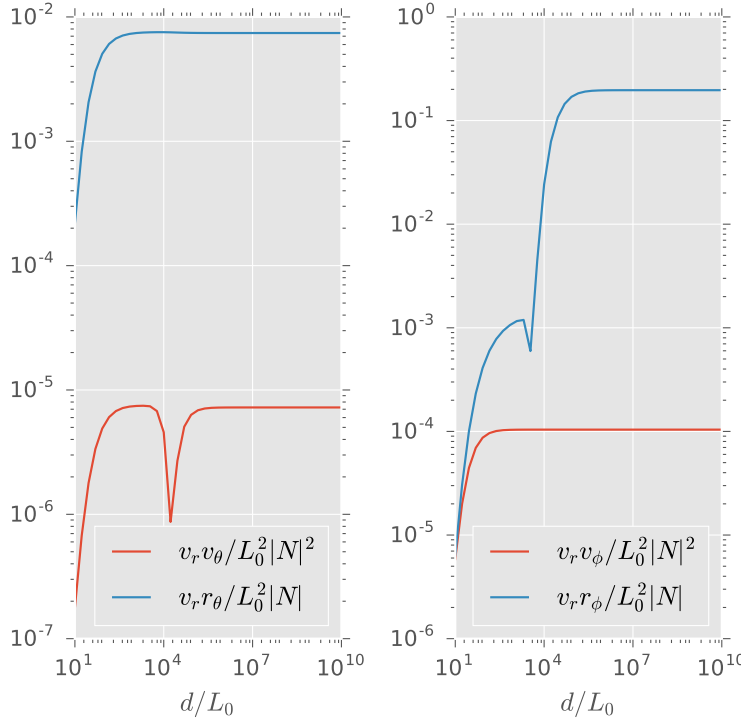


Figure 2.1: The absolute values of $\langle \delta v_r \delta v_\theta \rangle$ (left) and $\langle \delta v_r \delta v_\phi \rangle$ (right) are shown as a function of d , with both axes log-scaled. These results are for a stably stratified region with differential rotation in the radial direction with $|R \nabla \ln \Omega| = 10^{-3}$, $\Omega = 0.1|N|$ and no magnetic field. The data is computed for a point on the equator with differential rotation at an angle of $\pi/4$. Note that the dips in these curves are indicative of sign changes. All quantities are given in units of the mixing length and the Brunt-Väisälä frequency.

2.7 Results

In this section we exhibit a number of results which come from applying our model to a wide variety of astronomically- and physically-relevant circumstances. We also compare with the results of Lesaffre et al. (2013) and Kichatinov & Rudiger (1993). We modify the former to use the convention in equation (2.7) to avoid spurious differences in scale. We likewise assume that our L_0 is equal to three times the mixing length of Kichatinov & Rudiger (1993), as this is an inherent freedom in the formalism and resolves an otherwise-persistent scale difference between our model and theirs. These models have been well-tested against a variety of data, most notably helioseismic results, and so provide a useful reference for our work.

We have also included more direct comparisons but, because direct experiments are extremely difficult to perform under most circumstances

relevant to astrophysics, we have instead included comparisons with simulations and observations where available and applicable. Simulations are often the most useful comparison for stellar phenomena, because a variety of processes, including meridional circulation, can mask the effects of turbulent transport ⁴⁰. In accretion discs, however, there are several observable quantities which are thought to correlate closely with the underlying turbulence and these provide very helpful constraints ⁴¹.

⁴⁰ Kitchatinov 2013

⁴¹ King et al. 2007

These comparisons and calculations are not intended to be a complete collection of the results our model can produce, nor have we exhaustively explored the circumstances and dependencies of each result. Rather it is our hope to demonstrate that there is a great deal of interesting physics in this model, that our perturbative corrections give rise to realistic results and reproduce many known results, and that there is much to warrant further exploration along these lines.

2.7.1 Rotating Convection

We begin with the effect of rotation on convection in the case of a rotating system with radial pressure and entropy gradients. It is useful to start by comparing our results with those from simulations. Fig. 2.2 shows the ratios $\sqrt{\langle \delta v_r^2 \rangle / \langle \delta v^2 \rangle}$, $\sqrt{\langle \delta v_\theta^2 \rangle / \langle \delta v^2 \rangle}$ and $\sqrt{\langle \delta v_\phi^2 \rangle / \langle \delta v^2 \rangle}$ for several rotation rates as a function of latitude. The positive latitudes come from Table 2 of Chan (2001) while the negative are from Table 2 of Käpylä et al. (2004). In order to match the units for the rotation rates we put everything in terms of the coriolis number

$$\text{Co} \equiv \frac{\Omega h}{\langle \delta v^2 \rangle^{1/2}},$$

where, following the convention of Käpylä et al. (2004), $\langle \delta v^2 \rangle^{1/2}$ was computed for a non-rotating system and h is the pressure scale-height

$$h \equiv -\frac{dr}{d \ln p}.$$

Our model overestimates the anisotropy of the turbulence but captures its symmetries and trends. For instance we find that near the poles and in non-rotating systems the θ and ϕ components of the velocity fluctuations have identical magnitudes, in line with the simulations. We reproduce the trend of decreasing anisotropy towards the equator and decreasing anisotropy with increasing rotation, though we do not reproduce the reordering of velocity components which occurs at high rotation rates near the equator. Where there are differences between the θ and ϕ velocities

we typically reproduce both their sign and magnitude, though there are exceptions. Notably we find that $\langle \delta v_r^2 \rangle \geq \langle \delta v_\theta^2 \rangle \geq \langle \delta v_\phi^2 \rangle$, which is seen in these and other simulations⁴². Likewise we find that radial motion makes up a greater fraction of the total velocity near the poles than at the equator, and that as the Coriolis number increases $\langle \delta v_r^2 - \delta v_\theta^2 - \delta v_\phi^2 \rangle \rightarrow 0$, all of which is in agreement with the predictions of Rüdiger et al. (2005b).

⁴² Rüdiger et al. 2005a

Our overestimate of the anisotropy may be due to our model incorporating the large-scale fields on all scales, as noted by Lesaffre et al. (2013). This suggests that a future refinement might be to use estimates of the large-scale modes to compute the environment of those at smaller scales, but we do not treat such complications for now⁴³.

⁴³ For analyses of that sort see Winterberg (1968) and Canuto & Hartke (1986)

As a further comparison we consider the off-diagonal Reynolds stresses of both Chan (2001) and Käpylä et al. (2004). These numbers were extracted from Table 3 of the former and also Table 3 of the latter and are shown along with our predictions in Fig. 2.3. In the former they were straightforward to analyse but in the latter they do not provide a precise test because the simulations included a forced shear. To correct for this we used a linear expansion to subtract results across simulations which were identical in all conditions other than the rotation and thereby determine the effect of the rotation alone. As we will see in Section 2.7.2 this procedure is problematic because the shear may interact non-linearly with the rotation. Furthermore because these corrections are of the same order as the terms themselves some care must be taken in interpreting the results.

Despite these difficulties some trends are clear and sustained between both sets of data. For instance in the northern hemisphere⁴⁴ $\langle \delta v_r \delta v_\theta \rangle < 0$, while in both hemispheres $\langle \delta v_r \delta v_\phi \rangle < 0$, in keeping with predictions and simulations by Rüdiger et al. (2005b). Likewise we find that $\langle \delta v_\theta \delta v_\phi \rangle > 0$ in the northern hemisphere, in agreement with the findings of Rüdiger et al. (2005a).

⁴⁴ i.e. $\theta > 0$

Once more, however, our model overestimates these anisotropic terms by an amount which is largely invariant as a function of rotation. This suggests that this overestimate is a systematic offset rather than an error in scaling. We also have some difficulty to reproduce the signs of some of the stresses, particularly in the results of Käpylä et al. (2004), though this could simply be a subtraction difficulty. This is supported by the fact that the simulations themselves do not agree on the signs of these terms and highlights the challenges of making comparisons of terms which are small in magnitude relative to the scale of the turbulence.

To better understand which trends are significant and which are arte-

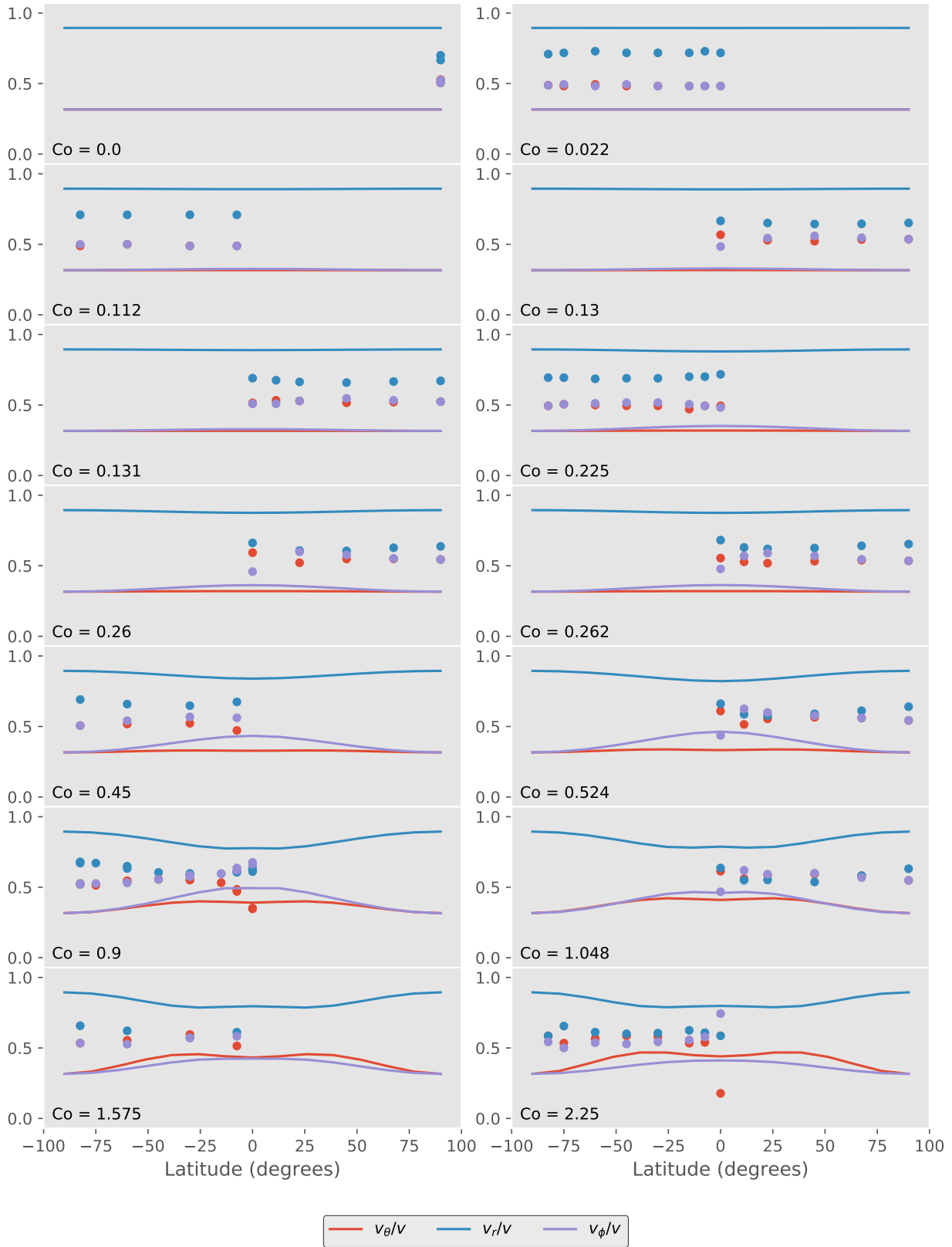


Figure 2.2: The ratios $\sqrt{\langle \delta v_r^2 \rangle / \langle \delta v^2 \rangle}$ (blue), $\sqrt{\langle \delta v_\theta^2 \rangle / \langle \delta v^2 \rangle}$ (red) and $\sqrt{\langle \delta v_\phi^2 \rangle / \langle \delta v^2 \rangle}$ (purple) are shown for our model (solid) and for simulations by Käpylä et al. (2004) (dots, negative latitude) and Chan (2001) (dots, positive latitude) for a wide range of rotation rates as a function of latitude. The rotation rate is captured by the Coriolis number $Co = \Omega h / \langle \delta v^2 \rangle^{1/2}$. Our model generally overestimates the anisotropy but captures its variation well.

facts we have placed data from comparable rotation rates for the two sets of simulations side-by-side in Fig. 2.4. The top five panels show the same data as in Fig. 2.2 while the bottom three show the data from Fig. 2.3. In general there is good agreement in the top five panels. The data of Käpylä et al. (2004) gives systematically larger anisotropies and the two sets of simulations occasionally differ on the relative magnitudes of the velocity components⁴⁵, but otherwise the two are in good agreement. By contrast the bottom three panels paint two very divergent pictures. Neither ordering, trends nor signs are consistent between the two sets of simulations. Only the magnitudes agree in these cases. Thus the two sets of simulations agree that our model systematically overestimates anisotropies and that, beyond that, our model agrees with them to the extent that they agree with one another.

⁴⁵ i.e. their ordering

Having compared in detail with these simulations we now consider predictions which go beyond the domain where simulations are possible. In convection with radial entropy and pressure gradients the leading order effect is to transport heat and material radially. Fig. 2.5 shows $\langle \delta v_r \delta v_r \rangle$ and $\langle \delta v_r \delta r_r \rangle$, which are the correlation functions controlling this transport.

Both correlators vary at second order in Ω in the slow rotation limit as expected⁴⁶. In the rapid rotation limit on the other hand they exhibit clear Ω^{-1} scaling, consistent with what is seen in other closure models and in simulations⁴⁷. The quenching of turbulence in this limit arises because the Coriolis effect acts as a restoring force, stabilising modes.

⁴⁶ Lesaffre et al. 2013; Kitchatinov 2013

⁴⁷ Garaud et al. 2010

The peak of each correlator is of order unity and occurs when $\Omega = 0$. In fact for the stress the maximum is 0.254647 while for the diffusivity it is 0.28125, both of which are consistent to this precision with Lesaffre et al. (2013), noting that we used the definition in equation (2.7) for their mixing length. This is because our model is precisely the same as theirs in this limit. Based on this and the observed scalings a good approximation is

$$\langle \delta v_r \delta r_r \rangle \approx \langle \delta v_r \delta v_r \rangle \approx \frac{1 - (\Omega/|N|)^2}{1 - (\Omega/|N|)^3},$$

where we have neglected factors of order unity.

Next we consider the effect of rotation on the $r - \theta$ correlation functions. These functions are responsible for latitudinal transport of heat, mass and momentum and vanish as a result of spherical symmetry in the non-rotating limit. Fig. 2.6 shows $\langle \delta v_r \delta v_\theta \rangle$ and $\langle \delta v_r \delta r_\theta \rangle$ as a function of the rotation rate.

In the slow-rotation regime both quantities scale as Ω^2 , while in the rapid rotation limit they scale as Ω^{-1} . The peak is of order unity and

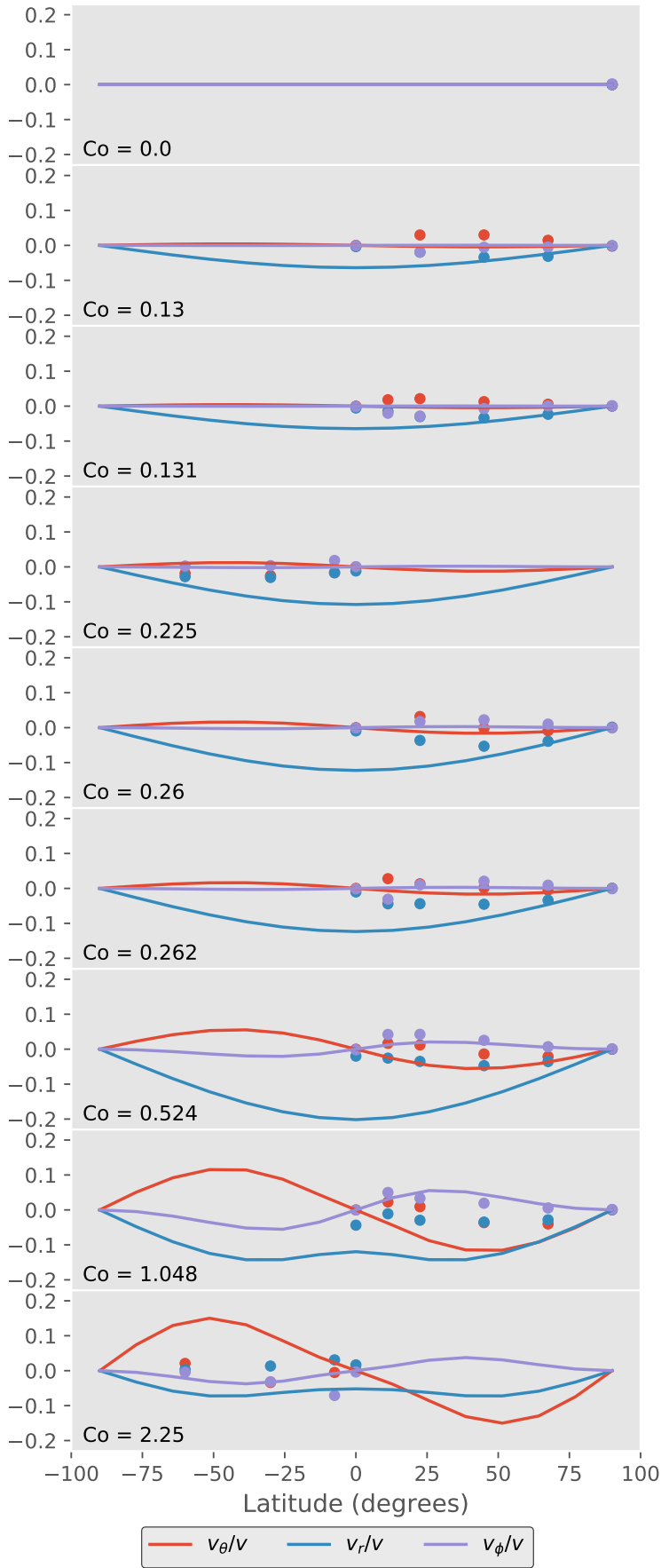


Figure 2.3: The ratios $\sqrt{\langle \delta v_r \delta v_\theta \rangle} / \langle \delta v^2 \rangle$ (red), $\sqrt{\langle \delta v_\theta \delta v_\phi \rangle} / \langle \delta v^2 \rangle$ (purple) and $\sqrt{\langle \delta v_r \delta v_\phi \rangle} / \langle \delta v^2 \rangle$ (blue) are shown from our model (solid) and from simulations by Käpylä et al. (2004) (dots, negative latitude) and Chan (2001) (dots, positive latitude) as a function of latitude. Note that Käpylä et al. (2004) cautions that the moderate rotation simulations had difficulty converging, and these results arise as the difference between two simulations, so it is not clear how significant this test is. Our model generally overestimates these stresses, and suggests a different symmetry for the variation, going as $\sin \theta$ rather than $\sin(2\theta)$.

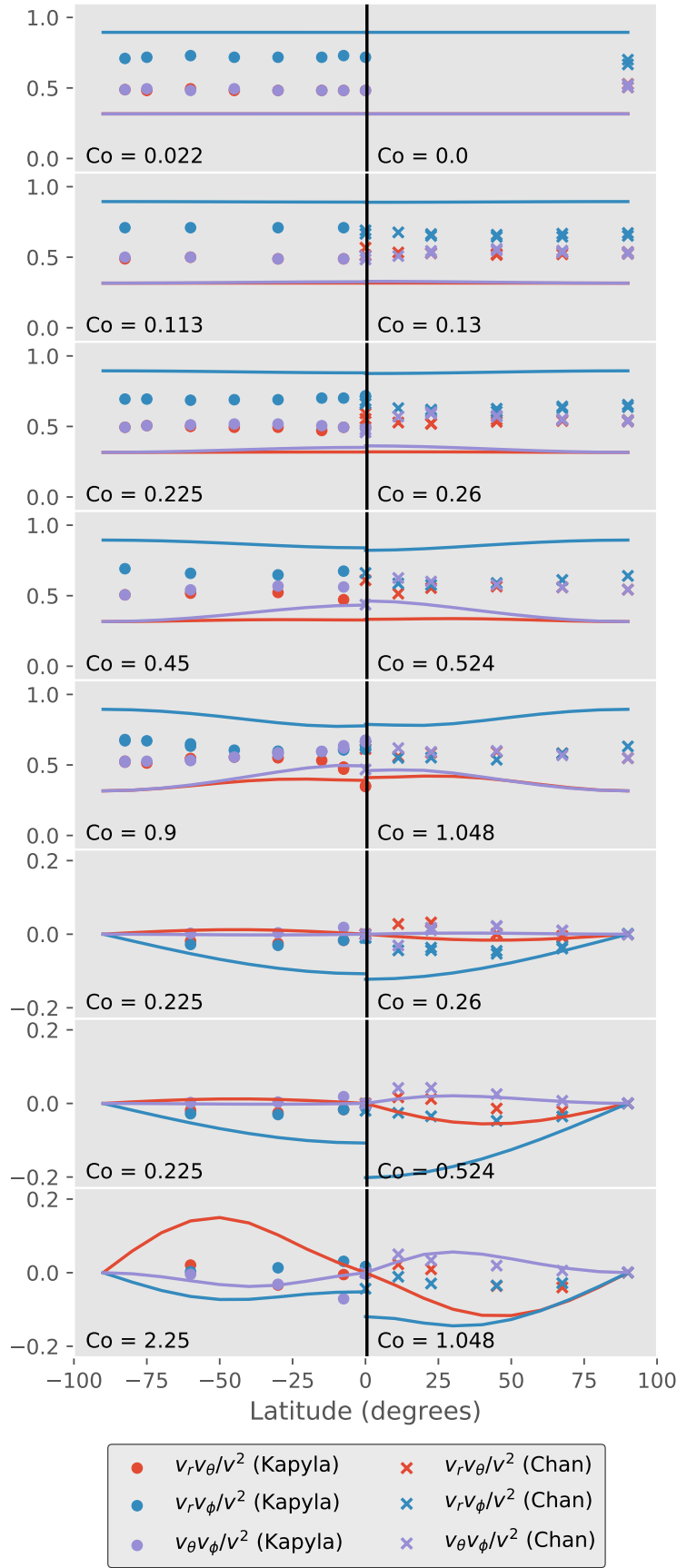


Figure 2.4: The functions shown in Figs. 2.2 and 2.3 are shown from our model (solid), simulations by [Käpylä et al. \(2004\)](#) (dots, negative latitude) and [Chan \(2001\)](#) (crosses, positive latitude) as a function of latitude. The most comparable pairs of rotation rates were placed side-by-side for each function. A solid black line is shown along the equator where the latitude is zero. There is reasonable agreement on the distribution of velocities in direction but not on the correlations between different velocity directions.

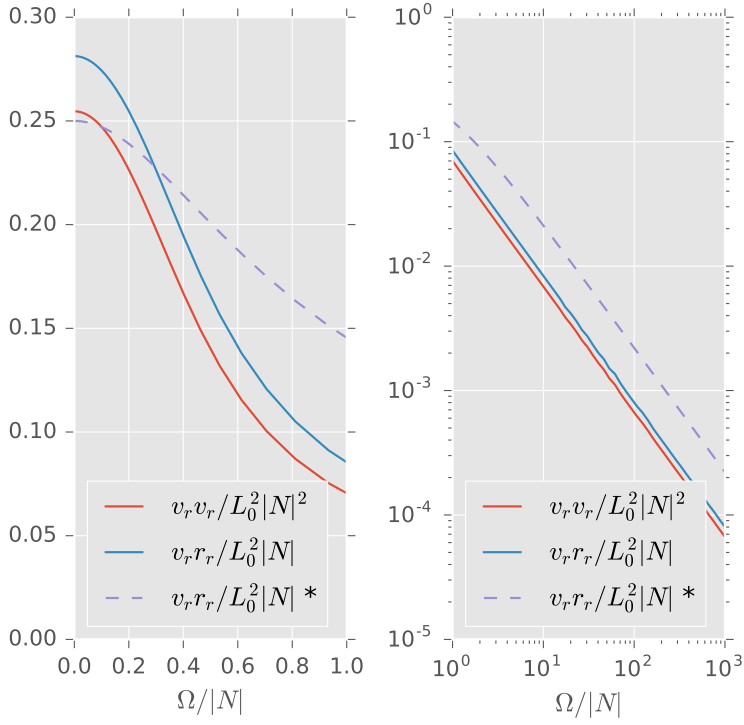


Figure 2.5: The radial velocity correlation function $\langle \delta v_r \delta v_r \rangle$ (red) and the radial diffusivity $\langle \delta v_r \delta r_r \rangle$ (blue) are shown in linear scale for $\Omega < |N|$ (left) and log-log scale for $\Omega > |N|$ (right). These results are for uniform rotation at a latitude of $\pi/4$ with no magnetic field. On this and all subsequent figures $v_r v_r / L_0^2 |N|^2$ should be read as $\langle \delta v_r \delta v_r \rangle / L_0^2 |N|^2$ and similarly for other correlations. Shown in purple (*, dashed) for comparison is the result of Kichatinov & Rudiger (1993) with an anisotropy factor of 2, which agrees in sign, scale and variation. The bumps in our results reflect parameter values where the numerical integration was more difficult. All quantities are given in units of the mixing length and the Brunt-Väisälä frequency.

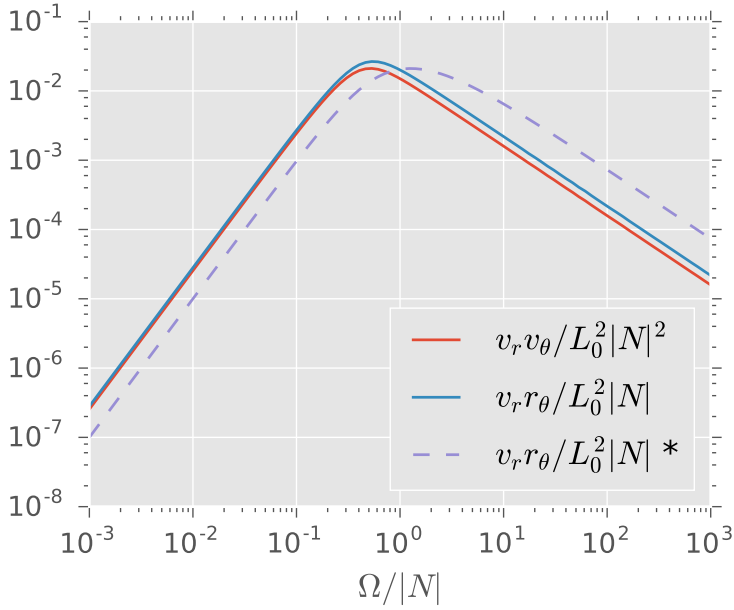


Figure 2.6: The absolute value of the $r - \theta$ velocity correlation function $\langle \delta v_r \delta v_\theta \rangle$ (red) and corresponding diffusivity $\langle \delta v_r \delta r_\theta \rangle$ (blue) are shown in log-log scale against rotation rate. These results are for uniform rotation at a latitude of $\pi/4$ with no magnetic field. Shown in purple (*, dashed) for comparison is the result of Kichatinov & Rudiger (1993) with an anisotropy factor of 2, which agrees in sign, scale and variation. All quantities are given in units of the mixing length and the Brunt-Väisälä frequency.

occurs near $\Omega = |N|$. This gives rise to the approximation

$$\langle v_r r_\theta \rangle \approx \langle v_r v_\theta \rangle \approx \frac{(\Omega/|N|)^2}{1 + (\Omega/|N|)^3}.$$

These scalings may be interpreted as a competition between symmetry breaking and quenching: the correlation function rises as rotation breaks symmetries but excessive rotation stabilises the system and quenches the turbulent motions. The symmetry is broken quadratically because, at first order, the Coriolis effect only couples radial and azimuthal motions.

The properties of turbulence vary with latitude in a rotating system because the rotation axis picks out a preferred direction. Fig. 2.7 shows the $r - r$ and $r - \theta$ stress and diffusivity correlations as a function of latitude. The $r - r$ correlations vary similarly to one another, exhibiting a minimum at the equator and maxima on-axis. On-axis the rotation drops out of the equations and so the on-axis functions are just those for non-rotating convection. The effect of rotation is then largest at the equator, where the convective motion is predominantly perpendicular to the rotation axis. The correlation functions are smallest where the rotation has the largest effect because rotation primarily acts to stabilise modes.

By contrast the $r - \theta$ correlator is largest in magnitude at mid-latitudes, vanishing both on-axis and at the equator. On-axis this correlation function must vanish because the $\hat{\theta}$ unit vector is ill-defined. The sign change between the northern and southern hemispheres occurs because $(\hat{r} \times \Omega)_\phi$ has the same sign everywhere while $(\hat{\theta} \times \Omega)_\phi$ changes sign between the hemispheres. This also explains the vanishing correlation at the equator.

The quantities of particular interest for studying the origins of differential rotation are the radial-azimuthal correlation functions $\langle \delta v_r \delta v_\phi \rangle$ and $\langle \delta v_r \delta r_\phi \rangle$. The former provides a stress coupling the angular momentum to radial motions known as the Λ -effect⁴⁸, while the latter provides a viscosity coupling radial shears to azimuthal motion and so acts as a proxy for the α -effect⁴⁹. Fig. 2.8 shows these quantities as a function of the rotation rate. In the slow-rotation limit both scale as Ω before peaking near unity and falling off as Ω^{-2} in the rapid-rotation limit. The linear scaling at slow rotation rates is a consequence of the Coriolis effect directly coupling radial and azimuthal motions. These quantities fall off more rapidly than the others in the case of rapid rotation because it is preferentially the modes which couple strongly to the Coriolis effect which are stabilised the most. The absolute scale of our Λ -effect is approximately what is seen in simulations, slightly overestimating relative to Käpylä et al. (2004) and similar to other theoretical predictions⁵⁰.

⁴⁸ The Λ -effect just refers to the terms proportional to Ω in the series expansion of $\langle \delta v_r \delta v_\phi \rangle$ and $\langle \delta v_\theta \delta v_\phi \rangle$. Such terms were initially expected to vanish because it was assumed that turbulence produces an isotropic viscous effect, analogous to the microscopic viscosity, which inherently cannot couple to rigid rotation. This fails when turbulence is anisotropic (Kippenhahn, 1963).

⁴⁹ Kichatinov & Rudiger 1993

⁵⁰ Kichatinov 2013; Gough 2012

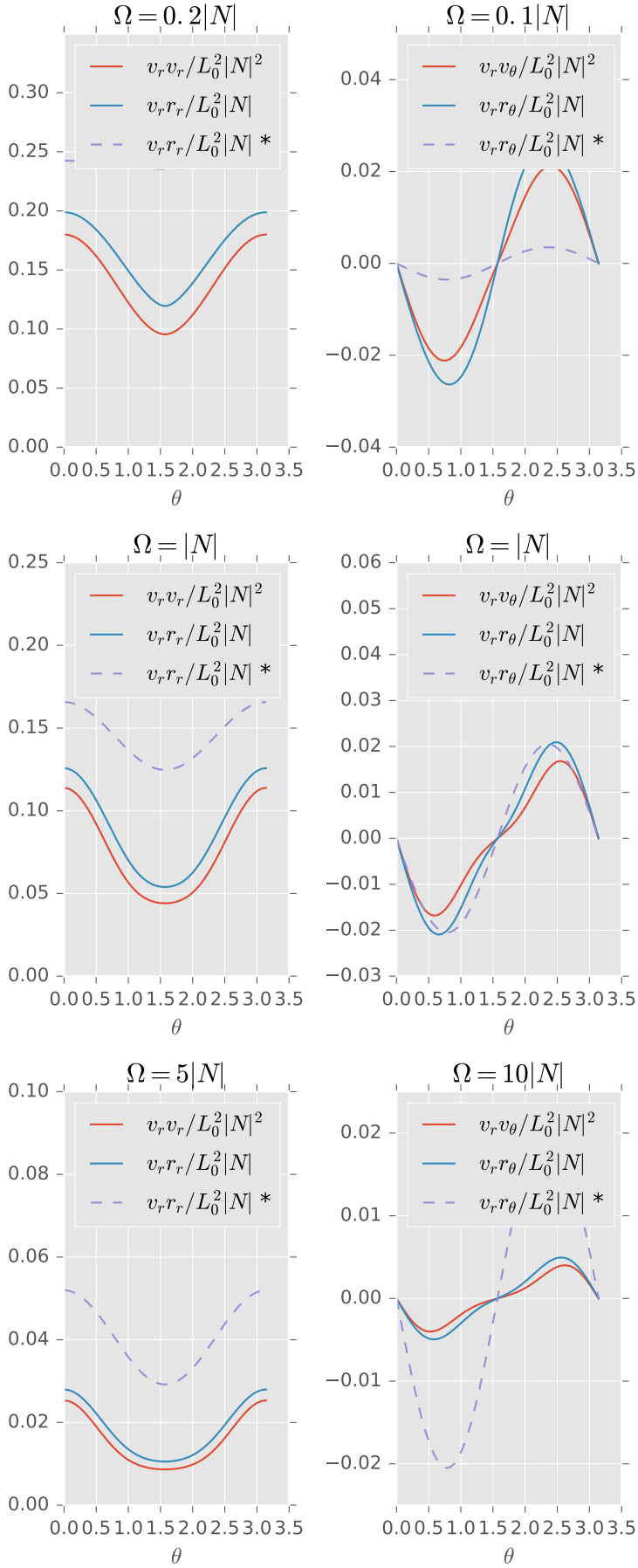


Figure 2.7: Various correlation functions are shown as a function of the angle θ from the rotation axis. The functions are the $r-r$ (left) and $r-\theta$ (right) velocity (red) and diffusivity (blue) correlation functions. These results are for uniform rotation at $\Omega = 0.2|N|$ (top), $\Omega = |N|$ (middle) and $\Omega = 5|N|$ (bottom). Shown in purple (*, dashed) for comparison is the KR result, which agrees in sign and variation but not scale. For slow rotation the scale of the variation is generally smaller than we predict, while for fast rotation the variation is somewhat larger. All quantities are given in units of the mixing length and the Brunt-Väisälä frequency.

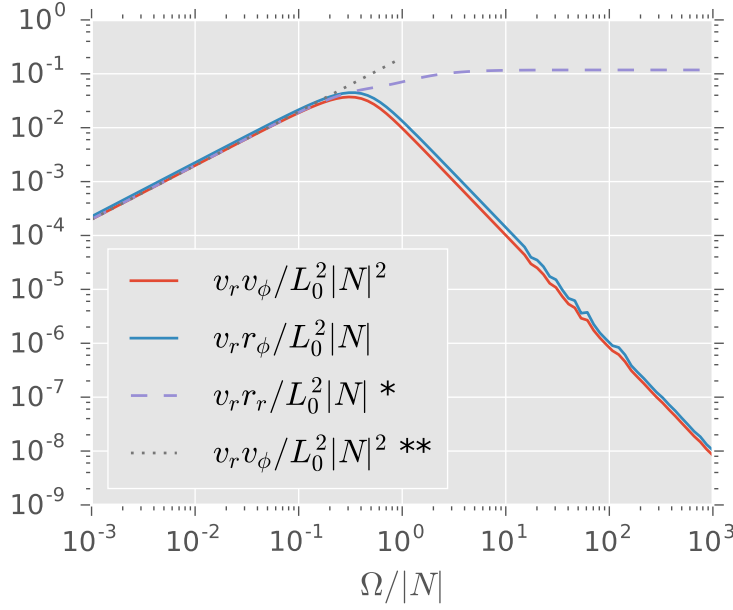


Figure 2.8: The absolute value of the $r - \phi$ velocity correlation function $\langle \delta v_r \delta v_\phi \rangle$ (red) and corresponding diffusivity $\langle \delta v_r \delta r_\phi \rangle$ (blue) are shown in log-log scale versus rotation rate. These results are for uniform rotation at a latitude of $\pi/4$ with no magnetic field. Shown in purple (*, dashed) for comparison is the result of Kichatinov & Rudiger (1993) with an anisotropy factor of 2 which agrees in sign, variation and scale up until $\Omega = |N|$, at which point the behaviour differs significantly. Shown in grey (**, dotted) for comparison is $\langle \delta v_r \delta v_\phi \rangle$ from that of Lesafre et al. (2013). This agrees precisely in the $\Omega \rightarrow 0$ limit and the agreement is good even near $\Omega \approx 0.5|N|$. All quantities are given in units of the mixing length and the Brunt-Väisälä frequency.

2.7.2 Differential Rotation and Convection

We now turn to the dependence of convective transport coefficients on differential rotation. We expand our closure model to linear order in the shear and so restrict this analysis to cases where the dimensionless shear $|R\nabla \ln \Omega|$ is at most of order unity.

Fig. 2.9 shows the $r - \theta$ and $r - \phi$ velocity and diffusivity correlation functions as a function of differential rotation for a situation where $\nabla \Omega$ is at an angle of $\pi/4$ relative to the pressure gradient. All four functions behave linearly near the origin, with intercept set by the stress and diffusivity in the uniform rotation limit. This is precisely as expected: the intercept is non-zero, giving rise to the Λ -effect, while the slope is non-zero, giving rise to the α -effect⁵¹. Note that the favourable comparison of our results with those of Kichatinov (2013) are helpful because their model was implemented in a two-dimensional solar model which compared well with helioseismic observations.

A key difference between our work and what we compare with in Fig. 2.9 is that, while we predict the same sign and comparable magnitude for the α -effect in the zero-shear limit, the effect greatly reduces near $R\nabla \ln \Omega \approx 0.1$, indicating that, at least for this configuration, this is the point at which non-linear effects become important. This does not represent a particularly severe shear and highlights a key point that the correlation functions we find are generally non-linear in all of the small parameters in which one might wish to expand. Our model captures this

⁵¹ Kichatinov & Rudiger 1993

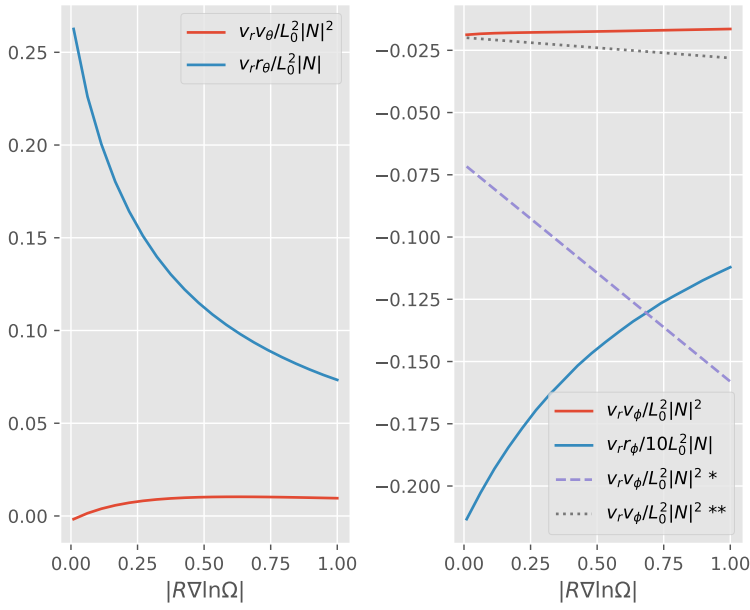


Figure 2.9: The $r - \theta$ (left) and $r - \phi$ (right) velocity (red) and diffusivity (blue) correlation functions are shown in log-scale versus the differential rotation. These results are for a convecting region with differential rotation in the cylindrical radial direction, $\Omega = 0.1|N|$ and no magnetic field at a latitude of $\pi/4$. Shown in purple (*, dashed) for comparison is the result of Kichatinov & Rudiger (1993) with an anisotropy factor of 2. This disagrees on the magnitude of the slope but agrees in the sign of the slope. Shown in grey (**, dotted) for comparison is $\langle \delta v_r \delta v_\phi \rangle$ of Lesaffre et al. (2013). This generally predicts smaller stresses though with the same sign and slope sign as our model. All quantities are given in units of the mixing length and the Brunt-Väisälä frequency.

nonlinear behaviour despite being carried out to linear order in $|R\nabla \ln \Omega|$. This is because, in our expansion, the time evolution operator is what is expanded linearly. The resulting eigenvalues and eigenvectors are generally non-linear functions of this operator.

This caution aside, there is a significant regime where the $\alpha - \Lambda$ expansion is valid and, in this regime, key quantities of interest are the derivatives of the various correlation functions with respect to the shear $|R\nabla \Omega|$. Fig. 2.10 shows these derivatives as a function of Ω . The $r - \phi$ stress derivative is constant in Ω . This means that the stress scales as $R\nabla \Omega$. This is as expected⁵² and indicates that there is a well-defined effective viscosity transporting angular momentum. This viscosity is given by

$$\nu_{r\phi} \approx L_0^2 |N|.$$

By contrast the derivatives of the $r - \theta$ correlations as well as the $r - \phi$ diffusivity all diverge in the limit as $\Omega \rightarrow 0$. In particular, the $r - \theta$ velocity correlation diverges as Ω^{-1} , the $r - \theta$ diffusivity correlation diverges as Ω^{-2} and the $r - \phi$ diffusivity diverges as Ω^{-2} . These divergences are signatures of symmetry breaking. They indicate that the direction in which the $R\nabla \Omega \rightarrow 0$ limit is approached matters. That is, this limit can be approached by first letting $\Omega \rightarrow 0$ and then differentiating or by differentiating and then taking $\Omega \rightarrow 0$ and the divergence we find in the latter approach indicates that the order matters. This means that the $r - \theta$ stress does not admit a linear expansion in terms of a viscosity, whereas the $r - \phi$ stress may be treated in that fashion.

⁵² See, e.g. Equation 79 of Lesaffre et al. (2013).

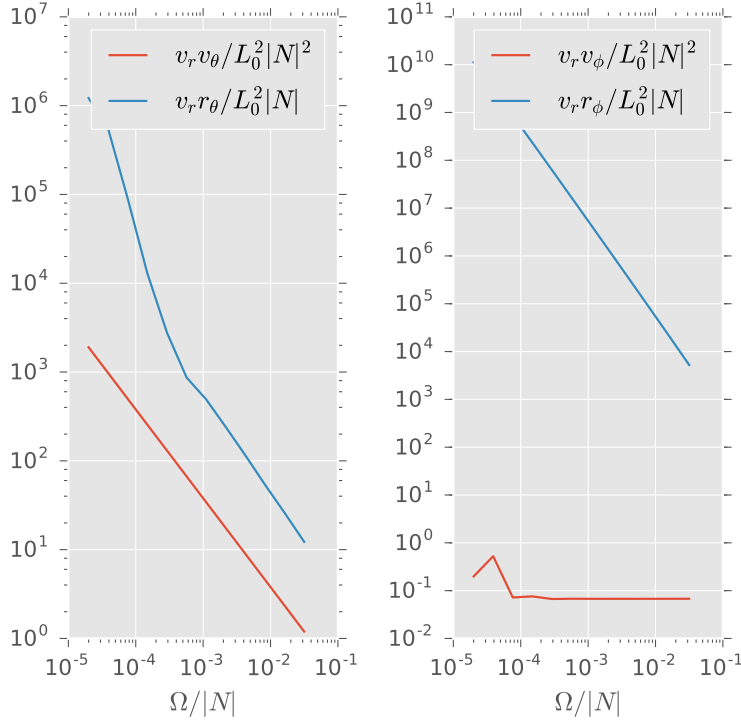


Figure 2.10: The derivatives of various correlation functions with respect to $|R\nabla\Omega|$ are shown as a function of Ω , with both axes log-scaled. The functions are the $r - \theta$ (left) and $r - \phi$ (right) velocity (red) and diffusivity (blue) correlation functions. These results are for a convecting region with differential rotation in the cylindrical radial direction and no magnetic field at a latitude of $\pi/4$. All quantities are given in units of the mixing length and the Brunt-Väisälä frequency.

When $\Omega = 0$ and $|R\nabla\Omega| = 0$ there is a symmetry between $\pm\theta$ and between $\pm\phi$. As a result both the $r - \theta$ and $r - \phi$ terms vanish in this limit. When $\Omega \neq 0$ these symmetries are broken by the rotation and we know from Figs. 2.6 and 2.8 that this occurs at first order for $r - \phi$ and second order for $r - \theta$. In the opposing limit the situation is different because in the time evolution described by equation (2.16) L is independent of $|R\nabla\Omega|$ when $\Omega = 0$. There is, however, a dependence on $|R\nabla\Omega|$ through the time-dependence of \mathbf{q} . This breaks the ϕ symmetry because $\partial_t \mathbf{q}$ is proportional to $q_\phi R\nabla\Omega$ and hence is sensitive to ϕ . It does not, however, break the θ symmetry, because $q_\phi R\nabla\Omega$ is symmetric with respect to changing the signs of both θ and \mathbf{q} . It follows then that we should find divergences in the $r - \theta$ correlation derivatives owing to the path-dependence of the zero-rotation limit and that we should find the $r - \phi$ derivatives to be generally well-behaved.

The curious divergence is then that in the $r - \phi$ diffusivity, because this correlation function does not suffer from a symmetry-derived path-dependence. Rather, the divergence arises because the differential rotation means that L is time-dependent. This introduces polynomial corrections to the usual exponential growth, as discussed in Section 2.3. This formalism captures the fact that the differential rotation turns vertical displacement into ϕ displacements which vary as polynomials in time. There are therefore modes with very small radial velocities which nevertheless have large

azimuthal displacements and these dominate the diffusivity derivative. These modes grow proportional to $|R\nabla\Omega|$ and their growth may proceed in the azimuthal direction until bounded by the Coriolis effect at a time Ω^{-1} . As a result these modes contribute to the diffusivity as $|R\nabla\ln\Omega|$ and hence lead to a diverging derivative in $|R\nabla\Omega|$ as $\Omega \rightarrow 0$. However, this is not physical because the autocorrelation time of turbulence is not infinite, so in practice this growth is cut off by fluctuations in the fastest-growing modes. This suggests a potential improvement to our formalism.

2.7.3 Differential Rotation and Stable Stratification

Stably stratified regions are those with

$$N^2 > 0,$$

such that buoyancy acts to counter perturbations in the vertical direction. This tends to damp turbulence.

In the presence of such damping there can still be turbulence if there is also a shear. The classic example of this is the Kelvin-Helmholtz phenomenon⁵³, which can occur in such a system if the Richardson criterion

$$\frac{|du/dz|^2}{|N|^2} > \frac{1}{4} \quad (2.17)$$

is satisfied⁵⁴. Here u is the velocity and z is the coordinate parallel to the stratification. Even when this criterion is not satisfied, latitudinal shear can still generate turbulence⁵⁵. These motions are suppressed in vertical extent by the stratification and hence are primarily confined to the plane perpendicular to the stratification direction.

Fig. 2.11 shows the dependence on shear strength of all non-vanishing stress components in a rotating stably stratified zone with latitudinal rotational shear. All exhibit linear scaling with the shear strength. This is unusual in an otherwise-stable zone because it implies a viscosity which, to leading order, does not depend on the shear. That is,

$$\nu_{ij} \approx L_0^2 N f_{ij} \left(\frac{\Omega}{|N|} \right),$$

where f_{ij} is some function of the angular velocity. Fig. 2.12 shows the dependence of the stress components on $\Omega/|N|$ for fixed $|R\nabla\ln\Omega| = 0.1$. The components all scale as Ω^2 in both regimes. Thus, for instance, $f_{r\phi} = \Omega/|N|$ because the viscosity is the derivative of the stress with respect to

⁵³ von Helmholtz 1868; Thomson 1871

⁵⁴ Zahn 1993

⁵⁵ Galperin et al. 2007; Canuto et al. 2008

the shear, and hence

$$v_{r\phi} \approx 10^{-5} L_0^2 \Omega. \quad (2.18)$$

The scaling in equation (2.18) arises owing to the centrifugal term, which has a destabilising effect when Ω increases with \hat{R} . When $|R\nabla\Omega| = 0$ this effect is not present so the system is stable but introducing a small differential rotation produces an acceleration proportional to $\Omega R \delta \mathbf{r} \cdot \nabla \Omega$ and hence

$$\partial_t^2 \delta \mathbf{r} \approx g^2 \delta \mathbf{r} \propto \hat{R} \Omega R \delta \mathbf{r} \cdot \nabla \Omega, \quad (2.19)$$

which means that the stress scales as $\Omega \nabla \Omega$ and thence the viscosity scales as Ω . This could be termed an epicyclic viscosity because it relies on the epicyclic term to relate motion to stress.

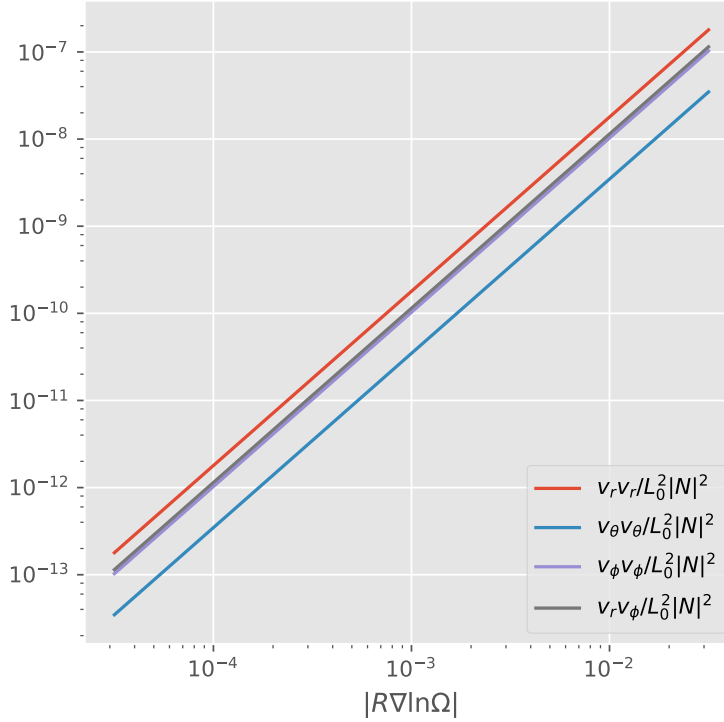


Figure 2.11: The absolute value of the r - r (red), θ - θ (blue), ϕ - ϕ (purple) and r - ϕ (grey) velocity correlation functions are shown as a function of $|R\nabla \ln \Omega|$, with both axes log-scaled. These results are for a stably stratified region with differential rotation in the radial direction, $\Omega = 0.1|N|$ and no magnetic field. The data is computed for a point on the equator with radial differential rotation. All quantities are given in units of the mixing length and the Brunt-Väisälä frequency.

To better understand the effect of our perturbative corrections we computed the same results without them. This produced stresses which were zero to within numerical precision in all cases, indicating that the entire contribution in this case is coming from the perturbation. This is consistent with findings that without thermal diffusion⁵⁶ or a magnetic field⁵⁷ equation (2.17) represents a strict criterion. However with a different angle of differential rotation we obtained non-zero results. This is consistent with the findings of Zahn (1992), who showed that horizontal turbulence⁵⁸

⁵⁶ Canuto & Hartke 1986

⁵⁷ Lecoanet et al. 2010

⁵⁸ i.e. turbulent motion on isobars

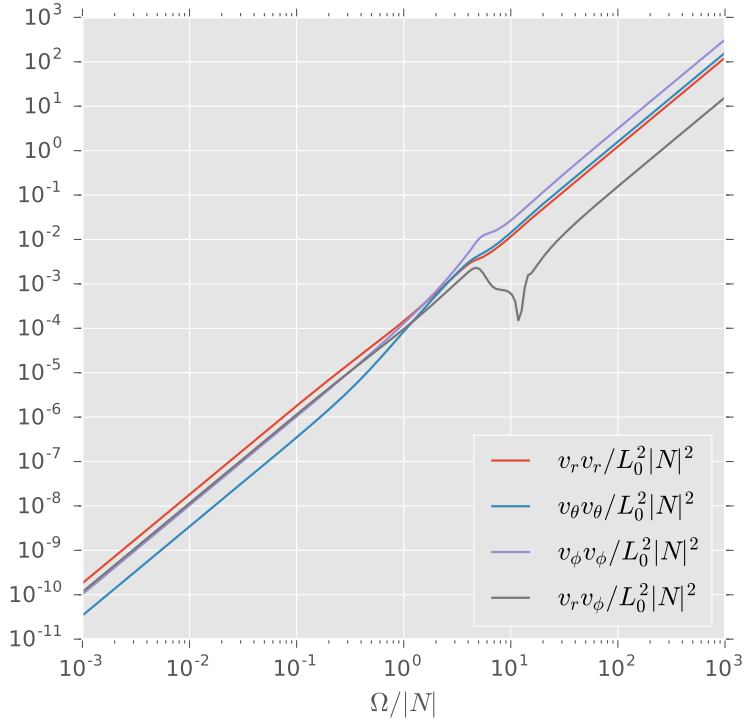


Figure 2.12: The absolute value of the r - r (red), θ - θ (blue), ϕ - ϕ (purple) and r - ϕ (grey) velocity correlation functions are shown as a function of $\Omega/|N|$ for fixed $|R\nabla \ln \Omega| = 0.1$ with both axes log-scaled. These results are for a stably stratified region with differential rotation in the radial direction and no magnetic field. The data is computed for a point on the equator with radial differential rotation. All quantities are given in units of the mixing length and the Brunt-Väisälä frequency. Note that the r - ϕ and θ - ϕ correlations undergo a sign change at $\Omega/|N| \approx 10 = |R\nabla \ln \Omega|^{-1}$, where terms which are linear in the differential rotation are overtaken by those which are quadratic.

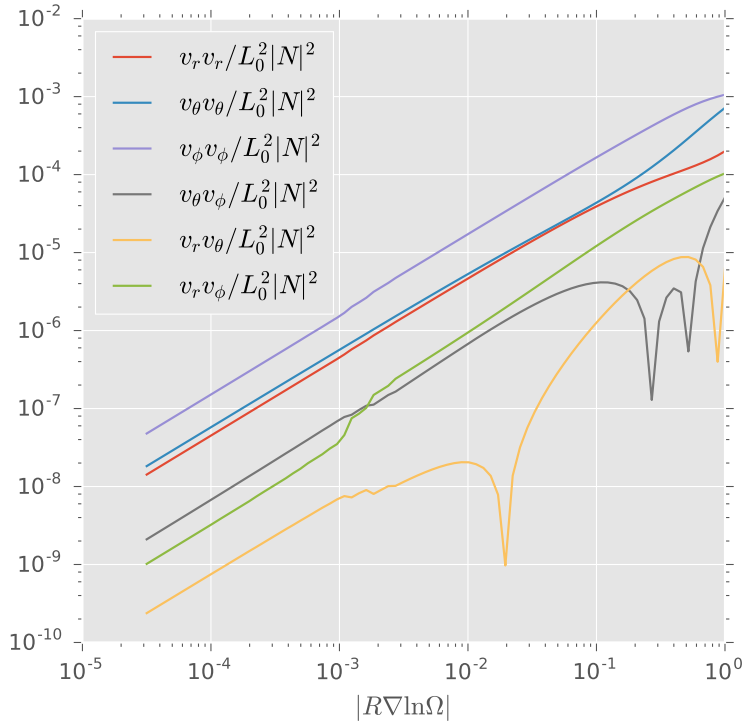


Figure 2.13: The absolute value of the r - r (red), θ - θ (blue), ϕ - ϕ (purple), θ - ϕ (grey), r - θ (yellow) and r - ϕ (green) velocity correlation functions are shown as a function of $|R\nabla \ln \Omega|$ with both axes log-scaled. The correlation functions are evaluated at first order in the perturbative expansion. These results are for a stably stratified region with differential rotation in the radial direction, $\Omega = 0.1|N|$ and no magnetic field. The data are computed for a point on the equator with differential rotation at an angle of $\pi/4$. All quantities are given in units of the mixing length and the Brunt-Väisälä frequency. Note that the r - θ correlation undergoes a sign change at $|R\nabla \ln \Omega| \approx 10^{-2} \approx (\Omega/|N|)^2$, where terms which are linear in the differential rotation are overtaken by those which are quadratic. Both this and the θ - ϕ component undergo sign changes near $|R\nabla \ln \Omega| = |N|$, where the shear competes directly with the stable stratification.

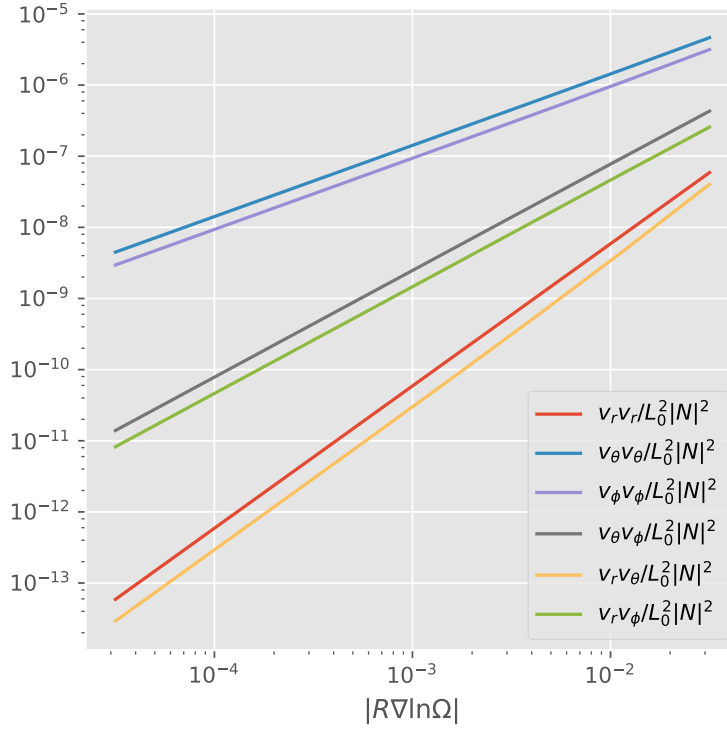


Figure 2.14: The absolute value of the r - r (red), θ - θ (blue), ϕ - ϕ (purple), θ - ϕ (grey), r - θ (yellow) and r - ϕ (green) velocity correlation functions are shown as a function of $|R\nabla \ln \Omega|$ with both axes log-scaled. The correlation functions are evaluated at zeroth order in the perturbative expansion rather than first order. These results are for a stably stratified region with differential rotation in the radial direction, $\Omega = 0.1|N|$ and no magnetic field. The data are computed for a point on the equator with differential rotation at an angle of $\pi/4$. All quantities are given in units of the mixing length and the Brunt-Väisälä frequency.

serves to enable vertical turbulence.

It is instructive then to compare Fig. 2.13 with Fig. 2.14. These show the same correlation functions as each other in the same physical scenario, with differential rotation this time at an angle of $\pi/4$, but the former uses the first order perturbative expansion while the latter only expands to zeroth order⁵⁹. The difference between the two calculations is striking: many of the correlation functions have fundamentally different scalings when the perturbative corrections are taken into account. In particular the non-vanishing stresses are quadratic in the shear, whereas they are all linear in the shear in the expanded calculation. This difference relates in part to the centrifugal term, which couples the displacement to the acceleration. Without expanding the equations of motion we would have $\delta r \propto \delta v$, because the mode would need to be an eigenvector of \mathbf{M} . The modes which couple to the centrifugal term would still grow according to equation (2.19) but, for most modes, arranging for the displacement to couple to this term requires coupling to the stabilising buoyant term too. To make this clearer, in Fig. 2.15 we have computed the growth rate as a function of wave-vector orientation without using the perturbative expansion. There are several rapidly-growing regions, oriented at angles of $\pm\pi/4$ relative to the vertical. These angles represent a compromise between maximising the magnitude of the centrifugal acceleration and

⁵⁹ By zeroth order we mean that L is represented by a constant in equation (2.9).

maximising its projection on to the velocity, both subject to the Boussinesq condition that motion be in the plane perpendicular to \mathbf{q} .

By contrast the growth rates in the expanded system, shown in Fig. 2.16, are significant over a much wider swath of parameter space. This is because, in the expanded system, the displacement and velocity need not be parallel so the displacement can be chosen to maximise the centrifugal term while the velocity can be chosen to maximise the projection of the acceleration on to the velocity.

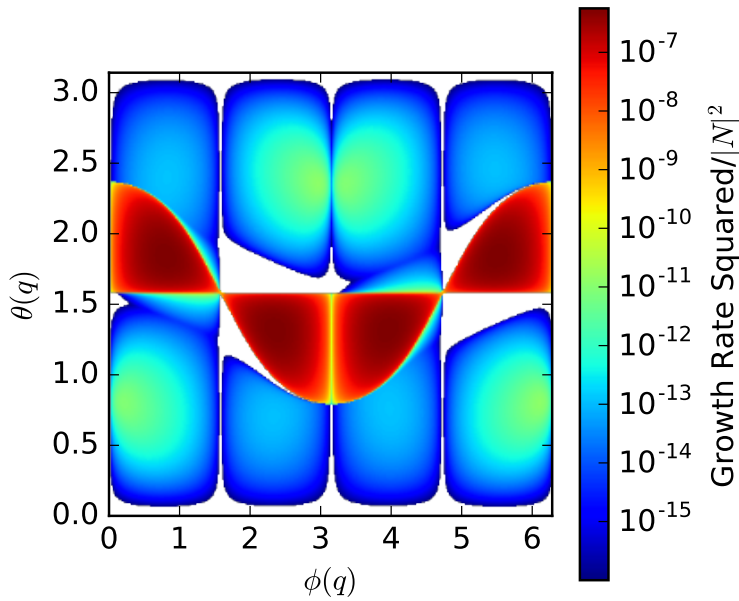


Figure 2.15: The square of the growth rate is shown as a function of wave-vector orientation on a logarithmic colour scale. The wave-vector is specified by a magnitude and two angles, $\theta(q)$ and $\phi(q)$, which are spherical angles relative to the rotation axis. These rates were computed with a zeroth-order expansion. Regions with squared growth rates below 10^{-16} are shown in white. All quantities are given in units of the mixing length and the Brunt-Väisälä frequency.

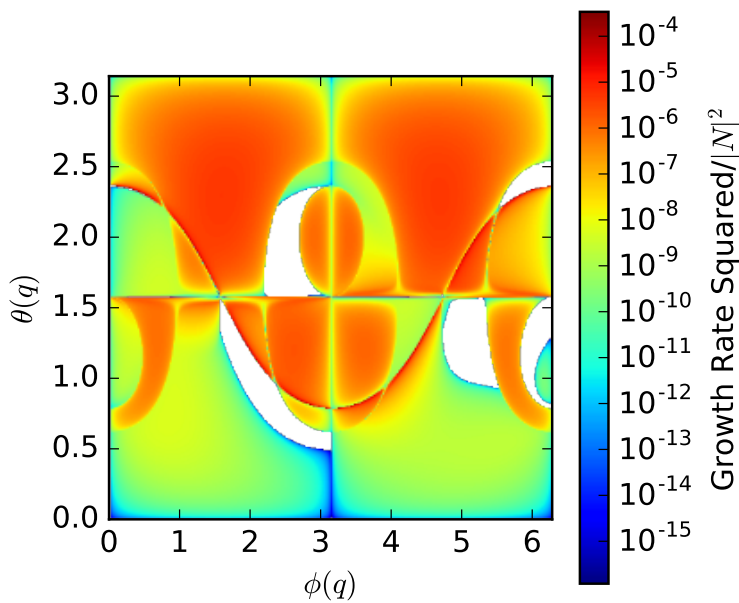


Figure 2.16: The square of the growth rate is shown as a function of wave-vector orientation on a logarithmic colour scale. The wave-vector is specified by a magnitude and two angles, $\theta(q)$ and $\phi(q)$, which are spherical angles relative to the rotation axis. These rates were computed with a first-order expansion. Regions with squared growth rates below 10^{-16} are shown in white. All quantities are given in units of the mixing length and the Brunt-Väisälä frequency.

2.7.4 Baroclinic Instability

The baroclinic instability arises in otherwise stably stratified fluids when the entropy gradient is not parallel to the pressure gradient⁶⁰. In fact this is part of a family of instabilities which includes the convective instability⁶¹. This family provides a continuous connection between the unstable convective and stably stratified limits. To explore it consider Fig. 2.17 which shows the variation of $r - r$ and $r - \theta$ correlation functions against the angle δ between the entropy gradient and the pressure gradient. The radial correlations peak when the two gradients are aligned. This is the convective limit. These correlations fall to zero in the opposing limit where the two gradients are anti-aligned, which is the stably stratified limit. In between these limits the behaviour is approximately that of $\cos^2 \delta$.

⁶⁰ Killworth 1980

⁶¹ Lebovitz 1965

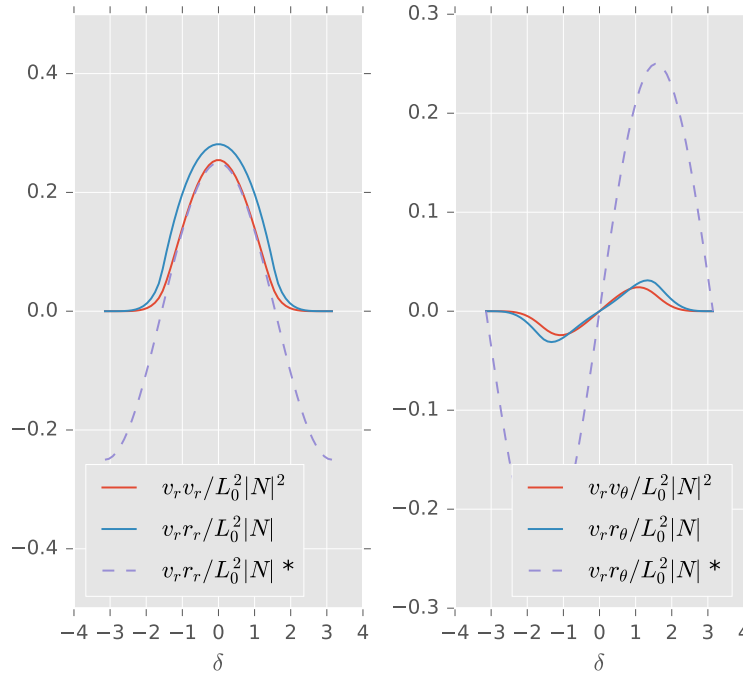


Figure 2.17: Various correlation functions are shown as a function of the angle δ between the entropy and pressure gradients. The functions are the $r - r$ (left) and $r - \theta$ (right) velocity (red) and diffusivity (blue) correlation functions. These results are for a non-rotating convective region on the equator and with no magnetic field. $|N|$ is evaluated for normalisation purposes for a system with $\delta = 0$. Shown in purple (*, dashed) for comparison is the KR result. This agrees in sign, and for $r - r$ agrees in scale, but their $r - \theta$ prediction is considerably larger. Notably this comparison is precisely as $\cos(\delta)$ (left) and $\sin(\delta)$ (right) and crosses zero at non-extremal angles. This is most likely because their theory is not designed for nearly-stable regions with extreme baroclinicity. All quantities are given in units of the mixing length and the Brunt-Väisälä frequency.

By contrast the $r - \theta$ correlations behave approximately as $\sin \delta$, and vanishes when $\delta = 0$. This is because both the aligned and the anti-aligned limits are spherically symmetric and so must have this correlation function vanish. Deviations from the convective limit give rise to linear scaling so the convective baroclinic instability transports heat and momentum at first order in the baroclinicity. This is an entirely distinct phenomenon from the thermal wind balance, which is a large-scale effect while this results from integrating out the small-scale turbulent modes. In the stable limit perturbations arise quadratically, a deviation from the behaviour of $\sin \delta$. This is because there are no existing turbulent motions to perturb, and

so each position and velocity component is linear in δ and gives rise to a quadratic two-point correlation function.

It is instructive to compare these results with the Schwarzschild criterion for dynamic stability⁶², namely

$$N^2 \cos^2 \delta > 0,$$

where δ is the angle between ∇p and ∇s , and N^2 is the Brunt-Väisälä frequency which would arise were the two parallel. From this we see that as $\delta \rightarrow \pm\pi/2$ the system becomes marginally stable so the stress ought to vanish. This is indeed what we see in Figure 2.17, which suggests that our model does indeed capture the relevant linear instability.

⁶² We use this rather than the Solberg-Høiland criteria because the systems considered in Figure 2.17 are not rotating and hence these more general criteria reduce to that of Schwarzschild.

2.7.5 Stellar Magnetism

We now turn to the impact of the magnetic field on convective turbulence in stars. Fig. 2.18 shows $\langle \delta v_r \delta v_r \rangle$ in a mildly rotating ($\Omega = 0.1|N|$) convection zone as a function of B for three polarisations; radial ($\mathbf{B} \parallel \hat{\mathbf{r}}$), latitudinal ($\mathbf{B} \parallel \hat{\boldsymbol{\theta}}$), and longitudinal ($\mathbf{B} \parallel \hat{\boldsymbol{\phi}}$). As the field increases the stress falls off. This is because the field quenches the turbulence by providing a stabilising restoring force, and is in general agreement with Canuto & Hartke (1986). Interestingly the only significant differences are between the radial and angular field polarisations! The θ and ϕ polarisations show precisely the same behaviour out to very strong fields. This is a result of symmetry, because the radial stress is not sensitive to rotation about the radial direction. The deviation seen with strong fields is a numeric artefact and decreases with increasing integration time.

By contrast consider $\langle \delta v_r \delta v_\phi \rangle$, shown in Fig. 2.19. This component, along with the corresponding Maxwell stress, is responsible for transporting angular momentum. Interestingly it shows differences amongst all polarisations, with the strongest difference between the θ polarisation and the others. This is because the stress is mixed between different directions and so is sensitive to all variations in the magnetic field direction. The large difference of the θ polarisation relative to the others reflects the fact that motion is damped perpendicular to the magnetic field so the θ polarisation damps motion in both directions involved in this component of the stress whereas the r and ϕ polarisations only damp motion in one of the two directions.

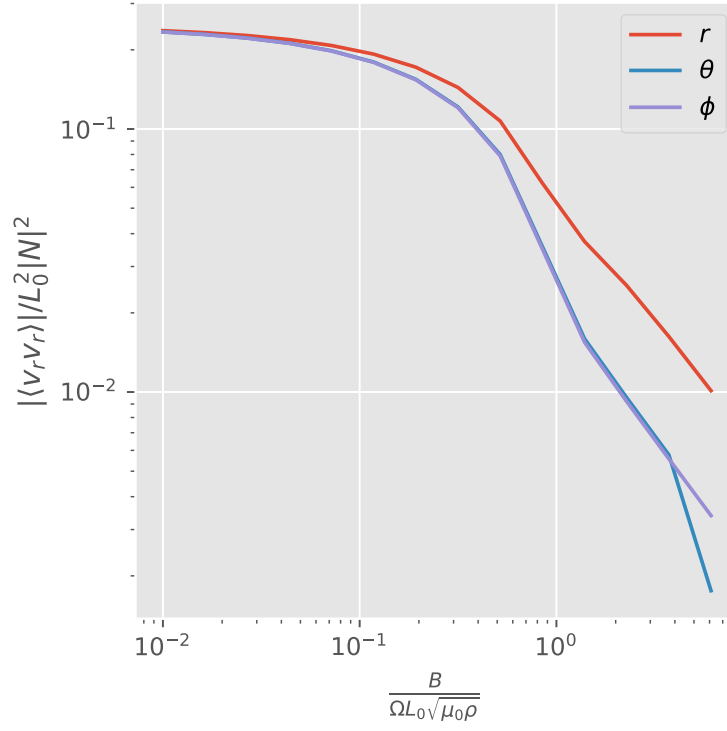


Figure 2.18: The stress $\langle \delta v_r \delta v_r \rangle$ is shown as a function of magnetic field strength. The magnetic field is polarised radially (red), longitudinally (purple) and latitudinally (blue). The system is rigidly rotating at $\Omega = 0.1|N|$ at a latitude of $\pi/4$. All quantities are given in units of the mixing length and Brunt-Väisälä frequency.

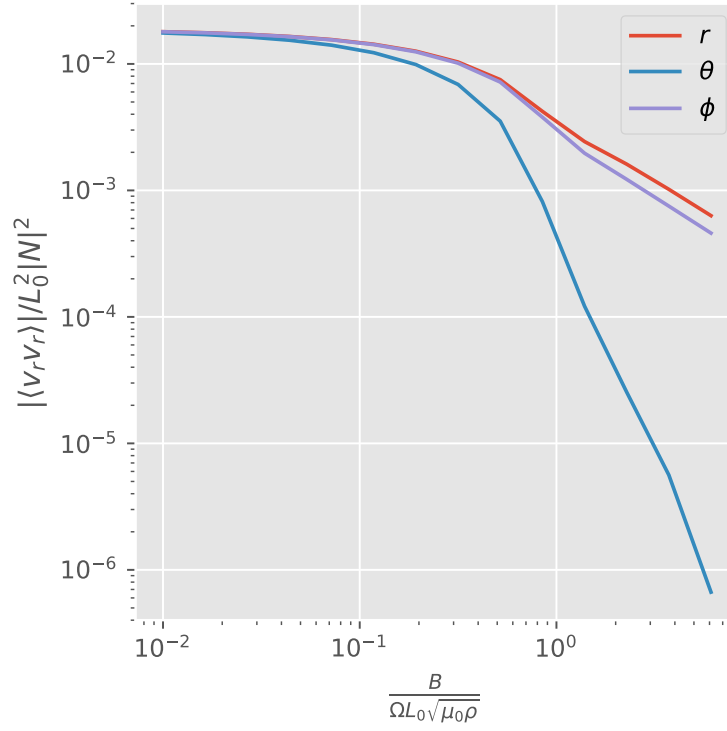


Figure 2.19: The stress $\langle \delta v_r \delta v_\phi \rangle$ is shown as a function of magnetic field strength. The magnetic field is polarised radially (red), longitudinally (purple) and latitudinally (blue). The system is rigidly rotating at $\Omega = 0.1|N|$ at a latitude of $\pi/4$. All quantities are given in units of the mixing length and Brunt-Väisälä frequency.

2.7.6 Magnetorotational Instability

As a final example we consider the magnetorotational instability ⁶³. This instability arises in magnetised fluids undergoing Keplerian orbital motion.

Fig. 2.20 shows the $r - r$ and $r - \phi$ Reynolds and Maxwell stresses for an accretion disc with a vertical magnetic field. Contrary to predictions ⁶⁴ not all of the Reynolds stresses vanish in the zero-field limit. This is because the linear system supports short-term growing modes but, while they only grow in the short-time limit, our numerical methods are not sensitive to that effect at this order. In principle, at higher order, this phenomenon should become evident and so this may be interpreted as an artefact associated with our expanding to low order in $|R\Omega| > 1$. Despite this, it has been proposed that other non-magnetic processes can destabilise these modes even in the long term and so we feel it is appropriate to at least consider them ⁶⁵. The Maxwell stresses by contrast do vanish as $B \rightarrow 0$. This is to be expected because they are proportional to B^2 . Additionally, the $\theta - \phi$ stresses vanish for all B because the system is symmetric under reversing both θ and ϕ , and similarly the $r - \theta$ stresses vanish because the system is symmetric under the simultaneous reversal of r and θ .

As the magnetic field increases the $r - \phi$ Reynolds stress changes sign. This indicates the onset of MRI modes, which have the opposite sign to the zero-field correlations. This effect saturates when $v_A \approx \Omega h$, where h is the scale height of the disc. We find that the total $r - \phi$ stress saturates at roughly $10^{-2}(h\Omega)^2$, which lies between those typically found in simulations and those inferred from observations ⁶⁶. Note that at the saturation point the Maxwell and Reynolds stresses are comparable, and beyond this point the Maxwell stress increases while the Reynolds stress falls off.

Above the saturation point the Reynolds stresses drop off as the magnetic field quenches the turbulence. This is precisely what is expected for the MRI ⁶⁷. The Maxwell stresses, however, continue to grow, again in line with expectations. Some care is required to interpret these results because they were computed for a fixed background field and that field may or may not be stable under the action of the turbulence it generates ⁶⁸. Furthermore there are challenges with the α -disk prescription which make the specific stress components more difficult to interpret ⁶⁹. Nevertheless it is encouraging that what we see matches well with both observations and simulations.

⁶³ Chandrasekhar 1960

⁶⁴ Chandrasekhar 1960

⁶⁵ cf. Luschgy & Pag  ls (2008)

⁶⁶ Starling et al. 2004; King et al. 2007

⁶⁷ Balbus & Hawley 1991

⁶⁸ Pessah et al. 2006

⁶⁹ Pessah et al. 2008

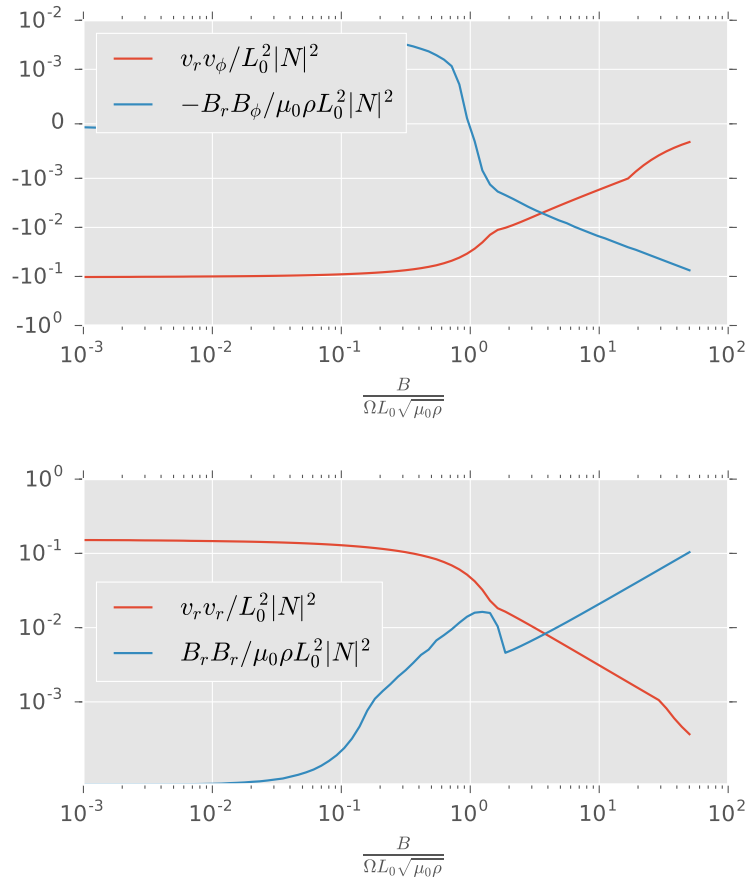


Figure 2.20: The $r-r$ (top) and $r-\phi$ (bottom) are shown as a function of B for a Keplerian disc. Reynolds (velocity) stresses are in red and the Maxwell (magnetic) stresses are in blue. Note that it is the negative $r-r$ Maxwell stress which is shown to make the comparison with the Reynolds stresses clearer. The magnetic field is taken parallel to \hat{z} . The system is taken to be stably stratified in the vertical direction with $|N| = \Omega$ and hence $L_0 = h = R$. All quantities are given in units of the mixing length and Ω .

2.8 *Discussion and Outlook*

We have derived a turbulent closure model which incorporates shear, rotation and magnetism as well as a three-dimensional spectrum of fluctuations. We have also presented a new perturbative approach to incorporate time-dependence in the evolution equations. This model, which is implemented in an open source numerical software package, fully reproduces many known phenomena such as the MRI, baroclinic instability, rotational quenching and more classic shear instabilities.

Using this model we have determined the asymptotic behaviour of a wide variety of correlation functions and transport coefficients under a wide range of circumstances, many of which do not appear in the literature. We have further explored the behaviour of turbulent transport coefficients in intermediate regimes where no single phenomenon dominates, such as in the critical MRI. In these cases the behaviour is generally complex and does not separate easily into components associated with the different pieces of input physics.

The closure formalism developed here fills a new niche in the landscape of solutions to turbulent transport, covering enough phenomena to be useful to understand those operating in stars, planets and accretion discs, while being rapid enough to be incorporated into stellar evolution codes on nuclear timescales.

In the future we hope to provide further refinements and comparisons with direct numerical simulations as well as experiments. In addition, it would be interesting to explore the results of this model to higher order in the shear and, even at this order, there are many results which deserve more analysis than we have given here.

3 *The Magnitude of Convective Differential Rotation*

I have slept out under the stars in Africa
for too many years not to know that they
sound and resound in the sky...
I had acquired also the dialect of the stars...

Sir Laurens Jan van der Post

Abstract

Differential rotation is central to a great many mysteries in stars. Asteroseismic data show that the internal rotation profiles of red giants as well as the Sun are strongly differential in the convection zone, while simulations of rapidly rotating stars show relatively mild shear. We analyse the vorticity equation from an order-of-magnitude and scaling perspective to derive the scaling of differential rotation in both slowly-rotating and rapidly-rotating convection zones. We also calculate the meridional circulation rate and baroclinicity, and examine the magnetic field strength in the rapidly rotating limit. These results are in good agreement with simulations and observations. Our findings are valid generally across stars and fluid planets and not limited to the Sun, though may be violated when tidal effects or externally imposed strong magnetic fields are present.

3.1 Introduction

Differential rotation is one of the key complications in the study of stars. It involves breaking symmetries, structure formation and both heat and momentum transport. Importantly the origin of magnetic fields ¹, the transport of angular momentum ² and the transport of material ³ are all critically influenced by its scale and geometry.

Over several decades helioseismology has permitted studies of the rotation profile of the solar convection zone ⁴. With time the data have become more precise and detailed, providing information on the time-variability of the rotation profile ⁵ as well as that of its gradients ⁶. Similarly related quantities such as the meridional circulation ⁷ have now been well-characterised. The overall picture that has emerged is one in which the differential rotation is of order $|\nabla\Omega| \approx \Omega/R$, with similar scale in both the cylindrical radial and vertical directions. This differential rotation reflects a shear which is large relative to the meridional circulation yet small relative to the characteristic scales of solar convection. These observations present a challenge: what phenomenon sets the scale of differential rotation in the solar convection zone?

Complementing the depth of solar observations, asteroseismic observations have begun to produce information on the rotation profiles of other convecting stars. Limits on the rotation profiles for several red giants are now known, and tell a remarkably similar picture. Detailed examination of Kepler-56 suggests that its convection zone exhibits some differential rotation, of order ⁸ $|\nabla\Omega| \lesssim 4\Omega/R$. This is in line with results from studies on a wider range of red giants which did not attempt to localise the difference rotation but find $|\nabla\Omega|$ typically of order ⁹ Ω/R . Similar results have also been found for solar-like stars ¹⁰.

In contrast to these observational successes, the theoretical study of differential rotation has historically struggled to reproduce observed rotation profiles. The earliest expectations were of solid body rotation ¹¹. Because turbulence and the microscopic viscosity together serve to dissipate energy, fluid bodies without any forcing are expected to come to rigid-body rotational equilibrium. The characteristic time-scale for this is the rotation period, as this is the only such scale for rotationally-driven kinetic turbulence. This is extremely rapid in the context of stellar and planetary lifetimes and so should preclude differential rotation. That this is not observed is evidence that stars host processes which inject energy into differential rotation. For instance in convecting bodies turbulence may be

¹ Miesch & Toomre 2009

² Cantiello et al. 2014

³ Chaboyer & Zahn 1992

⁴ Christensen-Dalsgaard & Schou 1988

⁵ Antia & Basu 2001

⁶ Antia et al. 2008

⁷ Rajaguru & Antia 2015

⁸ Klion & Quataert 2017

⁹ Deheuvels et al. 2015

¹⁰ Schunker et al. 2016; Nielsen et al. 2017

¹¹ Stewartson 1966

strongly isotropic¹². Such anisotropy drives differential rotation and, if the turbulence is powered by heating rather than by the shear itself, can maintain it indefinitely¹³.

In addition to the expectation of solid-body rotation there was also the expectation of cylindrical rotation. This was due to the Taylor-Proudman theorem, which states that the the rotation profile of an efficiently convecting¹⁴ region ought at least to have translational symmetry along the rotation axis¹⁵. This symmetry physically arises from a balance between the Coriolis and centrifugal effects, and so is very different in origin from the solid body expectation. Despite this clean result, observations indicate that the Sun obeys no such constraint¹⁶. The theorem neglects a variety of effects ranging from viscosity and turbulent stresses to MHD phenomena. Additionally convection zones are not perfectly isentropic, which results in the so-called thermal wind correction to the Taylor-Proudman state. One goal of this work is to determine which effects serve to break the Taylor-Proudman state and under what circumstances.

More recently, and in part owing to dramatic improvements in observational capabilities, differential rotation has garnered substantial theoretical attention. Some argue that thermal wind balance and entropy gradients dominate the solar rotation profile¹⁷, while others have called this into question¹⁸. Observations suggest that this is a significant effect, though there remain significant uncertainties¹⁹. Other models suggest that turbulent anisotropy is the most relevant factor²⁰, and more complex models with various parameterisations have also been proposed²¹.

Numerical investigations of these questions have proven more successful in reproducing details of the solar rotation profile²², though they face a different set of challenges²³. In particular, because it is not clear whether differential rotation is a secular phenomenon developing in stars over long periods of time²⁴ or if it is determined on short time-scales. In order to investigate the former case one must make significant simplifying assumptions about the nature of angular momentum transport so as to make the problem tractable with one-dimensional stellar evolution codes. Such simulations have proven helpful in identifying whether specific analytic or semi-analytic prescriptions for angular momentum transport are sufficient²⁵ and have had some success in reproducing the stellar period-radius relations, but do not currently reproduce the observed differential rotation profile in the Sun.

On the other hand if the rotation profile is set by physics acting on short time-scales then three-dimensional hydrodynamics simulations are

¹² There may also be a meridional circulation which pumps angular momentum. Indeed this is thought to be the dominant mechanism of angular momentum transport in radiative stars. As we shall show this is never the case in convective bodies.

¹³ Unno 1957; Kippenhahn 1963

¹⁴ i.e. isentropic

¹⁵ Hough 1897

¹⁶ Di Mauro et al. 1998; Gough & Thompson 1991

¹⁷ Miesch et al. 2006; Balbus & Scharf 2012; Balbus et al. 2012

¹⁸ Brun & Toomre 2002; Brun et al. 2010

¹⁹ Caccin et al. 1976; Rast et al. 2008; Teplit-skaya et al. 2015

²⁰ Ruediger 1989; Kitchatinov & Ruediger 1995; Kitchatinov 2013

²¹ Tuominen & Ruediger 1989; Tuominen et al. 1994; Brun & Rempel 2009; Kissin & Thompson 2015

²² Thompson et al. 2003; Miesch & Toomre 2009

²³ Käpylä 2011

²⁴ This is generally thought to be the case in radiative stars. See e.g. Maeder & Zahn (1998).

²⁵ Cantiello et al. 2014

possible, though global simulations remain challenging owing to the wide range of Mach numbers simultaneously present in stellar convection. A further challenge is that these simulations are sufficiently time-consuming that it is not currently possible to explore large parameter spaces and map out the dependence of differential rotation on key parameters such as angular momentum and luminosity. Nevertheless, the results which have been found in this way are intriguing. For instance, red giants are found in both simulation and asteroseismic inference to exhibit significant differential rotation, including cases where the angular velocity changes sign²⁶. There is also some evidence suggesting that baroclinicity at the tachocline plays a role²⁷.

Here we aim to understand the magnitude of differential rotation in the convection zones of stars, gaseous planets and accretion disks. That is, we aim to determine the approximate magnitude and scaling of $|\nabla\Omega|$ in these systems. **It is important to emphasise that our arguments are purely from an order-of-magnitude perspective.** In particular, we generally assume that dimensionless geometric factors are of order unity rather than being very small. We believe that this is likely in most cases, as the alternative is significant coincidence in the geometries of various fields that are determined by a variety of fundamentally dissimilar physical processes. Thus, for instance, we are agnostic on the question of whether baroclinic pumping or turbulent stresses play a greater role in the slow-rotation limit²⁸ because we find that they exhibit identical scaling and are related by a dimensionless factor of order unity.

We begin in Section 3.2 with a discussion of our assumptions. In Section 3.3 we examine the vorticity equation and derive the form which we use in all subsequent analysis. We then consider in turn magnetic fields²⁹, the condition of thermal equilibrium³⁰, and the thermal wind contribution³¹, deriving helpful expressions relating the magnitudes of different effects. Finally in Section 3.7 we introduce a perturbative paradigm which helps to organise the remainder of the calculation.

Subsequent sections of the paper focus on our key results. In Section 3.8 we derive the differential rotation in slowly rotating convection zones and find that

$$|\nabla\Omega| \approx \Omega R^{-1}.$$

In Section 3.10 we derive the same in rapidly rotating convection zones

²⁶ Brun & Palacios 2009; Klion & Quataert 2017

²⁷ Brun & Rempel 2009

²⁸ This has been a long-standing question. See Miesch et al. (2006) for a discussion of its status.

²⁹ Section 3.4

³⁰ Section 3.5

³¹ Section 3.6

and find that

$$|\nabla\Omega| \approx \Omega^{1/7} |N|^{6/7} R^{-1}$$

when the system is ionised and hence magnetised and

$$|\nabla\Omega| \approx \Omega^{1/3} |N|^{2/3} R^{-1}$$

otherwise. In both cases N is the Brunt-Väisälä frequency. In Section 3.12 we then discuss how the limit of rapid rotation transitions into a Keplerian state and find that the sub-Keplerian scaling of the rapid rotation limit necessarily becomes Keplerian once the scaling of effective gravity is taken into account. Taken together our results provide a unified theory of the magnitude of convective differential rotation which covers the full range from accretion discs to gas planets to the most massive stars.

The remainder of the paper is dedicated to comparisons with observations and simulations³². We find good agreement with data from the Sun, Jupiter and Red Giants. We likewise find good agreement with three-dimensional hydrodynamic and magnetohydrodynamic simulations of rotating convecting stars and planets even for extreme rotation rates. We conclude with a discussion of the limitations of our analysis³³ and a summary of our results³⁴.

³² Section 3.13

³³ Section 3.14

³⁴ Section 3.15

3.2 Assumptions

For simplicity we make a few assumptions.

1. Dimensionless factors arising from geometry are of order unity unless required to be otherwise.
2. All external perturbing forces such as tides or external heating are negligible in the regions of interest.
3. The material is non-degenerate and compressible ³⁵.
4. All microscopic³⁶ diffusivities are vanishingly small, such that:
 - Convection is efficient ³⁷.
 - Convection is well-developed ³⁸.
 - Magnetohydrodynamical processes are ideal.
 - Turbulent and/or advective processes are responsible for all macroscopic transport of heat, momentum and magnetism.
5. The system is axisymmetric in a time-averaged sense.
6. Convection is subsonic or, if supersonic, only mildly so.

³⁵ More specifically, we require that the entropy may be written in the form $a_1 \ln p - a_2 \ln \rho$ and the sound speed be related to the pressure by $c_s^2 = a_3 P / \rho$ for some $a_{1,2,3}$ of order unity. So for instance gases undergoing ionization or with a significant radiation component are still acceptable, but degenerate material with pressure and temperature decoupled is not.

³⁶ i.e. non-turbulent

³⁷ That is, the entropy gradient is much smaller than either the logarithmic pressure gradient or the logarithmic density gradient and an adiabatic law may be assumed except where the entropy gradient is the quantity of interest.

³⁸ That is, the Reynolds and Rayleigh numbers are much larger than critical.

7. The system is chemically homogeneous.

These assumptions are reasonable for the vast majority of systems and are generally not hard constraints. That is, small violations of them do not undermine our analysis. For instance the assumption that convection be subsonic is relied on implicitly in the relation $v_c \approx h|N|$, where h is the pressure scale height and $|N|$ is the Brunt-Väisälä frequency, in accordance with Böhm-Vitense (1992) and others. From a scaling perspective it is not a problem if convection is several-times supersonic, so long as this is just a proportionality constant independent of factors such as the rotation rate.

Similarly the assumption of axisymmetry is meant not in every instant but rather in a time-averaged sense. Thus for instance turbulence and dynamo cycles may produce temporary deviations from axisymmetry, but the long-run average behaviour must be axisymmetric. This is a much weaker condition which notably does not run afoul of Cowling's theorem ³⁹.

³⁹ Cowling 1933; Parker 1955

In Section 3.14 we discuss the limitations of our analysis in greater detail once it is complete. It is, however, worth discussing our treatment of geometric factors further at this stage. Broadly speaking there are two kinds of geometric factors which arise in this analysis, namely those associated with solutions to differential equations and those associated with the terms in those equations. We are highly concerned with the latter but pay less attention to the former. For instance a non-rotating self-gravitating system with no external or fossil magnetic fields is spherically symmetric and so even though the convective stresses do not vanish the angular momentum they transport does. Hence in the slowly-rotating regime there is a geometric factor associated with rotation breaking this symmetry. It relates the stress that transports angular momentum to that which does not. We pay significant attention to such terms. Similarly we pay considerable attention in our study of rapidly-rotating systems to the fact that the Taylor-Proudman term couples the azimuthal component of the vorticity to the projection of the differential rotation along the rotation axis but not to its projection along other axes. On the other hand we pay little attention to the geometric factors which result from precisely solving differential equations. In doing so we are, more or less, assuming that the boundary conditions imposed on the system are relatively generic, subject to whatever symmetries the system has. A consequence of this is that we generally avoid assuming that individual effects are tuned to be irrelevant in the solution unless their scaling properties make them so.

3.3 Vorticity

Here we derive the laws governing the evolution of angular momentum in axisymmetric systems, paying particular attention to the distinction between meridional and longitudinal contributions. We then argue that these systems are likely to be in a quasi-steady state and describe this steady state in the special case of a non-rotating system.

We begin by defining the vorticity of a fluid as

$$\boldsymbol{\omega} \equiv \nabla \times \mathbf{v}, \quad (3.1)$$

where \mathbf{v} is the velocity. Using equation (1.24) we see that in the absence of external forcing⁴⁰, the vorticity evolves according to

⁴⁰ e.g. tides

$$\frac{\partial \boldsymbol{\omega}}{\partial t} = \boldsymbol{\omega} \cdot \nabla \mathbf{v} - \boldsymbol{\omega} \nabla \cdot \mathbf{v} - \mathbf{v} \cdot \nabla \boldsymbol{\omega} + \frac{1}{\rho^2} \nabla \rho \times \nabla p + \nabla \times \left(\frac{1}{\rho} \nabla \cdot \mathbf{T} \right) + \nabla \times \left(\frac{\mathbf{F}_B}{\rho} \right), \quad (3.2)$$

where \mathbf{F}_B is the force due to the magnetic field, ρ is the density, p is the pressure and \mathbf{T} is the total fluid stress excluding magnetic effects. In particular T_{ij} is the flux along the unit vector \mathbf{e}_i of momentum along the direction \mathbf{e}_j .

The vorticity is the angular velocity of the fluid about a point, and so is closely related to the differential rotation. More explicitly, the connection between vorticity and differential rotation can be written in the limit where rotation dominates the flow as

$$\boldsymbol{\omega} = \boldsymbol{\Omega} + R \nabla \times (\boldsymbol{\Omega} \mathbf{e}_\phi),$$

where $\boldsymbol{\Omega}$ is the local angular velocity about the z axis and R is the cylindrical radial coordinate. We do not impose this limit, but it is worth keeping in mind as it gives an intuitive connection between vorticity and the force of rotation. In particular, it suggests that we should look to the meridional components of the vorticity for evidence of differential rotation.

We are interested in axisymmetric systems, where there is a natural distinction between the meridional and longitudinal components of the flow. To make this explicit we write the meridional flow as

$$\mathbf{u}(R, z) \equiv \mathbf{v}(R, z) - \Omega(R, z) R \mathbf{e}_\phi.$$

Then

$$\begin{aligned}
 \boldsymbol{\omega} \cdot \nabla \mathbf{v} &= \boldsymbol{\omega} \cdot \nabla \mathbf{u} + \boldsymbol{\omega} \cdot \nabla (\Omega R \mathbf{e}_\phi) \\
 &= \boldsymbol{\omega} \cdot \nabla \mathbf{u} - \mathbf{e}_R \Omega \omega_\phi + \mathbf{e}_\phi \boldsymbol{\omega} \cdot \nabla (\Omega R), \\
 \mathbf{v} \cdot \nabla \boldsymbol{\omega} &= \mathbf{u} \cdot \nabla \boldsymbol{\omega} + \Omega R \mathbf{e}_\phi \cdot \nabla \boldsymbol{\omega} \\
 &= \mathbf{u} \cdot \nabla \boldsymbol{\omega} - \Omega \omega_\phi \mathbf{e}_R + \Omega \omega_R \mathbf{e}_\phi,
 \end{aligned}$$

and

$$\begin{aligned}
 \boldsymbol{\omega} \nabla \cdot \mathbf{v} &= \boldsymbol{\omega} \nabla \cdot \mathbf{u} + \boldsymbol{\omega} \nabla \cdot (\mathbf{e}_\phi \Omega R) \\
 &= \boldsymbol{\omega} \nabla \cdot \mathbf{u}.
 \end{aligned}$$

Putting this together we find

$$\begin{aligned}
 \boldsymbol{\omega} \cdot \nabla \mathbf{v} - \boldsymbol{\omega} \nabla \cdot \mathbf{v} - \mathbf{v} \cdot \nabla \boldsymbol{\omega} \\
 &= \boldsymbol{\omega} \cdot \nabla \mathbf{u} - \mathbf{u} \cdot \nabla \boldsymbol{\omega} - \boldsymbol{\omega} \nabla \cdot \mathbf{u} \\
 &\quad + \mathbf{e}_\phi \boldsymbol{\omega} \cdot \nabla (\Omega R) - \mathbf{e}_\phi \Omega \omega_R.
 \end{aligned}$$

Combining this with equation (3.2) we find

$$\begin{aligned}
 \frac{\partial \boldsymbol{\omega}}{\partial t} &= \boldsymbol{\omega} \cdot \nabla \mathbf{u} - \boldsymbol{\omega} \nabla \cdot \mathbf{u} - \mathbf{u} \cdot \nabla \boldsymbol{\omega} + \mathbf{e}_\phi \boldsymbol{\omega} \cdot \nabla (\Omega R) - \mathbf{e}_\phi \Omega \omega_R \\
 &\quad + \frac{1}{\rho^2} \nabla \rho \times \nabla p + \nabla \times \left(\frac{1}{\rho} \nabla \cdot \mathbf{T} \right) + \nabla \times \left(\frac{\mathbf{F}_B}{\rho} \right). \quad (3.3)
 \end{aligned}$$

The first line of this equation describes kinematic effects associated with the geometry and the rotation. This includes the meridional circulation. The second line describes the effects of thermal wind, turbulent stresses and magnetic stresses respectively.

We now argue that astrophysical systems are likely to be near angular momentum equilibrium because the timescale over which shear turbulence transports momentum is quite short. This means both that the transient differential rotation associated with the formation of the system rings down rapidly to a more structured state (Fig. 3.1) but also that the secular evolution of the vorticity owing to nuclear evolution and wind losses may be neglected. To do this we first note that the diffusivity of shear turbulence over the whole system is of order

$$\nu \approx R^2 |\nabla \mathbf{v}|,$$

where R is the radius of the star. This is because the shear time-scale is set by $|\nabla \mathbf{v}|$ and its associated length-scale is set by the distance over which it

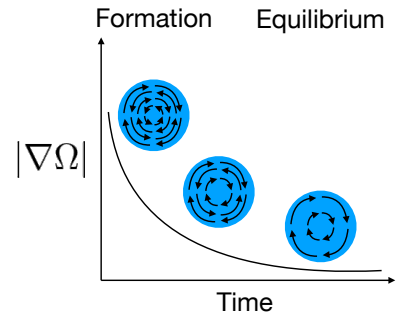


Figure 3.1: The ring-down of a system from an initial state with extreme and unstructured differential rotation to a steady state is shown schematically versus time. The final state need not obey solid-body rotation, but unlike the initial state it is not dependent on the details of the initial conditions and so is generally more structured.

persists. The diffusive timescale associated with a shear is therefore

$$\tau_{\text{diff}} \approx \frac{R^2}{\nu} \approx |\nabla \mathbf{v}|^{-1}.$$

When the star forms the differential rotation is likely at least of order ΩR^{-1} , because this is the scale expected for a collapsing gas cloud. As a result

$$|\nabla \mathbf{v}| \gtrsim \Omega^{-1}$$

and hence the transient highly-differential state rings down on a timescale

$$\tau_{\text{diff}} \lesssim \Omega^{-1}.$$

In practice this is an upper bound on the time-scale, because convective turbulence contributes as well. In systems which are rotating fast enough for differential rotation to be of interest, the rotation period is much shorter than the time-scale over which the system evolves, and so the system is likely to be in an instantaneous momentum equilibrium. So the secular evolution of the vorticity may be neglected in equation (3.3).

The only case of which we are aware in which this argument fails is in accretion discs, where the diffusivity is suppressed by the stability of non-magnetised Keplerian fluids, resulting in significantly less relative angular momentum transport and hence much longer equilibration time-scales. In this case, however, transients must ring-down on time-scales of order Ω^{-1} because non-Keplerian motion results in the fluid centrifugally adjusting its orbit on this time-scale. So once more we find that transient effects in the differential rotation decay quickly.

This is not the end of the story, however. Equation (3.3) supports linear oscillatory motions, such as Alfvén waves and sound waves, as well as non-linear instabilities such as those associated with the dynamo ⁴¹ and convection ⁴². We take these instabilities to have been averaged over, such that their root-mean-square effects appear in the stress tensor \mathbf{T} , and therefore neglect them wherever they appear in the vorticity equation. We also specifically neglect gravity waves because these damp rapidly in convection zones ⁴³.

Setting the time derivative in equation (3.3) to zero we find

$$\begin{aligned} 0 = & \boldsymbol{\omega} \cdot \nabla \mathbf{u} - \boldsymbol{\omega} \nabla \cdot \mathbf{u} - \mathbf{u} \cdot \nabla \boldsymbol{\omega} + \mathbf{e}_\phi \boldsymbol{\omega} \cdot \nabla (\Omega R) - \mathbf{e}_\phi \Omega \omega_R \\ & + \frac{1}{\rho^2} \nabla \rho \times \nabla p + \nabla \times \left(\frac{1}{\rho} \nabla \cdot \mathbf{T} \right) + \nabla \times \left(\frac{\mathbf{F}_B}{\rho} \right). \end{aligned} \quad (3.4)$$

⁴¹ Käpylä 2011

⁴² Böhm-Vitense 1958

⁴³ Fuller et al. 2014

Furthermore, in steady state conservation of mass requires

$$\nabla \cdot (\rho \mathbf{u}) = 0$$

so

$$\nabla \cdot \mathbf{u} = -\mathbf{u} \cdot \nabla \ln \rho. \quad (3.5)$$

Inserting this into equation (3.4) we find

$$\begin{aligned} 0 = & \boldsymbol{\omega} \cdot \nabla \mathbf{u} + \boldsymbol{\omega} \mathbf{u} \cdot \nabla \ln \rho - \mathbf{u} \cdot \nabla \boldsymbol{\omega} + \mathbf{e}_\phi \boldsymbol{\omega} \cdot \nabla (\Omega R) - \mathbf{e}_\phi \Omega \omega_R \\ & + \frac{1}{\rho^2} \nabla \rho \times \nabla p + \nabla \times \left(\frac{1}{\rho} \nabla \cdot \mathbf{T} \right) + \nabla \times \left(\frac{\mathbf{F}_B}{\rho} \right). \end{aligned} \quad (3.6)$$

At this stage it is useful to separate equation (3.6) into its meridional and \mathbf{e}_ϕ components. To do this we denote the projection of a vector into the meridional plane by the subscript m . In this notation then

$$\mathbf{u} \equiv \mathbf{v}_m.$$

Thus

$$\begin{aligned} 0 = & \boldsymbol{\omega}_m \cdot \nabla \mathbf{u} + \boldsymbol{\omega}_m \mathbf{u} \cdot \nabla \ln \rho + \mathbf{u} \cdot \nabla \boldsymbol{\omega}_m \\ & + \left[\nabla \times \left(\frac{1}{\rho} \nabla \cdot \mathbf{T} \right) \right]_m + \left[\nabla \times \left(\frac{\mathbf{F}_B}{\rho} \right) \right]_m \end{aligned} \quad (3.7)$$

and

$$\begin{aligned} 0 = & R^{-1} \omega_\phi u_R + \omega_\phi \mathbf{u} \cdot \nabla \ln \rho + \mathbf{u} \cdot \nabla \omega_\phi + \boldsymbol{\omega} \cdot \nabla (\Omega R) - \Omega \omega_R \\ & + \rho^{-2} \mathbf{e}_\phi \cdot \nabla \rho \times \nabla p + \mathbf{e}_\phi \cdot \nabla \times \left(\frac{1}{\rho} \nabla \cdot \mathbf{T} \right) + \mathbf{e}_\phi \cdot \nabla \times \left(\frac{\mathbf{F}_B}{\rho} \right). \end{aligned} \quad (3.8)$$

3.4 Magnetic Fields

The appearance of the magnetic field in the vorticity equation means that to close this equation we must address the source of magnetism. There are typically three sources of magnetic fields in the astrophysical context: fossil fields, turbulent dynamos, and externally imposed fields.

A fossil field is one present at the time of formation of the body. In convection zones the dynamo phenomenon processes magnetic fields on a variety of geometry-dependent time-scales. In the Sun these range from the convective turnover time, which is of order 10^6 s, up to several thousand

years. The longest of these time-scales is set by a variety of effects including the microscopic conductivity and the ratio of the convective time-scale to the rotation period. In any event this processing is quite rapid compared to the lifetime of the star, and so it appears that it may be neglected. Despite this it is possible for a fossil field to persist throughout the lifetime of the system if the convection zone is in contact with a magnetised radiative zone with little turbulence, as is the case for some white dwarfs and potentially in the Sun ⁴⁴. In this case the field may slowly leak out from the radiative zone over long time-scales. Consequently we cannot generically neglect fossil fields.

⁴⁴ Gough & McIntyre 1998; Gough 2017; Quentin & Tout 2018

Externally imposed magnetic fields are less common but nevertheless of astrophysical interest. For instance, in a star-pulsar binary system the star may be subject to significant magnetic fields which influence convection near the surface. From the perspective of a scaling analysis there is little difference between a fossil field and an externally imposed field. Both may break symmetries, including axisymmetry, and in both cases there is no a priori relationship between the magnitude of the field and other properties of the body. This means that these cases may be analysed together.

Such an analysis will wait for future work. For now we consider the many cases in which the fields are generated by turbulent dynamo processes. In such cases the field obeys the same symmetry, on average, as the turbulence which drives it, so its contribution vanishes in highly symmetric situations just as does the contribution of the turbulence. As a result the explicit contribution of the magnetic force may be absorbed into the turbulent stress, with the caveat that we must then account for this in determining the magnitude of that term. To that end we note that the magnetic force may be written as

$$\mathbf{F}_B = -\nabla \cdot \Pi_B,$$

where Π_B is given by equation (1.22) as

$$\Pi_{B,ij} \equiv -\frac{1}{4\pi} (B_i B_j - B^2 \delta_{ij}).$$

So the contribution to the stress tensor is just $-\Pi_B$. This scales proportional to ρv_A^2 , where

$$v_A \equiv \frac{B}{\sqrt{4\pi\rho}}$$

is the Alfvén speed. Hence what we must determine is how v_A compares with the characteristic velocity scale of the stress. For this there are two

regimes of interest, namely that of slow rotation and that of rapid rotation, which we discuss respectively in sections 3.8 and 3.10.

3.5 Thermal Equilibrium

Equations (3.7) and (3.8) involve the meridional circulation and the baroclinicity. In order to relate these we must close the system of equations with a study of heat transport. This analysis has all been conducted in equilibrium thus far so we do so through the equation of thermal equilibrium⁴⁵, which reads

$$\rho c_p T \mathbf{u} \cdot \nabla s + \nabla \cdot \mathbf{F} = 0, \quad (3.9)$$

where ρ is the density, c_p is the specific heat at constant pressure, T is the temperature, s is the dimensionless entropy given by equation (1.2) and

$$\mathbf{F} = \rho c_p T \mathbf{D} \cdot \nabla s \quad (3.10)$$

is the convective flux with diffusivity tensor \mathbf{D} . This tensor depends on the entropy gradient and so equation (3.10) is non-linear in s . For an ideal gas with homogeneous chemistry $p \propto \rho T$ so equation (3.9) may be written as

$$p \mathbf{u} \cdot \nabla s + \nabla \cdot (p \mathbf{D} \cdot \nabla s) = 0. \quad (3.11)$$

In the non-rotating limit this possesses barotropic solutions with ∇s and ∇p both radial. Outside of this limit that is generally not true, both because ∇p is distorted by the centrifugal effect⁴⁶ and because \mathbf{D} becomes anisotropic⁴⁷.

To proceed we define \mathbf{e}_p to be the unit vector along the pressure gradient and $\mathbf{e}_q \equiv \mathbf{e}_\phi \times \mathbf{e}_p$ to be a unit vector perpendicular to \mathbf{e}_p in the meridional plane. We likewise denote components of vectors by the subscripts p and q to mean the components along these unit vectors. It is also useful to define

$$\xi \equiv \frac{\mathbf{e}_\phi \cdot (\nabla \ln p \times \nabla s)}{|\nabla \ln p| |\nabla s|}, \quad (3.12)$$

which measures the extent to which the pressure and entropy gradients are misaligned. When ∇p and ∇s are nearly aligned, ξ measures the small angle between them. When they are further misaligned it approaches ± 1 . For convenience we also define

$$\bar{\xi} \equiv \sqrt{1 - \xi^2}.$$

⁴⁵ This is just equation (1.18) in steady state with $\epsilon = 0$, so that there is no heat generation. This is applicable in the bulk of the star or planet.

⁴⁶ Eddington 1929

⁴⁷ Kitchatinov 2013

With these definitions,

$$\nabla s = |\nabla s| (\mathbf{e}_p \bar{\xi} + \mathbf{e}_q \xi) \quad (3.13)$$

and

$$\mathbf{u} = \mathbf{e}_p u_p + \mathbf{e}_q u_q.$$

Hence equation (3.11) becomes

$$u_p \bar{\xi} + u_q \xi = -\frac{\nabla \cdot (p \mathbf{D} \cdot \nabla s)}{p |\nabla s|}. \quad (3.14)$$

It is now useful to relate ξ to the baroclinicity. This is given by

$$\lambda \equiv \frac{|\nabla \ln p \times \nabla \ln \rho|}{|\nabla \ln p| |\nabla \ln \rho|}, \quad (3.15)$$

which is directly proportional to the thermal wind term in equation (3.8). When ∇p and $\nabla \rho$ are nearly aligned, λ measures the small angle between them. When they are further misaligned λ approaches unity. In analogy with $\bar{\xi}$ we also define

$$\bar{\lambda} \equiv \sqrt{1 - \lambda^2}.$$

Equations (3.15) and (3.12) are related by equation (1.2), such that

$$\begin{aligned} \lambda &= \frac{|\nabla \ln p \times \frac{1}{\gamma} \nabla s|}{|\nabla \ln p| |\nabla \ln \rho|} \\ &= \frac{|\nabla s|}{\gamma |\nabla \ln \rho|} \xi. \end{aligned}$$

Recalling equation (1.2), the squared Brunt-Väisälä frequency is

$$\begin{aligned} N^2 &= -\gamma^{-1} \mathbf{g} \cdot \nabla s \\ &= -\frac{1}{\gamma \rho} \nabla p \cdot \nabla s \\ &= -\frac{p}{\gamma \rho} |\nabla \ln p| |\nabla s| \bar{\xi}, \end{aligned} \quad (3.16)$$

where there is a convectively unstable gradient. Thus

$$\lambda = \frac{-\rho N^2}{p |\nabla \ln \rho| |\nabla \ln p|} \frac{\xi}{\bar{\xi}}.$$

When ∇p and $\nabla \rho$ are aligned, $|\nabla \ln \rho| = \gamma^{-1} |\nabla \ln p|$ because convection enforces a near-adiabatic relation. When they are not the density gradient along the pressure gradient remains adiabatic because convective motions

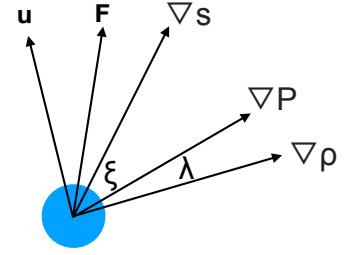


Figure 3.2: The vectors and angles which arise in analysing equation (3.9) are shown together. Note that the entropy gradient is on the opposite side of the pressure gradient from the density gradient. This is required by equation (1.2).

are primarily along the pressure gradient⁴⁸, so we instead find

$$|\nabla \ln \rho| = \frac{1}{\gamma \bar{\lambda}} |\nabla \ln p|, \quad (3.17)$$

so

$$\frac{\lambda}{\bar{\lambda}} = -\frac{\gamma \rho N^2}{p |\nabla \ln p|^2} \frac{\xi}{\bar{\xi}}.$$

Noting that

$$|\nabla \ln p| = h^{-1}, \quad (3.18)$$

where

$$h = \frac{p}{\rho g} \quad (3.19)$$

is the pressure scale height⁴⁹, we find

$$\frac{\lambda}{\bar{\lambda}} = -\frac{\gamma h^2 N^2 \rho}{p} \frac{\xi}{\bar{\xi}}.$$

Making use of $c_s = \sqrt{\gamma p / \rho}$ and ⁵⁰ $v_c \approx h|N|$ we find

$$\frac{\lambda}{\bar{\lambda}} = \gamma^3 \frac{v_c^2}{c_s^2} \frac{\xi}{\bar{\xi}}. \quad (3.20)$$

Thus λ and ξ are just related by a function of the convective Mach number

$$\mathcal{M} \equiv v_c / c_s.$$

Combining equation (3.20) with equations (3.5) and (3.17), we find

$$\begin{aligned} 0 &= \nabla \cdot (\rho \mathbf{u}) \\ &= \mathbf{u} \cdot \nabla \ln \rho + \nabla \cdot \mathbf{u}. \end{aligned}$$

We may evaluate the first term as

$$\begin{aligned} \mathbf{u} \cdot \nabla \ln \rho &= (u_p \mathbf{e}_p + u_q \mathbf{e}_q) \cdot \nabla \ln \rho \\ &= h(u_p \nabla \ln p + u_q \mathbf{e}_\phi \times \nabla \ln p) \cdot \nabla \ln \rho \\ &= |\nabla \ln \rho| (\lambda u_q + u_p \bar{\lambda}) \\ &= (h\gamma)^{-1} \left(\frac{\lambda}{\bar{\lambda}} u_q + u_p \right). \end{aligned} \quad (3.21)$$

The second may be expanded as

$$\begin{aligned} \nabla \cdot \mathbf{u} &= \nabla \cdot (\mathbf{e}_p u_p + \mathbf{e}_q u_q) \\ &= \mathbf{e}_p \cdot \nabla u_p + \mathbf{e}_q \cdot \nabla u_q + u_p \nabla \cdot \mathbf{e}_p + u_q \nabla \cdot \mathbf{e}_q. \end{aligned}$$

⁴⁸ This is because the pressure gradient is the source of the convective restoring force. See e.g. Fig. 16 of Chapter 2.

⁴⁹ Equation (3.19) arises from hydrostatic equilibrium. In systems with circulation currents, stresses, and differential rotation there are deviations from this, but these are only large when the rotation is nearly Keplerian, and so we may ignore such corrections except in that regime.

⁵⁰ Böhm-Vitense 1958

Because \mathbf{e}_p is parallel to the gravitational field its variation is set by the overall scale and symmetry of the system, rather than local thermodynamic properties. The unit vector \mathbf{e}_q is then determined as a linear function of \mathbf{e}_p and so varies over the same scales. Thus we expect that $\nabla \cdot \mathbf{e}_p \approx \nabla \cdot \mathbf{e}_q \approx 1/r$, where r is the spherical radial scale and comes in due to the large-scale structure of the system.

On the other hand u_p and u_q generally vary more rapidly than this because equation (3.14) shows that the velocity is related to the local condition of thermal equilibrium. As a result we expect that the variation of u_p and u_q is due to the variation of local thermodynamic properties as well as global effects having to do with the scale and symmetry of the system. Along the pressure gradient then

$$|\mathbf{e}_p \cdot \nabla \ln u_p| \approx |\mathbf{e}_q \cdot \nabla \ln u_q| \approx |\nabla \ln p| + r^{-1} = h^{-1} + r^{-1},$$

where once more r arises due to the large-scale structure of the system. Perpendicular to the pressure gradient only the density varies, so

$$|\mathbf{e}_q \cdot \nabla \ln u_p| \approx |\mathbf{e}_q \cdot \nabla \ln u_q| \approx |\mathbf{e}_q \cdot \nabla \ln \rho| + r^{-1} \approx \frac{\lambda}{\gamma \bar{\lambda} h} + r^{-1}.$$

In general the pressure scale height is somewhat less than the radius, so

$$|\nabla \cdot \mathbf{u}| \approx h^{-1}|u_p| + \left(\frac{\lambda}{\gamma \bar{\lambda} h} + r^{-1} \right) |u_q|,$$

where we have neglected the signs of terms and just written down their magnitudes. Incorporating this with equation (3.21) and dropping factors of order unity we find

$$|\nabla \cdot (\rho \mathbf{u})| = 0 \approx \frac{1}{h} \left(|u_p| + \left(\frac{h}{r} + \frac{\lambda}{\bar{\lambda}} \right) |u_q| \right),$$

where once more we have just written down the scaling of each term and have neglected potential signs, terms of order unity and geometric factors. Because we assume minimal geometric tuning it must be that motion along \mathbf{e}_p balances that along \mathbf{e}_q in this equation, so

$$|u_p| \approx \left(\frac{h}{r} + \frac{\lambda}{\bar{\lambda}} \right) |u_q|. \quad (3.22)$$

Inserting equation (3.22) into equation (3.14) we find

$$|u_q| \xi \left[1 + \frac{\bar{\xi}}{\xi} \left(\frac{h}{r} + \frac{\lambda}{\bar{\lambda}} \right) \right] \approx \frac{|\nabla \cdot (p \mathbf{D} \cdot \nabla s)|}{p |\nabla s|}.$$

Inserting equation (3.20) and dropping factors of order unity we find

$$|u_q|\xi \left[1 + \frac{\bar{\xi}h}{\xi r} + \mathcal{M}^2 \right] \approx \frac{|\nabla \cdot (p\mathbf{D} \cdot \nabla s)|}{p|\nabla s|}.$$

Examining equation (3.22) and using $h < r$ and⁵¹ $\lambda < \bar{\lambda}$ we see that $u_q > u_p$. Hence we may write the magnitude

$$u \approx u_q \approx \frac{|\nabla \cdot (p\mathbf{D} \cdot \nabla s)|}{p|\nabla s| \left[\xi(1 + \mathcal{M}^2) + \bar{\xi}h/r \right]}. \quad (3.23)$$

Equation (4.12) relates the magnitude of the meridional circulation to the conditions of thermal equilibrium, which in turn we related to the baroclinicity by the diffusivity tensor. This does not intrinsically mean that thermal equilibrium drives the circulation, just that thermal equilibrium demands that this equation be satisfied. Thus, for instance, if the vorticity equation is stiffer in the meridional circulation than the momentum equation it could be that the momentum equation drives a circulation, in which case the causation runs from left-to-right and the circulation determines the baroclinicity⁵². Likewise in the reverse case baroclinicity drives and determines the circulation⁵³. In fact both possibilities appear to occur depending on the context. An interesting result from recent simulations is that in the slow-rotation limit these two effects actually scale with rotation in a similar manner⁵⁴ with the momentum imbalance generally providing a somewhat stronger impetus. This may be why rather different approaches have historically had comparable success at explaining the observations.

⁵¹ This follows because were it not the case ∇p and $\nabla \rho$ would need to be at an angle of order unity relative to one another, which can only be the case near breakup rotational velocities.

⁵² Miesch & Toomre 2009; Brun & Rempel 2009

⁵³ Eddington 1929; Osaki 1982; Maeder & Zahn 1998

⁵⁴ Miesch & Toomre 2009

3.6 Thermal Wind

We now turn to the thermal wind term appearing in equations (3.8), namely $\rho^{-2}(\nabla p \times \nabla \rho)_\phi$. Noting that ∇p and $\nabla \rho$ lie in the meridional plane we find

$$|\rho^{-2}(\nabla p \times \nabla \rho)_\phi| = \frac{p}{\rho} |\nabla \ln p \times \nabla \ln \rho|.$$

Inserting equation (3.15) yields

$$|\rho^{-2}(\nabla p \times \nabla \rho)_\phi| = \frac{p}{\rho} |\nabla \ln p| |\nabla \ln \rho| \lambda.$$

Equation (3.17) then gives

$$|\rho^{-2}(\nabla p \times \nabla \rho)_\phi| = \frac{p}{\rho} |\nabla \ln p|^2 \frac{\lambda}{\gamma \bar{\lambda}}.$$

Recalling equations (3.18) and (3.19) we find

$$|\rho^{-2}(\nabla p \times \nabla \rho)_\phi| = \frac{g}{h} \frac{\lambda}{\gamma \bar{\lambda}}.$$

Neglecting factors of order unity such as γ we finally obtain

$$|\rho^{-2}(\nabla p \times \nabla \rho)_\phi| \approx \frac{g}{h} \frac{\lambda}{\bar{\lambda}}. \quad (3.24)$$

Hence the thermal wind term is purely determined by the baroclinicity.

3.7 Stiffness

We now introduce a concept which will be helpful in determining the magnitudes of terms in our equations, namely the stiffness of a solution. The stiffness indicates how strongly the solution of a differential equation responds to perturbations in its parameters. In this section we construct a basic framework for calculating this quantity.

Suppose we have a series of differential equations of the form

$$\mathcal{F}_i[\{\phi_j\}] = 0,$$

where each \mathcal{F} is a possibly-nonlinear yet local functional of each ϕ , and where some ϕ_j may be derivatives of other $\phi_{j'}$. If we perturb this system of equations by modifying one ϕ_k then

$$\mathcal{F}_i[\{\phi_j\}] = d\mathcal{F}_i = \frac{\delta \mathcal{F}_i}{\delta \phi_k} d\phi_k,$$

where δ indicates the functional derivative.⁵⁵ If we require a solution to the system of equations then the other variables must be perturbed such that $d\mathcal{F}_i = 0$, so

$$\sum_{j \neq k} \frac{\delta \mathcal{F}_i}{\delta \phi_j} d\phi_j = -\frac{\delta \mathcal{F}_i}{\delta \phi_k} d\phi_k.$$

So long as the number of variables exceeds the number of equations by one this linear system may be inverted to find

$$d\phi_j = -\sum_i \mathcal{J}_{ji}^{-1} \frac{\delta \mathcal{F}_i}{\delta \phi_k} d\phi_k = -\mathcal{J}^{-1} \cdot \mathbf{q} d\phi_k, \quad (3.25)$$

where

$$\mathcal{J}_{ij} \equiv \frac{\delta \mathcal{F}_i}{\delta \phi_j} \quad \forall j \neq k \quad (3.26)$$

⁵⁵ We could equally well perform this analysis using partial derivatives by discretising space and projecting our functions onto that discretisation, but such notation is considerably more cumbersome and obscures the analysis.

and

$$\mathbf{q} \equiv \frac{\delta \mathcal{F}_i}{\delta \phi_k}. \quad (3.27)$$

In keeping with our general neglect of geometric factors we now ignore the spatial dependence of \mathbf{q} as well as of \mathcal{J} and its inverse. We further specialise to the case of three equations, namely the heat equation and the meridional and azimuthal components of the vorticity equation. Because we have related the two components of the velocity in equation (3.22) and evaluated their derivatives, \mathbf{u} and its derivatives are determined for our purposes just by the scalar u . Likewise we parameterise the entropy gradient simply by ξ because $|\nabla s|$ must vary proportional to the total flux and we have evaluated the action of derivatives on this object ⁵⁶. Where we must be more cautious is with the rotation. We have not determined the differential rotation, indeed that is our goal, so we treat Ω and $R\nabla\Omega$ separately. We thus have four variables and three equations as desired. Slightly more carefully, note that there are two components of the meridional vorticity equation, but there are also two components of $R\nabla\Omega$, and so the count remains correct.

While in principle any variable could be taken to be the perturbing one, Ω is the natural choice. There is a continuum of solutions for systems at various rotation rates, and our concern is with how ξ , u and of course $R\nabla\Omega$ vary with Ω .

In practice using equation (5.34) we estimate the functional derivatives rather than compute them precisely, and as noted we are neglecting the spatial dependence of \mathcal{J} , so we treat \mathcal{J} as a regular matrix. When there are three equations this may be written as

$$\mathcal{J}_{ij}^{-1} = \frac{1}{\det(\mathcal{J})} \epsilon_{ilk} \mathcal{J}_{lp} \mathcal{J}_{km} \epsilon_{pmj},$$

where ϵ_{ijk} is the Levi-Civita symbol. Hence

$$\frac{d\phi_i}{d\phi_j} = -\frac{1}{\det(\mathcal{J})} \epsilon_{ilk} \epsilon_{pmj} \mathcal{J}_{lp} \mathcal{J}_{km} \mathbf{q}_j.$$

3.8 Slow Rotation

In the special case of a non-rotating body with no fossil field, every term in the vorticity equation vanishes. This follows from symmetry, as the only preferred direction is radial, which implies that the system is spherically symmetric. All vector fields of interest must therefore be radial. Every term in the vorticity equation results from the curl of a vector field, and the curl

⁵⁶ Specifically, derivatives are broken into a contribution from the simultaneous variation of pressure and density, which contribute a factor of h^{-1} multiplied by the projection of the derivative direction on to those gradients, and a contribution from the geometry, which produces a factor of r^{-1} .

of a radial field with spherical symmetry is zero and consequently every term in equation (3.6) vanishes. This provides a useful starting point for perturbation theory in the slow-rotation limit. Note that here slow is with respect to the Brunt-Väisälä frequency $|N|$, so we assume that $\Omega \ll |N|$.

3.8.1 Magnetic Field

When the rotation is slow relative to the convective turnover time, the field approaches equipartition with the turbulent flow ⁵⁷ and the Alfvén speed v_A is comparable to the convection speed. This is what is typically found in simulations ⁵⁸ even up to rotation rates comparable to the turnover time ⁵⁹. So in this regime the magnetic term scales with the turbulent term, and we only need to retain one of these terms in the angular momentum balance to capture the scaling. Because there are situations in which the magnetic term is sub-dominant, such as weakly ionised fluids, we choose to retain the turbulent term. With this equations (3.7) and (3.8) become

$$0 = \boldsymbol{\omega}_m \cdot \nabla \mathbf{u} + \boldsymbol{\omega}_m \mathbf{u} \cdot \nabla \ln \rho + \mathbf{u} \cdot \nabla \boldsymbol{\omega}_m + \left[\nabla \times \left(\frac{1}{\rho} \nabla \cdot \mathbf{T} \right) \right]_m \quad (3.28)$$

and

$$0 = R^{-1} \omega_\phi u_R + \omega_\phi \mathbf{u} \cdot \nabla \ln \rho + \mathbf{u} \cdot \nabla \boldsymbol{\omega}_\phi + \boldsymbol{\omega} \cdot \nabla (\Omega R) - \Omega \omega_R + \rho^{-2} \mathbf{e}_\phi \cdot \nabla p \times \nabla \rho + \mathbf{e}_\phi \cdot \nabla \times \left(\frac{1}{\rho} \nabla \cdot \mathbf{T} \right). \quad (3.29)$$

3.8.2 Stress

When there is symmetry breaking the solution is generally quite complicated, but it may be understood by examining the scaling of each term in equations (3.7) and (3.8). We have already discussed the magnetic and meridional flow terms, so we turn to the contributions from the convective stress. When the rotation is slow the turbulence is primarily convective, with characteristic length scale h and characteristic time scale $|N|^{-1}$. So ⁶⁰

$$\mathbf{T} \approx \rho h^2 |N|^2,$$

where \mathbf{T} is the typical magnitude of entries in \mathbf{T} .

⁵⁷ Roberts & Glatzmaier 2000; Sreenivasan & Jones 2006

⁵⁸ Hotta et al. 2015; Augustson et al. 2011

⁵⁹ Augustson et al. 2013

⁶⁰ Böhm-Vitense 1958

In the non-rotating limit $T \neq 0$, and by symmetry must be of the form

$$\mathbf{T} \approx \begin{pmatrix} T_{rr} & 0 & 0 \\ 0 & T_{\theta\theta} & 0 \\ 0 & 0 & T_{\phi\phi} \end{pmatrix},$$

where we have written this tensor in spherical coordinates and the diagonal terms are of the same order of magnitude ⁶¹. In this limit we know that

$$\nabla \times \left(\frac{1}{\rho} \nabla \cdot \mathbf{T} \right) = 0.$$

That is, the angular momentum transported by turbulence is protected by spherical symmetry. Hence we find

$$\nabla \times \left(\frac{1}{\rho} \nabla \cdot \mathbf{T} \right) = \nabla \times \left(\frac{1}{\rho} \nabla \cdot \mathbf{T} \right) - \nabla \times \left(\frac{1}{\rho} \nabla \cdot \mathbf{T} \right) \Big|_{\Omega=0}.$$

When there is rotation this symmetry is broken and \mathbf{T} is perturbed as ⁶²

$$\mathbf{T} \approx \begin{pmatrix} T_{rr,0} \left(1 + \frac{\Omega^2}{|N|^2} \right) & \frac{\Omega^2}{|N|^2} & \frac{\Omega}{|N|} \\ \frac{\Omega^2}{|N|^2} & T_{\theta\theta,0} \left(1 + \frac{\Omega^2}{|N|^2} \right) & \frac{\Omega}{|N|} \\ \frac{\Omega}{|N|} & \frac{\Omega^2}{|N|^2} & T_{\phi\phi,0} \left(1 + \frac{\Omega^2}{|N|^2} \right) \end{pmatrix},$$

where we have neglected dimensionless factors of order unity which multiply the various factors of $\Omega/|N|$. The first order perturbations arise in the $r\phi$, ϕr , $\phi\theta$ and $\theta\phi$ components because the Coriolis effect couples motion along other directions to motion along \mathbf{e}_ϕ , while the perturbations to the remaining components are second order because a second application of the Coriolis effect is required to couple motion along two directions neither of which is \mathbf{e}_ϕ . Finally, the perturbations on the diagonal are second order, both because of the centrifugal effect and because it takes two applications of the Coriolis effect to couple motion in a direction to itself.

To proceed further we must know which stress components appear in which parts of the vorticity equation. In spherical coordinates we write

$$\mathbf{T} = \begin{pmatrix} T_{rr} & T_{r\theta} & T_{r\phi} \\ T_{\theta r} & T_{\theta\theta} & T_{\theta\phi} \\ T_{\phi r} & T_{\phi\theta} & T_{\phi\phi} \end{pmatrix},$$

where T_{ij} refers to momentum along \mathbf{e}_j being transported along \mathbf{e}_i . The stress terms appearing in equation (3.2) are then ⁶³

⁶¹ Gough 1978

⁶² See Chapter 2 and Kitchatinov (2013).

⁶³ This calculation was performed with Mathematica (Inc., 2016).

$$\begin{aligned}\nabla \times \left(\frac{1}{\rho} \nabla \cdot \mathbf{T} \right)_r &= \frac{1}{r^2 \rho^2} \left[\rho \partial_\theta \mathbf{T}_{r\phi} + \mathbf{T}_{r\phi} (\cot(\theta) \rho - \partial_\theta \rho) \right. \\ &\quad + \cot(\theta) \rho \partial_\theta \mathbf{T}_{\theta\phi} - \mathbf{T}_{\theta\phi} (\cot(\theta) \partial_\theta \rho + \rho) \\ &\quad - r \partial_\theta \rho \partial_r \mathbf{T}_{\phi r} + 2 \rho \partial_\theta \mathbf{T}_{\phi r} + r \rho \partial_r \partial_\theta \mathbf{T}_{\phi r} \\ &\quad + r \cot(\theta) \rho \partial_r \mathbf{T}_{\phi r} - 2 \partial_\theta \rho \mathbf{T}_{\phi r} + 2 \cot(\theta) \rho \mathbf{T}_{\phi r} \\ &\quad - \partial_\theta \rho \partial_\theta \mathbf{T}_{\phi\theta} + \rho \partial_\theta^2 \mathbf{T}_{\phi\theta} + 2 \cot(\theta) \rho \partial_\theta \mathbf{T}_{\phi\theta} \\ &\quad \left. - \cot(\theta) \partial_\theta \rho \mathbf{T}_{\phi\theta} - \rho \mathbf{T}_{\phi\theta} \right],\end{aligned}$$

$$\begin{aligned}\nabla \times \left(\frac{1}{\rho} \nabla \cdot \mathbf{T} \right)_\theta &= \frac{1}{r \rho^2} \left[\partial_r \rho (\mathbf{T}_{r\phi} + \cot(\theta) (\mathbf{T}_{\theta\phi} + \mathbf{T}_{\phi\theta})) \right. \\ &\quad + r \partial_r \mathbf{T}_{\phi r} + 2 \mathbf{T}_{\phi r} + \partial_\theta \mathbf{T}_{\phi\theta}) \\ &\quad - \rho (\partial_r \mathbf{T}_{r\phi} + \cot(\theta) \partial_r (\mathbf{T}_{\theta\phi} + \partial_r \mathbf{T}_{\phi\theta})) \\ &\quad \left. + 3 \partial_r \mathbf{T}_{\phi r} + r \partial_r^2 \mathbf{T}_{\phi r} + \partial_r \partial_\theta \mathbf{T}_{\phi\theta} \right]\end{aligned}$$

and

$$\begin{aligned}\nabla \times \left(\frac{1}{\rho} \nabla \cdot \mathbf{T} \right)_\phi &= \frac{1}{r^2 \rho^2} \left[\rho (-2 \partial_\theta \mathbf{T}_{rr} - \partial_\theta^2 \mathbf{T}_{r\theta} \right. \\ &\quad - \cot(\theta) \partial_\theta \mathbf{T}_{r\theta} + \partial_\theta \mathbf{T}_{\theta\theta} + \partial_\theta \mathbf{T}_{\phi\phi}) \\ &\quad + r (-\partial_r \partial_\theta \mathbf{T}_{rr} + \partial_r \mathbf{T}_{r\theta} + 3 \partial_r \mathbf{T}_{\theta r} + r \partial_r^2 \mathbf{T}_{\theta r} \\ &\quad + \partial_r \partial_\theta \mathbf{T}_{\theta\theta} + \cot(\theta) \partial_r (\mathbf{T}_{\theta\theta} - \partial_r \mathbf{T}_{\phi\phi})) \\ &\quad + \partial_\theta \rho (r \partial_r \mathbf{T}_{rr} + 2 \mathbf{T}_{rr} + \partial_\theta \mathbf{T}_{r\theta} - \mathbf{T}_{\theta\theta} - \mathbf{T}_{\phi\phi}) \\ &\quad + \mathbf{T}_{r\theta} (-r \partial_r \rho + \cot(\theta) \partial_\theta \rho + \csc^2(\theta) \rho) \\ &\quad - r \partial_r \rho (r \partial_r \mathbf{T}_{\theta r} + 2 \mathbf{T}_{\theta r} + \partial_\theta \mathbf{T}_{\theta\theta} \\ &\quad \left. + \cot(\theta) (\mathbf{T}_{\theta\theta} - \mathbf{T}_{\phi\phi})) \right].\end{aligned}$$

Inspection of these equations reveals that only the off-diagonal components of \mathbf{T} contribute to the r and θ components of the vorticity equation, while all but the $r\phi$, θr , ϕr , and $r\theta$ components of \mathbf{T} contribute to the ϕ component of the vorticity equation. As before we take radial gradients to produce factors of h^{-1} and latitudinal ones to produce factors of $r^{-1} + h^{-1}\lambda/\bar{\lambda}$. Because λ is small and $h < r$, terms with fewer latitudinal derivatives are dominant. In equation (3.30) there are several terms involving just one latitudinal derivative which are perturbed at first order, so these are the most important. In equation (3.31) there is a term involving no latitudinal derivatives which is perturbed at first order, so that is the dominant term. In equation (3.32) there is one term which is perturbed at leading order⁶⁴ and which has only radial derivatives, so that is the important term. Hence

⁶⁴ In this case the leading order is quadratic.

we find that

$$\nabla \times \left(\frac{1}{\rho} \nabla \cdot \mathbf{T} \right)_r \approx \frac{1}{\rho h^2} \left(\frac{h}{r} + \frac{\lambda}{\bar{\lambda}} \right) \mathbf{T} \frac{\Omega}{|N|}, \quad (3.30)$$

$$\nabla \times \left(\frac{1}{\rho} \nabla \cdot \mathbf{T} \right)_\theta \approx \frac{1}{\rho h^2} \mathbf{T} \frac{\Omega}{|N|} \quad (3.31)$$

and

$$\nabla \times \left(\frac{1}{\rho} \nabla \cdot \mathbf{T} \right)_\phi \approx \frac{1}{\rho h^2} \mathbf{T} \frac{\Omega^2}{|N|^2}. \quad (3.32)$$

Differential rotation likewise breaks spherical symmetry. The $r\phi$, ϕr , $\theta\phi$ and $\phi\theta$ components of \mathbf{T} break this symmetry at first order because they directly couple to the shear, while the remaining terms break the symmetry at second order both by coupling to the shear twice and by coupling once to the shear and once to the rotation itself. To see this note that the differential rotation acts in the plane of \mathbf{e}_ϕ and the shear direction, so if motions along \mathbf{e}_r , \mathbf{e}_θ and \mathbf{e}_ϕ are not correlated initially then motions between \mathbf{e}_r and \mathbf{e}_θ cannot be coupled at first order by the differential rotation. Thus either the Coriolis effect is needed to couple these components or else a higher order perturbation is needed. For the same reason the differential rotation cannot perturb the diagonal components of \mathbf{T} to first order, and two applications are needed to turn motion along, say, \mathbf{e}_r into motion along another axis and back into motion along \mathbf{e}_r . Another way to understand this is to note that the mapping $v_\phi \rightarrow -v_\phi$ also maps $\Omega \rightarrow -\Omega$ and $\nabla\Omega \rightarrow -\nabla\Omega$, which may be undone by then letting $\phi \rightarrow -\phi$. This spatial transformation negates the components of \mathbf{T} which involve the direction \mathbf{e}_ϕ an odd number of times but not those involving it an even number of times⁶⁵, and so the latter must be even functions of Ω . It follows that they must be at least quadratic in Ω and hence only terms of the form $\Omega|R\nabla\Omega|$ and $|R\nabla\Omega|^2$ are allowed at leading order. This is in agreement with the model of [Kitchatinov et al. \(1994\)](#).

Based on these symmetry arguments we write the leading order term in the differential rotation

$$\nabla \times \left(\frac{1}{\rho} \nabla \cdot \mathbf{T} \right)_r \approx \frac{1}{\rho h^2} \left(\frac{h}{r} + \frac{\lambda}{\bar{\lambda}} \right) \mathbf{T} \frac{R\nabla\Omega}{|N|}, \quad (3.33)$$

$$\nabla \times \left(\frac{1}{\rho} \nabla \cdot \mathbf{T} \right)_\theta \approx \frac{1}{\rho h^2} \mathbf{T} \frac{|R\nabla\Omega|}{|N|}$$

⁶⁵ One might ask why this transformation is not also undone by letting $z \rightarrow -z$. The reason is that while \mathbf{v} is a vector, Ω is a pseudovector generated by a cross-product with \mathbf{e}_ϕ , so its component along the \mathbf{e}_z axis is left invariant upon reflection about that axis.

and

$$\nabla \times \left(\frac{1}{\rho} \nabla \cdot \mathbf{T} \right)_{\phi} \approx \frac{1}{\rho h^2} \mathbf{T} \frac{\Omega |R \nabla \Omega|}{|N|^2}.$$

A similar argument produces the couplings to the meridional circulation, which is rather symmetric with respect to the meridional plane and hence

$$\begin{aligned} \nabla \times \left(\frac{1}{\rho} \nabla \cdot \mathbf{T} \right)_r &\approx \frac{1}{\rho h^2} \left(\frac{h}{r} + \frac{\lambda}{\bar{\lambda}} \right) \mathbf{T} \frac{|\nabla \mathbf{u}|}{|N|} \left(\frac{\Omega}{|N|} + \frac{|R \nabla \Omega|}{|N|} \right), \\ \nabla \times \left(\frac{1}{\rho} \nabla \cdot \mathbf{T} \right)_{\theta} &\approx \frac{1}{\rho h^2} \mathbf{T} \frac{|\nabla \mathbf{u}|}{|N|} \left(\frac{\Omega}{|N|} + \frac{|R \nabla \Omega|}{|N|} \right) \end{aligned}$$

and

$$\nabla \times \left(\frac{1}{\rho} \nabla \cdot \mathbf{T} \right)_{\phi} \approx \frac{1}{\rho h^2} \mathbf{T} \frac{|\nabla \mathbf{u}|}{|N|}. \quad (3.34)$$

That is, \mathbf{u} only couples to the stress via the perturbed terms in the meridional vorticity equation whereas it couples directly in the azimuthal component.

Note that the couplings in equations (3.30) and (3.31) are the leading order contributions to the Λ -effect⁶⁶, while those in equations (3.33)–(3.34) produce an effective turbulent viscosity with magnitude $|N|^{-1} \mathbf{T}$ ⁶⁷. These expansions are consistent with standard closure models such as those used by Gough (2012) and Lesaffre et al. (2013), as well as with simulations of slowly rotation convection⁶⁸.

There is one further effect which may contribute to the stress at leading order, namely baroclinicity⁶⁹. This effect lies inside the meridional plane and hence is invariant with respect to the mapping $\phi \rightarrow -\phi$. It follows that it only contributes at leading order to components of \mathbf{T} which incorporate the direction \mathbf{e}_{ϕ} an even number of times. As a result

$$\nabla \times \left(\frac{1}{\rho} \nabla \cdot \mathbf{T} \right)_{\phi} \approx \frac{1}{\rho h^2} \mathbf{T} \xi.$$

In order to couple ξ into the remaining components of the vorticity equation we need other effects to break this symmetry. Hence

$$\nabla \times \left(\frac{1}{\rho} \nabla \cdot \mathbf{T} \right)_r \approx \frac{1}{\rho h^2} \left(\frac{h}{r} + \frac{\lambda}{\bar{\lambda}} \right) \mathbf{T} \xi \left(\frac{|\nabla \mathbf{u}|}{|N|} + \frac{\Omega}{|N|} + \frac{|R \nabla \Omega|}{|N|} \right)$$

and

$$\nabla \times \left(\frac{1}{\rho} \nabla \cdot \mathbf{T} \right)_{\theta} \approx \frac{1}{\rho h^2} \mathbf{T} \xi \left(\frac{|\nabla \mathbf{u}|}{|N|} + \frac{\Omega}{|N|} + \frac{|R \nabla \Omega|}{|N|} \right).$$

⁶⁶ For a discussion of this effect see Chapter 2.

⁶⁷ Ruediger 1989; Kitchatinov 2013

⁶⁸ Käpylä et al. 2011

⁶⁹ See Chapter 2 and Ruediger (1989).

Putting it all together we find

$$\begin{aligned}\nabla \times \left(\frac{1}{\rho} \nabla \cdot \mathbf{T} \right)_r &\approx \left(\frac{h}{r} + \frac{\lambda}{\bar{\lambda}} \right) |N| (\Omega + |R \nabla \Omega|) \\ &\quad + |N|^2 \left(\xi + \frac{u}{h|N|} + \frac{\Omega}{|N|} + \frac{|R \nabla \Omega|}{|N|} \right)^2, \\ \nabla \times \left(\frac{1}{\rho} \nabla \cdot \mathbf{T} \right)_\theta &\approx |N| (\Omega + |R \nabla \Omega|) \\ &\quad + |N|^2 \left(\xi + \frac{u}{h|N|} + \frac{\Omega}{|N|} + \frac{|R \nabla \Omega|}{|N|} \right)^2\end{aligned}$$

and

$$\nabla \times \left(\frac{1}{\rho} \nabla \cdot \mathbf{T} \right)_\phi \approx |N|^2 \left(\xi + \frac{u}{h} + \frac{\Omega^2}{|N|^2} + \frac{\Omega |R \nabla \Omega|}{|N|^2} \right),$$

where we have used the fact⁷⁰ that $|\nabla \mathbf{u}| \approx u/h$ and where we have added additional terms at higher order to permit a more compact representation. These are not necessarily present, though there is no symmetry which prohibits them.

⁷⁰ See Section 3.5.

3.9 Advective Terms

We now evaluate the various terms directly involving either \mathbf{u} or $\boldsymbol{\omega}$. We begin with the meridional vorticity equation. The first term is $\boldsymbol{\omega}_m \cdot \nabla \mathbf{u}$. Expanding equation (4.10) and projecting into the meridional plane we find

$$\boldsymbol{\omega}_m = \mathbf{e}_r \left(2 \cos \theta \Omega + \sin \theta \frac{\partial \Omega}{\partial \theta} \right) - \mathbf{e}_\theta \sin \theta \left(2\Omega + r \frac{\partial \Omega}{\partial r} \right). \quad (3.35)$$

Expanding \mathbf{u} in the basis formed by the pressure gradient and the perpendicular unit vector in the meridional plane we obtain

$$\mathbf{u} = u_p \mathbf{e}_p + u_q \mathbf{e}_q.$$

When the system is slowly rotating, $\mathbf{e}_p \approx \mathbf{e}_r$ and $\mathbf{e}_q \approx \mathbf{e}_\theta$, with corrections to both of order λ . Neglecting such corrections we find

$$\begin{aligned}\boldsymbol{\omega}_m \cdot \nabla \mathbf{u} &\approx \mathbf{e}_r [\partial_r u_r (2 \cos \theta \Omega + \sin \theta \partial_\theta \Omega) \\ &\quad - \sin \theta \partial_r u_\theta (2\Omega + r \partial_r \Omega)] \\ &\quad + \frac{1}{r} \mathbf{e}_\theta [(\partial_\theta u_r - u_\theta) (2 \cos \theta \Omega + \sin \theta \partial_\theta \Omega) \\ &\quad - \frac{\sin \theta}{r} (2\Omega + r \partial_r \Omega) (u_r + \partial_\theta u_\theta)].\end{aligned}$$

Making the approximation that radial derivatives of \mathbf{u} produce factors of h^{-1} while latitudinal derivatives produce factors of r^{-1} and taking $h \ll r$ we find

$$|\boldsymbol{\omega}_m \cdot \nabla \mathbf{u}| \approx \frac{1}{h} [\Omega u_r + \Omega u_\theta + u_r |R \nabla \Omega| + u_\theta |R \nabla \Omega|],$$

where we have estimated $\partial_\theta \Omega$ and $r \partial_r \Omega$ by $|R \nabla \Omega|$. Equation (3.22) then tells us that $u \approx u_\theta \ll u_r$ so

$$|\boldsymbol{\omega}_m \cdot \nabla \mathbf{u}| \approx \frac{u}{h} [\Omega + |R \nabla \Omega|].$$

The relative corrections to this are at least of order h/r , λ and $\Omega/|N|$. Because the non-rotating system is spherically symmetric λ must be at least of order $\Omega/|N|$, hence this expansion is accurate to leading order in both h/r and $\Omega/|N|$.

We next turn to the term $\boldsymbol{\omega}_m \mathbf{u} \cdot \nabla \ln \rho$. The magnitude of this is just

$$|\boldsymbol{\omega}_m \mathbf{u} \cdot \nabla \ln \rho| = |\boldsymbol{\omega}_m| |\mathbf{u} \cdot \nabla \ln \rho|.$$

The first term we may find using equation (3.35) to be

$$|\boldsymbol{\omega}_m| = \sqrt{4\Omega^2 + |R \nabla \times (\Omega \mathbf{e}_\phi)|^2 + 4\Omega \cdot R \nabla \times (\Omega \mathbf{e}_\phi)}.$$

Approximating the radical by the sum of the square roots of its parts, which is of the same order of magnitude in the absence of significant geometric coincidence, and neglecting factors of order unity we find

$$|\boldsymbol{\omega}_m| = |R \nabla \Omega| + \Omega. \quad (3.36)$$

The remaining term we have already computed in equation (3.21) and found to be

$$|\mathbf{u} \cdot \nabla \ln \rho| \approx \frac{1}{h\gamma} \left(u_p + u_q \frac{\lambda}{\bar{\lambda}} \right).$$

Inserting equation (3.22) and dropping factors of order unity we find

$$|\mathbf{u} \cdot \nabla \ln \rho| \approx \frac{u}{h} \left(\frac{h}{r} + \frac{\lambda}{\bar{\lambda}} \right),$$

hence

$$|\boldsymbol{\omega}_m \mathbf{u} \cdot \nabla \ln \rho| \approx \frac{u}{h} (|R \nabla \Omega| + \Omega) \left(\frac{h}{r} + \frac{\lambda}{\bar{\lambda}} \right)$$

as desired.

Finally we examine the term $\mathbf{u} \cdot \nabla \boldsymbol{\omega}_m$. Again using $\mathbf{e}_p \approx \mathbf{e}_r$ and $\mathbf{e}_q \approx \mathbf{e}_\theta$ we find

$$\begin{aligned} \mathbf{u} \cdot \nabla \boldsymbol{\omega}_m &\approx \mathbf{e}_r [u_r (2 \cos \theta \partial_r \Omega + \sin \theta \partial_r \partial_\theta \Omega) \\ &\quad + \frac{u_\theta}{r} (3 \cos \theta \partial_\theta \Omega + \sin \theta (\partial_\theta^2 \Omega + r \partial_r \Omega))] \\ &\quad - \mathbf{e}_\theta [u_r \sin \theta (3 \partial_r \Omega + r \partial_r^2 \Omega) \\ &\quad + \frac{u_\theta}{r} (r \cos \theta \partial_r \Omega + \sin \theta (\partial_\theta \Omega + r \partial_r \partial_\theta \Omega))] . \end{aligned}$$

Making the same approximations as in equation (3.36) we find

$$|\mathbf{u} \cdot \nabla \boldsymbol{\omega}_m| \approx \frac{u}{h} [\Omega + |R \nabla \Omega|] .$$

We now turn to the azimuthal vorticity equation. The first term is $R^{-1} \omega_\phi u_R$. Expanding the azimuthal vorticity we find

$$\omega_\phi = \partial_r u_\theta + r^{-1} u_\theta - r^{-1} \partial_\theta u_r . \quad (3.37)$$

Noting that $u_\theta \approx u_q \approx u$ we may approximate the first term by u/h . This is larger than the remaining terms, so

$$\omega_\phi \approx \frac{u}{h} .$$

Hence

$$R^{-1} \omega_\phi u_R \approx \frac{u_R u}{h R}$$

Averaged over latitudes u_R projects comparably onto both u_q and u_p , so $u_R \approx u$ hence

$$|R^{-1} \omega_\phi u_R| \approx \frac{u^2}{h R} .$$

The next term is $\boldsymbol{\omega} \cdot \nabla(\Omega R)$. Using equation (3.35) we find

$$\boldsymbol{\omega} \cdot \nabla(\Omega R) = -\Omega \sin \theta (r \cos \theta \partial_r \Omega - \partial_\theta \Omega \sin \theta) .$$

Neglecting the geometric factors this is just

$$|\boldsymbol{\omega} \cdot \nabla(\Omega R)| \approx \Omega |R \nabla \Omega|$$

as desired.

The next term is $\mathbf{u} \cdot \nabla \omega_\phi$. Expanding the vorticity as in equation (3.37)

we find

$$\begin{aligned} \mathbf{u} \cdot \nabla \omega_\phi &\approx \frac{\mathbf{e}_\phi}{r^2} \left[u_\theta \left(\partial_\theta u_\theta - \partial_\theta^2 u_r + r \partial_r \partial_\theta u_\theta \right) \right. \\ &\quad \left. + u_r \left(\partial_\theta u_r - u_\theta + r \left(\partial_r u_\theta - \partial_r \partial_\theta u_r + r \partial_r^2 u_\theta \right) \right) \right]. \end{aligned}$$

This contains a term involving two radial derivatives and $u_\theta \approx u_q \approx u$ so that term dominates the expression. Hence we write

$$|\mathbf{u} \cdot \nabla \omega_\phi| \approx \frac{u^2}{h^2}.$$

The next term is $\Omega \omega_R$. Writing the vorticity in cylindrical coordinates we see that

$$\boldsymbol{\omega} = \mathbf{e}_R(-R\partial_z \Omega) + \mathbf{e}_z(2\Omega + R\partial_r \Omega) + \mathbf{e}_\phi(\partial_z u_r - \partial_r u_z).$$

Hence,

$$|\Omega \omega_R| = |R\Omega \partial_z \Omega| \approx \Omega |R\nabla \Omega|.$$

The final term is $\omega_\phi \mathbf{u} \cdot \nabla \ln \rho$. The first factor is given in spherical polar coordinates as

$$\omega_\phi = \partial_r u_\theta + r^{-1} u_\theta - r^{-1} \partial_\theta u_r.$$

Noting that $u_\theta \approx u_q \approx u$ we may approximate the first term by u/h . This is larger than the remaining terms, so

$$\omega_\phi \approx \frac{u}{h}.$$

The remaining piece of this term we have already computed in equation (3.21), so

$$|\omega_\phi \mathbf{u} \cdot \nabla \ln \rho| \approx \frac{u^2}{h^2} |N|^2 \left(\frac{h}{r} + \frac{\lambda}{\bar{\lambda}} \right).$$

We have only incurred errors of order h/r and $\lambda/\bar{\lambda}$ in computing this term because we have approximated u_θ by u , so the expansion is accurate to leading order in both factors. These results as well as those from earlier sections are summarised in Table 3.1.

3.9.1 Baroclinicity

To proceed further we must determine the baroclinicity. To do so we note that the diffusivity tensor is of the form ⁷¹

⁷¹ Rüdiger et al. 2005b; Lesaffre et al. 2013

| Term | Magnitude |
|---|--|
| Meridional (3.28) | |
| $\boldsymbol{\omega}_m \cdot \nabla_m \mathbf{u}$ | $\frac{u}{h}(\Omega + R\nabla\Omega)$ |
| $\boldsymbol{\omega}_m \mathbf{u} \cdot \nabla \ln \rho$ | $\frac{u}{h}(\Omega + R\nabla\Omega) \left(\frac{h}{r} + \frac{\lambda}{\lambda} \right)$ |
| $\left(\nabla \times \left(\frac{1}{\rho} \nabla \cdot \mathbf{T} \right) \right)_m$ | $ N (\Omega + R\nabla\Omega) + N ^2 \left(\xi + \frac{u}{h N } + \frac{\Omega}{ N } + \frac{ R\nabla\Omega }{ N } \right)^2$ |
| Azimuthal (3.29) | |
| $\boldsymbol{\omega} \cdot \nabla(\Omega R)$ | $\Omega R\nabla\Omega $ |
| $\Omega \omega_R$ | $\Omega R\nabla\Omega $ |
| $\omega_\phi \mathbf{u} \cdot \nabla \ln \rho$ | $\frac{u^2}{h^2} \left(\frac{h}{r} + \frac{\lambda}{\lambda} \right)$ |
| $\rho^{-2}(\nabla p \times \nabla \rho)_\phi$ | $\frac{g}{h} \frac{\lambda}{\lambda}$ |
| $\left(\nabla \times \left(\frac{1}{\rho} \nabla \cdot \mathbf{T} \right) \right)_\phi$ | $ N ^2 \left(\xi + \frac{u}{h N } + \frac{\Omega^2}{ N ^2} + \frac{\Omega R\nabla\Omega }{ N ^2} \right)$ |

Table 3.1: The magnitudes of the terms in equations (3.28) and (3.29) are summarised here. Factors of order unity have been dropped for simplicity. We have also dropped terms which we have argued are never relevant.

$$\mathbf{D} \approx h^2 |N|^{-1} \begin{pmatrix} |N|^2 & \Omega^2 \\ \Omega^2 & |N|^2 \end{pmatrix}, \quad (3.38)$$

where we have neglected multiplicative factors of order unity, the first column and row reflect \mathbf{e}_p and the second of each reflects \mathbf{e}_q . We have omitted the components of the diffusivity associated with \mathbf{e}_ϕ because axisymmetry means that both the entropy gradient and the derivative of the flux vanish in that direction. There is a second-order contribution of the form $\Omega |R\nabla\Omega|/|N|^2$, analogous to that in \mathbf{T} , but we shall argue that $|R\nabla\Omega|$ is no greater than Ω and so absorb that contribution into the Ω^2 terms. Similarly there is a contribution from the baroclinicity proportional to ξ , but we shall show that this is at most of order $\Omega^2/|N|^2$ and so we may likewise absorb it into the Ω^2 terms.

Inserting equations (3.13) and (3.38) into equation (3.11) and neglecting the meridional circulation we find

$$\begin{aligned} \nabla \cdot (p\mathbf{D} \cdot \nabla s) &= \nabla \cdot \left[h^2 p |\nabla s| \left(\mathbf{e}_p \left(D_{pp} \bar{\xi} + D_{pq} \xi \right) \right. \right. \\ &\quad \left. \left. + \mathbf{e}_q \left(D_{qp} \bar{\xi} + D_{qq} \xi \right) \right) \right] \\ &= \nabla \cdot \left[p |\nabla s| \mathbf{e}_p (|N|^2 \bar{\xi} + \Omega^2 \xi) + \mathbf{e}_q (\Omega^2 \bar{\xi} + |N|^2 \xi) \right]. \end{aligned} \quad (3.39)$$

This vanishes with $\xi = 0, \bar{\xi} = 1$ when $\Omega = 0$, so in that limit

$$\nabla \cdot (p\mathbf{D} \cdot \nabla s) = \nabla \cdot \left[\frac{h^2}{|N|} p |\nabla s| \mathbf{e}_p |N|^2 \right] = 0.$$

Subtracting this from equation (3.39) we find

$$\begin{aligned} \nabla \cdot (p\mathbf{D} \cdot \nabla s) &= \nabla \cdot \left[\frac{h^2}{|N|} p |\nabla s| \mathbf{e}_p (|N|^2 (\bar{\xi} - 1) + \Omega^2 \xi) \right. \\ &\quad \left. + \mathbf{e}_q (\Omega^2 \bar{\xi} + |N|^2 \xi) \right]. \end{aligned}$$

Because it is the rotation that breaks spherical symmetry and allows $\xi \neq 0$, we expect ξ to be small in this limit so we may write

$$\bar{\xi} - 1 \approx -\frac{1}{2}\xi^2.$$

Hence,

$$\begin{aligned} \nabla \cdot (p\mathbf{D} \cdot \nabla s) = \nabla \cdot \left[\frac{h^2}{|N|} p |\nabla s| \mathbf{e}_p \left(-\frac{1}{2}\xi^2 |N|^2 + \Omega^2 \xi \right) \right. \\ \left. + \mathbf{e}_q (\Omega^2 \bar{\xi} + |N|^2 \xi) \right]. \end{aligned}$$

Retaining only the leading-order terms we find

$$\nabla \cdot (p\mathbf{D} \cdot \nabla s) = \nabla \cdot \left[\frac{h^2}{|N|} p |\nabla s| \mathbf{e}_q (\Omega^2 \bar{\xi} + |N|^2 \xi) \right]. \quad (3.40)$$

Without invoking geometric fine-tuning, this may be made to vanish if

$$|\xi| \approx \frac{\Omega^2}{|N|^2}. \quad (3.41)$$

Because this is small our earlier expansion around $\xi = 0$ is justified.

3.9.2 Circulation

We now argue using the methods of Section 3.7 that the solution to equation (3.40) typically involves both a circulation and baroclinicity of comparable order, rather than just one or the other as equation (3.41) suggests. This is because equation (3.6) is comparably stiff in both the baroclinicity and the circulation.

To begin let \mathcal{H} be the left-hand side of equation (3.9), \mathcal{V}_m be the first component of the right-hand side of equation (3.28) and \mathcal{V}_ϕ be the right-hand side of equation (3.29). We perturb in Ω , so let

$$\begin{aligned} \phi_1 &\equiv \xi, \\ \phi_2 &\equiv u, \\ \phi_3 &\equiv |R\nabla\Omega| \end{aligned}$$

and

$$\phi_4 \equiv \Omega.$$

We consider the two components of the differential rotation together because in this limit none of the dominant terms preferentially couple to one or the other.

We now evaluate \mathcal{J} and \mathbf{q} in the slowly rotating limit. Turning first to the heat equation we see that Ω does not actually enter except via \mathbf{D} , where we have argued that it is perturbed to leading order as $\Omega^2/|N|^2$. Using equations (3.10) and (3.11) and assuming derivatives produce factors of h^{-1} , we find that

$$\frac{\delta\mathcal{H}}{\delta\Omega} \approx \frac{\Omega}{|N|^2} h^{-1} F.$$

The perturbation owing to ξ may be seen from equations (3.14) and (3.40), from which we find

$$\frac{\delta\mathcal{H}}{\delta\xi} \approx p|\nabla s|u + h^{-1} F.$$

Inserting equation (3.16) and neglecting corrections owing to $\bar{\xi}$ we obtain

$$\frac{\delta\mathcal{H}}{\delta\xi} \approx p|N|^2 \frac{u}{g} + h^{-1} F.$$

Recalling equation (3.19)

$$\frac{\delta\mathcal{H}}{\delta\xi} \approx \rho h|N|^2 u + h^{-1} F.$$

Finally using $v_c \approx h|N|$ and ⁷² $F \approx \rho v_c^3$ we find

$$\frac{\delta\mathcal{H}}{\delta\xi} \approx h^{-1} F \left(1 + \frac{u}{v_c} \right) \approx h^{-1} F.$$

We additionally have

$$\frac{\delta\mathcal{H}}{\delta u} \approx p|\nabla s| + \frac{F}{v_c} \approx \frac{F}{hv_c}$$

because \mathbf{D} is perturbed by the circulation current. Note that this happens at leading order because the current lies in the meridional plane. Finally, the differential rotation perturbs the heat transport at second order, or equivalently at first order by coupling to the rotation ⁷³, so

$$\frac{\delta\mathcal{H}}{\delta(R\partial_z\Omega)} \approx \frac{\Omega F}{|N|v_c}$$

and

$$\frac{\delta\mathcal{H}}{\delta(R\partial_R\Omega)} \approx \frac{\Omega F}{|N|v_c}.$$

We next examine the azimuthal vorticity equation. Using Table 3.1

⁷² Böhm-Vitense 1992

⁷³ This matter is discussed in the context of the stress in Section 3.8.2, and the considerations for the diffusivity are precisely the same.

and equation (3.24) we find

$$\begin{aligned}\frac{\delta \mathcal{V}_\phi}{\delta \xi} &\approx |N|^2, \\ \frac{\delta \mathcal{V}_\phi}{\delta u} &\approx \frac{u}{h^2} \left(\frac{h}{r} + \frac{\lambda}{\bar{\lambda}} \right) + h^{-1} |N| \approx h^{-1} |N|, \\ \frac{\delta \mathcal{V}_\phi}{\delta |R\nabla\Omega|} &\approx \Omega\end{aligned}$$

and

$$\frac{\delta \mathcal{V}_\phi}{\delta \Omega} \approx |R\nabla\Omega| + \Omega \approx \Omega.$$

Likewise using Table 3.1 we find for the meridional component

$$\begin{aligned}\frac{\delta \mathcal{V}_m}{\delta \xi} &\approx |N|^2 \xi + \frac{u}{h} |N| + \Omega |N| + |R\nabla\Omega| |N| \approx \Omega |N|, \\ \frac{\delta \mathcal{V}_m}{\delta u} &\approx h^{-1} \left(\xi |N| + \Omega + |R\nabla\Omega| + h^{-1} u \right) \approx h^{-1} \Omega, \\ \frac{\delta \mathcal{V}_m}{\delta |R\nabla\Omega|} &\approx |N| + \frac{u}{h} + \left(|R\nabla\Omega| + h^{-1} u + \Omega + \xi |N| \right) \approx |N|\end{aligned}$$

and

$$\frac{\delta \mathcal{V}_m}{\delta \Omega} \approx |N| + \frac{u}{h} + \left(|R\nabla\Omega| + h^{-1} u + \Omega + \xi |N| \right) \approx |N|.$$

Note that in both cases we have assumed $|R\nabla\Omega| \lesssim \Omega$ and taken equations (3.42) and (3.41) to bound u and ξ respectively.

Using equations (3.26) and (3.27) as well as Table 3.1 we find

$$\mathcal{J} \approx \begin{pmatrix} h^{-1} F & \frac{F}{h v_c} & \frac{\Omega F}{|N| v_c} \\ |N|^2 & h^{-1} |N| & \Omega \\ \Omega |N| & h^{-1} \Omega & |N| \end{pmatrix}$$

and

$$\mathbf{q} \approx \begin{pmatrix} \frac{\Omega}{|N|^2} h^{-1} F \\ |N| \\ |N| \end{pmatrix}.$$

We do not actually need to calculate the inverse of \mathcal{J} to estimate the magnitude of the solution. In particular we have only computed the magnitudes, not the signs, of its components, and so we do not have enough information to calculate the inverse. Rather we proceed more along the lines of Gaussian elimination. First though, we rescale our variables such

that

$$\begin{aligned}
 d\phi_1 &\rightarrow d\phi_1, \\
 d\phi_2 &\rightarrow h^{-1}|N|^{-1}d\phi_2, \\
 d\phi_3 &\rightarrow |N|^{-1}d\phi_3, \\
 d\phi_4 &\rightarrow |N|^{-1}d\phi_4, \\
 \mathcal{H} &\rightarrow hF^{-1}\mathcal{H}, \\
 \mathcal{V}_m &\rightarrow |N|^{-2}\mathcal{V}_m, \\
 \mathcal{V}_\phi &\rightarrow |N|^{-2}\mathcal{V}_\phi
 \end{aligned}$$

Then

$$\mathcal{J} \approx \begin{pmatrix} 1 & 1 & \frac{\Omega}{|N|} \\ 1 & 1 & \frac{\Omega}{|N|} \\ \frac{\Omega}{|N|} & \frac{\Omega}{|N|} & 1 \end{pmatrix}$$

and

$$\mathbf{q} \approx \begin{pmatrix} \frac{\Omega}{|N|} \\ \frac{\Omega}{|N|} \\ 1 \end{pmatrix}.$$

From this form we see that the meridional component of the vorticity equation is essentially decoupled from the meridional circulation and the baroclinicity, and is chiefly determined by the rotation and differential rotation balancing against one another. On the other hand, the azimuthal component of the vorticity equation and the heat equation are both quite stiff in the baroclinicity and the circulation, and notably are equally stiff in each. Hence unless there is significant geometric tuning, such that the heat and vorticity equations both support a solution with one of ξ or u vanishing, we expect that

$$|N|d\xi \approx h^{-1}du \approx \frac{\Omega}{|N|}d\Omega,$$

and so we generally expect $\xi \approx \Omega^2/|N|^2$ and⁷⁴ $u \approx \Omega^2 h/|N|$. Furthermore we have found that $|R\nabla\Omega| \approx \Omega$, though we leave a full discussion of this for the next subsection.

⁷⁴ It is interesting to note that there is another permitted scaling: the circulation velocity and baroclinicity may be made to be of the same arbitrarily large order. In that case they straightforwardly produce thermal equilibrium and come to dominate the vorticity equation. This scenario is not, however, physical, because it requires that the circulation current be one of the two largest effects, and hence nothing other than the baroclinicity may drive it in this scenario. The baroclinicity, though, arises as a result of the circulation in this case, and so cannot drive it. As a result this scenario is not physical. This is actually reflective of a more general result: because the system is dissipative the largest terms in each equation must be driven and in some way tap the heat flux through the system. Thus, for instance, it is fine for the Λ -effect to drive differential rotation because it draws energy from the convective turbulence, but the reverse would not be sustainable.

Returning to equation (3.40), we see that

$$\begin{aligned} |\nabla \cdot (p\mathbf{D} \cdot \nabla s)| &\approx \nabla \cdot \left[\frac{h^2}{|N|} p |\nabla s| \mathbf{e}_q (\Omega^2 \bar{\xi} + |N|^2 \xi) \right] \\ &\approx \nabla \cdot \left[\frac{h^2}{|N|} p |\nabla s| \mathbf{e}_q \left(\Omega^2 \left(1 - \frac{\xi^2}{2} \right) + |N|^2 \xi \right) \right] \\ &\approx \nabla \cdot \left[\frac{h^2}{|N|} p |\nabla s| \mathbf{e}_q \Omega^2 \right]. \end{aligned}$$

Expanding the divergence yields

$$\frac{|N| |\nabla \cdot (p\mathbf{D} \cdot \nabla s)|}{h^2 p |\nabla s| \Omega^2 \bar{\xi}} \approx \nabla \cdot \mathbf{e}_q + \mathbf{e}_q \cdot \nabla \ln \left[\frac{h^2}{|N|} p |\nabla s| \mathbf{e}_q \Omega^2 \bar{\xi} \right].$$

The divergence of the unit vector is of order r^{-1} because this is the scale over which the effective gravitational field varies. The gradient of the logarithmic function is dominated by the thermodynamic terms in the logarithm and so as argued in Section 3.5 produces a factor of order $h^{-1} (\mathbf{e}_p + \mathbf{e}_q (h/r + \lambda/\bar{\lambda}))$, where the scale r arises owing to geometric factors and $\lambda/\bar{\lambda}$ measures the extent to which the direction perpendicular to the pressure gradient overlaps with the density gradient. Hence

$$|\nabla \cdot (p\mathbf{D} \cdot \nabla s)| \approx \frac{h}{|N|} p |\nabla s| \Omega^2 \bar{\xi} \left(\frac{h}{r} + \frac{\lambda}{\bar{\lambda}} \right).$$

Inserting this into equation (4.12) we find

$$u \approx \frac{h}{|N|} \left(\frac{h}{r} + \frac{\lambda}{\bar{\lambda}} \right) \frac{\Omega^2 \bar{\xi}}{\xi (1 + \mathcal{M}^2) + \bar{\xi} h/r}.$$

Using equation (3.20) this may be written as

$$\begin{aligned} u &\approx h|N| \left(\frac{h}{r} + \frac{\lambda}{\bar{\lambda}} \right) \frac{\mathcal{M}^2 (\Omega^2 / |N|^2)}{(\lambda/\bar{\lambda})(1 + \mathcal{M}^2) + \mathcal{M}^2 h/r} \\ &\approx h|N| \left(1 + \frac{r\lambda}{h\bar{\lambda}} \right) \left(\frac{\Omega^2}{|N|^2} \right) \left(\frac{1}{1 + \frac{\lambda r}{\bar{\lambda} h} (1 + \mathcal{M}^{-2})} \right) \\ &= qh|N|, \end{aligned}$$

where

$$q \approx \left(\frac{\Omega^2}{|N|^2} \right) \left(1 + \frac{r\lambda}{h\bar{\lambda}} \right) \left(\frac{1}{1 + \frac{\lambda r}{\bar{\lambda} h} (1 + \mathcal{M}^{-2})} \right).$$

Recalling equation (3.20) and that $\xi \approx \Omega^2 / |N|^2$ we find

$$\frac{\lambda r}{\bar{\lambda}} h \approx \gamma \mathcal{M}^2 \frac{\Omega^2}{|N|^2}.$$

Hence to leading order in⁷⁵ Ω ,

⁷⁵ We shall later find that the meridional circulation is a small component of the vorticity balance, and this approximation only ever results in an overestimation, so this does not alter our subsequent arguments.

$$q \approx \frac{\Omega^2}{|N|^2}.$$

Thus we find

$$u \approx h|N| \frac{\Omega^2}{|N|^2}. \quad (3.42)$$

3.9.3 Results

| Term | Magnitude |
|---|--|
| Meridional (3.28) | |
| $\boldsymbol{\omega}_m \cdot \nabla_m \mathbf{u}$ | $\frac{\Omega^2}{ N } (\Omega + R\nabla\Omega)$ |
| $\boldsymbol{\omega}_m \mathbf{u} \cdot \nabla \ln \rho$ | $\frac{\Omega^2}{ N } (\Omega + R\nabla\Omega) \left(\frac{h}{r} + \frac{\lambda}{\bar{\lambda}} \right)$ |
| $\left(\nabla \times \left(\frac{1}{\rho} \nabla \cdot \mathbf{T} \right) \right)_m$ | $ N ^2 \left(\frac{\Omega}{ N } + \frac{ R\nabla\Omega }{ N } \right)$ |
| Azimuthal (3.29) | |
| $\boldsymbol{\omega} \cdot \nabla(\Omega R)$ | $\Omega R\nabla\Omega $ |
| $\Omega \omega_R$ | $\Omega R\nabla\Omega $ |
| $\omega_\phi \mathbf{u} \cdot \nabla \ln \rho$ | $\Omega^4 N ^{-2} \left(\frac{h}{r} + \frac{\lambda}{\bar{\lambda}} \right)$ |
| $\rho^{-2} (\nabla p \times \nabla \rho)_\phi$ | $\frac{g}{h} \frac{\lambda}{\bar{\lambda}}$ |
| $\left(\nabla \times \left(\frac{1}{\rho} \nabla \cdot \mathbf{T} \right) \right)_\phi$ | $ N ^2 \left(\xi + \frac{\Omega^2}{ N ^2} + \frac{\Omega R\nabla\Omega }{ N ^2} \right)$ |

Table 3.2: The magnitudes of the terms in equations (3.28) and (3.29) are summarised here. Factors of order unity have been dropped for simplicity. We have also dropped terms which we have argued are never relevant.

Our results thus far are summarised in Table 3.2, where we have inserted our results for u into the expressions in Table 3.1. Putting it all together and dropping sub-dominant terms these equations may be written in terms of the magnitudes of their terms as

$$0 = |N|^2 \left(\frac{\Omega}{|N|} + \frac{|R\nabla\Omega|}{|N|} \right) \quad (3.43)$$

and

$$0 = (\Omega + |R\nabla\Omega|)^2 + \frac{g}{h} \frac{\lambda}{\bar{\lambda}} + |N|^2 \left(\xi + \frac{\Omega^2}{|N|^2} + \frac{\Omega |R\nabla\Omega|}{|N|^2} \right). \quad (3.44)$$

In this case we do not need to go through the formalism of Section 3.7, though we have employed it in getting this far, because equation (3.43) and (3.44) immediately indicate that $|R\nabla\Omega| \approx \Omega$. Equation (3.44) is satisfied with this solution, so as promised we find that

$$|\nabla\Omega| \approx \frac{\Omega}{R}. \quad (3.45)$$

This justifies our earlier assumption that $|R\nabla\Omega|$ is no greater than Ω in scaling. Note that we found this too in our analysis of the circulation velocity, though there the result was not so evident from the form of the

vorticity equation.

To summarise, we have found that in a slowly rotating axisymmetric convection zone with no fossil magnetic field

$$|\nabla\Omega| \approx \frac{\Omega}{R}.$$

This is consistent with the solar rotation profile ⁷⁶ as well as the profiles of other slowly-rotating systems ⁷⁷. Physically this results from a balance between turbulent viscosity and the Λ -effect in both equations, in agreement with arguments by ⁷⁸. This means that in slowly rotating convection zones thermal wind balance is unlikely to be the dominant source of differential rotation. It does not, however, mean that it is not significant or even dominant in the Sun, because in the bulk of the convection zone $\Omega/|N|$ varies from 0.1 up to 1, only that in the regions where $|N|$ is larger it ought to be less important than other terms. This is in good agreement with the work of Balbus et al. (2012), who find that thermal wind balance produces a good match to the solar rotation profile in the bulk of the solar convection zone but that near the surface, where $|N|$ rises rapidly, the fit worsens. Of course the fit also worsens towards the tachocline, where $\Omega/|N| \gg 1$, but in that case there may be significant boundary effects coupling the rotation profile and potentially the magnetic field to that in the interior of the Sun and so it is not worth reading too extensively into that disagreement.

Furthermore though it was not our aim we have found that

$$\begin{aligned} u_r &\approx \frac{h}{r} u_\theta, \\ u_\theta &\approx u \approx h|N| \left(\frac{\Omega^2}{|N|^2} \right) \end{aligned}$$

and

$$\lambda \lesssim \mathcal{M} \left(\frac{\Omega^2}{|N|^2} \right) \approx \frac{\Omega^2 h}{g}.$$

The velocity field is in agreement with both the Sun ⁷⁹ and simulations ⁸⁰, and as we shall discuss later the baroclinicity λ is in agreement with (albeit uncertain) measurements of the solar pole-equator temperature difference ⁸¹.

⁷⁶ Rajaguru & Antia 2015

⁷⁷ Brun & Palacios 2009; Käpylä et al. 2011

⁷⁸ Ruediger 1989

⁷⁹ Rajaguru & Antia 2015

⁸⁰ Brun & Palacios 2009

⁸¹ Teplitskaya et al. 2015

3.10 Rapid Rotation

In this section we examine the case of rapid rotation, here meant with respect to the Brunt-Väisälä frequency. It is important to be careful, however, because the relationship between the Brunt-Väisälä frequency and various convective quantities is altered in the limit of rapid rotation, so to be clear we take $|N|$ to be the actually realised Brunt-Väisälä frequency and $|N|_0$ to be what the Brunt-Väisälä frequency would be were the rotation slow and all else held constant. In this notation, the rapid rotation limit is the one in which $\Omega \gg |N|_0$. We are not, however, interested in arbitrarily large rotation. In particular the system must remain primarily pressure supported, and so we also require that $\Omega \ll \sqrt{g/r}$. Note that the combination of these two limits is only sensible because unlike in radiative zones, in convection zones $|N|$ may be significantly less than $\sqrt{gr^{-1}}$.

3.10.1 Magnetic Fields

In the limit of rapid rotation the case of magnetism is more complex than in that of slow rotation. In this work we primarily follow the analysis of Christensen & Aubert (2006), who argue for a balance between the convective heat flux and ohmic dissipation. Our aim is to cast their results into our notation and framework.

We begin by considering a convecting region of thickness D , ranging from $r = r_i$ on the inner edge to $r = r_o$ on the outer one. In this region let

$$R_Q \equiv \frac{\alpha g F}{4\pi r_i r_o \rho c_p \Omega^3 D^2}, \quad (3.46)$$

where α is the thermal expansion coefficient. This is the quantity Christensen & Aubert (2006) defines in their equation (19) and call Ra_Q^* . Furthermore we approximate the turbulent kinetic energy density as

$$K \approx v_c^2. \quad (3.47)$$

This is the quantity Christensen & Aubert (2006) refer to as Ro . With these we may write the scaling⁸²

$$v_A = \frac{B}{\sqrt{4\pi\rho}} \approx \Omega D \sqrt{f_{\text{ohm}} V_s \frac{R_Q}{K}},$$

where f_{ohm} is a dimensionless factor of order unity and V_s is the volume in which a dynamo is active. For simplicity we neglect the dimensionless

⁸² See equations (11) and (32) of Christensen & Aubert (2006).

factor f_{ohm} because it is of order unity. We also take $D \approx h$ and write

$$V_s \approx 4\pi r^2 h,$$

Hence

$$v_A \approx \Omega h \sqrt{4\pi r^2 h \frac{R_Q}{K}}.$$

Inserting equation (3.47) we find

$$v_A \approx \sqrt{4\pi r^2 h \frac{(\Omega h)^3 R_Q}{v_c}}.$$

Now making use of equation (3.46) noting that for an ideal gas the thermal expansion coefficient $\alpha = T^{-1}$ we find

$$v_A \approx \sqrt{\frac{hgF}{\rho c_p T v_c}}.$$

For an ideal gas

$$p = \frac{2}{5} \rho c_p T$$

so using equation (3.19) we find

$$c_p T = \frac{5}{2} hg,$$

hence

$$v_A \approx \sqrt{\frac{2F}{5\rho v_c}}, \quad (3.48)$$

This is in very good agreement with the extensive suite of simulations they performed over a wide range of parameter space, and gives good agreement with a wide variety of observed stars ⁸³ as well as with observations of Jupiter Christensen & Aubert (2006). It is also in good agreement with the findings of Augustson et al. (2016a). There is more significant error when compared with the observed surface field of Saturn, but there there is reason to believe that the observed field does not reflect that in the interior ⁸⁴.

It is tempting to insert the relation for the non-rotating convective flux ⁸⁵

$$F \approx \rho v_c^3$$

⁸³ Christensen et al. 2009

⁸⁴ Stevenson 1982

⁸⁵ Böhm-Vitense 1992

into equation (3.48) and thereby find that

$$v_A \approx v_c,$$

which is the equipartition result. This is incorrect, however, because in rapidly rotating and magnetised convection the convective motions are arrested by the Coriolis effect while the magnetic dynamics are not. This means that, as Ω rises, an increasing fraction of the convective flux is carried magnetically. Hence significantly super-equipartition fields are possible in this case, in agreement with what is seen in simulations ⁸⁶.

To be more careful we turn to empirical fits to simulations, which show that at constant heat flux ⁸⁷

$$v_c \propto \Omega^{-0.23}.$$

This is in quite good agreement with closure models and scaling arguments for rapidly rotating turbulence. For instance at fixed Brunt-Väisälä frequency $|N|$,

$$v_c \approx h|N|^{3/2}\Omega^{-1/2} \quad (3.49)$$

⁸⁸. If the magnetic diffusivity is vanishing the growth of the dynamo is limited only by the fact that above equipartition the field begins to quench convection ⁸⁹. Hence we expect $v_A \approx h|N|$. Using equations (3.48) and (3.49) we find at fixed heat flux and density that ⁹⁰

$$|N| \approx v_c^{-1/2} \propto \Omega^{1/4}|N|^{-3/4},$$

or

$$|N| \propto \Omega^{1/7}.$$

From this we see that

$$v_c \propto \Omega^{-2/7},$$

hence by equation (3.48) we find

$$\frac{v_A}{v_c} \approx \left(\frac{\Omega}{|N|_0} \right)^{3/7},$$

where we have non-dimensionalised the equation using $|N|_0$, which is what the Brunt-Väisälä frequency would be were the system non-rotating. We may similarly non-dimensionalise the other relations we have found

⁸⁶ Roberts & Glatzmaier 2000; Sreenivasan & Jones 2006; Brun et al. 2005

⁸⁷ See equation (30) of Christensen & Aubert (2006).

⁸⁸ Showman et al. 2011

⁸⁹ Moreno-Inertis & Spruit 1989

⁹⁰ Equation (3.49) was derived for non-magnetic circumstances, so it is worth considering whether or not its use here is justified. The key to this is that the magnetic field has scale set by $|N|$. Hence it is always significant in the equations of motion at a level comparable to the buoyant term. Importantly this remains true even as $\Omega \rightarrow \infty$ and so does not alter the scaling of the velocity with Ω . This justifies using the scaling derived in its absence, and numerical experiments done with the formalism in Chapter 2 confirm this, though we have not investigated these circumstances systematically.

and obtain

$$|N| \approx |N|_0 \left(\frac{\Omega}{|N|_0} \right)^{1/7}, \quad (3.50)$$

$$v_c \approx h|N|_0 \left(\frac{\Omega}{|N|_0} \right)^{-2/7}, \quad (3.51)$$

and

$$v_A \approx h|N|_0 \left(\frac{\Omega}{|N|_0} \right)^{1/7} \approx h|N|. \quad (3.52)$$

The net result then is that in the limit of rapid rotation we expect magnetic fields to be in super-equipartition. In this limit equations (3.7) and (3.8) become

$$0 = \boldsymbol{\omega}_m \cdot \nabla_m \mathbf{u} + \boldsymbol{\omega}_m \mathbf{u} \cdot \nabla \ln \rho + \left[\nabla \times \left(\frac{1}{\rho} \nabla \cdot \mathbf{T} \right) \right]_m$$

and

$$\begin{aligned} 0 = & \boldsymbol{\omega} \cdot \nabla(\Omega R) - \Omega \boldsymbol{\omega}_R + \omega_\phi \mathbf{u} \cdot \nabla \ln \rho + \rho^{-2} \mathbf{e}_\phi \cdot \nabla p \times \nabla \rho \\ & + \mathbf{e}_\phi \cdot \nabla \times \left(\frac{1}{\rho} \nabla \cdot \mathbf{T} \right), \end{aligned}$$

with the bulk magnetic field explicitly eliminated and the fluctuating magnetic field still included in the stress.

3.10.2 Stress

In this limit the turbulence is dominated by the convective dynamo so long as $|R\nabla\Omega| < |N|$, which we verify to be the case further on. Following equation (3.52) we take the magnetic field to be superequipartition and write

$$\mathbf{T} \approx \rho v_A^2 \approx \rho h^2 |N|_0^2 \left(\frac{\Omega}{|N|_0} \right)^{2/7}.$$

This time the stress is not symmetry protected because the rotation is rapid and the off-diagonal components of \mathbf{T} are of the same order as those on the diagonal⁹¹. Hence in the absence of shear and baroclinicity we write

$$\nabla \times \left(\frac{1}{\rho} \nabla \cdot \mathbf{T} \right)_r \approx \left(\frac{h}{r} + \frac{\lambda}{\bar{\lambda}} \right) |N|_0^2 \left(\frac{\Omega}{|N|_0} \right)^{2/7} \quad (3.53)$$

$$\nabla \times \left(\frac{1}{\rho} \nabla \cdot \mathbf{T} \right)_\theta \approx |N|_0^2 \left(\frac{\Omega}{|N|_0} \right)^{2/7} \quad (3.54)$$

⁹¹ See Chapter 2 and [Kitchatinov \(2013\)](#).

and

$$\nabla \times \left(\frac{1}{\rho} \nabla \cdot \mathbf{T} \right)_{\phi} \approx |N|_0^2 \left(\frac{\Omega}{|N|_0} \right)^{2/7}, \quad (3.55)$$

where we have followed the prescription in Section 3.8 to evaluate the derivatives.

Similarly the MHD turbulence couples viscously to the differential rotation and any meridional shear. Because there is no symmetry protection, this produces a coupling generically at first order. The relevant diffusivity is just the stress divided by its characteristic time-scale $|N| = |N|_0(\Omega/|N|_0)^{1/7}$, hence

$$\nabla \times \left(\frac{1}{\rho} \nabla \cdot \mathbf{T} \right)_r \approx \left(\frac{h}{r} + \frac{\lambda}{\bar{\lambda}} \right) |N|_0 |R \nabla \Omega| \left(\frac{\Omega}{|N|_0} \right)^{1/7} \quad (3.56)$$

$$\nabla \times \left(\frac{1}{\rho} \nabla \cdot \mathbf{T} \right)_{\theta} \approx |N|_0 |R \nabla \Omega| \left(\frac{\Omega}{|N|_0} \right)^{1/7} \quad (3.57)$$

and

$$\nabla \times \left(\frac{1}{\rho} \nabla \cdot \mathbf{T} \right)_{\phi} \approx |N|_0 |R \nabla \Omega| \left(\frac{\Omega}{|N|_0} \right)^{1/7}. \quad (3.58)$$

There is likewise a coupling to the meridional circulation of the form

$$\nabla \times \left(\frac{1}{\rho} \nabla \cdot \mathbf{T} \right)_r \approx \left(\frac{h}{r} + \frac{\lambda}{\bar{\lambda}} \right) |N|_0 |\nabla \mathbf{u}| \left(\frac{\Omega}{|N|_0} \right)^{1/7} \quad (3.59)$$

$$\nabla \times \left(\frac{1}{\rho} \nabla \cdot \mathbf{T} \right)_{\theta} \approx |N|_0 |\nabla \mathbf{u}| \left(\frac{\Omega}{|N|_0} \right)^{1/7} \quad (3.60)$$

and

$$\nabla \times \left(\frac{1}{\rho} \nabla \cdot \mathbf{T} \right)_{\phi} \approx |N|_0 |\nabla \mathbf{u}| \left(\frac{\Omega}{|N|_0} \right)^{1/7}, \quad (3.61)$$

where $|\nabla \mathbf{u}|$ is the magnitude of the tensor formed of derivatives of the velocity components.

Finally we must consider the contribution of baroclinicity to the stress. In this case there is nothing additional to add: the baroclinicity ξ is at most of order unity, and its presence breaks no additional symmetries, so it contributes a term at most of the same order as those in equations (3.53), (3.54) and (3.55). Combining this with equations (3.53), (3.56) and (3.59) and

letting $|\nabla \mathbf{u}| \approx u/h$ we find

$$\nabla \times \left(\frac{1}{\rho} \nabla \cdot \mathbf{T} \right)_r \approx |N|^2 \left(1 + \xi + \frac{|R\nabla\Omega|}{|N|} + \frac{u}{h|N|} \right),$$

where we have reverted to using $|N|$ rather than $|N|_0$ for compactness.

Likewise equations (3.54), (3.57) and (3.60) give

$$\nabla \times \left(\frac{1}{\rho} \nabla \cdot \mathbf{T} \right)_\theta \approx |N|^2 \left(1 + \xi + \frac{|R\nabla\Omega|}{|N|} + \frac{u}{h|N|} \right),$$

and finally equations (3.55), (3.58) and (3.61) produce

$$\nabla \times \left(\frac{1}{\rho} \nabla \cdot \mathbf{T} \right)_\phi \approx |N|^2 \left(1 + \xi + \frac{|R\nabla\Omega|}{|N|} + \frac{u}{h|N|} \right).$$

3.10.3 Advective Terms

We now evaluate the terms which depend on \mathbf{v} and its derivatives but which are not a part of the stress. None of our analysis in determining the terms involving \mathbf{u} in the meridional vorticity equation depended on the rotation being slow, so those are given by

$$\begin{aligned} \boldsymbol{\omega}_m \cdot \nabla_m \mathbf{u} &\approx \frac{u}{h} (\Omega + |R\nabla\Omega|), \\ \boldsymbol{\omega}_m \mathbf{u} \cdot \nabla \ln \rho &\approx \frac{u}{h} (\Omega + |R\nabla\Omega|) \left(\frac{h}{r} + \frac{\lambda}{\bar{\lambda}} \right) \end{aligned}$$

and

$$\omega_\phi \mathbf{u} \cdot \nabla \ln \rho \approx \frac{u^2}{h^2} \left(\frac{h}{r} + \frac{\lambda}{\bar{\lambda}} \right),$$

where all we have done is followed our analysis in the slowly-rotating limit up until the point where we would have substituted $h\Omega^2/|N|^2$ for u .

The only remaining terms we must evaluate are the terms coupling to rotation in the azimuthal equation as well as the magnetic term in that equation. The only difference in the rotational terms from our previous analysis is that it now matters that these *only* couple the rotation to the \mathbf{e}_z component of the differential rotation⁹², so

$$\boldsymbol{\omega} \cdot \nabla(\Omega R) \approx R\Omega |\partial_z \Omega|$$

and

$$\Omega \omega_R \approx R\Omega |\partial_z \Omega|.$$

The magnetic term may be found by way of equation (3.52) and by taking

⁹² This is important because, as we shall see, these terms are crucial in setting the scale of the differential rotation and so different components scale differently with Ω .

the angle between the density gradient and the magnetic field to be order unity. In fact doing so we see that this contributes the same as the regular stress terms in equations (3.53), (3.54) and (3.55) and so what we assume about it does not actually matter.

3.10.4 Baroclinicity

In addition to its contribution to the stress tensor, the baroclinicity ξ enters into the vorticity balance both in relation to the scale of the meridional circulation and by means of the thermal wind term. In order to proceed, therefore, we must estimate ξ . In fact we will not go quite so far, but will simply provide bounds on various terms which depend on ξ .

The circulation speed is given by equation (4.12) as

$$u \approx \frac{|\nabla \cdot (p\mathbf{D} \cdot \nabla s)|}{p|\nabla s| [\xi(1 + \mathcal{M}^2) + \bar{\xi}h/r]}.$$

This may be bounded by noting that

$$|\mathbf{D} \cdot \nabla s| \leq D|\nabla s|,$$

where once more we use D to denote the typical magnitude of the components of \mathbf{D} (e.g. an l^2 -norm). Taking the divergence to produce a factor of h^{-1} , which produces the largest possible effect⁹³, we find

$$|\nabla \cdot (p\mathbf{D} \cdot \nabla s)| \leq h^{-1}pD|\nabla s|.$$

Hence

$$\begin{aligned} u &\leq \frac{D/h}{\xi(1 + \mathcal{M}^2) + \bar{\xi}h/r} \\ &\leq \frac{D/h}{\xi + \bar{\xi}h/r}. \end{aligned}$$

If both ξ and $\bar{\xi}$ are of order unity then

$$u \lesssim h^{-1}D.$$

If a significant fraction of order unity of the heat flux is transported turbulently then

$$pD|\nabla s| \approx F,$$

⁹³ A more conservative choice would be r^{-1} , if the deviation were a result of the large-scale geometry of the system.

so

$$u \lesssim \frac{F}{hp|\nabla s|}.$$

Inserting equation (3.48) this becomes

$$u \lesssim \frac{\rho v_c v_A^2}{hp|\nabla s|}.$$

With equation (3.16) this becomes

$$u \lesssim \frac{\rho g v_c v_A^2}{hp|N|^2}.$$

Inserting equation (3.19) we find

$$u \lesssim \frac{v_c v_A^2}{h^2|N|^2}.$$

Using equations (3.50) and (3.52) we find

$$u \lesssim v_c.$$

Next we argue that the thermal wind term is always irrelevant in this limit. Starting with equation (3.24), we have

$$|\rho^{-2}(\nabla p \times \nabla \rho)_\phi| \approx \frac{g}{h} \frac{\lambda}{\bar{\lambda}}.$$

Taking ξ to be at most of order unity and $\bar{\xi}$ to be at least of order unity ⁹⁴ we find from equation (3.20) that

$$\frac{\lambda}{\bar{\lambda}} \approx \gamma \frac{v_c^2}{c_s^2} \frac{\xi}{\bar{\xi}} \lesssim \gamma \frac{v_c^2}{c_s^2}.$$

Hence

$$|\rho^{-2}(\nabla p \times \nabla \rho)_\phi| \lesssim \gamma \frac{g v_c^2}{h c_s^2}.$$

For an ideal gas $c_s^2 = \gamma p / \rho$ so

$$|\rho^{-2}(\nabla p \times \nabla \rho)_\phi| = \frac{\rho g v_c^2}{hp}.$$

Using equation (3.19) we find

$$|\rho^{-2}(\nabla p \times \nabla \rho)_\phi| = \frac{v_c^2}{h^2}.$$

⁹⁴ This just precludes tuning to have $\nabla p \perp \nabla s$, and is in keeping with our assumption that the geometry of the solution is not fine-tuned.

By equation (3.51) we have

$$v_c \approx h|N|_0 \left(\frac{\Omega}{|N|_0} \right)^{-2/7},$$

so

$$|\rho^{-2}(\nabla p \times \nabla \rho)_\phi| = |N|_0^2 \left(\frac{\Omega}{|N|_0} \right)^{-4/7}.$$

This is less than the stress terms we have already found⁹⁵ and so may be neglected. Likewise we may ignore the magnetic term because it just contributes the same amount as the unit contribution to the stress.

⁹⁵ e.g. equations (3.53), (3.54) and (3.55)

3.10.5 Results

| Term | Magnitude |
|---|--|
| Meridional (3.7) | |
| $\omega_m \cdot \nabla_m \mathbf{u}$ | $\frac{u}{h}(\Omega + R\nabla\Omega)$ |
| $\omega_m \mathbf{u} \cdot \nabla \ln \rho$ | $\frac{u}{h}(\Omega + R\nabla\Omega) \left(\frac{h}{r} + \frac{\lambda}{\lambda} \right)$ |
| $\left(\nabla \times \left(\frac{1}{\rho} \nabla \cdot \mathbf{T} \right) \right)_m$ | $ N ^2 \left(1 + \xi + \frac{u}{h N } + \frac{ R\nabla\Omega }{ N } \right)$ |
| Azimuthal (3.8) | |
| $\omega \cdot \nabla(\Omega R)$ | $R\Omega \partial_z \Omega $ |
| $\Omega \omega_R$ | $R\Omega \partial_z \Omega $ |
| $\omega_\phi \mathbf{u} \cdot \nabla \ln \rho$ | $\frac{u^2}{h^2} \left(\frac{h}{r} + \frac{\lambda}{\lambda} \right)$ |
| $\left(\nabla \times \left(\frac{1}{\rho} \nabla \cdot \mathbf{T} \right) \right)_\phi$ | $ N ^2 \left(1 + \xi + \frac{u}{h N } + \frac{ R\nabla\Omega }{ N } \right)$ |

Table 3.3: The magnitudes of the terms in equations (3.7) and (3.8) are summarised here. Factors of order unity have been dropped for simplicity. We have also dropped terms which we have argued are never relevant.

Our results thus far are summarised in Table 3.3. Note that we have dropped the thermal wind term and the explicit magnetic term, the former because it is strictly smaller than many other terms and the latter because it scales in the same manner as the stress terms which have already been included.

To proceed we must solve equations (3.9), (3.7) and (3.8) for u , ξ and $R\nabla\Omega$. We do this using the methods of Section 3.7 in a calculation similar to that used to determine the circulation velocity in the slowly-rotating case. To begin let \mathcal{H} be the left-hand side of equation (3.9), $\mathcal{V}_{m,1}$ be the first component of the right-hand side of equation (3.7), $\mathcal{V}_{m,2}$ be the second component of the same and \mathcal{V}_ϕ be the right-hand side of equation (3.8).

We perturb in Ω , so let

$$\begin{aligned}\phi_1 &\equiv \xi, \\ \phi_2 &\equiv u, \\ \phi_3 &\equiv R\partial_z\Omega, \\ \phi_4 &\equiv R\partial_R\Omega,\end{aligned}$$

and

$$\phi_5 \equiv \Omega.$$

We consider the two components of the differential rotation separately because in this limit there are dominant terms which only couple to one or the other.

We now evaluate \mathcal{J} and \mathbf{q} in the rapidly rotating limit. Turning first to the heat equation we see that Ω does not actually enter except via \mathbf{D} . Using equations (3.10) and (3.11) and neglecting the possibility of geometric tuning we find

$$\mathbf{D} \approx \frac{F}{p|\nabla s|}.$$

Inserting equation (3.16) and assuming that $\bar{\xi}$ is of order unity produces

$$\mathbf{D} \approx \frac{gF}{p|N|^2}.$$

Recalling equations (3.48) and (3.52) we see that

$$\mathbf{D} \approx \frac{p}{\rho g} v_c \approx h v_c.$$

Now using equation (3.51) we see that

$$\mathbf{D} \approx h^2 |N|_0 \left(\frac{\Omega}{|N|_0} \right)^{-2/7}.$$

From this it follows that with F held fixed \mathbf{D} is perturbed at leading order as $\Omega^{-2/7}$. There are additional terms associated with the geometry of \mathbf{D} but, because we are not working in a highly symmetric limit like the non-rotating one, we need only focus on the overall magnitude. Taking derivatives to produce factors of h^{-1} , we find that

$$\frac{\delta \mathcal{H}}{\delta \Omega} \approx \frac{2}{7\Omega} h^{-1} F,$$

where we have dropped the minus sign because we only care about the

magnitude of this term. The perturbation owing to ξ is as before, and we find

$$\frac{\delta\mathcal{H}}{\delta\xi} \approx p|\nabla s|u + F \approx F \left(1 + \frac{u}{hv_c}\right) \approx h^{-1}F.$$

We additionally have

$$\frac{\delta\mathcal{H}}{\delta u} \approx p|\nabla s| + \frac{F}{v_c} \approx \frac{F}{hv_c}$$

because \mathbf{D} is perturbed by the circulation current. Note that this happens at leading order because we are no longer perturbing away from a spherically symmetric state. Finally, the differential rotation perturbs the heat transport at first order, so

$$\frac{\delta\mathcal{H}}{\delta(R\partial_z\Omega)} \approx \frac{F}{v_c}$$

and

$$\frac{\delta\mathcal{H}}{\delta(R\partial_R\Omega)} \approx \frac{F}{v_c}.$$

We next examine the azimuthal vorticity equation. Using Table 3.3 we find

$$\begin{aligned} \frac{\delta\mathcal{V}_\phi}{\delta\xi} &\approx |N|^2, \\ \frac{\delta\mathcal{V}_\phi}{\delta u} &\approx h^{-1}|N|, \\ \frac{\delta\mathcal{V}_\phi}{\delta(R\partial_z\Omega)} &\approx |N| + \Omega \approx \Omega, \\ \frac{\delta\mathcal{V}_\phi}{\delta(R\partial_R\Omega)} &\approx |N|, \end{aligned}$$

and

$$\frac{\delta\mathcal{V}_\phi}{\delta\Omega} \approx R\partial_z\Omega + \frac{2}{7\Omega}|N|^2.$$

Likewise using Table 3.3 we find for the two meridional components

$$\begin{aligned}
\frac{\delta \mathcal{V}_{m,1}}{\delta \xi} &\approx |N|^2, \\
\frac{\delta \mathcal{V}_{m,1}}{\delta u} &\approx h^{-1}|N|, \\
\frac{\delta \mathcal{V}_{m,1}}{\delta(R\partial_z\Omega)} &\approx \frac{u}{h} + |N| \approx |N|, \\
\frac{\delta \mathcal{V}_{m,1}}{\delta(R\partial_R\Omega)} &\approx \frac{u}{h} + |N| \approx |N|, \\
\frac{\delta \mathcal{V}_{m,1}}{\delta \Omega} &\approx \frac{u}{h} + \frac{2|N|^2}{7\Omega}, \\
\frac{\delta \mathcal{V}_{m,2}}{\delta \xi} &\approx |N|^2, \\
\frac{\delta \mathcal{V}_{m,2}}{\delta u} &\approx h^{-1}|N|, \\
\frac{\delta \mathcal{V}_{m,2}}{\delta(R\partial_z\Omega)} &\approx \frac{u}{h} + |N| \approx |N|, \\
\frac{\delta \mathcal{V}_{m,2}}{\delta(R\partial_R\Omega)} &\approx \frac{u}{h} + |N| \approx |N|,
\end{aligned}$$

and

$$\frac{\delta \mathcal{V}_{m,2}}{\delta \Omega} \approx \frac{u}{h} + \frac{2|N|^2}{7\Omega}.$$

Putting it all together with equations (3.26) and (3.27) we find

$$\mathcal{J} \approx \begin{pmatrix} h^{-1}F & \frac{F}{hv_c} & \frac{F}{v_c} & \frac{F}{v_c} \\ |N|^2 & h^{-1}|N| & \Omega & |N| \\ |N|^2 & h^{-1}|N| & |N| & |N| \\ |N|^2 & h^{-1}|N| & |N| & |N| \end{pmatrix}$$

and

$$\mathbf{q} \approx \begin{pmatrix} \frac{2}{7\Omega}h^{-1}F \\ R\partial_z\Omega + \frac{2|N|^2}{7\Omega} \\ \frac{u}{h} + \frac{2|N|^2}{7\Omega} \\ \frac{u}{h} + \frac{2|N|^2}{7\Omega} \end{pmatrix}.$$

We do not actually need to calculate the inverse of \mathcal{J} to estimate the magnitude of the solution. In particular we have only computed the magnitudes, not the signs, of its components, and so we do not have enough information to calculate the inverse. Rather we proceed more along the lines of Gaussian elimination. First though, we rescale our variables such

that

$$\begin{aligned}
d\phi_1 &\rightarrow d\phi_1, \\
d\phi_2 &\rightarrow |N|^{-1}d\phi_2, \\
d\phi_3 &\rightarrow |N|^{-1}d\phi_3, \\
d\phi_4 &\rightarrow |N|^{-1}d\phi_4, \\
d\phi_5 &\rightarrow \Omega^{-1}d\phi_5, \\
\mathcal{H} &\rightarrow hF^{-1}\mathcal{H}, \\
\mathcal{V}_{m,1} &\rightarrow |N|^{-2}\mathcal{V}_{m,1}, \\
\mathcal{V}_{m,2} &\rightarrow |N|^{-2}\mathcal{V}_{m,2}, \\
\mathcal{V}_\phi &\rightarrow |N|^{-2}\mathcal{V}_\phi
\end{aligned}$$

Then

$$\mathcal{J} \approx \begin{pmatrix} 1 & 1 & 1 & 1 \\ 1 & 1 & \frac{\Omega}{|N|} & 1 \\ 1 & 1 & 1 & 1 \\ 1 & 1 & 1 & 1 \end{pmatrix}$$

and

$$\mathbf{q} \approx \begin{pmatrix} \frac{2}{7} \\ R\partial_z \ln \Omega + \frac{2}{7} \\ \frac{u}{h\Omega} + \frac{2}{7} \\ \frac{u}{h\Omega} + \frac{2}{7} \end{pmatrix}.$$

Because $u \lesssim v_c < v_A \approx h|N| \ll h\Omega$ we may write

$$\mathbf{q} \approx \begin{pmatrix} \frac{2}{7} \\ R\partial_z \ln \Omega + \frac{2}{7} \\ \frac{2}{7} \\ \frac{2}{7} \end{pmatrix}.$$

Because \mathcal{J} is equally stiff in ϕ_1 , ϕ_2 and ϕ_4 and because $q_1 \approx q_2 \approx q_4 \approx 2/7$, we expect $d\phi_1 \approx d\phi_2 \approx d\phi_4 \approx 2/7$. The remaining equation is of the form

$$\begin{aligned}
d\phi_1 + d\phi_2 + \frac{\Omega}{|N|}d\phi_3 + d\phi_4 &\approx \left(\frac{2}{7} + R\partial_z \ln \Omega \right) d \ln \Omega \\
&\approx \left(\frac{2}{7} + \frac{|N|}{\Omega} \phi_3 \right) d \ln \Omega.
\end{aligned}$$

Now suppose that $|N|\phi_3/\Omega$ increases with Ω . Then the right-hand side is dominated by this term. None of $d\phi_1$, $d\phi_2$ or $d\phi_4$ are large enough to

satisfy this equation so this must be done by the term involving $d\phi_3$. Hence

$$d \ln \phi_3 \approx \frac{|N|^2}{\Omega^2} d \ln \Omega.$$

This implies that $\phi_3 \propto \Omega^{-2}$ as $\Omega \rightarrow \infty$, which contradicts our assumption. It follows that the right-hand side asymptotes to $(2/7)d \ln \Omega$. Because we have assumed that the solution is not fine-tuned and because $d\phi_1$, $d\phi_2$ and $d\phi_4$ are all of this order we conclude that each term on the left-hand side contributes comparably. Hence

$$d\phi_3 \approx \frac{|N|}{\Omega} d\Omega.$$

The net result is that

$$\begin{aligned} \frac{d\phi_1}{d \ln \Omega} &\approx 1, \\ \frac{d\phi_2}{d \ln \Omega} &\approx 1, \\ \frac{d\phi_3}{d \ln \Omega} &\approx \frac{|N|}{\Omega}, \end{aligned}$$

and

$$\frac{d\phi_4}{d \ln \Omega} \approx 1.$$

In more physical terms,

$$\begin{aligned} \frac{d\xi}{d \ln \Omega} &\approx 1, \\ \frac{du}{d \ln \Omega} &\approx h|N|, \\ \frac{d(R\partial_z \Omega)}{d \ln \Omega} &\approx \frac{|N|^2}{\Omega}, \end{aligned}$$

and

$$\frac{d(R\partial_R \Omega)}{d \ln \Omega} \approx |N|.$$

In other words, ξ is of order unity, and u is of order $h|N|$, $R\partial_R \Omega$ is of order $|N|$, and $R\partial_z \Omega$ is of order $|N|^2/\Omega$. Inserting equation (3.50) we find

$$\begin{aligned} R\partial_z \Omega &\approx |N|_0 \left(\frac{\Omega}{|N|_0} \right)^{-5/7}, \\ R\partial_R \Omega &\approx |N|_0 \left(\frac{\Omega}{|N|_0} \right)^{1/7}, \\ u &\approx h|N|_0 \left(\frac{\Omega}{|N|_0} \right)^{1/7} \end{aligned} \tag{3.62}$$

and

$$\xi \approx 1.$$

Or in terms of $|R\nabla\Omega|$,

$$|R\nabla\Omega| \approx |N|_0 \left(\frac{\Omega}{|N|_0} \right)^{1/7}. \quad (3.63)$$

This is in good agreement with three-dimensional simulations of rapidly rotating solar-type stars ⁹⁶, though it is in disagreement with at least some two-dimensional simulations ⁹⁷. In particular, we obtain differential rotation which increases sub-linearly with Ω and which asymptotically approaches a Taylor-Proudman balance ⁹⁸. This arises because inertial/advective terms come to balance the turbulent viscosity, but these preferentially couple to shear in the \mathbf{e}_z direction and hence the system comes to preferentially shear orthogonal to this.

As a final note, if the system were not magnetised or were non-ionised the analysis would proceed in the same manner but instead of equation (3.48) we would have ⁹⁹

$$F \approx \rho v_c^3.$$

With equation (3.49) we find

$$F \approx \rho h^3 |N|^{9/2} \Omega^{-3/2}.$$

Hence at fixed flux

$$|N| = |N|_0 \left(\frac{\Omega}{|N|_0} \right)^{1/3}. \quad (3.64)$$

None of the rest of the analysis is altered, and so we instead find

$$\begin{aligned} R\partial_z\Omega &\approx |N|_0 \left(\frac{\Omega}{|N|_0} \right)^{-1/3} \\ R\partial_R\Omega &\approx |N|_0 \left(\frac{\Omega}{|N|_0} \right)^{1/3} \\ u &\approx h|N|_0 \left(\frac{\Omega}{|N|_0} \right)^{1/3} \end{aligned} \quad (3.65)$$

and

$$\xi \approx 1.$$

⁹⁶ Brown et al. 2007; Matt et al. 2011; Käpylä et al. 2011

⁹⁷ Sun & Schubert 1995

⁹⁸ Brun & Palacios 2009

⁹⁹ Gough 1978

Or in terms of $|R\nabla\Omega|$,

$$|R\nabla\Omega| \approx |N|_0 \left(\frac{\Omega}{|N|_0} \right)^{1/3}. \quad (3.66)$$

3.11 Inverse Cascade

In our analysis we have assumed that solutions to the governing equations contain no geometric factors which differ significantly from order unity. In effect we have assumed that any structures which form are in some fashion generic and do not depend specifically on $\Omega/|N|$, though they may depend on the regime in which the system lies. While this assumption is usually quite good, there is an important known exception in the case of rapidly-rotating two-dimensional turbulence ¹⁰⁰. This phenomenon, first noted by Rhines (1973), is known as the inverse cascade or Rhines cascade, and results from the Coriolis effect preferentially scattering waves into large-scale modes. This produces feedback between small-scale convective motions and the overall geometry of the solution.

¹⁰⁰ Sukoriansky et al. 2006

The reason that two-dimensional turbulence is of interest for our purposes is that stars and planets exhibit significant density stratification. This makes turbulence effectively two-dimensional by preventing strong correlations between regions with significant vertical separation.

The net result of the Rhines cascade has been found, both analytically and numerically ¹⁰¹, to result in the formation of alternating bands of differential rotation. In particular, the number of jets is seen to scale as ¹⁰²

¹⁰¹ Danilov & Gurarie 2002

¹⁰² See equation 22 of Verhoeven & Stellmach (2014).

$$n \approx \sqrt{\frac{\Omega h}{w}}, \quad (3.67)$$

where we have used $d = h$ as the relevant vertical length-scale and w is the characteristic velocity scale of the system, given by v_c when the primary means of energy transport is convective ¹⁰³. This has been seen in a broad array of simulations ¹⁰⁴ and agrees well with observations of the four gas giant planets in the solar system ¹⁰⁵.

¹⁰³ When the jets are driven more by surface temperature variations this is instead the jet velocity, but we are not interested in such cases here because they only change the rotational structure in a boundary layer, not in the bulk of the system.

¹⁰⁴ Gastine et al. 2013; Verhoeven & Stellmach 2014

¹⁰⁵ Ingersoll & Pollard 1982; Galperin et al. 2001

From the perspective of our analysis this interesting geometric effect changes little unless $n > R/h$. This is because the jets introduce a correction only into the latitudinal derivatives, all of which have turned out to be irrelevant because h is typically considerably less than R . That is, the jets are only relevant locally if they cause the horizontal scale of convection cells to be significantly less than their vertical scale. Substituting $w = v_c$

into equation (3.67) and using $v_c \approx h|N|$ we find

$$n \approx \sqrt{\frac{\Omega}{|N|}}.$$

Hence for $n > R/h$ it must be that

$$\frac{\Omega}{|N|} > \frac{R^2}{h^2}. \quad (3.68)$$

When inequality (3.68) is satisfied the latitudinal derivatives of the stress are enhanced above the radial derivatives by a factor of nh/R and thereby become dominant. In the meridional vorticity equation (3.7) the balance is chiefly between the asymmetric stress and the viscous term. Both are enhanced by this factor because both couple to the turbulent motions and so we expect to see no change in the resulting differential rotation. Because that equation sets $R\partial_R\Omega$, we therefore expect this to be unchanged by these geometric considerations.

By contrast in the azimuthal vorticity equation the balance is primarily between the asymmetric components of the stress and the coupling of rotation to vorticity. The former is enhanced by the presence of jets while the latter is not, so we expect to see enhanced differential rotation. Because this equation sets $R\partial_z\Omega$, we expect that

$$R\partial_z\Omega \rightarrow nh\partial_z\Omega \approx \frac{h}{R}\sqrt{\frac{\Omega}{|N|}}(R\partial_z\Omega)_0,$$

where $(R\partial_z\Omega)_0$ is the differential rotation along \mathbf{e}_z we would expect in the absence of the Rhines cascade. In non-magnetised systems we combine this with equation (3.65) to find

$$R\partial_z\Omega \approx \frac{h}{R}|N|_0.$$

In the magnetised limit we instead use equation (3.62) to find

$$R\partial_z\Omega \approx \frac{h}{R}|N|_0 \left(\frac{\Omega}{|N|_0} \right)^{-2/7}.$$

The overall effect of the Rhines cascade on our results is then somewhat underwhelming. The cascade is only relevant when $\Omega > |N|R^2/h^2$, which in practice makes it only relevant for a small population of extremely rapid rotators¹⁰⁶. Furthermore the cascade does not modify the scaling of $R\partial_R\Omega$. Because this dominates the overall differential rotation, the Rhines cascade also does not modify the scaling of $|R\nabla\Omega|$. Hence the only real effect is to slow the transition to the limit of shellular rotation, making the very small

¹⁰⁶ In the bulk of a polytropic self-gravitating body h is of order 0.1 – 0.2 of R , so this requires Ω at least 10 – 100 times greater than $|N|$. This limit is readily seen in planets but is quite difficult to achieve in stars.

vertical differential rotation slightly larger yet still never dominant.

3.12 Breakup Rotation

Stable systems cannot rotate faster than the Keplerian velocity

$$\Omega_K \equiv \sqrt{\frac{g}{R}}$$

without invoking pressure profiles that increase outwards. As a system approaches this velocity it nears the state of an accretion disk, where

$$R\partial_z\Omega = 0$$

and

$$R\partial_R\Omega = -\frac{3}{2}\Omega.$$

The derivation of this state is straightforward so we do not dwell on it. What we are interested in, however, is how this limit is approached.

To see why this is not simply an extension of the rapidly rotating limit, note that in both the magnetised and the hydrodynamic limits we found that $|R\nabla\Omega|$ increases sub-linearly in that limit, such that

$$|R\nabla\ln\Omega| \rightarrow 0$$

as $\Omega/|N| \rightarrow \infty$. This is incompatible with the Keplerian limit and so something different must happen in between the two limits.

The first important point is that the window of rotation rates we considered in Section 3.10 is not infinite. In particular, we considered

$$|N| \ll \Omega \ll \sqrt{\frac{g}{R}} = \Omega_K,$$

so the window has width

$$\frac{\Omega_{\max}}{\Omega_{\min}} = \sqrt{\frac{g}{R|N|^2}}.$$

For $\Omega > \Omega_{\max}$ certain terms which could be ignored because $h \ll r$ become significant, though this does not explain the difference between our results and the Keplerian limit because those terms do not scale sufficiently quickly with Ω as to produce $|R\nabla\Omega| \propto \Omega$.

The second point to note is that as the rotation rate increases so does $|N|$. To incorporate both the hydrodynamic and the magnetised limits

discussed in the previous section we write

$$|N| = |N|_0 \left(\frac{\Omega}{|N|_0} \right)^\alpha$$

for some $\alpha > 0$. Using equation (3.16)¹⁰⁷ we may relate this to the entropy gradient and find that

$$|\nabla s| = \frac{|N|_0^2}{g\bar{\xi}} \left(\frac{\Omega}{|N|_0} \right)^{2\alpha}. \quad (3.69)$$

¹⁰⁷ Once more we assume that $\bar{\xi}$ is of order unity.

In the simple case of an ideal gas with aligned pressure and density gradients this may be related to the temperature gradient using equation (1.2), so

$$\begin{aligned} |\nabla s| &= |\nabla \ln p - \gamma \nabla \ln \rho| \\ &= |(1 - \gamma) \nabla \ln p + \gamma \nabla \ln T| \\ &= \frac{1}{h} \left[1 - \gamma + \gamma \frac{d \ln T}{d \ln p} \right] \\ &= \frac{\gamma}{h} [\nabla - \nabla_a], \end{aligned}$$

where ∇_a and ∇ are the adiabatic and actual logarithmic temperature gradients respectively. But ∇ is bounded above by the radiative temperature gradient ∇_R , so

$$|\nabla s| \leq \frac{\gamma}{h} [\nabla_R - \nabla_a]. \quad (3.70)$$

Combining equations (3.69) and (3.70) we find

$$|N|_0^2 \left(\frac{\Omega}{|N|_0} \right)^{2\alpha} \leq \frac{\gamma g \bar{\xi}}{h} [\nabla_R - \nabla_a].$$

Using equation (3.19) and recalling that $c_s^2 = \gamma p / \rho$ we see that

$$|N|_0^2 \left(\frac{\Omega}{|N|_0} \right)^{2\alpha} \leq \bar{\xi} \left(\frac{\gamma g}{c_s} \right)^2 [\nabla_R - \nabla_a].$$

To proceed note that g in this equation is the effective¹⁰⁸ gravity, such that

$$\mathbf{g} = \mathbf{g}_0 - \mathbf{e}_R \Omega^2 R \quad (3.71)$$

¹⁰⁸ i.e. centrifugally-corrected

where \mathbf{g}_0 is the actual acceleration of the gravitational interaction. Hence on the equator, where $\mathbf{g}_0 \propto \mathbf{e}_R$,

$$g = g_0 \left(1 - \frac{\Omega^2 R}{g_0} \right).$$

So

$$\xi \left(\frac{\gamma g_0}{c_s |N|_0} \right)^2 \left(1 - \frac{\Omega^2 R}{g_0} \right) \left(\frac{\Omega}{|N|_0} \right)^{-2\alpha} [\nabla_R - \nabla_a] \geq 1.$$

As Ω increases this breaks down because the left-hand side vanishes, both as $\Omega^{-2\alpha}$ and as a result of the centrifugal term. In other words at some point the system must become radiative. Of course this is only a problem in regions near the equator, but it may have significant consequences for the transport of angular momentum and hence may suffice to explain the discrepancy between the Keplerian and sub-Keplerian regimes.

Finally, and perhaps most importantly, in approaching the Keplerian limit we face a breakdown of the steady state assumption. To understand this consider a system spinning with $\Omega_K \gg \Omega \gg |N|_0$. Because $\Omega \gg |N|_0$ the rotation rate is nearly uniform in relative terms. Furthermore because Ω_K decreases with increasing R the outermost parts of the system are those with Ω closest to the Keplerian rate.

Suppose we now inject angular momentum into the system in small doses and wait for it to come to equilibrium. After each injection and equilibration the system has a new Ω , which is still nearly uniform in relative terms. Eventually the outermost regions reach Ω_K . They cannot rotate faster than Ω_K because doing so would push them out to larger radii, and with fixed specific angular momentum they will reach a radius at which $\Omega = \Omega_K$.

It follows that further injection of angular momentum creates a region near the surface where $\Omega(R) = \Omega_K(R)$. This is the region in which

$$R > R_K = \frac{g}{\Omega^2},$$

where now Ω is the rotation rate for $R < R_K$. However this solution does not represent an equilibrium. This is because the Keplerian region is rotating slower than the interior, with an angular velocity gradient that exceeds that which equations (3.7) and (3.8) support. We have found that angular momentum is transported in this limit so as to reduce $|R \nabla \ln \Omega|$, so angular momentum is carried out from the interior into the Keplerian region. In essence a decretion disk is formed.

As angular momentum flows into the disk Ω decreases, R_K moves outward and the disk spreads away from the central body. Should this flow continue indefinitely the system will reach an equilibrium in which R_K equals the radius of the body, but at this point the majority of the system is no longer Keplerian and the results from Section 3.10 apply. Upon

injecting more angular momentum the process repeats, but eventually the system will have too much angular momentum to remain bound and must lose mass to infinity. In this case the assumption that the system remains in equilibrium is violated and there is no reason to expect our equilibrium solution to continuously connect to the Keplerian one.

3.13 Tests

To test our results we turn to simulations and observations. Fig. 3.4 shows our scaling relations for non-magnetised (left, equations (3.45) and (3.63)) and magnetised (right, equations (3.45) and (3.66)) rotating convection as a function of $\Omega/|N|$. Observations are shown with solid shapes and simulations are shown as open shapes. Data for the Sun and Jupiter are shown as lines. Details of how the data were processed are included at the end of this Chapter in Section 3.16.

The first point to note is that there is significant disagreement between different simulation suites and different kinds of observations. Much of this may be attributed to differences in which quantities were reported, and indeed there is somewhat better agreement among data of the same type. For instance reports of surface latitudinal variation from both simulation and observation generally agree with one another and with the analytic results, and likewise for reports of core–envelope differential rotation, but neither group agrees well with the other. The exceptions to this are reports of equatorial–mean differential rotation, which agree on the general trend of the data but exhibit many outliers. Some of this is due to the fact that this data was most often extracted digitally from figures rather than from data tables. Fig. 3.5 shows the same comparison as Fig. 3.4 but with these points excluded and there is evidently more consistency amongst datasets determined from data tables than amongst those extracted from figures. Furthermore Fig. 3.5 shows considerably better agreement with our scaling relations, suggesting that the data extraction is indeed partly to blame for the discrepancies in Fig. 3.4.

The rapidly-rotating non-magnetised scaling exhibits mild tension with Juno upper bounds on core differential rotation in Jupiter, though it is in better agreement with Juno measurements of the shallow differential rotation than the magnetised scaling. This is in agreement with previous work ¹⁰⁹ and the finding that the transition between shallow and deep differential rotation in Jupiter are associated with a large change in electrical conductivity ¹¹⁰.

There are unfortunately very few observed systems at extreme rotation

¹⁰⁹ Kirk & Stevenson 1987; Liu et al. 2008

¹¹⁰ Guillot et al. 2018

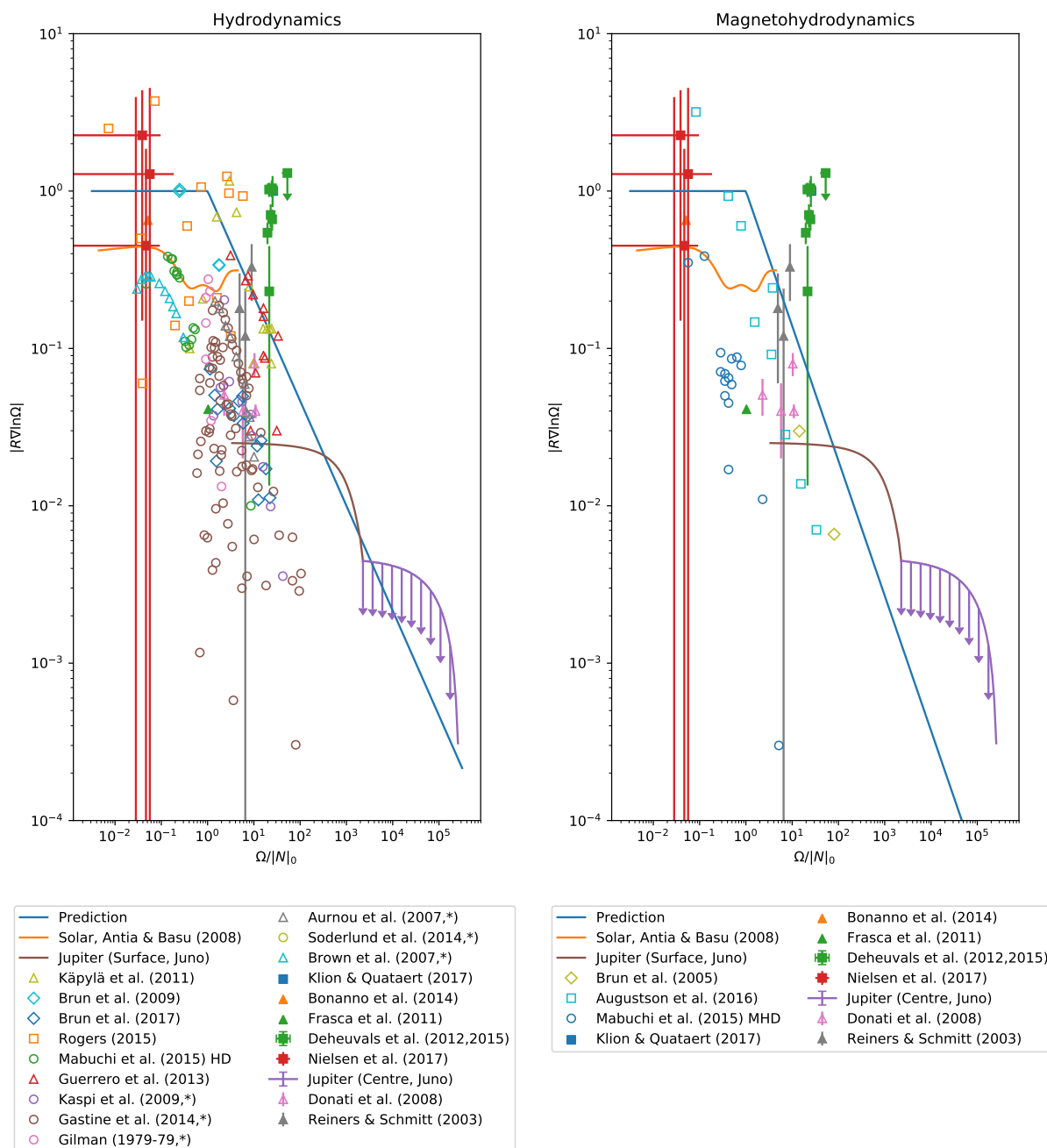


Figure 3.4: (Left) The differential rotation given by equations (3.45) and (3.66) as functions of $\Omega/|N|_0$ and normalised by Ω . (Right) The differential rotation given by equations (3.45) and (3.63) as functions of $\Omega/|N|_0$ and normalised by Ω . (Both) The proportionality constant was taken to be unity and the transition between slow and rapid rotation was taken to be at $\Omega = |N|$. Observations are shown with solid shapes and simulations are shown as open shapes. Data for the Sun and Jupiter are shown as lines. The surface–centre distinction in Jupiter is made at a depth of 3000km, beyond which point [Guillot et al. \(2018\)](#) report only upper bounds on the shear. Triangles are used to show latitudinal differential rotation at the surface of an object. Circles are used to show the difference between the mean rotation and that at the equator on the surface. Diamonds are used to show the differential rotation inferred from the energy in rotational motion in the globally co-rotating frame. Squares are used to show differential rotation inferred from core–envelope rotation ratios. Simulations are shown in the panel appropriate to their conditions (i.e. magnetised or not). Note that in some cases data (marked with *) were extracted digitally from figures, and these cases produced the majority of anomalously low points, suggesting that the uncertainties in this process are significant. Full details of how the data were processed are included in Appendix 3.16. Data were taken from the following works: [Brown et al. \(2007\)](#); [Brun & Palacios \(2009\)](#); [Brun et al. \(2005\)](#); [Augustson et al. \(2016b\)](#); [Brun et al. \(2017\)](#); [Rogers \(2015\)](#); [Gilman \(1977, 1979\)](#); [Mabuchi et al. \(2015\)](#); [Käpylä et al. \(2011\)](#); [Bonanno et al. \(2014\)](#); [Guerrero et al. \(2013\)](#); [Gastine et al. \(2014\)](#); [Soderlund et al. \(2013\)](#); [Kaspi et al. \(2009\)](#); [Aurnou et al. \(2007\)](#); [Klion & Quataert \(2017\)](#); [Donati et al. \(2008\)](#); [Nielsen et al. \(2017\)](#); [Reiners & Schmitt \(2003\)](#); [Frasca et al. \(2011\)](#); [Deheuveils et al. \(2012, 2015\)](#); [Kaspi et al. \(2018\)](#); [Guillot et al. \(2018\)](#); [Antia et al. \(2008\)](#).

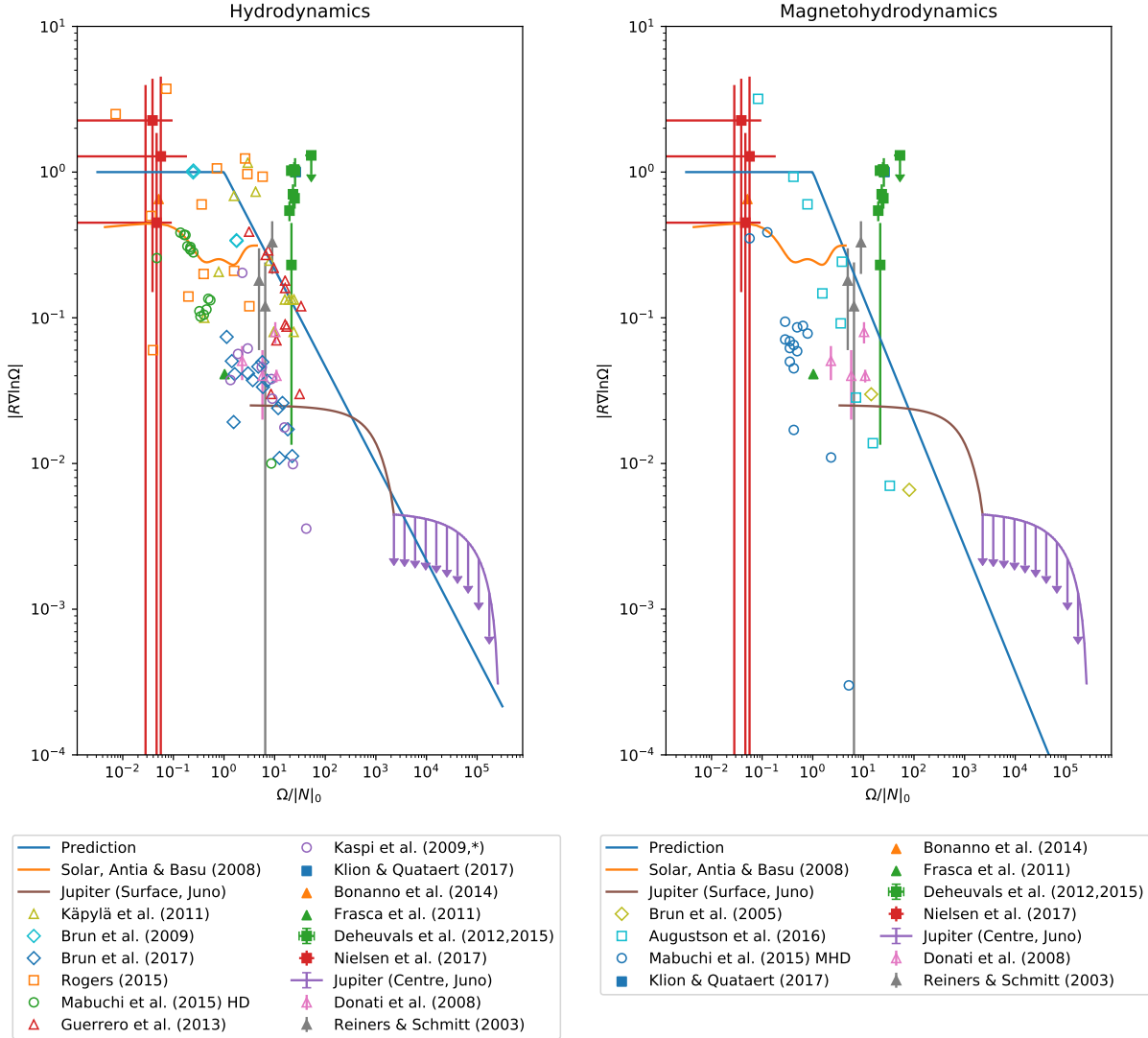


Figure 3.5: (Left) The differential rotation given by equations (3.45) and (3.66) as functions of $\Omega/|N|_0$ and normalised by Ω . (Right) The differential rotation given by equations (3.45) and (3.63) as functions of $\Omega/|N|_0$ and normalised by Ω . (Both) The proportionality constant was taken to be unity and the transition between slow and rapid rotation was taken to be at $\Omega = |N|$. Observations are shown with solid shapes and simulations are shown as open shapes. Data for the Sun and Jupiter are shown as lines. The surface–centre distinction in Jupiter is made at a depth of 3000km, beyond which point Guillot et al. (2018) report only upper bounds on the shear. Triangles are used to show latitudinal differential rotation at the surface. Circles are used to show the difference between the mean rotation and that at the equator on the surface. Diamonds are used to show the differential rotation inferred from the energy in rotational motion in the globally co-rotating frame. Squares are used to show differential rotation inferred from core–envelope rotation ratios. Simulations are shown in the panel appropriate to their conditions (i.e. magnetised or not). Full details of how the data were processed are included in Appendix 3.16. Data were taken from the following works: Brun & Palacios (2009); Brun et al. (2005); Augustson et al. (2016b); Brun et al. (2017); Rogers (2015); Mabuchi et al. (2015); Käpylä et al. (2011); Bonanno et al. (2014); Guerrero et al. (2013); Klion & Quataert (2017); Donati et al. (2008); Nielsen et al. (2017); Reiners & Schmitt (2003); Frasca et al. (2011); Deheuvels et al. (2012, 2015); Kaspi et al. (2018); Guillot et al. (2018); Antia et al. (2008).

rates other than Jupiter. To understand this note that

$$\frac{\Omega^2}{|N|_0^2} < \frac{g}{R|N|_0^2}$$

because the system must be stable against rotational breakup. Next recall that

$$|N|_0 \approx \frac{v_{c,0}}{h},$$

where $v_{c,0} \approx (F/\rho)^{1/3}$ is the convection speed which would be required were the system non-rotating and non-magnetised. Hence

$$|N|_0 \approx \left(\frac{F}{\rho h^3} \right)^{1/3}.$$

Because central convection zones maximise ρh^3 , we let $h \approx R$ to find

$$|N|_0 \gtrsim \left(\frac{F}{\rho R^3} \right)^{1/3} \approx \left(\frac{F}{M} \right)^{1/3}.$$

Hence

$$\begin{aligned} \frac{\Omega^2}{|N|_0^2} &< \frac{g}{R|N|_0^2} \\ &< \left(\frac{G^3 M^5}{F^2 R^9} \right)^{1/3} \\ &\approx \left(\frac{G^3 M^5}{L^2 R^5} \right)^{1/3}. \end{aligned}$$

Because R and L both increase with mass for main-sequence stars, and $L^2 R^5$ does so more rapidly¹¹¹ than M^5 , this bound is loosest at low masses. Hence the objects with the potential for the most extreme rotation are also those which are most difficult to observe.

There are likewise few simulations at these extreme rotation rates because the dominant wave-vectors become quite large and so the required resolution becomes difficult to resolve. Advances are likely to continue in this direction, but for the moment the strongest constraints on differential rotation in rapidly rotating systems come from Jupiter.

Both the Sun and Jupiter exhibit asymptotically fixed differential rotation¹¹² as $\Omega/|N| \rightarrow 0$. In the Sun this occurs near the transition between slow and rapid convection and so may be regarded as being reflective of slowly rotating systems more generally. In Jupiter, however, it occurs well above the knee, when $\Omega \approx 3 \times 10^2 |N|$. In this case the near-fixed differential rotation is actually reflective of differential rotation in the bulk,

¹¹¹ See scaling relations in [Böhm-Vitense \(1992\)](#).

¹¹² [Antia et al. 2008](#); [Kaspi et al. 2018](#)

where the rotation isosurfaces are nearly cylindrical. In effect each region on the surface couples primarily to its neighbours in latitude and to the Taylor-Proudman cylinder on which it sits. These cylinders rotate according to a balance set in the bulk of the planet because that is where most of the mass and interaction area lies. This sets a decidedly non-generic lower boundary condition which damps the surface differential rotation that our analysis predicts would otherwise emerge.

The plateau in Jupiter's differential rotation may also be seen as highlighting that differential rotation cannot vary wildly from point to point within a system because of geometric considerations. Hence when we refer to $|N|_0$ within a given system we are really speaking of the typical $|N|_0$ in the bulk of the convection zone, rather than at any specific location.

An interesting systematic trend is that asteroseismic measurements of differential rotation in red giants, which make up most of the filled squares in Figs. 3.4 and 3.5, generally lie a factor of several above any other observations made at comparable rotation rates. This may be understood by noting that the quantity we have calculated is

$$\frac{|R\nabla\Omega|}{\Omega} = |R\nabla \ln \Omega|.$$

Assuming that there is little geometric tuning, the difference between the rotation rate in the core and that in the envelope rotation ratio is therefore of order

$$\frac{\Delta\Omega}{\Omega} \approx \int_{R_{\text{core}}}^{R_{\text{surface}}} |\nabla \ln \Omega| dR.$$

We have argued that $|\nabla \ln \Omega| \approx kR^{-1}$ for some function $k(\Omega/|N|)$, so

$$\frac{\Delta\Omega}{\Omega} \approx k \ln \frac{R_{\text{surface}}}{R_{\text{core}}}.$$

For objects with large envelopes and small cores the logarithm may produce a factor of several, and that is indeed what we see in the data. Our underprediction may therefore be attributed simply to the large amount of room in which giant stars may develop differential rotation.

Looking at more minor trends, the solar data suggests that the transition point between slow and rapid rotation is closer to $\Omega \approx 0.2|N|$, rather than $\Omega \approx |N|$ as we have assumed. This is in agreement with closure models¹¹³ and some simulations such as those of Brown et al. (2007). Additionally these simulations and data suggest that the asymptotic differential rotation is closer to $0.3\Omega/R$ rather than Ω/R , in agreement with the calculations of¹¹⁴. On the other hand the simulations of Gastine et al. (2014) and the

¹¹³ See Chapter 2 as well as Küker & Rüdiger (2005).

¹¹⁴ Küker & Rüdiger 2005

observations of [Deheuvels et al. \(2015\)](#) both argue for a knee at mildly stronger rotation. Furthermore the latter and observations by [Nielsen et al. \(2017\)](#) suggest somewhat stronger asymptotic differential rotation than what is found in the Sun. This is rather strange because they were looking primarily at solar-like stars, though the error bars are so large that their results are consistent with what is seen in the Sun. More broadly, these differences are all at the same level as the uncertainties associated with standardising these very disparate sources of data and so are unlikely to be indicative of the scaling of the differential rotation.

In summary, both scaling relations are in reasonable agreement with both observations and simulations. This is particularly the case when one examines a single suite of simulations. It is then clear which regime the system is in (i.e. magnetic or not) and there are no systematic differences in which quantities are reported. For instance the slope we have found of $-2/3$ for the non-magnetised case is in good agreement with fits performed on individual sets of simulations ¹¹⁵. The magnetised scaling is a better match to observation overall, though there are indications in the data that Jupiter actually switches from the hydrodynamic regime to the magnetised one ¹¹⁶ at a depth of around 3000 km.

¹¹⁵ [Brown et al. 2007](#)

¹¹⁶ [Kaspi et al. 2018](#)

3.14 Limitations

To reiterate from Section 3.2, we have made the following assumptions.

1. Dimensionless factors arising from geometry are of order unity unless required to be otherwise.
2. All external perturbing forces such as tides or external heating are negligible in the regions of interest.
3. The material is compressible and non-degenerate.
4. All microscopic (i.e. non-turbulent) diffusivities are vanishingly small, such that:
 - convection is efficient;
 - convection is well-developed;
 - magnetohydrodynamical processes are ideal;
 - and turbulent and/or advective processes are responsible for all macroscopic transport of heat, momentum and magnetism.
5. The system is axisymmetric.
6. Convection is subsonic or, if supersonic, only mildly so.

7. The system is chemically homogeneous.

We now consider each of these assumptions and explain how they limit our results.

We have already discussed the first of these extensively at various points, but it is worth emphasising that the plateau in Jupiter's differential rotation profile near the surface is evidence of the limitations imposed by our neglect of geometry. Our analysis provides a local prediction for what is actually a globally-determined phenomenon, and so really is only suitable to relate, for instance, the mean $\Omega/|N|$ in a convection zone to the mean $|R\nabla\Omega|$, rather than to calculate anything at any specific point in a system. With appropriate consideration of boundary conditions this may be remedied, but such an analysis rapidly becomes quite complex to perform generally, even as an order of magnitude exercise, and so we are content to leave this for the future.

The next assumption is that perturbing forces such as tides or external heating may be neglected. In single systems this is correct, but in binary or planetary systems it may fail. In order for tides to be relevant the angular momentum transport they induce must be at least of order the steady state flux which is transported by the various terms which balance in the vorticity equation. Likewise in order for heating to be relevant it must be at least of order that owing to the rotational perturbations to the equation of thermal equilibrium. In either case these are large but not insurmountable barriers. In hot Jupiter systems heating owing either to tides or to insolation may even exceed the heat flux from the centre ¹¹⁷. Likewise in a slowly-rotating close binary system the non-equilibrium tidal potential could easily be the dominant mode of angular momentum transport. It is more difficult to arrange for this to be the case in rapidly rotating systems, but such scenarios likely exist.

¹¹⁷Jermyn et al. 2017

Our third assumption really enters the analysis only insofar as it allows us to use an ideal gas-type equation of state. In particular, in several places we have used the fact that the pressure depends on both temperature and density. Removing the dependence on temperature changes the structure of these arguments significantly and so we have simply ignored such cases. This means that our analysis cannot be applied robustly to compact objects, rocky or otherwise solid bodies, or to degenerate planetary cores. In such systems though the microscopic viscosity may be quite large and convection may not be fully developed, and so we would need to exclude them anyway.

The fourth assumption is principally one of convenience: by neglecting

microscopic diffusivities we achieve significant simplifications of the equations of thermal and vorticity equilibrium. Indeed the true momentum diffusivity in systems for which the third assumption holds is genuinely expected to be extremely small ¹¹⁸. On the other hand the thermal diffusivity may not be small, and near the tachocline this assumption definitely fails. Nevertheless, for systems in which a convecting region is large enough to matter for the rotation of the system we expect it to also be large enough that the tachocline does not dominate its dynamics. In effect this is an extension of the assumption that geometry, and hence boundary effects, are not too important.

¹¹⁸ Spitzer 1956

Related to this, there is one place in which the microscopic thermal diffusivity cannot be neglected, namely near breakup rotation. As we have mentioned, the scaling laws we have derived do not hold all the way to the breakup velocity. We have shown that this is because a system which does not reconfigure to follow Keplerian rotation cannot continue to convect as the rotation approaches the breakup rate. The way in which convection is disrupted, however, is by reducing the effective gravity such that a radiative temperature gradient may be convectively stable. This requires that there be a finite radiative gradient, and so requires that the diffusivity not vanish. It may be arbitrarily small because reducing the diffusivity just shifts the rotation rate at which convection ceases closer to the breakup rate, but for any non-zero diffusivity there is a rotation rate at which convection fails. This may seem a pedantic technical point, but it is important to note because it precludes smoothly connecting the rapidly-rotating convecting solution to that of a Keplerian disk. Notably this points to one of the key open problems in understanding heat transport in W UMa ¹¹⁹ systems ¹²⁰, namely that there must be regions in which convection fails because the effective gravity vanishes.

¹¹⁹ i.e. low-mass contact binary

¹²⁰ Li et al. 2004

Along similar lines, in Jupiter the microscopic conductivity changes dramatically at the depths at which ionization occurs. This is responsible for the transition from hydrodynamic to magnetohydrodynamic scaling. This is captured in our analysis by a change in the turbulence closure equations, and so is explicitly handled, but even so there is a transition region in which neither analysis is quite right. Similar to the tachocline, we require that this region not be too important. However Jupiter's geometry is such that its surface layers strain this assumption.

The fifth assumption, that of axisymmetry, is a strong one. It is responsible for a myriad of simplifications in our equations, and in particular controls the orders of various perturbations which are protected by this

symmetry. As a result any phenomena which break this symmetry may introduce new modes of heat and momentum transport which disagree with our calculations by an amount which is proportional to the symmetry breaking. This is a concern for systems which exhibit tides or non-axisymmetric external heating. In many cases these effects are either very low in amplitude, as in a long-period binary, or very high in frequency, as in a short-period binary. In the former case they may be neglected owing to their amplitude, while in the latter they may produce no leading order effect because they are not well-matched frequency-wise to the turbulence. This was first noted by Goldreich & Keeley (1977) in the context of tides, where at high frequencies relative to $|N|$ convection only couples weakly to the tidal potential. Nevertheless there are cases in which axisymmetry strongly fails, such as in W UMa systems¹²¹, and so this assumption is worth considering carefully when applying our results.

¹²¹ Li et al. 2004

We have already discussed the assumption that convection is subsonic and so merely note that this assumption would only result in incorrect scaling relations if the Mach number were to exceed unity by a factor which depended strongly on $\Omega/|N|$. That is, if the Mach number exceeds unity by a factor of a few which is set by thermodynamic considerations our analysis is unchanged, but if the Mach number can increase without bound as $\Omega \rightarrow 0$ or ∞ we have a problem because then we cannot bound the convection speed by thermodynamic considerations. In fact we have shown that this is not the case, because the convection speed is largely independent of Ω as $\Omega \rightarrow 0$ and decreases for fixed $|N|$ as $\Omega \rightarrow \infty$. This assumption is therefore not one which we expect to be violated in any significant way.

Finally we must consider chemistry. We have assumed everywhere that the system is chemically homogeneous. This is actually quite straightforward because convection rapidly mixes chemical composition and so we do not expect to find substantial violation of this assumption unless, for instance, material is being injected into a convection zone at a rate comparable to the convective mass flux. This is a rather exotic scenario though, and with a few notable exceptions¹²² does not reflect a system which is undergoing evolution on secular/nuclear time-scales, so we suffer no great loss by excluding it.

¹²² e.g. hot bottom burning in Asymptotic Giant Branch stars

3.15 Discussion and Outlook

In this work we studied differential rotation in both slowly and rapidly rotating convection zones in both the hydrodynamic and magnetohydro-

dynamic limits. We have found that when the system is rotating slowly

$$|\nabla\Omega| \approx \Omega R^{-1}.$$

When it is rotating rapidly and is magnetised we found that

$$|\nabla\Omega| \approx \Omega^{1/7} |N|_0^{6/7} R^{-1},$$

and when non-magnetised

$$|\nabla\Omega| \approx \Omega^{1/3} |N|_0^{2/3} R^{-1}.$$

In the last two equations $|N|_0$ is the Brunt-Väisälä frequency which would arise if the system were not rotating. This is related to the actual Brunt-Väisälä frequency $|N|$ by

$$|N| = |N|_0 \left(\frac{\Omega}{|N|_0} \right)^{1/7}$$

and

$$|N| = |N|_0 \left(\frac{\Omega}{|N|_0} \right)^{1/3}$$

for non-magnetised systems. In addition we have explored the scaling of the meridional circulation u and baroclinicity ξ , and found that these increase as Ω^2 before reaching plateaus at $u \approx \Omega^2 h / |N|$ and $\xi \approx 1$.

In the slow-rotation limit we did not find any preference for different shear directions which scaled with the rotation rate. There the angular momentum balance is chiefly between the turbulent viscosity and the Λ -effect, with all other terms scaling more slowly with angular velocity.

By contrast in the rapid-rotation limit the shear is preferentially in the cylindrical radial direction, and that preference is enforced by a factor of $\Omega / |N|$. Thus the Taylor-Proudman theorem becomes increasingly relevant. This is because the term which couples the shear in the direction along the rotation axis scales more strongly with Ω than any other in the azimuthal vorticity equation, followed by the turbulent stress terms, and so these are the effects which balance asymptotically. In the meridional vorticity equation the former term does not appear, and so the radial differential equation balances the stress and ends up asymptotically larger.

An important consequence of this is that a great many details of a convecting system are irrelevant to the question of the magnitude of its differential rotation. All that matters to leading order is the bulk ratio $\Omega / |N|_0$, which is readily computed from observable parameters such as the

rotation rate, surface temperature and mean density. This allows a wide range of systems to be approximately characterised with minimal data, and should help to support future studies of momentum and magnetic flux transport in convection zones.

3.16 Data Processing

We now detail the way in which data were processed to produce Fig. 3.4. The two variables of interest in each case are $|R\nabla\Omega|/\Omega$ and $\Omega/|N|_0$. All scripts used in this data processing shall be made available at github.com/adamjermyn/DifferentialRotation2018.

3.16.1 Solar Data

Helioseismic inversions were obtained from Antia (2016), corresponding to that appearing in Antia et al. (2008). This includes Ω as a function of position throughout the convective envelope as well as in the upper portions of the radiative envelope. This profile was then supersampled onto a grid running from $0.5R_\odot$ to R_\odot in the radial direction with 100 points uniformly spaced and from 0 to π in the latitude with 70 points uniformly spaced. By applying a differentiating gaussian filter with width equal to five grid points in each of the radial and latitudinal directions we computed $R\nabla\Omega/\Omega$ from this profile. We then averaged the square of this over latitude, weighted by $\sin\theta$, and took the square root of the result to produce a measure of the mean differential rotation at each radial slice.

The radial profile of $|N|$ was obtained from a model computed by G. Houdek and D. O. Gough, which is the same model used by Chaplin et al. (2005) in their study of the power spectral density of solar p modes. This was used to compute $\Omega/|N|$ everywhere in the solar convection zone. We then averaged $\Omega^2/|N|^2$ over latitudes again weighting by $\sin\theta$ and computed the square root to determine the mean $\Omega/|N|$ in each radial slice. This was then plotted alongside our measure of the differential rotation in each radial slice.

3.16.2 Jupiter Data

The profile of differential rotation in the surface layers of Jupiter was taken to be that in Kaspi et al. (2018). This yields the variation of the characteristic zonal flow rate with depth but does not provide the shear itself. To compute this we first note that roughly 30 per-cent of Jupiter's latitudes are covered in bands with velocities of order 100km s^{-1} , while the remaining latitudes contain bands with velocities of order $^{123} 25\text{km s}^{-1}$. The former are also approximately twice as wide per band as the latter. There are approximately 15 bands in total, and so we define the typical

¹²³ Kaspi et al. 2018

shear at the surface as

$$|R\nabla\Omega| \approx \frac{15}{\pi R_J} \left(0.3 \times 25 \text{ km s}^{-1} + \frac{1}{2} \times 0.7 \times 100 \text{ km s}^{-1} \right),$$

where $R_J \approx 7 \times 10^9 \text{ cm}$ is the radius of Jupiter. We then assume that the band velocities scale with depth as found by [Kaspi et al. \(2018\)](#) while the mean rotation period remains ¹²⁴ 9.92hr.

¹²⁴ [Kaspi et al. 2018](#)

For regions deeper than 3000km we bound the band velocity above by the inferred ¹²⁵ 6 m s^{-1} and use the band structure above to compute the shear. Furthermore we treat the number of bands as varying linearly in radial coordinate between 1 near the centre of the planet and 15 at the surface. This is an approximation of the cylindrical nature of Jupiter's differential rotation.

¹²⁵ [Guillot et al. 2018](#)

All that remains is to compute $|N|_0$. To do this we recall that

$$|N|_0 \approx h^{-1} \left(\frac{F}{\rho} \right)^{1/3}.$$

Jupiter has ¹²⁶ $F \approx 5000 \text{ erg cm}^{-2} \text{ s}^{-1}$. We take h to be approximately equal to the depth at any given point in the planet. Using equation (3.19) and matching the ratio of p/ρ against the profile in [Guillot et al. \(2004\)](#) we find that at 3000km, $\rho \approx 0.4 \text{ g cm}^{-3}$. With this we find that at a depth of 3000km, $|N|_0 \approx 8 \times 10^{-8} \text{ s}^{-1}$. Because Jupiter is approximately adiabatic in its convection zone and neglecting changes in radius we may write

¹²⁶ [Liu et al. 2008](#)

$$h = \frac{p}{\rho g} \propto \rho^{\gamma-1} \propto \rho^{2/3},$$

hence

$$|N|_0 \propto \rho^{-1} \propto h^{-3/2}.$$

This may be used to find $|N|_0$ everywhere. We truncate the model where $h \approx 40 \text{ km}$, which is the approximate scale height at the cloud deck, obtained using a temperature of ¹²⁷ 300K and solar composition. The precise choice of truncation point is not relevant so long as it is not too far from the convective-radiative transition.

¹²⁷ [Seiff et al. 1998](#)

3.16.3 *Reiners Observations*

Data were taken from Table 5 of [Reiners & Schmitt \(2003\)](#). The reported differential rotation is in the form of the coefficient α defined in equation (6.5) and we treat it as we have previously. The rotation rate is reported as $v \sin i$, where v is the surface rotation velocity. Inclinations are

also reported, so we use these to compute v and propagate errors using the formula

$$d\mu = \sqrt{\sum_j \left(\frac{\partial \mu}{\partial x_j} \right)^2 dx_j^2},$$

where μ is a function of interest and x_j are variables on which it depends. This amounts to assuming that errors are uncorrelated and small relative to the scale over which higher-order derivatives are relevant.

To proceed further we need an estimate of the radius of each star. We obtain this from stellar scaling relations, noting that

$$R \propto M^{0.7}$$

and

$$L \propto M^{3.7}$$

¹²⁸. Hence $T \propto L^{1/4} R^{-1/2} \propto M^{0.58}$. Using this we may compute M from the provided temperatures. We then let $|N|_0$ be the mean $|N|$ in the solar convection zone (spatially averaged), scaled to each star as $(T/T_\odot)^{4/3}$ because

¹²⁸ Demircan & Kahraman 1991

$$|N|_0 \approx h^{-1} \left(\frac{F}{\rho} \right)^{1/3} \propto T^{4/3} h^{-1} \rho^{-1/3}.$$

We neglect the variation of ρ because it enters to a much lower power than that of T . We further neglect the variation of h because it is just of order the depth of the convection zone, which we expect to be comparable to within a factor of a few across the stars in the sample. Providing better estimates of its depth requires more detail about each object, including ages and compositional information, and so we do not attempt to capture this detail. Given R and $|N|_0$ we may calculate first $\Omega = v/R$ and thereby compute $\Omega/|N|_0$.

3.16.4 Deheuvels Observations

Data were taken from Deheuvels et al. (2012) and Deheuvels et al. (2015). The reported differential rotation is in the form of the difference between the core and envelope rotation rates divided by the envelope rotation rate, which we take to equal $|R\nabla\Omega|/\Omega$.

The rotation rate is provided in the text and we estimate $|N|$ for the red

giants as

$$|N|_0 \approx h^{-1} \left(\frac{F}{\rho} \right)^{1/3},$$

taking ρ to be the mean density of the star and $h \approx R$. Given the extent of convection zones in these systems both are reasonable approximations.

3.16.5 *Donati Observations*

Data were taken from [Donati et al. \(2008\)](#). The reported differential rotation rate is the surface equator–pole difference in Ω normalised against that of the equator. Because this spans 1.5 radians we divide by 1.5 to place it in the same units as $\partial_\theta \Omega / \Omega$. We take this as to be approximately $|R\nabla\Omega|/\Omega$.

The paper reports the Rossby number, defined as $|N|_0/\Omega$, so we let

$$\frac{\Omega}{|N|_0} \approx \text{Ro}^{-1}.$$

3.16.6 *Frasca Observations*

Data were taken from [Frasca et al. \(2011\)](#). The reported differential rotation is in the form of the coefficient α defined in equation (6.5) and we treat it as we have previously. The rotation rate is reported as $v \sin i$, where v is the surface rotation velocity. The inclination is also reported, so we use it to compute v . As with the observations of [Reiners & Schmitt \(2003\)](#) we take $|N|_0 \propto T^{4/3}$, where in this case T is reported at the surface. With this we may calculate first $\Omega = v/R$ and thereby compute $\Omega/|N|_0$.

3.16.7 *Bonanno Observations*

Data were taken from [Bonanno et al. \(2014\)](#). The reported differential rotation is in the form of a latitudinal variation $d\Omega$ in the rotation rate. We normalise this against the mean rotation rate. We take this as to be approximately $|R\nabla\Omega|/\Omega$. As with the observations of [Reiners & Schmitt \(2003\)](#) we take $|N|_0 \propto T^{4/3}$, where in this case T is reported at the surface.

3.16.8 *Nielson Observations*

Data were taken from Table 1 of [Nielsen et al. \(2017\)](#). The reported differential rotation is in the form of the difference between the core and envelope rotation rates divided by the envelope rotation rate, which we take to equal $|R\nabla\Omega|/\Omega$. We then let $|N|_0$ be the mean $|N|$ in the solar

convection zone because these stars are all very similar to the Sun in mass and radius. From this we compute $\Omega/|N|_0$.

3.16.9 *Klion Observations*

Data were taken from the text of [Klion & Quataert \(2017\)](#) with $|R\nabla\Omega|/\Omega$ taken from the best-fitting power law to be 1. The rotation rate is provided in the text and we estimate $|N|$ for the red giant as before with

$$|N|_0 \approx h^{-1} \left(\frac{F}{\rho} \right)^{1/3},$$

taking ρ to be the mean density of the star and $h \approx R$.

3.16.10 *Brown 2008 Simulations*

The data are from the simulations in [Brown et al. \(2007\)](#). These were extracted with automated graphic data extraction software which uses the positions of points on a figure along with calibration of the figure axes to determine the underlying data. This provided the surface difference of the rotation between the equator and the line of 60 degrees of colatitude. We normalise this against the mean rotation rate and take it as measuring $|R\nabla\Omega|/\Omega$. We compute $\Omega/|N|_0$ using $|N|_0$ as being that from the Sun averaged spatially over the convection zone, as these are simulations of solar-type stars.

3.16.11 *Brun 2005 Simulations*

The data are from the simulations in [Brun et al. \(2005\)](#). The differential rotation is reported as the mass-weighted average of the squared difference between the rotation rate and the mean rotation rate. We therefore compute

$$|R\nabla\Omega| \approx \sqrt{\langle (\Omega - \bar{\Omega})^2 \rangle},$$

where $\langle \dots \rangle$ denote the mass-weighted average and $\bar{\Omega}$ is the mean rotation rate.

The Rossby number actually realised in the flow is also reported. This is defined in that work as

$$\text{Ro} = \frac{v_c}{2\Omega R},$$

In these hydrodynamic simulations we may use $F \approx \rho v_c^3$ to find that v_c is approximately invariant with respect to Ω and hence $v_c \approx h|N|_0$. Taking

$h \approx R$ because the depth is comparable to the radius we find

$$\frac{\Omega}{|N|_0} \approx 2\text{Ro}^{-1}.$$

3.16.12 Brun 2009 Simulations

The data are from the simulations in [Brun & Palacios \(2009\)](#). The differential rotation is reported as the mass-weighted average of the squared difference between the rotation rate and the mean rotation rate. We therefore compute

$$|R\nabla\Omega| \approx \sqrt{\langle(\Omega - \bar{\Omega})^2\rangle},$$

where $\langle...\rangle$ denote the mass-weighted average and $\bar{\Omega}$ is the mean rotation rate.

The Rossby number actually realised in the flow is also reported. This is defined in that work as

$$\text{Ro} = \frac{\omega_{\phi,\text{convective}}}{2\Omega},$$

where $\omega_{\phi,\text{convective}} \approx v_c/h$ is the root-mean-squared vorticity of the convective flow. Thus we find

$$\frac{\Omega}{|N|_0} \approx 2\text{Ro}^{-1}.$$

3.16.13 Augustson 2016 Simulations

The data are from the simulations in [Augustson et al. \(2016b\)](#). The differential rotation is reported as the mass-weighted average of the squared difference between the rotation rate and the mean rotation rate. We therefore compute

$$|R\nabla\Omega| \approx \sqrt{\langle(\Omega - \bar{\Omega})^2\rangle},$$

where $\langle...\rangle$ denote the mass-weighted average and $\bar{\Omega}$ is the mean rotation rate.

The Rossby number actually realised in the flow is also reported. This is defined in that work as

$$\text{Ro} = \frac{\omega_{\phi,\text{convective}}}{2\Omega},$$

where $\omega_{\phi,\text{convective}} \approx v_c/h$ is the root-mean-squared vorticity of the con-

vective flow. Thus we find

$$\frac{\Omega}{|N|_0} \approx 2\text{Ro}^{-1}.$$

3.16.14 Brun 2017 Simulations

The data are from the simulations in [Brun et al. \(2017\)](#). The differential rotation is reported as the surface difference in rotation rate between the equator and the line of 60 degrees of colatitude. We normalise this against the mean rotation rate and take it as measuring $|R\nabla\Omega|/\Omega$.

The Rossby number actually realised in the flow is also reported. This is defined in that work as

$$\text{Ro} = \frac{v_c}{2\Omega R},$$

In these hydrodynamic simulations we may use $F \approx \rho v_c^3$ to find that v_c is approximately invariant with respect to Ω and hence $v_c \approx h|N|_0$. Taking $h \approx R$ because the depth is comparable to the radius we find

$$\frac{\Omega}{|N|_0} \approx 2\text{Ro}^{-1}.$$

3.16.15 Gastine Simulations

The data are from the simulations in [Gastine et al. \(2014\)](#). These were extracted with automated graphic data extraction software, providing the quantity

$$\alpha \equiv \frac{\Omega - \bar{\Omega}}{\bar{\Omega}}, \quad (3.72)$$

where $\bar{\Omega}$ is the rotation rate of the frame with zero total angular momentum and Ω is evaluated at the surface of the simulated star on the equator. We treat α as measuring $|R\nabla\Omega|/\Omega$ and in that way determine the differential rotation.

To measure the rotation we note that α is provided as a function of the convective Rossby number, which is defined in that work as $|N|/\Omega$. We then use the scaling in equation (3.64) to compute $\Omega/|N|_0$.

3.16.16 Aurnou Simulations

The data from the simulations by [Aurnou et al. \(2007\)](#) appear in the second summary figure in [Gastine et al. \(2014\)](#). These were extracted with

automated graphic data extraction software, providing the quantity

$$\alpha \equiv \frac{\Omega - \bar{\Omega}}{\bar{\Omega}}, \quad (3.73)$$

where $\bar{\Omega}$ is the rotation rate of the frame with zero total angular momentum and Ω is evaluated at the surface of the simulated star on the equator. We treat α as measuring $|R\nabla\Omega|/\Omega$ and in that way determine the differential rotation.

To measure the rotation we note that α is provided as a function of the convective Rossby number, which is defined in that work as $|N|/\Omega$. We then use the scaling in equation (3.64) to compute $\Omega/|N|_0$.

3.16.17 Soderlund Simulations

The data from the simulations by Soderlund et al. (2013) appear in the second summary figure in Gastine et al. (2014). These were extracted with automated graphic data extraction software, providing the quantity

$$\alpha \equiv \frac{\Omega - \bar{\Omega}}{\bar{\Omega}}, \quad (3.74)$$

where $\bar{\Omega}$ is the rotation rate of the frame with zero total angular momentum and Ω is evaluated at the surface of the simulated star on the equator. We treat α as measuring $|R\nabla\Omega|/\Omega$ and in that way determine the differential rotation.

To measure the rotation we note that α is provided as a function of the convective Rossby number, which is defined in that work as $|N|/\Omega$. We then use the scaling in equation (3.64) to compute $\Omega/|N|_0$.

3.16.18 Kaspi Simulations

The data from the simulations by Kaspi et al. (2009) appear in the second summary figure in Gastine et al. (2014). These were extracted with automated graphic data extraction software, providing the quantity

$$\alpha \equiv \frac{\Omega - \bar{\Omega}}{\bar{\Omega}}, \quad (3.75)$$

where $\bar{\Omega}$ is the rotation rate of the frame with zero total angular momentum and Ω is evaluated at the surface of the simulated star on the equator. We treat α as measuring $|R\nabla\Omega|/\Omega$ and in that way determine the differential rotation.

To measure the rotation we note that α is provided as a function of the convective Rossby number, which in that work is $|N|/\Omega$. We then use the

scaling in equation (3.64) to compute $\Omega/|N|_0$.

3.16.19 Rogers Simulations

Data were taken from the table in Rogers (2015). The text surrounding the table provides v_c for the two extremal convective forcing functions and so we linearly interpolate as

$$v_c = [2.9 + (q - 1.5) * (4.5 - 2.9)] \text{ km s}^{-1},$$

where $q \equiv \bar{Q}/c_v$ is the convective forcing. We take the scale height to be the size of their convection zone, which is $0.3R_\odot$. For slow rotation we use $|N| \approx v_c/h$, while for fast convection we use equation (3.64) to find

$$|N|^{3/2} \Omega^{-1/2} \approx h^{-1} v_c,$$

so

$$|N|_0 \approx h^{-1} v_c.$$

In both cases we find the same result, because in slow rotation $|N| \approx |N|_0$.

The output of the simulation is the ratio of the core rotation rate to the envelope rotation rate, which we take to be $|R\nabla\Omega|/\Omega$.

3.16.20 Mabuchi Simulations

Data were taken from Table 1 of Mabuchi et al. (2015). The reported differential rotation is in the form of α as defined in equation (6.5). The Rossby number actually realised in the flow is also reported. This is defined in that work as

$$\text{Ro} = \frac{\pi v_c}{\Omega d},$$

where d is the radial extent of the convection zone.

In the hydrodynamic simulations we may use $F \approx \rho v_c^3$ to find that v_c is approximately invariant with respect to Ω and hence $v_c \approx h|N|_0$. Taking $d \approx h$ we find

$$\frac{\Omega}{|N|_0} \approx \pi \text{Ro}^{-1}.$$

In the magnetohydrodynamic simulations we instead use the convective Rossby number Ro_c , which is approximately $\pi|N|/\Omega$, in combination with

the scaling in equation (3.50) to find

$$\frac{\Omega}{|N|_0} \approx (\pi \text{Ro}_c^{-1})^{7/6}.$$

3.16.21 *Käpylä Simulations*

Data were taken from Table 1 of Käpylä et al. (2011). The reported differential rotation rate is the surface equator-pole difference in Ω normalised against that of the equator. Because this spans 1.5 radians we divide by 1.5 to place it in the same units as $\partial_\theta \Omega / \Omega$. We take this as to be approximately $|R\nabla\Omega|/\Omega$.

The paper reports the Rossby number actually realised in the flow, defined as in the simulations by Mabuchi et al. (2015), so as before we simply let

$$\frac{\Omega}{|N|_0} \approx \pi \text{Ro}^{-1}.$$

3.16.22 *Guerrero Simulations*

Data were taken from Table 1 of Guerrero et al. (2013). The reported differential rotation rate is the surface equator-pole difference in Ω normalised against that of the equator. Because this spans 1.5 radians we divide by 1.5 to place it in the same units as $\partial_\theta \Omega / \Omega$. We take this as to be approximately $|R\nabla\Omega|/\Omega$.

The paper reports the Rossby number actually realised in the flow, defined as $2|N|_0/\Omega$, so we simply let

$$\frac{\Omega}{|N|_0} \approx 2\text{Ro}^{-1}.$$

3.16.23 *Gilman Simulations*

These simulations were reported in Gilman (1977) and Gilman (1979) and appear in the second summary figure in Gastine et al. (2014). These were extracted with automated graphic data extraction software, providing the quantity

$$\alpha \equiv \frac{\Omega - \bar{\Omega}}{\bar{\Omega}}, \quad (3.76)$$

where $\bar{\Omega}$ is the rotation rate of the frame with zero total angular momentum and Ω is evaluated at the surface of the simulated star on the equator. We treat α as measuring $|R\nabla\Omega|/\Omega$ and in that way determine the differential rotation.

To measure the rotation we note that α is provided as a function of the convective Rossby number, which in that work is $|N|/\Omega$. We then use the scaling in equation (3.64) to compute $\Omega/|N|_0$.

4 *Rotational Mixing in Massive Stars*

Your assumptions are your windows on
the world. Scrub them off every once in a
while, or the light won't come in.

Isaac Asimov

Abstract

Convection in the cores of massive stars becomes anisotropic when they rotate. This anisotropy leads to a misalignment of the thermal gradient and the thermal flux, which in turn results in baroclinicity and circulation currents in the upper radiative zone. We show that this induces a much stronger meridional flow in the radiative zone than previously thought. This drives significantly enhanced mixing, though this mixing does not necessarily reach the surface. The extra mixing takes on a similar form to convective overshooting, and may help explain the large overshoot distances inferred from observations. This has significant consequences for the evolution of these stars by enhancing core-envelope mixing.

4.1 Introduction

The problem of meridional mixing in the radiative zones of rotating stars has been studied for nearly a century ¹. The understanding that has emerged is based on the famed von Zeipel theorem ², which states that in a radiative zone there is no way to satisfy the equations of hydrostatic and thermal equilibrium without allowing the pressure and temperature to vary separately. Hence in rotating stars thermodynamic quantities are not solely determined by the pressure; they exhibit baroclinicity. This baroclinicity drives a circulation current that mixes material in the meridional plane.

The scale of this current is proportional to the heat flux, to the reciprocal of the entropy gradient and to $\Omega^2 R/g$, where Ω is the angular velocity and g and R are the typical gravity and cylindrical radial coordinate in the radiative zone. The interpretation of this effect, either as due to transient damping or a genuinely driven flow, has led to some controversy ³ but it is generally agreed that the mixing itself occurs ⁴.

Underlying the standard analysis of this mixing is the assumption that baroclinicity is set locally in the radiative zone by the requirements of thermal and hydrostatic equilibrium. A key result of this work is that this is not true in stars with central convection zones⁵. In such stars rotation distorts convective motions, which sets a baroclinic boundary condition at the base of the radiative zone. This boundary condition is often more significant than the locally-generated baroclinicity and so results in enhanced circulation. This scenario has not been adequately studied and constitutes a novel driver for meridional flows in the radiative zones of massive rotating stars.

A related scenario that has been studied extensively is that of circulation driven by mechanical pumping in the convection zone. For instance (Garaud & Brummell, 2008; Garaud & Acevedo Arreguin, 2009) examined the transmission of mechanical forcing across the tachocline and (Garaud & Bodenheimer, 2010) extended this to stars with multiple convection zones, where there may be interesting interactions between the zones mediated by the intervening radiative zone. A key insight of these studies which also holds for our scenario is that the circulation cannot be transmitted and propagated without significant mechanical stresses in the radiative zone. Such stresses have also been considered as drivers of circulation (Zahn, 1992; Maeder & Zahn, 1998) and so must be taken into account in any analysis of these phenomena.

The possibility of enhanced mixing in these systems is particularly rele-

¹ Eddington 1929; Maeder & Zahn 1998

² Zeipel 1924

³ Busse 1981

⁴ Osaki 1982

⁵ These are those with masses above $1.2M_{\odot}$

vant in light of the recent discovery of gravitational waves from merging binary black holes ⁶. This has led to increased interest in formation mechanisms for massive stellar cores the subsequent evolution of which can produce massive black holes. Many such mechanisms are quite sensitive to the magnitude of rotational mixing, particularly in the most massive stars ⁷, and so understanding this phenomenon in more depth is extremely important.

⁶ Abbott et al. 2016

⁷ Marchant, Pablo et al. 2016

In Section 4.2 we review the derivation of the meridional velocity by Eddington (1929), Sweet (1950) and Zeipel (1924). Briefly, the centrifugal effect distorts isobars, causing a flux anisotropy which violates thermal equilibrium⁸. Thermal equilibrium is then restored by inducing baroclinicity⁹ and hence introducing a circulation current¹⁰.

⁸ Fig. 4.1, top panel

⁹ Fig. 4.1, middle panel

¹⁰ Fig. 4.1, bottom panel

In Section 4.4 we argue that turbulent anisotropy in the convection zone makes the zone baroclinic. This arises because the Coriolis effect couples different components of the velocity and so produces heat transport at an angle to the entropy gradient, as shown in Fig. 4.2. We show in Section 4.5 that this effect is much greater than that caused by the centrifugal acceleration. As in the case of radiative zones this results in a circulation current, which we characterise in Section 4.6. Notably this is significantly enhanced relative to what would occur in a radiative zone because the radial entropy gradient is much smaller in convection zones.

A further consequence of turbulent anisotropy is that the heat flux in the zone is highly aspherical¹¹. This is important in massive stars with convective cores because this flux perturbation produces baroclinicity at the base of the radiative zone. In Section 4.7 we argue that this baroclinic boundary condition serves to drive additional mixing in the radiative zone. This mixing is often orders of magnitude greater than what the Eddington–Sweet calculation alone provides. We then comment on the prospects for similar mechanisms in stars of lower mass.

¹¹ This is related to the baroclinicity because the convective flux depends strongly on the entropy gradient.

In Section 4.9 we argue that these circulation currents are actually the source of the extra mixing normally attributed to convective overshooting. Finally we discuss the physical interpretation of the circulation in light of historical difficulties with the Eddington–Sweet circulation.

4.2 Origins of Meridional Flow

The meridional velocity arises from the impossibility of thermal and hydrostatic equilibrium when the pressure gradient is misaligned with the thermal flux. In the case considered by Eddington (1929) and von Zeipel ¹² this arises because of a bending of the isobars owing to $O(\Omega^2)$ centrifugal

¹² Zeipel 1924

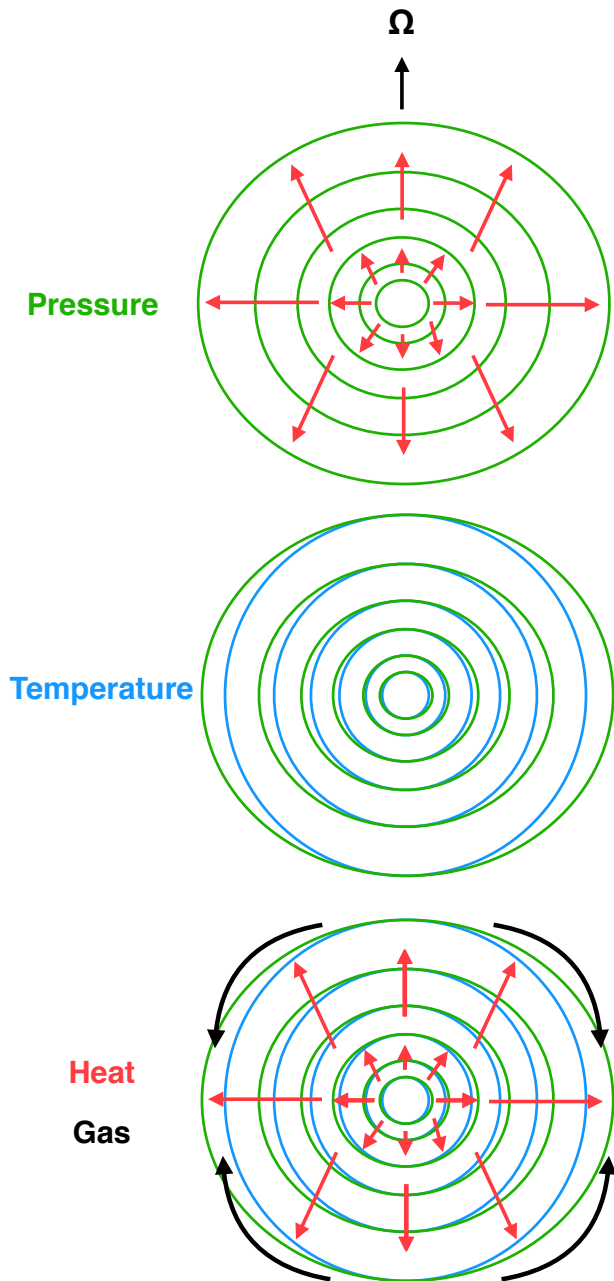


Figure 4.1: Centrifugal effects distort isobars. Variation in the magnitude of the pressure gradient along isobars leads to a flux anisotropy (top panel). This pushes the system out of thermal equilibrium, and a new equilibrium is established with baroclinicity (i.e. mismatched entropy and pressure surfaces, middle panel) and circulation currents (bottom panel). The length of the arrows is not meaningful. Likewise the geometry of the gas circulation is only meant schematically.

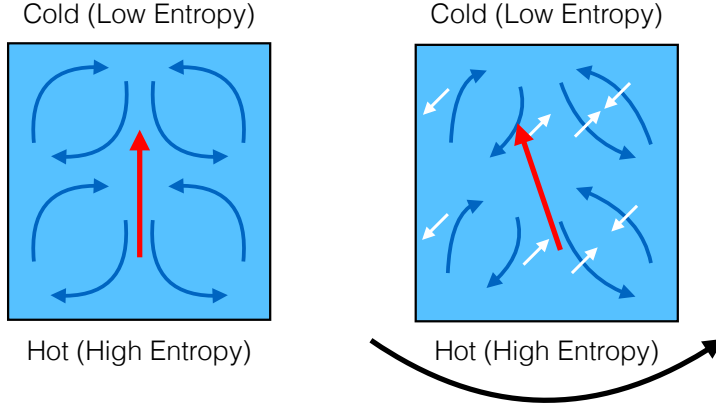


Figure 4.2: Non-rotating convection (left, blue arrows) transports heat along the entropy gradient. Rotating convection (right, blue arrows) is distorted by the Coriolis force (white arrows) and so transports heat at an angle relative to the entropy gradient.

effects. We now review this derivation.

To begin note that, in the absence of differential rotation, there exists an effective potential satisfying

$$\nabla^2 \Phi = 4\pi G\rho - 2\Omega^2. \quad (4.1)$$

With hydrostatic equilibrium we also have

$$\nabla p = -\rho \nabla \Phi \quad (4.2)$$

This means that

$$\nabla \times \left(\frac{1}{\rho} \nabla p \right) = -\nabla \times \nabla \Phi = 0$$

and so

$$\nabla \rho \times \nabla p = 0, \quad (4.3)$$

hence isobars and isochors coincide. From equation (4.2) it follows that these coincide with surfaces of constant Φ and so p and ρ may be written solely as functions of Φ .

The energy balance in stars is given by equation (1.18) as

$$c_p \rho T \frac{\partial s}{\partial t} = \frac{\partial F_i}{\partial x_i} + \rho \varepsilon - \rho c_p T u_i \frac{\partial s}{\partial x_i},$$

where F is the diffusive flux, ε is the specific rate of energy generation from nuclear processes, s is the dimensionless entropy, ρ is the density, T is the temperature, u_i is the velocity and summation is over repeated indices.

In the case of radiation we may write the diffusive flux as

$$F_i = -\rho c_p \chi \frac{\partial T}{\partial x_i} \quad (4.4)$$

where χ is the thermal diffusivity and c_p is the specific heat at constant pressure. In steady state $\partial_t s$ vanishes and with no nuclear burning we may set $\varepsilon = 0$ so that

$$\frac{\partial F_i}{\partial x_i} - \rho c_p T u_i \frac{\partial s}{\partial x_i} = 0. \quad (4.5)$$

Now suppose that there is no meridional flow, $u = 0$. We have then

$$\frac{\partial F_i}{\partial x_i} = 0. \quad (4.6)$$

So from equation (4.4)

$$\frac{\partial}{\partial x_i} \left(\rho c_p \chi \frac{\partial T}{\partial x_i} \right) = 0. \quad (4.7)$$

All these quantities are thermodynamic variables which may be written as functions of p and ρ using the equation of state. Because p and ρ are functions only of Φ equation (4.7) may be written as

$$\frac{\partial}{\partial x_i} \left(q(\Phi) \frac{\partial \Phi}{\partial x_i} \right) = 0,$$

where q is a function only of potential. Expanding the divergence yields

$$\frac{dq}{d\Phi} |\nabla \Phi|^2 + q(\Phi) \nabla^2 \Phi = 0$$

and hence

$$|\nabla \Phi|^2 = -\frac{q(\Phi) \nabla^2 \Phi}{dq/d\Phi}. \quad (4.8)$$

The right-hand side may be evaluated with equation (4.1) to find a function only of Φ . The left-hand side, by contrast, may be written as

$$|\nabla \Phi|^2 = |\mathbf{g} - \Omega^2 R \mathbf{e}_r|^2,$$

where R is the distance from the rotation axis, \mathbf{e}_r is the cylindrical radial unit vector and \mathbf{g} is the acceleration due to gravity. This generally varies along isobars because the direction of \mathbf{g} changes while that of the centrifugal acceleration does not, and the magnitude of the centrifugal acceleration varies while, to leading order, that of gravity does not. As a result equation (4.8) cannot be satisfied simultaneously with equation (4.3). This is the original Eddington–Sweet argument for radiative zones ¹³.

¹³ Zeipel 1924

From this it follows that there must at a minimum be either a meridional

flow or differential rotation or both. The original Eddington–Sweet argument does not address the possibility of differential rotation as an alternative and so just concludes that a meridional flow arises with scale set by equation (4.5). In the next section we address this point and demonstrate that in fact both a meridional flow and differential rotation generally arise, with this equation setting the scale of the flow.

4.3 Differential Rotation

The derivation of the Eddington–Sweet circulation relies on it being impossible to satisfy equation (4.7) when the system is perfectly barotropic. One might think from the structure of the argument that this is just a mathematical difficulty rather than a physical one. After all, valid solutions could exist if one introduces an arbitrarily small differential rotation, introducing baroclinicity and allowing the cross-product in equation (4.3) to be non-zero.

While this is mathematically a valid concern, it runs up against physical difficulties because what matters is how rapidly the diffusivity and other thermodynamic variables may vary along an isobar. Suppose that equation (4.7) fails to be satisfied by a dimensionless amount of order ϵ . Differential rotation may arise and introduce baroclinicity, or misalignment of isobars and isotherms. If the angle of misalignment is of order $\lambda \ll 1$, logarithmic derivatives of the diffusivity along isobars must be at least of order ϵ/λ in order to satisfy equation (4.7). These derivatives ought to be of order unity so we must have $\lambda \approx \epsilon$ or $\lambda > \epsilon$.

There is then a degeneracy between differential rotation and the meridional circulation as far as the condition of thermal equilibrium is concerned. In Chapter 3 we used the vorticity equation to break this degeneracy and demonstrate that both effects are generically of the same order in convection zones. We now repeat that analysis for radiative zones¹⁴. For simplicity we neglect magnetic fields¹⁵ Hence equation (3.3) becomes

$$\begin{aligned} \frac{\partial \boldsymbol{\omega}}{\partial t} = & \boldsymbol{\omega} \cdot \nabla \mathbf{u} - \boldsymbol{\omega} \nabla \cdot \mathbf{u} - \mathbf{u} \cdot \nabla \boldsymbol{\omega} + \mathbf{e}_\phi \boldsymbol{\omega} \cdot \nabla (\Omega R) - \mathbf{e}_\phi \Omega \boldsymbol{\omega}_R \\ & + \frac{1}{\rho^2} \nabla \rho \times \nabla p + \nabla \times \left(\frac{1}{\rho} \nabla \cdot \mathbf{T} \right). \end{aligned} \quad (4.9)$$

where as before $\boldsymbol{\omega}$ is the vorticity and \mathbf{u} is the meridional velocity.

Suppose that differential rotation arises which satisfies equation (4.7) with no meridional flow. So $\mathbf{u} = 0$ and

$$\boldsymbol{\omega} = \mathbf{e}_z \frac{1}{R} \frac{\partial (\Omega R^2)}{\partial R} - \mathbf{e}_R R \frac{\partial \Omega}{\partial z}.$$

¹⁴ A similar and in many ways more detailed analysis was done by [Caleo et al. \(2015\)](#), but they neglect turbulent stresses, which we find to be crucial to the angular momentum balance. [Caleo & Balbus \(2016\)](#) studied linear modes in the solar radiative zone and found them to be asymptotically stable, though many such modes grow significantly in the short run. This is consistent with the findings of [Galperin et al. \(2007\)](#), who show that such modes which are not asymptotically unstable nevertheless generate turbulence for arbitrarily small shears, scaling in the manner predicted by [Canuto & Hartke \(1986\)](#) and [Zahn \(1993\)](#). This has been verified in simulations ([Prat, V. et al., 2016](#)) and is what we assume here.

¹⁵ When such fields are present they may serve an important role in suppressing circulations and differential rotation, though there is usually no dynamo in radiative zones so such a field may need to be primordial in origin.

This rotation must then also satisfy equation (3.3). In steady state this reduces to

$$0 = \mathbf{e}_\phi \mathbf{e}_z \cdot \nabla(\Omega^2 R) + \frac{1}{\rho^2} \nabla \rho \times \nabla p + \nabla \times \left(\frac{\nabla \cdot \mathbf{T}}{\rho} \right). \quad (4.10)$$

We refer to the first term as advective because it is related to the advection of angular momentum. The second is the thermal wind term ¹⁶ and the third reflects the turbulent stress.

¹⁶ Balbus et al. 2012

Because equation (4.10) is a vector equation it contains three scalar equations,

$$\begin{aligned} 0 &= \mathbf{e}_z \cdot \nabla(\Omega^2 R) + \frac{1}{r\rho^2} \left(\frac{\partial \rho}{\partial r} \frac{\partial p}{\partial \theta} - \frac{\partial p}{\partial r} \frac{\partial \rho}{\partial \theta} \right) + \mathbf{e}_\phi \cdot \nabla \times \left(\frac{\nabla \cdot \mathbf{T}}{\rho} \right), \quad (4.11) \\ 0 &= \mathbf{e}_R \cdot \nabla \times \left(\frac{\nabla \cdot \mathbf{T}}{\rho} \right) \end{aligned}$$

and

$$0 = \mathbf{e}_z \cdot \nabla \times \left(\frac{\nabla \cdot \mathbf{T}}{\rho} \right),$$

where r is the spherical radial coordinate. Given p and ρ satisfying equation (4.7) it is possible to solve for Ω with the first of these equations because ω is just a function of Ω . The remaining two equations must then be satisfied by that solution. Because they depend on the turbulent flux there is no reason to expect them to be satisfied by a rotation profile arrived at independently. As a result the vorticity equation is unlikely to be satisfied without a meridional flow.

From this we conclude that satisfying both the vorticity equation and thermal equilibrium requires a meridional flow. Now suppose that differential rotation permits baroclinicity of order λ . If $\lambda \ll \epsilon$ then thermal equilibrium relies on the meridional flow. If $\lambda \gg \epsilon$ then thermal equilibrium could be satisfied without such a circulation. Because the flow appears in the vorticity equation at first order multiplied by the rotation, and the differential rotation also appears at first order multiplied by the rotation, the flow must be at least as large as the differential rotation, possibly larger if turbulent stresses dominate. In this case then the flow is at least of order λ and hence also suffices to satisfy thermal equilibrium. This means that, no matter what, there is a meridional flow which is at least of order ϵ .

To be more precise note that because the system is axisymmetric the

thermal wind term has magnitude

$$\begin{aligned}\frac{1}{\rho^2} |\mathbf{e}_\phi \cdot \nabla p \times \nabla \rho| &= \frac{1}{\rho^2} |\nabla p \times \nabla \rho| \\ &= \frac{\lambda}{\rho^2 \gamma} |\nabla p| |\nabla \rho|,\end{aligned}$$

where we have used the definition λ as the small angle between the density and pressure gradients. Taking both derivatives to produce factors of order h^{-1} we find

$$\frac{1}{\rho^2} |\nabla p \times \nabla \rho| \approx \frac{\lambda p}{h^2 \rho^2 \gamma}.$$

Using $p = \rho g h$ and neglecting γ because it is of order unity yields

$$|\mathbf{e}_\phi \cdot (\nabla p \times \nabla \rho)| \approx \lambda \frac{g}{h}.$$

There are now two cases to consider. First suppose that in radiative zones the stress term in equation (4.11) balances the thermal wind term. Then as shown in Chapter 3

$$\left| \mathbf{e}_\phi \cdot \nabla \times \left(\frac{\nabla \cdot \mathbf{T}}{\rho} \right) \right| \approx \frac{\mathbf{T}}{\rho h^2} \approx \frac{g}{h} \lambda,$$

where we have approximated derivatives by factors of h^{-1} and where $\mathbf{T} = |\mathbf{T}| = \max(\mathbf{T}_{ij})$. Using equation (4.9) we may now calculate the circulation implied by the vorticity equation. Because the meridional circulation enters the meridional components of the vorticity equation in the form of gradients multiplied by Ω , we have

$$\mathbf{u} \approx \frac{1}{h \rho \Omega} \mathbf{T} \approx \lambda \frac{g}{\Omega}. \quad (4.12)$$

In essence we are balancing terms like $\boldsymbol{\omega} \cdot \nabla \mathbf{u}$ and $\boldsymbol{\omega} \nabla \cdot \mathbf{u}$ with the stress induced by the differential rotation and using¹⁷ $|\boldsymbol{\omega}| \approx \Omega$. The rate at which heat is deposited per unit volume by this flow is of order

$$Q = \rho c_p T \mathbf{u} |\nabla s| \approx \rho c_p T \frac{u}{h}, \quad (4.13)$$

because, in radiative zones, the entropy gradient is on the order of h^{-1} . Noting that c_p is of order k_B and so $p \approx \rho c_p T$ for an ideal gas, we find

$$Q \approx \lambda p \frac{g}{h \Omega}.$$

¹⁷ See Chapter 3 for a more detailed discussion of the geometry and magnitudes of these terms.

The flux anisotropy is

$$\Delta F \approx \epsilon F.$$

This deposits heat at a rate

$$\Delta Q = \nabla \cdot \Delta F \approx \epsilon \frac{F}{h},$$

where we have used the fact that the characteristic scale of the flux anisotropy is the pressure scale height. So

$$\frac{Q}{\Delta Q} \approx \frac{\lambda}{\epsilon} \left(\frac{gp}{\Omega F} \right) > \frac{gp}{\Omega F} = \frac{p\sqrt{gh}}{F} \left(\frac{g}{\Omega^2 h} \right)^{1/2} \gg \frac{p}{F} \sqrt{gh},$$

when $\lambda \geq \epsilon$ and $\Omega^2 \ll g/h$. Noting that

$$\sqrt{gh} = \sqrt{\frac{p}{\rho}} = c_s \sqrt{\gamma},$$

where c_s is the adiabatic sound speed, and that the heat flux in a radiative zone is bounded above by¹⁸ $c_s p$, we find that $Q > \Delta Q$. The heat transported in this way is therefore greater than the initial flux disturbance. As a result this flow does more to relieve the violation of thermal equilibrium than the differential rotation and so, in practice, a much milder differential rotation develops, with the circulation on the order of the baroclinicity.

A similar outcome can be seen in the case where the advective¹⁹ term balances the thermal wind term. Recall that the advective term is

$$\mathbf{e}_z \cdot \nabla(\Omega^2 R) \approx \Omega^2 |R \nabla \ln \Omega|,$$

where we have assumed that the differential rotation is not strongly preferentially along \mathbf{e}_R . In this case

$$|R \nabla \ln \Omega| \approx \lambda \frac{g}{h \Omega^2}. \quad (4.14)$$

Noting that $\lambda \geq \Omega^2 r/g$ we find²⁰

$$|R \nabla \ln \Omega| \geq \frac{r}{h} \approx 1, \quad (4.15)$$

where we have approximated r/h as unity because this is the case in the bulk of the star. Now note²¹ that the turbulent viscosity for vertical shear is of order

$$\nu \approx \alpha K \frac{S^2}{N^2}, \quad (4.16)$$

where α is a dimensionless constant of order unity, S is the shear, $N^2 \approx g/h$

¹⁸ To see this note that $F = 16\sigma|\nabla T^4|/3\kappa\rho$. If the medium is optically thick over a scale height then $\kappa\rho h > 1$, so $F < 16\sigma h|\nabla T^4| = 4acT^4 h|\nabla \ln T|$. The onset of convection occurs when $|\nabla \ln T| > (2/5)|\nabla \ln p| = 2/5h$, so $F < 8acT^4/5$. Noting that radiation pressure is given by $p = aT^4/3$, $F/p < (24/5)c(p_{\text{rad}}/p)$. The sound speed is $c_s = \sqrt{\gamma p/\rho} = c\sqrt{\gamma p/\rho c^2}$, so $F/p c_s \leq (p_{\text{rad}}/p)\sqrt{p/\rho c^2}$. The first factor is at most unity by definition and the second is much less than unity (for non-relativistic gases) or of order unity (for relativistic gases), so the bound holds.

¹⁹ e.g. Taylor-Proudman

²⁰ We showed that λ receives a contribution from the centrifugal term of order $\Omega^2 r/g$, but there may be additional contributions from other effects such as flux anisotropies. For the purposes of this argument though it suffices to have a lower bound.

²¹ Maeder 1997

is the square of the Brunt-Väisälä and

$$K = \frac{k}{\rho c_p}$$

is the thermal diffusivity with k the thermal conductivity. In order for this prescription to apply we require that

$$\frac{N^2}{c'S^2} \left(\frac{\nu_{\text{micro}}}{K} \right) < 1, \quad (4.17)$$

where ν_{micro} is the microscopic viscosity and c' is a constant which has been variously estimated as lying between 10^{-2} and 1²². We shall later verify that this holds in most cases of interest. Even when it does not a comparable diffusivity may be provided by turbulence in the non-stratified direction²³. In Chapter 2 we found no minimum shear threshold for this to be active, though that analysis neglected the microscopic viscosity which [Caleo & Balbus \(2016\)](#) have argued plays an important stabilising role in the linear regime even when quite small. Following equation (36) of [Menou et al. \(2004\)](#) we find that so long as the colatitude θ is such that $\sin^2 \theta$ is small compared with the reciprocal of the left-hand side of equation (4.17) this effect is active. Furthermore it is active if the specific angular momentum decreases outward. Hence even when equation (4.17) is not precisely satisfied equation (4.16) likely still applies in much of the star.

²² [Kulenthirarajah & Garaud 2018](#)

²³ [Zahn 1993](#)

Taking $\alpha = 1$ and noting that

$$\mathbf{T} \approx \rho D\mathbf{S}$$

we find

$$\rho^{-1}\mathbf{T} \approx \frac{kh}{\rho c_p g} S^3.$$

In a system with differential rotation

$$S \approx |R\nabla\Omega| \quad (4.18)$$

so

$$\rho^{-1}\mathbf{T} \approx \frac{kh}{\rho c_p g} \Omega^3 |R\nabla \ln \Omega|^3.$$

Using equations (4.14) and the first equality of (4.12) we may now calculate the circulation implied by the vorticity equation. So we have

$$u \approx \frac{1}{h\rho\Omega} \mathbf{T} \approx \lambda^3 \frac{k}{\rho c_p g} \frac{g^3}{h^3 \Omega^4}.$$

Noting that $F = |k\nabla T|$ and $|\nabla T| \approx T/h$ we find

$$u \approx \lambda^3 \frac{F}{\rho c_p T} \frac{g^2}{h^2 \Omega^4},$$

Noting again that $\lambda \gtrsim \Omega^2 r/g$,

$$u \gtrsim \lambda \frac{F}{\rho c_p T} \frac{g}{h \Omega^2} \left(\frac{r}{h}\right)^2.$$

Because the star is spinning below breakup, $\sqrt{g/h}$ is greater than Ω , and we have $r > h$, so when $\lambda \geq \epsilon$

$$u > \lambda \frac{F}{\rho c_p T} \geq \epsilon \frac{F}{\rho c_p T}. \quad (4.19)$$

The heat deposited by this flow is again (4.13) of order

$$Q = \rho c_p T u |\nabla s| \approx \rho c_p T \frac{u}{h},$$

because, in radiative zones, the entropy gradient is on the order of h^{-1} . With equation (4.19) we find

$$Q > \epsilon \frac{F}{h} \approx \Delta F.$$

Once more the heat transported by the circulation is greater than the initial flux disturbance, so we expect a much milder differential rotation to develop, with the circulation on the order of the baroclinicity.

We now determine the conditions under which inequality (4.17) gives rise to a vertical instability. Using equation (4.18) this may be written as

$$\frac{N^2}{|R\nabla\Omega|^2} \left(\frac{\nu_{\text{micro}}}{K} \right) < c'.$$

Near the cores of stars, which is where we shall ultimately be interested in this expression, the viscosity is predominantly radiative²⁴, so that ²⁵

$$\nu_{\text{micro}} \approx \frac{K c_p T}{4c^2},$$

where $c \approx 3 \times 10^{10} \text{ cm s}^{-1}$ is the speed of light. Hence the condition is that

$$\frac{N^2}{|R\nabla\Omega|^2} \left(\frac{c_p T}{4c^2} \right) < c'.$$

We now need a better estimate of the differential rotation than that provided by equation (4.15). Near the cores of these stars, where equation (4.17) is hardest to satisfy because N^2 and T are largest, we shall later show that $\lambda \approx \Omega^2 / |N|_{\text{core}}^2$, with an upper bound of order unity,

²⁴ Higher up in the atmosphere the particle viscosity dominates, but there h/r is small and equation (4.15) indicates that the shear is large, so we do not expect that limit to violate equation (4.17).

²⁵ Jeans. 1926

where $|N|_{\text{core}}^2$ is the average Brunt-Väisälä frequency in the convection zone. Hence with equation (4.14) we find

$$\frac{\min(|N|_{\text{core}}/\Omega, 1)^2 N^2 h}{g} \left(\frac{c_p T}{4c^2} \right) < c'.$$

Noting that $g/h \approx N^2$ we find

$$\min \left(1, \frac{|N|_{\text{core}}^2}{\Omega^2} \right) \left(\frac{c_p T}{4c^2} \right) < c'.$$

Noting that $c_p T \approx c_s^2$, we obtain

$$\min \left(1, \frac{|N|_{\text{core}}^2}{\Omega^2} \right) \left(\frac{c_s^2}{4c^2} \right) < c',$$

or

$$\min \left(1, \frac{|N|_{\text{core}}}{\Omega} \right) \left(\frac{c_s}{c} \right) < 2c',$$

In the cores of massive stars such as those we consider in Section 4.7, $c_s \approx 3^7 \text{ cm}^2 \text{ s}^{-2}$ and we take $R \approx 0.2R_\odot \approx 10^{10} \text{ cm}$ so

$$\min \left(1, \frac{|N|_{\text{core}}}{\Omega} \right) < 2 \times 10^3 c'.$$

Using $2 \times 10^3 c' > 1$ this reduces to

$$\Omega > \frac{|N|_{\text{core}}}{2 \times 10^3 c'}.$$

In the stars of interest $|N|_{\text{core}} \approx 10^{-8} \text{ s}^{-1}$, so even with the pessimistic estimate $c' \approx 10^{-2}$ the cutoff frequency is around 10^{-9} s^{-1} , which accommodates the vast majority of stars. Away from the core we shall show that the flux anisotropy drops off so the shear falls to that given by equation (4.15). As this occurs h falls, equation (4.15) becomes a tighter bound, NT falls and the criterion becomes looser, so we do not expect this to represent a significant limitation, though there could be stars for which equation (4.17) fails at some intermediate point. Such objects are potentially of interest, though even when the criterion is not precisely satisfied horizontal turbulence of comparable magnitude may still be active in a region in the vicinity of the poles. This means that at a minimum turbulence is present in many stars, even those which rotate quite slowly, though the latitudinal extent of the circulation may be restricted in the slowest-rotating stars.

It is useful to note that this argument may be recast in the language

of Garaud & Bodenheimer (2010) by writing their parameter

$$\sigma \equiv \frac{|N|}{\Omega} \sqrt{\frac{\nu}{K}} = \frac{S}{\Omega} \sqrt{\alpha}.$$

We have found that $S \gtrsim \Omega$ so

$$\sigma \gtrsim \sqrt{\alpha},$$

which is of order unity. Hence we are in the rather special limit where the decay scale for the circulation is of order R and yet the flow is not mechanically constrained, which we see from the fact that the heat flow of the mechanically forced circulation exceeds that of the thermally forced one.

4.4 Anisotropic Convection

We now turn to the convection zone. When viewed on large length-scales convective turbulence acts to diffuse heat. The effective diffusivity tensor is of the form

$$D_{ij} \approx \langle \delta x_i \delta u_j \rangle.$$

Physically this just means that material located at $\delta \mathbf{x}$ relative to the centre of an eddy is transported along with velocity $\delta \mathbf{u}$.

In the presence of an entropy gradient, this diffusivity gives rise to a heat flux

$$F_i = -c_p \rho T D_{ij} \frac{\partial s}{\partial x_j}. \quad (4.20)$$

Crucially, the convective viscosity is not isotropic²⁶. This is because the Coriolis acceleration of a fluid parcel owing to its velocity \mathbf{u} is

$$\mathbf{a}_c = 2\mathbf{u} \times \Omega, \quad (4.21)$$

where Ω is the angular velocity of rotation. Because this expression contains a cross product, the Coriolis effect generically leads to a coupling between different components of the velocity, and hence between different components of the position and velocity of the eddy. In rotating systems this means that the heat flux is not aligned parallel to the entropy gradient²⁷, and it is this effect that drives baroclinicity.

A subtlety in this argument is that while equation (4.21) produces an acceleration, for certain modes that acceleration may be matched by non-azimuthal perturbations in the pressure balance²⁸. This matching is complete for modes with wave-vector \mathbf{k} in the azimuthal direction

²⁶ Lesaffre et al. 2013; Gough 1978; Unno 1957

²⁷ Kichatinov & Rudiger 1993; Lesaffre et al. 2013

²⁸ This may be seen from equation (2.16), which is the dispersion relation for rotating convection.

and motion in the meridional plane ²⁹ but decreases monotonically and eventually vanishes away from $\mathbf{k} \propto \mathbf{e}_\phi$. Hence while the net effect of rotation is not quite that in equation (4.21), that relation serves to give both its scaling and symmetry-breaking properties.

In spherical coordinates the diffusivity tensor may be written as

$$\mathbf{D} = D_0 \mathbf{D}' = D_0 \begin{pmatrix} 1 & \epsilon_{\theta r} & \epsilon_{\phi r} \\ \epsilon_{r\theta} & c_1 & \epsilon_{\phi\theta} \\ \epsilon_{r\phi} & \epsilon_{\theta\phi} & c_2 \end{pmatrix}, \quad (4.22)$$

where D_0 is a scalar function ³⁰. When $\Omega = 0$ this tensor is diagonal because of spherical symmetry. The terms on the diagonal do not vanish when $\Omega = 0$, so we let c_1 and c_2 be constants of order unity. Perturbing away from this limit we argue that all components involving the azimuthal direction are linear in Ω because a single application of the Coriolis effect suffices to correlate meridional motion with azimuthal motion. By contrast $\epsilon_{r\theta}$ and $\epsilon_{\theta r}$ are quadratic in Ω at leading order because it takes two applications of this effect to correlate one component of meridional motion with another, as shown in Fig. 4.4. This form is in agreement with the works of Kitchatinov (2013) as well as Chapter 2 and Lesaffre et al. (2013), each of which have been verified with data from 3D simulations of rotating convection.

To see how this drives baroclinicity we first calculate the corrections that the convective anisotropy introduces in the equation of thermal equilibrium. For this we assume that there is no meridional flow in the convection zone. We then introduce a meridional flow in the convection zone and demonstrate that it does not change the overall magnitude of the baroclinicity.

Inserting equation (4.22) and equation (4.20) into equation (4.6) we find

$$\nabla \cdot (\mathbf{D}' \cdot \nabla s) + \nabla \ln(\rho T D_0) \cdot (\mathbf{D}' \cdot \nabla s) = 0. \quad (4.23)$$

Taking the system to be axisymmetric, we may write the function D_0 as

$$D_0 = D_{0,0}(p, T) + \Omega^2 D_{0,1}(p, T, \theta) + O(\Omega^3).$$

The dependence of $D_{0,1}$ on θ and the independence of $D_{0,0}$ on the same reflects the symmetry of the problem: only contributions coupling to the rotation may depend on latitude because in the absence of rotation latitude

²⁹ Cowling 1951

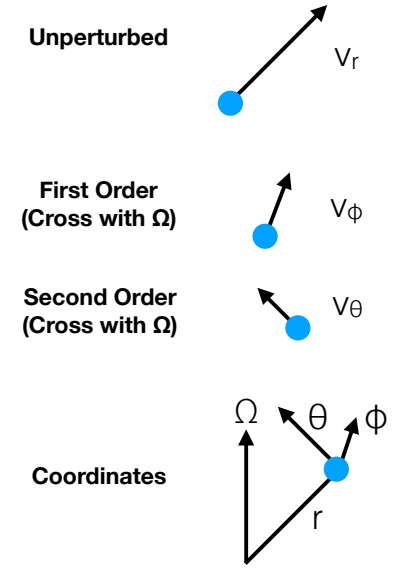


Figure 4.3: The radial motion v_r of a convective eddy is shown unperturbed. The Coriolis force acting on this creates an azimuthal component v_ϕ at first order. Acting on this the Coriolis force creates a latitudinal component v_θ at second order. So two applications of the Coriolis effect are required to generate motion along \mathbf{e}_θ from motion along \mathbf{e}_r .

³⁰ Gough 2012

is an arbitrary coordinate. In addition, we write

$$\nabla s = \mathbf{e}_r s_r + \mathbf{e}_\theta s_\theta,$$

where s_θ is $O(\Omega^2)$, and

$$\nabla \ln(\rho T D_0) = \mathbf{e}_r t_r + \mathbf{e}_\theta t_\theta,$$

where t_θ is $O(\Omega^2)$. In both cases we have used axisymmetry, so that $\partial/\partial\phi = 0$. Inserting these into equation (4.23) gives

$$0 = (\nabla + t_r \mathbf{e}_r + t_\theta \mathbf{e}_\theta) \cdot [\mathbf{e}_r (s_r + \epsilon_{r\theta} s_\theta) + \mathbf{e}_\theta (s_r \epsilon_{r\theta} + s_\theta c_1)]. \quad (4.24)$$

Expanding equation (4.24) then gives us

$$\begin{aligned} 0 = & \frac{1}{r^2} \frac{\partial}{\partial r} (r^2 (s_r + \epsilon_{r\theta} s_\theta)) + \frac{1}{r \sin \theta} \frac{\partial}{\partial \theta} (\sin \theta (s_r \epsilon_{r\theta} + s_\theta c_1)) \\ & + t_r (s_r + \epsilon_{r\theta} s_\theta) + t_\theta (s_r \epsilon_{r\theta} + s_\theta c_1). \end{aligned}$$

We now drop terms which we know to be of order Ω^3 and higher so that

$$0 = \frac{1}{r^2} \frac{\partial}{\partial r} (r^2 s_r) + \frac{1}{r \sin \theta} \frac{\partial}{\partial \theta} (\sin \theta (s_r \epsilon_{r\theta} + s_\theta c_1)) + t_r s_r.$$

As before terms which couple to latitude must be at least second order in Ω . This includes derivatives in θ of terms which themselves are non-zero for $\Omega = 0$. This allows us to neglect the term $\epsilon_{r\theta} \partial_\theta s_r$ but does not allow any such simplification for the remaining terms because those which are $O(\Omega^2)$ do not necessarily become of higher order when differentiated with respect to latitude. Thus we have

$$\begin{aligned} 0 = & \frac{1}{r^2} \frac{\partial}{\partial r} (r^2 s_r) + \frac{1}{r} \left(s_r \frac{\partial \epsilon_{r\theta}}{\partial \theta} + c_1 \frac{\partial s_\theta}{\partial \theta} \right) \\ & + \frac{\cot \theta}{r} (s_r \epsilon_{r\theta} + s_\theta c_1) + t_r s_r. \end{aligned}$$

Reorganising terms we write

$$0 = \frac{\partial \epsilon_{r\theta}}{\partial \theta} + \frac{c_1}{s_r} \frac{\partial s_\theta}{\partial \theta} + \cot \theta \left(\epsilon_{r\theta} + \frac{s_\theta c_1}{s_r} \right) + 2 + r t_r + \frac{\partial \ln s_r}{\partial \ln r}.$$

Now $\epsilon_{r\theta}$, $\partial_\theta \epsilon_{r\theta}$, s_θ and $\partial_\theta s_\theta$ vanish when $\Omega = 0$ because these terms can only be non-zero when spherical symmetry is broken. So

$$0 = \frac{\partial \epsilon_{r\theta}}{\partial \theta} + \frac{c_1}{s_r} \frac{\partial s_\theta}{\partial \theta} + \cot \theta \left(\epsilon_{r\theta} + \frac{s_\theta c_1}{s_r} \right) + \Delta \left(r t_r + 2 + \frac{\partial \ln s_r}{\partial \ln r} \right), \quad (4.25)$$

where Δ refers to the difference between the expression evaluated in the

rotating and non-rotating cases. Hence the term in parentheses is at least of order Ω^2 .

Because the fourth term in equation (4.25) does not contain an explicit dependence on θ it may well vanish in a barotropic setting if the other terms all vanish as well. However if the other terms do not vanish then either their explicit dependence on θ must cancel among them, in which case it must be that s_θ is non-zero, or else they must introduce a θ dependence into the fourth term. In either case the system becomes baroclinic, and by the same argument as in the Eddington–Sweet case and Section 4.3 this comes along with a circulation current of the order of the implied baroclinicity. This is in good agreement with our analysis the previous chapter but with additional geometric detail, which will be useful to study how these effects propagate through the star.

We have argued that $\epsilon_{r\theta}$ is $O(\Omega^2)$. The only relevant time-scale to non-dimensionalise this is the Brunt–Väisälä frequency $|N|$, so up to a dimensionless factor of order unity we expect

$$\epsilon_{r\theta} \approx \frac{\Omega^2}{|N|^2} \quad (4.26)$$

and

$$\frac{\partial \epsilon_{r\theta}}{\partial \theta} \approx \frac{\Omega^2}{|N|^2}, \quad (4.27)$$

which is in good agreement with the results of Kichatinov & Rudiger (1993) and Chapter 2. This may also be seen by noting that these quantities are locally determined and are perturbed to second order, so the magnitude of each is just its characteristic scale (unity in the case of $\epsilon_{r\theta}$, D_0 in the case of ΔD_0) multiplied by the dimensionless parameter $\Omega^2/|N|^2$.

The quantities t_r , s_θ and s_r and their derivatives, by contrast, are primarily determined non-locally by the perturbing terms throughout the atmosphere. To find them we must integrate outward from the centre of the star, where they all vanish by symmetry. We approximate these integrals by the integral of the magnitude of the perturbation from the centre to the point of interest. That is, each of these quantities acquires a perturbation of order $\Omega^2/|N|^2$ from the local perturbations to the convective flux (driven by ΔD_0 and $\epsilon_{r\theta}$). The relevant radial length scale is the pressure scale height h so radial derivatives of these quantities are characterised by

$$\left| \frac{d}{dr} \Delta(r t_r) \right| \approx \frac{d}{dr} \left| \frac{s_\theta}{s_r} \right| \approx \left| \frac{d}{dr} \Delta \frac{\partial \ln s_r}{\partial \ln r} \right| \approx \frac{1}{h} \left(\frac{\Omega}{|N|} \right)^2.$$

Integrating up from the centre of the core where $p = p_c$ then gives

$$\Delta(rt_r) \approx \frac{s_\theta}{s_r} \approx \Delta \frac{\partial \ln s_r}{\partial \ln r} \approx \alpha, \quad (4.28)$$

where

$$\alpha \equiv \int_{\ln p}^{\ln p_c} \frac{\Omega(\mathcal{P})^2}{|N|(\mathcal{P})^2} d \ln \mathcal{P}$$

and \mathcal{P} is the pressure. We use this as a proxy for the radial coordinate because even in highly baroclinic regions the pressure gradient is predominantly radial.

Now let λ be the small angle between ∇p and $\nabla \rho$ as in equation (3.15). Noting that in a nearly-adiabatic region

$$|\nabla \ln \rho| \approx \gamma^{-1} |\nabla \ln p|,$$

where γ is the adiabatic index, we find that for small angles

$$\begin{aligned} \lambda &\equiv \sin^{-1} \left(\frac{|\nabla p \times \nabla \rho|}{|\nabla p| |\nabla \rho|} \right) \\ &\approx \frac{|\nabla \ln p \times \nabla \ln \rho|}{|\nabla \ln p| |\nabla \ln \rho|} \\ &\approx \gamma \frac{|\nabla \ln p \times \nabla \ln \rho|}{|\nabla \ln p|^2}. \end{aligned}$$

Using the fact that ∇p and $\nabla \rho$ both lie in the meridional plane we find

$$\begin{aligned} \lambda &\approx \gamma \frac{|\mathbf{e}_\phi \cdot (\nabla \ln p \times \nabla \ln \rho)|}{|\nabla \ln p|^2} \\ &\approx \gamma |\mathbf{e}_\phi \cdot ((h \nabla \ln p) \times (h \nabla \ln \rho))|, \end{aligned}$$

where as usual h is the pressure scale height. If we approximate the pressure gradient as radial then

$$\begin{aligned} \lambda &\approx |\mathbf{e}_\phi \cdot (-\mathbf{e}_r \times (h \nabla \ln \rho))| \\ &\approx \frac{h}{r} |\partial_\theta \ln \rho|. \end{aligned}$$

Recalling equation (1.2) we find

$$\lambda \approx \gamma h |s_\theta|.$$

This parametrises the baroclinicity. Because it is of order unity we neglect the factor of γ and use equation (4.28) to find

$$\lambda \approx h |s_r \alpha|. \quad (4.29)$$

This is our leading order estimate of the baroclinicity in the convection zone.

4.5 Centrifugal Effects

In addition to anisotropic turbulence there is another source of baroclinicity, namely the centrifugal acceleration. This is given by

$$\mathbf{a}_\Omega \equiv \Omega^2 R \mathbf{e}_R.$$

Because this acceleration does not depend on the meridional velocity of the fluid it may be absorbed into the gravitational acceleration. This produces a modified effective gravity³¹

$$\mathbf{g}_{\text{eff}} = \mathbf{g} + \mathbf{a}_\Omega$$

which, in the hydrostatic limit, satisfies

$$\nabla p = -\rho \mathbf{g}_{\text{eff}}.$$

Hence the centrifugal acceleration serves to disort isobars by an amount of order $\rho \Delta(\nabla \Phi) \approx \rho \Omega^2 R$. If the density did not adjust as well this would influence λ as

$$\Delta \lambda \approx h \Delta(\nabla \ln p) \approx \frac{h}{p} \rho \Omega^2 R = \frac{\Omega^2 R}{g}.$$

However in reality the density gradient adjusts as well and it is instead the entropy gradient which is perturbed by the requirement of thermal equilibrium³². The corresponding perturbation to the baroclinicity is therefore multiplied by a factor of $h s_r$, so

$$\Delta \lambda \approx \frac{\Omega^2 R}{g} h s_r,$$

which is much less than $h s_r \alpha$ because $N^2 \ll g/R$. Thus the total baroclinicity is well approximated by equation (4.29).

4.6 Meridional Circulation in the Convection Zone

Having considered both relevant effects in convection zones, we now examine the consequences for the circulation in those regions³³. We know that it is not possible for rotating radiative zones to avoid circulation currents because they cannot satisfy the condition of thermal equilibrium without becoming baroclinic, and once baroclinic a flow is generically driven with magnitude set by the baroclinicity. The same is true for

³¹ This is the same modification which appears in equation (3.71).

³² Eddington 1929

³³ This is not our focus and we have performed a local treatment in Chapter 3, but it is useful for our later study of circulation in radiative zones to understand how the circulation acts to damp the flux anisotropy which generates it.

convection zones, and so there is a meridional flow. Incorporating such a flow³⁴ and recalling the assumption of axisymmetry, this equation becomes

$$0 = -\frac{r}{D_0 s_r} (u_r s_r + u_\theta s_\theta) + \Delta \left(r t_r + 2 + \frac{\partial \ln s_r}{\partial \ln r} \right) + \frac{\partial \epsilon_{r\theta}}{\partial \theta} + \frac{c_1}{s_r} \frac{\partial s_\theta}{\partial \theta} + \cot \theta \left(\epsilon_{r\theta} + \frac{s_\theta c_1}{s_r} \right). \quad (4.30)$$

Now noting that s_θ is $O(\Omega^2)$ and u_θ is at least $O(\Omega)$ we may drop their product and find

$$\frac{r}{D_0} u_r = \frac{\partial \epsilon_{r\theta}}{\partial \theta} + \frac{c_1}{s_r} \frac{\partial s_\theta}{\partial \theta} + \cot \theta \left(\epsilon_{r\theta} + \frac{s_\theta c_1}{s_r} \right) + \Delta \left(r t_r + 2 + \frac{\partial \ln s_r}{\partial \ln r} \right),$$

from which we see that the magnitude of the flow is set by the typical magnitude of the remaining terms, so we expect

$$u_r \approx \frac{D_0}{r} \alpha', \quad (4.31)$$

where equations (4.26), (4.27) and (4.28) give

$$\alpha' \equiv \frac{\Omega^2}{|N|^2} + \alpha. \quad (4.32)$$

This is similar to the result of [Roxburgh \(1991\)](#), except that the denominator of the perturbing parameter here is correctly identified as $|N|^2$ rather than g/r .

In steady state conservation of mass gives $\nabla \cdot (\rho \mathbf{u}) = 0$, so

$$\frac{r}{\sin \theta} \frac{\partial(u_\theta \sin \theta)}{\partial \theta} = -\frac{\partial(r^2 u_r)}{\partial r} - u_r r^2 \frac{\partial \ln \rho}{\partial r},$$

where we have dropped $\partial_\theta \ln \rho$ because it is higher-order in Ω than $\partial_r \ln \rho$. We can evaluate the derivatives approximately by noting that D_0 , and hence u_r , has characteristic scale h as does ρ . This is because all of these owe their spatial dependence primarily to the variation of thermodynamic quantities, which ultimately all vary with the same spatial scale as p . This produces the scaling relation

$$u_\theta \approx u_r \frac{r}{h}, \quad (4.33)$$

and thence

$$u_\theta \approx \frac{D_0}{h} \alpha'. \quad (4.34)$$

³⁴ This is done by starting the derivation with equation (4.5) rather than equation (4.6) and propagating the effects through to equation (4.25).

From simple mixing length theory of convection

$$D_0 \approx \frac{1}{3} h v_c,$$

where v_c is the convective velocity ³⁵ Inserting this into equations (4.31) and (4.34) we find

³⁵ Gough 1978

$$u_r \approx \frac{1}{3} v_c \frac{h}{r} \alpha' \quad (4.35)$$

and

$$u_\theta \approx \frac{1}{3} v_c \alpha'. \quad (4.36)$$

As argued in Chapter 3, the actual baroclinicity is reduced by virtue of our including the meridional circulation. We have argued that what is left over after this is accounted for is of the same order as what we began with, but to be careful about the distinction **in what follows when we discuss baroclinicity we are talking about that which would exist in the absence of a meridional circulation**. That is, we are using it as a proxy for the anisotropy of the flux distribution, which is the quantity which sets the magnitude of the circulation.

The flow given by equations (4.35) and (4.36) generally acts to damp the flux anisotropy because it is driven by this effect. The term that appears in equation (4.30) associated with this flow is

$$\begin{aligned} Q_{\text{flow}} &\equiv \frac{r}{D_0 s_r} (u_r s_r + u_\theta s_\theta) \\ &= \frac{r}{D_0} \left(u_r + u_\theta \frac{s_\theta}{s_r} \right). \end{aligned}$$

Inserting equations (4.31) and (4.34) we find

$$Q_{\text{flow}} \approx \alpha' + \alpha' \frac{r}{h} \frac{s_\theta}{s_r},$$

and with equation (4.28) we arrive at

$$Q_{\text{flow}} \approx \alpha' + \alpha' \alpha' \frac{r}{h}.$$

Because both α and α' are quadratic in the rotation we drop the second term and find

$$Q_{\text{flow}} \approx \alpha'.$$

Because the terms in equation (4.30) are those which contribute to α

and α' , and because this must act to damp the baroclinicity³⁶, we find

$$\begin{aligned}\frac{d\alpha}{d \ln p} &= Q_{\text{flow}} - \frac{d}{d \ln p} \left[\int_{\ln p}^{\ln p_c} \frac{\Omega^2}{|N|^2} d \ln \right] \\ &= \alpha' - \frac{\Omega^2}{|N|^2}.\end{aligned}$$

Because the term proportional to α' is responsible for damping α' , the coefficient may matter, so we write

$$\frac{d\alpha}{d \ln p} = y' \alpha' - \frac{\Omega^2}{|N|^2},$$

where y' is a dimensionless factor of order unity. With equation (4.32) this becomes

$$\frac{d\alpha}{d \ln p} = y \alpha - \frac{\Omega^2}{|N|^2},$$

where y is a further dimensionless factor of order unity. Applying the boundary condition $\alpha(p_c) = 0$, which must be true because all latitudinal derivatives vanish at the origin, we find

$$\alpha = p^y \int_p^{p_c} \frac{\Omega(\mathcal{P})^2}{|N|(\mathcal{P})^2} \frac{d\mathcal{P}}{\mathcal{P}^{1+y}}.$$

The effect of the damping is then just to change how we weight the average of the perturbation rather than to change the fundamental scalings.

As a final consideration, equations (4.26) and (4.27) do not hold for arbitrarily large Ω . In particular, we have shown³⁷ in Chapter 2 that the convective anisotropy saturates for Ω large relative to $|N|$. So we use the prescription

$$\epsilon = \epsilon_{\text{max}} \min \left(1, \frac{\Omega^2}{|N|^2} \right), \quad (4.37)$$

where³⁸ $\epsilon_{\text{max}} \approx 0.2$, and hence find that

$$\alpha \approx p^y \int_p^{p_c} \epsilon_{\text{max}} \min \left(1, \frac{\Omega(\mathcal{P})^2}{|N|(\mathcal{P})^2} \right) \frac{d\mathcal{P}}{\mathcal{P}^{1+y}}.$$

As a test of this model, Fig. 4.4 shows the radial and latitudinal velocities, (4.35) and (4.36), in the solar convection zone compared with the circulation velocity inferred from helioseismic observations (Rajaguru & Antia, 2015). The solar model envelope, computed by G. Houdek and D. O. Gough, is the model used by Chaplin et al. (2005) in their study of the power spectral density of solar p-modes. We fitted the parameter y so as to minimise the root mean square error in the logarithm of the velocity components. This produced $y = 0.2$, in agreement with the gen-

³⁶ This is because the work which powers the flow comes from the baroclinicity, or equivalently the flux anisotropy, and so thermodynamically the only option is for the flow to damp it.

³⁷ as have Lesaffre et al. (2013); Kitchatinov (2013).

³⁸ See Chapter 2.

eral magnitude we expect. The variation in the radial component of the flow is well modelled by equation (4.35) except near the surface, where the sharp density gradient means that inertial effects become increasingly important relative to thermal considerations. It is therefore worth noting that equation (4.35) is really a lower bound on the radial velocity set by the condition of thermal equilibrium: greater velocities are, of course, permitted. The overall magnitude and trend in the θ component of the flow is reasonably captured by equation (4.36), but the details are not. In particular, the dips in the observed u_θ are due to cell boundaries in the meridional flow structure, and these geometric features are not captured by our simplified analysis. Furthermore we generally predict velocities which are larger than what is observed in deeper regions. This could be a result of geometric or magnetic effects near the tachocline or else could indicate that we ought to have used a more precise prescription in equation (4.37).

A further test is provided by the simulations of Brun & Palacios (2009), who find that in simulations of slowly rotating³⁹ convecting giant stars of order 5 to 10 per-cent of the kinetic energy resides in the meridional circulation, such that the circulation velocity is of order 30 per-cent of the convective velocity. This is in good agreement with equations (4.35) and (4.36).

³⁹ $\Omega < |N|$

4.7 *Effects in Massive Stars*

In massive stars it is typical to have a convective core and a radiative envelope. If the convection is anisotropic then the core is baroclinic and a meridional flow is present. Here we argue that this produces baroclinicity in the radiative zone, which ultimately drives a circulation current there⁴⁰. We then examine the decay of this circulation into the radiative zone and examine how these effects scale in stellar models.

⁴⁰ This follows the standard Eddington–Sweet argument once we establish the magnitude of the baroclinicity.

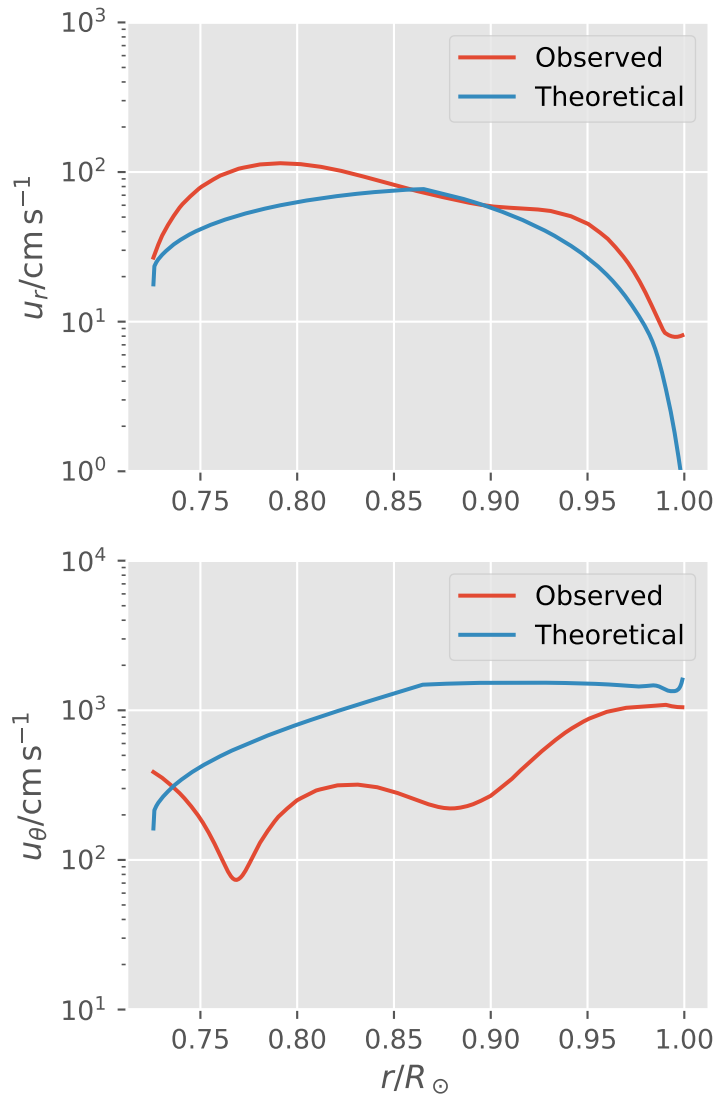


Figure 4.4: The root mean square meridional velocity taken over latitudinal slices of the data is shown (red) for radial (top) and angular (bottom) components from [Rajaguru & Antia \(2015\)](#). In blue are the predicted velocities using $\Omega_\odot \approx 2.5 \times 10^{-6} \text{Hz}$.

4.7.1 Transmitting Baroclinicity

To analyse the transmission of baroclinicity we begin by noting that in radiative zones

$$\begin{aligned} hs_r &= h \frac{\partial s}{\partial r} \\ &= h \left[\frac{\partial \ln p}{\partial r} - \gamma \frac{\partial \ln p}{\partial r} \right] \\ &= h \left[(1 - \gamma) \frac{\partial \ln p}{\partial r} + \gamma \frac{\partial \ln T}{\partial r} \right] \\ &= \gamma - 1 - \gamma \frac{d \ln T}{d \ln p}, \end{aligned}$$

where we have taken the mean molecular weight μ to be constant and made use of equation (1.2) as well as the ideal gas law $p = \rho k_B T / \mu$. In radiative zones $d \ln T / d \ln p$ is generally small compared to the adiabatic gradient, so $hs_r \approx \gamma - 1$ is of order unity. Thus according to equation (4.29)

$$\lambda \approx \alpha. \quad (4.38)$$

At the tachocline, the boundary of the convection zone, we expect

$$\alpha \approx p_{\text{tachocline}}^y \int_{p_{\text{tachocline}}}^{p_c} \epsilon_{\text{max}} \min \left(1, \frac{\Omega(\mathcal{P})^2}{|N|(\mathcal{P})^2} \right) \frac{d\mathcal{P}}{\mathcal{P}^{1+y}},$$

because α accumulates perturbations to the entropy gradient⁴¹. In this way effects which would be small in the radiative zone, which is difficult to perturb because $|N|$ tends to be quite large there, are enhanced because they accumulate in the convection zone, where $|N|$ is small, and are then transmitted to the radiative zone at the tachocline.

To more precisely examine this transmission we write the heat flux as

$$\mathbf{F} = \mathbf{e}_r F_0(r) + A(r) \mathbf{e}_r \cos \theta + B(r) \mathbf{e}_\theta \sin \theta, \quad (4.39)$$

where

$$F_0 = \frac{L}{4\pi r^2}$$

is the unperturbed flux of the star, L its luminosity and A and B are of order αF_0 at the tachocline. There is no $\cos \theta$ term along \mathbf{e}_θ because $\mathbf{e}_\theta \cdot \mathbf{F}$ must vanish for $\theta = 0$ and $\theta = \pi$, and we neglect higher-order harmonics for simplicity. Within the radiative zone and in the absence of a meridional flow, the thermal flux obeys equation (4.4), which may be written as

$$\mathbf{F} = -k \nabla T, \quad (4.40)$$

⁴¹ It is important to note that it is α , not α' , which matters in radiative zones. This is because the additional factor of $\Omega^2 / |N|^2$ which arises through convective anisotropy vanishes in radiative zones.

where the thermal conductivity

$$k \equiv \rho c_p \chi$$

depends solely on the temperature, pressure and opacity. Hence

$$\nabla T = -\frac{1}{k} [\mathbf{e}_r F_0(r) + A(r) \mathbf{e}_r \cos \theta + B(r) \mathbf{e}_\theta \sin \theta]. \quad (4.41)$$

It follows that when α is small

$$\frac{\partial_\theta T}{r \partial_r T} \approx \frac{B \sin \theta}{F_0},$$

which is of order α . Thus the heat flux transmits baroclinicity from the convection zone into the radiative zone to an extent given by equation (4.38).

Note that the *mechanical* transmission of currents across the tachocline has been studied in great detail by [Garaud & Bodenheimer \(2010\)](#) and in the context of that work these stars are in a limit of efficient transmission, being neither mechanically nor thermally constrained⁴². Hence it is possible that mechanical pumping plays a significant role as well.

⁴² [Garaud & Bodenheimer \(2010\)](#) define $\sigma = (|N|/\Omega)\sqrt{\nu/K}$, where ν is the (effective) viscosity and K is the thermal diffusivity. Recalling the formalism of [Canuto & Hartke \(1986\)](#) we see that $\nu/K \approx S^2/|N|^2$, where S is the shear. Hence $\sigma \approx S/\Omega$. Given order unity differential rotation in the convection zone, which is what results from the balance of the α and Λ effects ([Kitchatinov, 2013](#)), $S \approx \Omega$ so $\sigma \approx 1$. In this limit [Garaud & Bodenheimer \(2010\)](#) find the mechanical damping scale to be of order R , meaning that the flow is not thermally constrained, and turbulence makes the effective viscosity in the radiative zone large enough that the velocity bound of ν/R does not provide a mechanical constraint. This simultaneous limit only exists when h is of order R , which is the case in the cores of massive stars. See Appendix 4.3 for further details.

4.7.2 Decay Profile

Within the radiative zone the flux perturbation generally decays. We now aim to determine the scale over which this occurs. In equilibrium and in the absence of any meridional flow or heat generation, the flux obeys the conservation law

$$\nabla \cdot \mathbf{F} = 0$$

and, by equation (4.40),

$$\nabla \times \mathbf{F} = -k \nabla \times \nabla T - \nabla k \times \nabla T = \nabla \ln k \times \mathbf{F}. \quad (4.42)$$

From

$$\nabla \cdot \mathbf{F} = 0$$

and equation (4.39) we obtain

$$\frac{\partial A}{\partial r} + \frac{2}{r}(A + B) = 0 \quad (4.43)$$

and from equation (4.42)

$$\begin{aligned} \frac{\partial B}{\partial r} + \frac{1}{r}(B - A) &= \frac{\partial \ln k}{\partial r} B - \frac{2}{\pi} \int_0^\pi \frac{\partial \ln k}{\partial \theta} \left[F_0 + \frac{1}{r} A(r) \cos \theta \right] \sin \theta d\theta \\ &= \frac{\partial \ln k}{\partial r} B - \frac{2F_0}{\pi r} \int_0^\pi \frac{\partial \ln k}{\partial \theta} \sin \theta d\theta. \end{aligned} \quad (4.44)$$

Because we have assumed a chemically homogeneous star we can relate k in the limit of small α to the derivatives of k in temperature and pressure. That is,

$$\frac{\partial \ln k}{\partial \theta} \approx \frac{\partial \ln k}{\partial \ln T} \frac{\partial \ln T}{\partial \theta} + \frac{\partial \ln k}{\partial \ln p} \frac{\partial \ln p}{\partial \theta}, \quad (4.45)$$

where the thermodynamic derivatives of k are taken with respect to the unperturbed state and so are independent of θ . The pressure only acquires a dependence on θ through the centrifugal force, so

$$\frac{\partial \ln p}{\partial \theta} \approx \frac{\Omega^2 R}{g} \approx \frac{\Omega^2 r}{g} \sin \theta. \quad (4.46)$$

The temperature depends on θ through equation (4.41) so

$$\frac{\partial \ln T}{\partial \theta} = -\frac{rB(r)}{kT} \sin \theta. \quad (4.47)$$

Inserting equations (4.45), (4.46) and (4.47) into equation (4.48) we find

$$\frac{\partial B}{\partial r} + \frac{1}{r}(B - A) = \frac{\partial \ln k}{\partial r} B - \frac{F_0}{r} \left(-\frac{rB}{kT} \frac{\partial \ln k}{\partial \ln T} + \frac{\Omega^2 r}{g} \frac{\partial \ln k}{\partial \ln p} \right).$$

From equation (4.41) we find

$$\frac{F_0}{kT} \approx |\nabla \ln T| \approx -\frac{d \ln p}{dr} \frac{d \ln T}{d \ln p} = \frac{1}{h} \frac{d \ln T}{d \ln p}.$$

So

$$\frac{\partial B}{\partial r} + \frac{1}{r}(B - A) = \left(\frac{\partial \ln k}{\partial r} - \frac{1}{h} \frac{d \ln T}{d \ln p} \frac{\partial \ln k}{\partial \ln T} \right) B - F_0 \frac{\Omega^2 r}{g} \frac{\partial \ln k}{\partial \ln p}.$$

The final term in this equation is important near the surface, where it is necessary to reproduce the usual Eddington–Sweet circulation. However deeper in the star it may be neglected because there $B/F_0 \approx \alpha \gg \Omega^2 r/g$ and logarithmic derivatives of k with respect to each of pressure and temperature are of order unity. Hence we find

$$\frac{\partial B}{\partial r} + \frac{1}{r}(B - A) = \left(\frac{\partial \ln k}{\partial r} - \frac{1}{h} \frac{d \ln T}{d \ln p} \frac{\partial \ln k}{\partial \ln T} \right) B,$$

which may be written as

$$\frac{\partial B}{\partial r} + \frac{1}{r}(B - A) \approx -\frac{b}{h}B, \quad (4.48)$$

where

$$b \equiv \frac{d \ln k}{d \ln p} + \frac{d \ln T}{d \ln p} \frac{\partial \ln k}{\partial \ln T}.$$

Combining equations (4.43) and (4.48) we find

$$\frac{\partial}{\partial r} \begin{pmatrix} A \\ B \end{pmatrix} = \begin{pmatrix} -\frac{2}{r} & -\frac{2}{r} \\ +\frac{1}{r} & -\frac{1}{r} - \frac{b}{h} \end{pmatrix} \begin{pmatrix} A \\ B \end{pmatrix}.$$

Treating b and r as constants, the eigenvalues of this system are

$$\lambda_{\pm} = -\frac{1}{r} \left[\frac{3}{2} + \frac{br}{2h} \pm \frac{1}{2} \sqrt{\frac{b^2 r^2}{h^2} - 2b \frac{r}{h} - 7} \right].$$

In and around the cores of stars r is typically smaller than h , and b is of order unity, so for simplicity we neglect terms involving b and find that the slowest-decaying mode is

$$\lambda_- \approx -\frac{3}{2r} - i \frac{\sqrt{7}}{2},$$

so

$$\Re(\lambda) \approx -\frac{3}{2r}.$$

Taking only this mode, because it is the one that persists for the largest distance, we find that

$$\frac{d \ln A}{d \ln r} = \frac{d \ln B}{d \ln r} = \Re(\lambda).$$

Hence

$$\frac{A(r)}{A(r_c)} \approx \frac{B(r)}{B(r_c)} \approx \left(\frac{p}{p_{\text{tachocline}}} \right)^{\beta},$$

where r_c is the radius of the convective core and

$$\beta \equiv -h \Re(\lambda_-) \approx \frac{3h}{2r}. \quad (4.49)$$

Thus the baroclinicity is of order

$$\alpha \approx \alpha(r_c) \left(\frac{p}{p_{\text{tachocline}}} \right)^{\beta}.$$

This generally prevents solutions which do not involve $O(\alpha)$ meridional flows for the same reason as outlined in section 4.2.

The standard Eddington–Sweet derivation for baroclinic radiative zones finds that the radial circulation velocity is of order that required to balance the flux anisotropy. That is ⁴³,

⁴³ Eddington 1929

$$\rho c_p T u_r s_r \approx \nabla \cdot F.$$

Noting that hs_r is of order unity we find

$$u_r \approx \frac{h \nabla \cdot F}{\rho c_p T}.$$

The length-scale associated with the flux anisotropy is r , because that is the latitudinal scale, and the flux scale of the anisotropy is set by αF , so

$$u_r \approx \alpha \frac{h F}{r \rho c_p T}.$$

Using equation (4.33) we find

$$u \approx \alpha \frac{F}{\rho c_p T}. \quad (4.50)$$

In an efficient convection zone the luminosity equals the convective luminosity. This is well approximated by the power flux of a fluid moving with the convection speed, so

$$L \approx 4\pi r^2 \rho u_c^3,$$

where u_c is the convection speed, the heat flux outside of the core may be related to that at the boundary of the core by

$$F \approx \rho_c u_{c,\text{core}}^3 \left(\frac{r_c}{r} \right)^2.$$

and so

$$\frac{u_r}{u_{c,\text{core}}} \approx \left(\frac{\rho_c}{\rho} \right) \left(\frac{u_{c,\text{core}}}{c_s} \right)^2 \left(\frac{r_c}{r} \right)^2 \left(\frac{p}{p_{\text{tachocline}}} \right)^\beta \alpha(r_c), \quad (4.51)$$

where c_s is the sound speed and

$$\alpha(r_c) = p_{\text{tachocline}}^y \int_{p_{\text{tachocline}}}^{p_c} \epsilon_{\text{max}} \min \left(1, \frac{\Omega(\mathcal{P})^2}{|N|(\mathcal{P})^2} \right) \frac{d\mathcal{P}}{\mathcal{P}^{1+y}}.$$

It is worth noting that the ratio $p/p_{\text{tachocline}}$ scales exponentially in the radial coordinate while the flow speed scales as a power law in this ratio. The latter scaling persists even after accounting for the additional heat flux

transported by the meridional flow. To see this note that the rate at which α changes with r is proportional to the flux transported latitudinally by the meridional flow because this flow damps α . This flux scales as α because the flow transports material radially at a rate which scales as α and the radial gradient is largely independent of α . This means that $d\alpha/dr \approx -(h/r^2)\alpha$, which produces a power-law in p , which merely modifies the exponent β . The modification is approximately

$$\beta \rightarrow \beta + \frac{h}{r},$$

applied to equation (4.49), so that

$$\beta \approx \frac{5h}{2r}. \quad (4.52)$$

As one final simplification, it is worth noting that when the exponent β is unity equation (4.50) may be written as

$$u_r \approx \left(\frac{F}{p_c} \right) \alpha_{\text{core}}.$$

This form has the disadvantage of not generalising should the exponent differ from one and of lacking the clear dimensionless ratios of equation (4.51), but has the advantage that the origin of the flow is clear: rotationally-driven anisotropy forces a meridional flow to carry a portion of the flux, with the speed set by the energy density, which is proportional to p .

4.7.3 *Scaling in Stellar Models*

To understand these effects quantitatively we define

$$\tau \equiv \frac{h}{u_r}$$

as the analogue of the local Eddington–Sweet time. Noting that h is approximately the distance $z = R - r$ to the surface of the star we see that τ is an estimate of the time needed to bring material to the surface. Fig. 4.5 shows this time as a function of mass coordinate for three different stellar models made with the Cambridge STARS code (Eggleton, 1971; Pols et al., 1995). These calculations were made with a surface rotation of $u_{\text{rot}} = 3 \times 10^6 \text{ cm s}^{-1}$ and we assume that the mixing rate cannot fall below that of the Eddington circulation. For simplicity we took $\beta = 3/2$ though in practice this parameter varies with r .

A few implications are clear from this figure. First, rotating massive stars mix near the core much more rapidly than would normally be expected

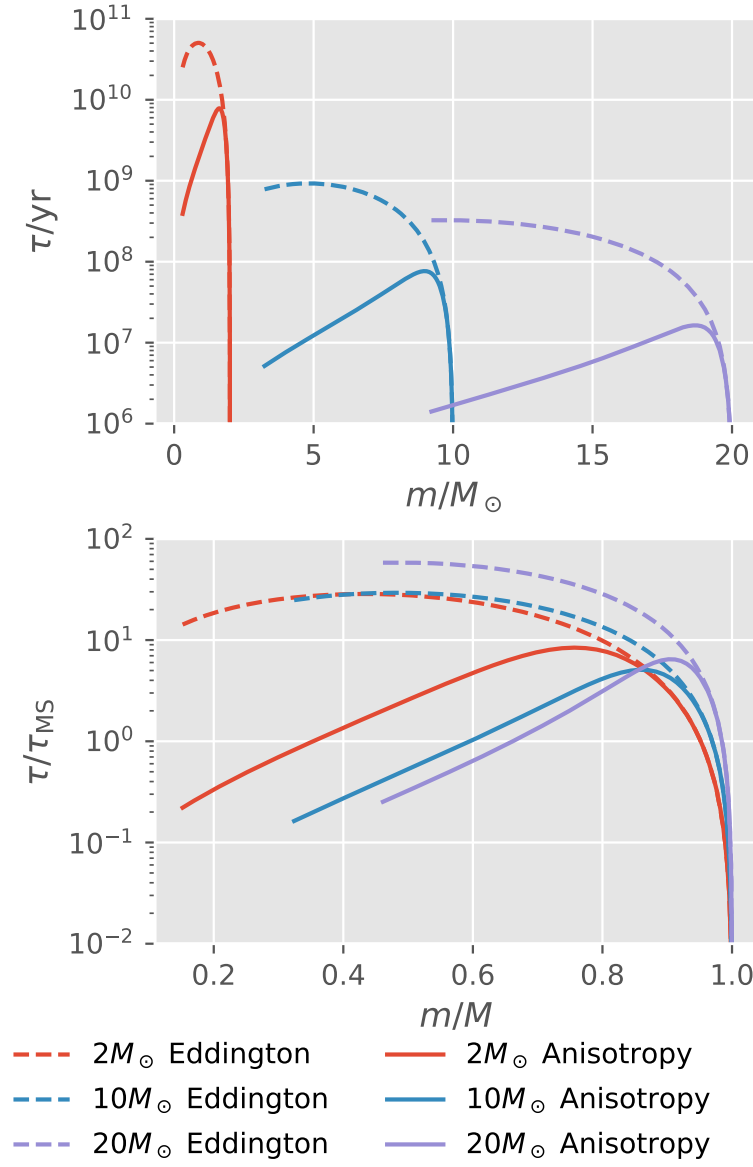


Figure 4.5: The analogue of the Eddington-Sweet time $\tau = z/u_r$ is shown as a function of mass m for three stellar models on the main sequence with masses of $2M_\odot$, $10M_\odot$ and $20M_\odot$. For each model results from both the Eddington-Sweet mechanism and the mechanism presented in this paper are shown. These calculations were made with $\beta = 3/2$ and rigid rotation with a surface velocity of $u_{\text{rot}} = 3 \times 10^6 \text{ cm s}^{-1}$. The bottom panel shows the same timescales τ normalised to the main-sequence lifetime τ_{MS} , with the mass normalised to the total mass of the star M .

without accounting for convective anisotropy, which increases the effective core mass and acts very much like convective overshooting (Prather & Demarque, 1974), a topic we explore in more detail in Section 4.9. This enhancement arises because $|N|$ in the core is generally much smaller than $\sqrt{g/R}$, and so the convective boundary condition drives baroclinicity much more than the simple Eddington–Sweet mechanism. Secondly, this effect damps strongly as we approach the surface and is eventually overtaken by the Eddington circulation, so there would not necessarily be strong observable chemical signatures of the enhanced mixing except by virtue of making material more readily available to other mixing processes.

To understand how effectively this mechanism transports material through the star we now examine the travel time from the tachocline to a point at radius r , given by

$$\tau' \equiv \int_{r_c}^r \frac{dr}{u_r}.$$

This is shown in Figure 4.6. In each of the stellar models in Fig. 4.5 τ' is less than the lifetime of the star almost everywhere and so, at least at this rotation rate, a significant amount of material ought to reach the core. By contrast, the time

$$\tau'' \equiv - \int_{r_{\text{surface}}}^r \frac{dr}{u_r}.$$

to mix to the surface exceeds the main-sequence lifetime in most of the star. Hence at least at this rotation rate the amount of material mixed from the core to the surface from this region ought to be minimal. For more rapidly rotating stars this effect is stronger and considerably more material may reach the surface from the core.

A similar story may be seen in Fig. 4.7, which shows the radial velocity of the circulation as a function of position in the star. The results are for the same stellar models as in Fig. 4.5 and, once more, the Eddington curves only contain the Eddington–Sweet circulation while the Anisotropy curves contain both effects. Because the anisotropy-induced circulation declines towards the surface it is clear from this where the Eddington–Sweet mechanism becomes dominant. In the top panel, which was made with a surface velocity of $u_{\text{rot}} = 30 \text{ km s}^{-1}$, this point is typically around a mass fraction of 0.9. By contrast in the bottom panel, which was made with a surface velocity of $u_{\text{rot}} = 300 \text{ km s}^{-1}$, the transition occurs between 0.5 and 0.7. This is because the anisotropy-driven circulation saturates at much lower rotation rates and so does not scale with rotation in this

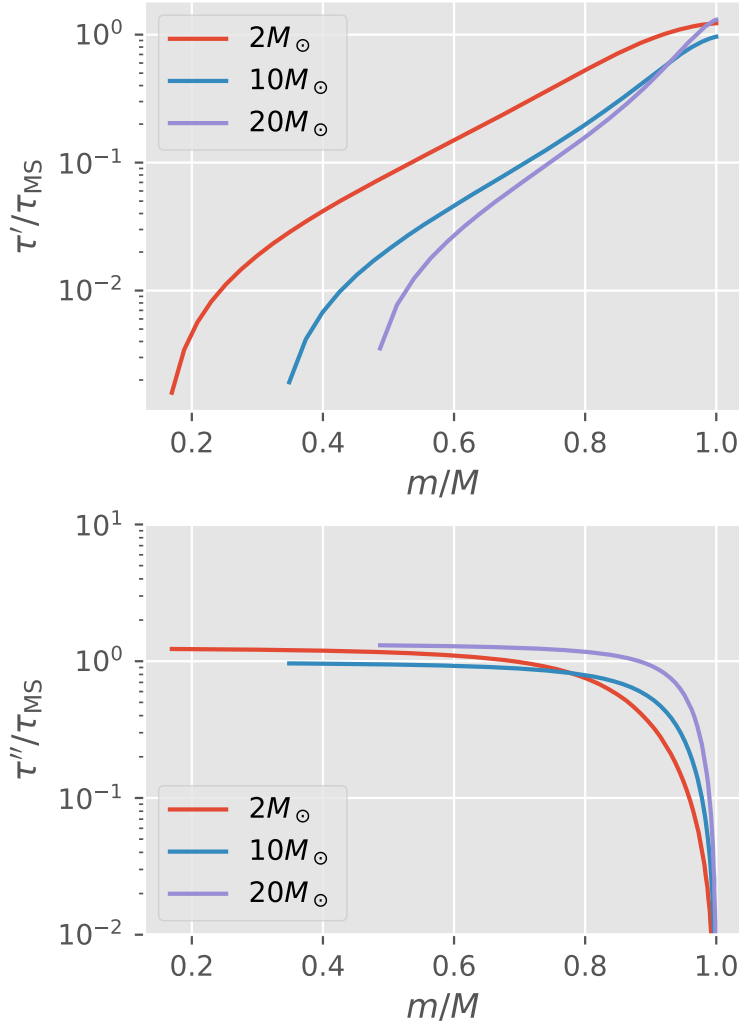


Figure 4.6: The time τ' required for material to flow to the core (top) and the time τ'' required for material to flow to the surface (bottom) are shown as functions of mass fraction m/M for three stellar models on the main sequence with masses of $2M_{\odot}$, $10M_{\odot}$ and $20M_{\odot}$. Both times are normalised to the main-sequence lifetime τ_{MS} . For each model the velocity u_r is assumed to be the sum of that owing to the Eddington–Sweet mechanism and that owing to the mechanism presented in this paper. These calculations were made with $\beta = 3/2$ and rigid rotation with a surface velocity of $u_{\text{rot}} = 3 \times 10^6 \text{ cm s}^{-1}$, corresponding respectively to 4×10^{-3} , 2×10^{-3} and 10^{-3} of the surface breakup rate for the three stars.

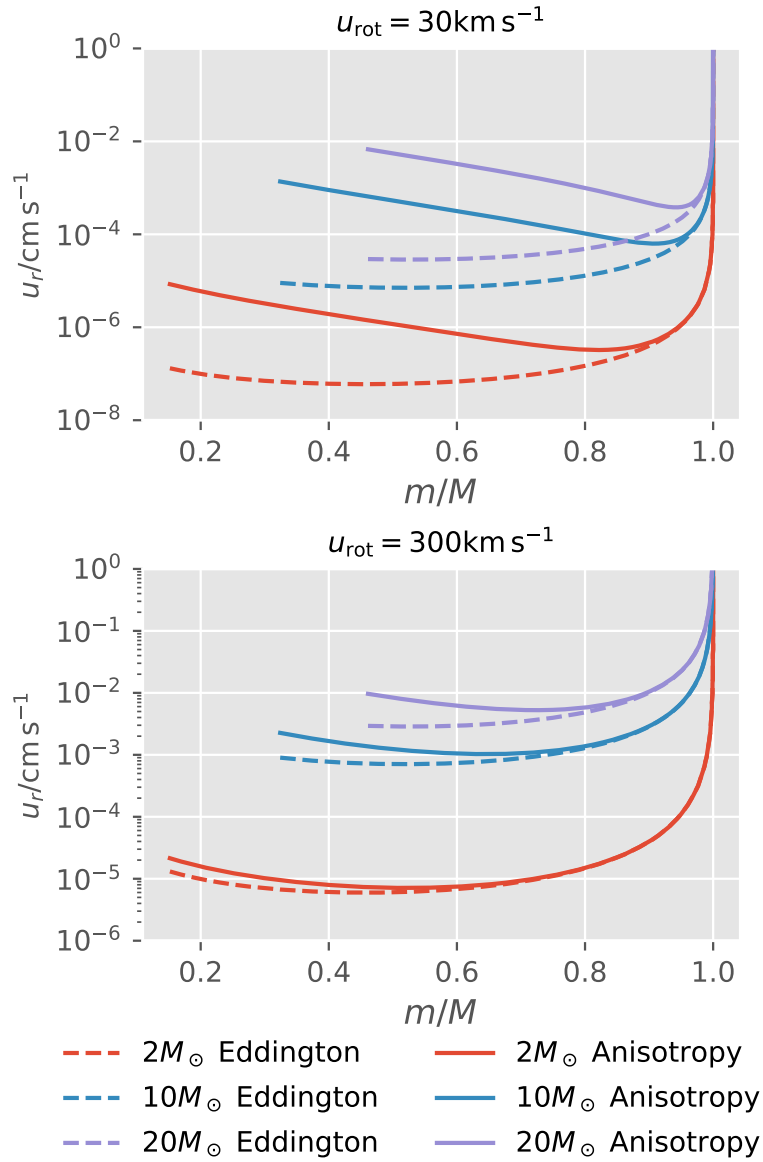


Figure 4.7: The radial velocity u_r is shown as a function of mass fraction m/M for three stellar models on the main sequence with masses of $2M_\odot$, $10M_\odot$ and $20M_\odot$. For each model results from both the Eddington–Sweet mechanism and the mechanism presented in this paper are shown. These calculations were made with $\beta = 3/2$ and for simplicity assume rigid rotation. The top panel has surface velocity of $u_{\text{rot}} = 3 \times 10^6 \text{ cm s}^{-1}$, corresponding respectively to 4×10^{-3} , 2×10^{-3} and 10^{-3} of the surface breakup velocity for the three stars. The bottom panel has $u_{\text{rot}} = 3 \times 10^7 \text{ cm s}^{-1}$, corresponding respectively to 0.4, 0.2 and 0.1 of the breakup velocity.

regime while the Eddington–Sweet mechanism scales quadratically with rotation rate.

It is worth noting that a similar effect is possible in stars of lower mass, where the anisotropy in the outer convection zone induces baroclinicity in the radiative core. This effect is more strongly damped because the characteristic damping scale is h , which is much shorter at an outer radiative–convective boundary than at a core convective–radiative boundary. Equivalently, the damping goes as $p_{\text{tachocline}}/p$ in this case, and $p_{\text{tachocline}}$ may be quite small relative to the core pressure. In addition the velocity damps towards the core because the temperature increases, making it easier to dissipate the flux accumulation. Finally, the anisotropy for a given rotation is smaller because the relevant $|N|$ is greater. Still, in the Sun $h \approx R_{\odot}/10$ near the tachocline, so this likely causes some mixing between the convection zone and the material a few tenths of a solar radius below it.

4.8 Chemical Composition Gradients

In the convection zones of massive stars chemical composition gradients are generally wiped out by turbulent mixing. So there are significant composition gradients only in the radiative zones of these bodies.

Because the circulation in radiative zones is driven by the same criterion of thermal equilibrium as the Eddington–Sweet circulation such gradients act on it in the same manner as they do that mechanism. The only place where there might be a difference in how composition gradients impact the mechanism we have introduced is in the transmission of baroclinicity from the convection zone to the radiative zone. However this transmission is achieved by the core emitting an aspherical heat flux and this is not at all changed by the chemistry in the vicinity of the core. Hence the effect of composition ought to be the same in both mechanisms. This has been examined in detail by [Meynet & Maeder \(2000\)](#), who provide a prescription for correcting the circulation velocity and find that such corrections are typically of order unity. This is therefore what we expect.

4.9 Convective Overshooting

The fact that these circulations drive extra mixing in radiative zones close to convective cores suggests that this may be the source of extra mixing which is commonly, though probably erroneously, called convective overshooting ⁴⁴. Such extra mixing naturally prolongs the main-sequence lifetime as required to match a number of evolved binary systems ⁴⁵ and

⁴⁴ Prather & Demarque 1974

⁴⁵ Schroder et al. 1997; Farmer et al. 2015; Eggleton & Yakut 2017

so is of significant interest for the purposes of stellar modelling.

Convective overshooting is often incorporated in stellar models by modelling a region beyond the convection zone as isentropic and well-mixed⁴⁶. This region has width

$$l_{\text{ov}} = \alpha_{\text{ov}} h, \quad (4.53)$$

where α_{ov} is a dimensionless parameter^{47 48}. A long-standing problem with this prescription is that the overshoot distance $\alpha_{\text{ov}} h$ required to match observations is often much larger than what calculations of the stiffness of the radiative-convective boundary suggest⁴⁹. What appears more likely is that the physical overshooting is small as predicted by stiffness calculations but that there is additional mixing caused by the baroclinic mechanism developed in the previous section.

The most immediate comparison with observations that can be made to test this hypothesis is to calculate α_{ov} from our model. To do so we calculate l_{ov} such that in the lifetime of the star the material within this distance of the tachocline is well-mixed with that at the tachocline. This is just the statement that

$$\frac{l_{\text{ov}}}{u_r} \approx \tau_{\text{MS}},$$

or

$$l_{\text{ov}} \approx u_r \tau_{\text{MS}},$$

where τ_{MS} is the main-sequence lifetime of the star. This is not quite right, however, because vertical chemical mixing is less efficient than the circulation velocity alone suggests. Using the correction of [Maeder & Zahn \(1998\)](#)⁵⁰ we find

$$l_{\text{ov}} \approx \frac{1}{30} u_r \tau_{\text{MS}}.$$

Inserting equation (4.51) we find

$$l_{\text{ov}} \approx \frac{u_{\text{c,core}}}{30} \tau_{\text{MS}} \left(\frac{\rho_{\text{c}}}{\rho} \right) \left(\frac{u_{\text{c,core}}}{c_s} \right)^2 \left(\frac{r_{\text{c}}}{r} \right)^2 \left(\frac{p}{p_{\text{tachocline}}} \right)^{\beta} \alpha_{\text{core}}.$$

In massive stars with even mild rotation, $\Omega > |N|$ everywhere in the core

⁴⁶ This is known as a penetrative overshoot model.

⁴⁷ Confusingly, this is also called f_{ov} by some authors.

⁴⁸ [Schroder et al. 1997](#)

⁴⁹ [Saslaw & Schwarzschild 1965](#)

⁵⁰ The correction is that the vertical diffusivity, rather than being hu_r , is $D_v = (1/30)(ru_r)^2/(D_h)$, where D_h is the horizontal diffusivity. Taking $D_h \approx u_{\theta} r = r(r/h)u_r$ yields $D_v = (1/30)hu_r$ and hence the overall correction is a factor of $1/30$.

so

$$\begin{aligned}\alpha_{\text{core}} &= p_{\text{tachocline}} \int_{p_{\text{tachocline}}}^{p_c} \min \left(\epsilon_{\text{max}}, \frac{\Omega(\mathcal{P})^2}{|N|(\mathcal{P})^2} \right) \frac{d\mathcal{P}}{\mathcal{P}^2} \\ &= \epsilon_{\text{max}} p_{\text{tachocline}} \int_{p_{\text{tachocline}}}^{p_c} \frac{d\mathcal{P}}{\mathcal{P}^2} \\ &\approx \epsilon_{\text{max}},\end{aligned}$$

because $p_{\text{tachocline}} \ll p_c$. Hence

$$\begin{aligned}l_{\text{ov}} &\approx \frac{\epsilon_{\text{max}}}{30} u_{\text{c,core}} \tau_{\text{MS}} \left(\frac{\rho_c}{\rho} \right) \left(\frac{u_{\text{c,core}}}{c_s} \right)^2 \left(\frac{r_c}{r} \right)^2 \left(\frac{p}{p_{\text{tachocline}}} \right)^\beta \\ &\approx \frac{\epsilon_{\text{max}}}{30} u_{\text{c,core}} \tau_{\text{MS}} \left(\frac{u_{\text{c,core}}}{c_{\text{s,core}}} \right)^2 \left(\frac{r_c}{r} \right)^2 \left(\frac{p}{p_{\text{tachocline}}} \right)^{\beta-1},\end{aligned}$$

where we have used the fact that $p \propto \rho c_s^2$. Noting that near the tachocline

$$r \approx r_c$$

and

$$p \approx p_{\text{tachocline}} e^{-\Delta r/h},$$

where Δr is the distance to the tachocline, we find that

$$l_{\text{ov}} \approx \frac{\epsilon_{\text{max}}}{30} u_{\text{c,core}} \tau_{\text{MS}} \left(\frac{u_{\text{c,core}}}{c_{\text{s,core}}} \right)^2 e^{-l_{\text{ov}}(\beta-1)/h}.$$

Inserting equation (4.53) we find

$$\alpha_{\text{ov}} \approx \frac{\epsilon_{\text{max}}}{30} \frac{u_{\text{c,core}}}{h} \tau_{\text{MS}} \left(\frac{u_{\text{c,core}}}{c_{\text{s,core}}} \right)^2 e^{-\alpha_{\text{ov}}(\beta-1)}$$

and making use of equation (4.52)

$$\alpha_{\text{ov}} \approx \frac{\epsilon_{\text{max}}}{30} \frac{u_{\text{c,core}}}{h} \tau_{\text{MS}} \left(\frac{u_{\text{c,core}}}{c_{\text{s,core}}} \right)^2 e^{-\alpha_{\text{ov}}(5h/2r-1)}. \quad (4.54)$$

This may be solved in terms of the Lambert W function or else numerically.

Fig. 4.8 shows α_{ov} as a function of stellar mass for a fine grid of stellar models made with the Cambridge STARS code ⁵¹. ϵ_{max} was taken to be 0.2 as suggested by various turbulence closure schemes ^{52,53}. The stellar lifetime was computed with the main-sequence fit of Eggleton et al. (1989). The variation of α_{ov} with mass suggests that it rises rapidly with mass in the window between 1 and $2 M_\odot$ and then asymptotically shortly thereafter $\alpha_{\text{ov}} \approx 0.25$. This behaviour is in very good agreement with the findings of Ribas et al. (2000), ⁵⁴ and Stancliffe et al. (2015), while yielding

⁵¹ Eggleton 1971; Pols et al. 1995

⁵² Kitchatinov 2013

⁵³ See Chapter 2.

⁵⁴ Moravveji et al. 2016

a slight overestimate relative to those of [Claret & Torres \(2017\)](#), who find an asymptote of $\alpha_{\text{ov}} \approx 0.2$.

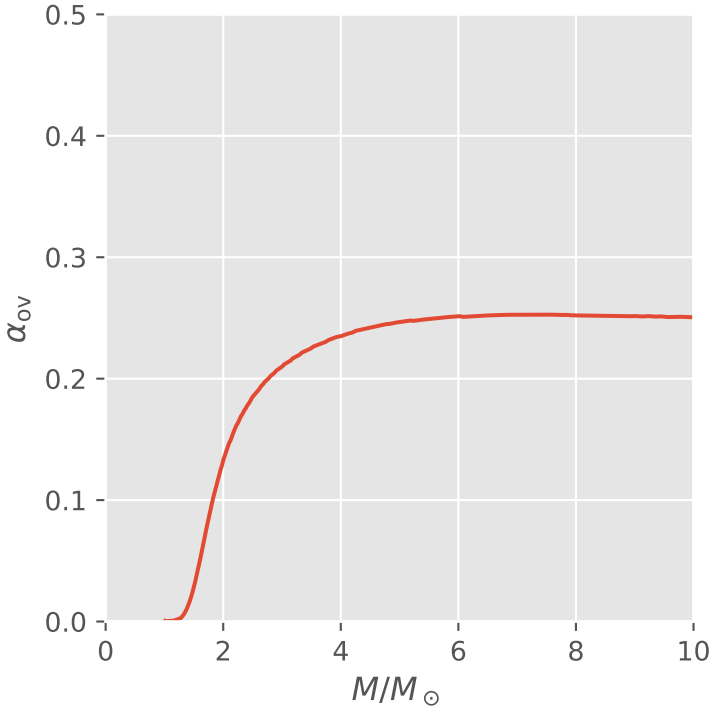


Figure 4.8: The convective overshoot parameter α_{ov} is shown as a function of stellar mass, computed with equation (4.54) and $\epsilon_{\text{max}} \approx 0.2$ as various turbulence closure schemes suggest. See e.g. Chapter 2.

An alternate way to parametrise convective overshooting is as an additional diffusivity in the radiative zone of the form

$$D_{\text{overshoot}} = D_{\text{convective}} e^{-2\Delta r / (f_{\text{ov}} h)} \quad (4.55)$$

⁵⁵, where f_{ov} is the exponential overshoot parameter, Δr is the distance to the radiative-convective boundary and

$$D_{\text{convective}} \equiv u_{\text{c,core}} h. \quad (4.56)$$

There are two ways to compare this prescription with our calculations. First, we may note from a practical perspective that the f_{ov} and α_{ov} prescriptions agree with one another, and so the fact that our calculated α_{ov} are consistent with those inferred from observations implies consistency with the f_{ov} prescription. Secondly, we can calculate an effective f_{ov} from our model. Because we predict different spatial behaviour from that of equation (4.55) there is no unique way to do this and different prescriptions yield different results. Indeed to self-consistently map from mixing via circulation currents to an exponential convective overshoot model requires a detailed comparison of stellar models with each prescription which we

⁵⁵ [Herwig et al. 1997](#); [Paxton et al. 2011](#)

leave for future work. Nevertheless one straightforward way to perform this mapping is to insist that one scale-height from the convective-radiative boundary, the effective diffusivity owing to the meridional circulation

$$D_{\text{merid}} \approx uh \quad (4.57)$$

equals the overshoot diffusivity. Following the same procedure as before to calculate u and incorporating the correction to chemical mixing we find

$$D_{\text{merid}} \approx \frac{\epsilon_{\text{max}}}{30} u_{\text{c,core}} h \left(\frac{u_{\text{c,core}}}{c_{\text{s,core}}} \right)^2 \left(\frac{r_c}{r} \right)^2 \left(\frac{p}{p_{\text{tachocline}}} \right)^{\beta-1}.$$

With equation (4.56) this becomes

$$\frac{D_{\text{merid}}}{D_{\text{convective}}} \approx \frac{\epsilon_{\text{max}}}{30} \left(\frac{u_{\text{c,core}}}{c_{\text{s,core}}} \right)^2 \left(\frac{r_c}{r} \right)^2 \left(\frac{p}{p_{\text{tachocline}}} \right)^{\beta-1}.$$

Setting this equal to one and letting $D_{\text{merid}} = D_{\text{overshoot}}$ we obtain

$$e^{-2\Delta r / (f_{\text{ov}} h)} \approx \frac{\epsilon_{\text{max}}}{30} \left(\frac{u_{\text{c,core}}}{c_{\text{s,core}}} \right)^2 \left(\frac{r_c}{r} \right)^2 \left(\frac{p}{p_{\text{tachocline}}} \right)^{\beta-1}.$$

Noting that near the tachocline $r \approx r_c$ and

$$p \approx p_{\text{tachocline}} e^{-\Delta r / h},$$

we find

$$e^{-2\Delta r / (f_{\text{ov}} h)} \approx \frac{\epsilon_{\text{max}}}{30} e^{-(\beta-1)\Delta r / h} \left(\frac{u_{\text{c,core}}}{c_{\text{s,core}}} \right)^2.$$

Hence

$$\left[\frac{2}{f_{\text{ov}}} - (\beta - 1) \right] \frac{\Delta r}{h} = \ln \frac{30}{\epsilon_{\text{max}}} - 2 \ln \frac{u_{\text{c,core}}}{c_{\text{s,core}}}.$$

Letting $\Delta r = h$ we find

$$\frac{2}{f_{\text{ov}}} - (\beta - 1) = \ln \frac{30}{\epsilon_{\text{max}}} - 2 \ln \frac{u_{\text{c,core}}}{c_{\text{s,core}}}.$$

Once more inserting equation (4.52) and taking $r \approx r_c$ we find

$$\frac{2}{f_{\text{ov}}} - \left(\frac{5h}{2r_c} - 1 \right) = \ln \frac{30}{\epsilon_{\text{max}}} - 2 \ln \frac{u_{\text{c,core}}}{c_{\text{s,core}}}. \quad (4.58)$$

Fig. 4.9 shows f_{ov} as a function of stellar mass with the same stellar models and parameters as were used for Fig. 4.8. The results qualitatively capture the inferred dependence on stellar mass, but we overestimate f_{ov} by a factor

of approximately ⁵⁶ 2. This is not surprising given the ad-hoc nature of our matching between equations (4.55) and (4.57) but it is encouraging that the overall magnitude is approximately correct and that the dependence on mass reproduces what is observed.

⁵⁶ Stancliffe et al. 2015; Moravveji et al. 2016

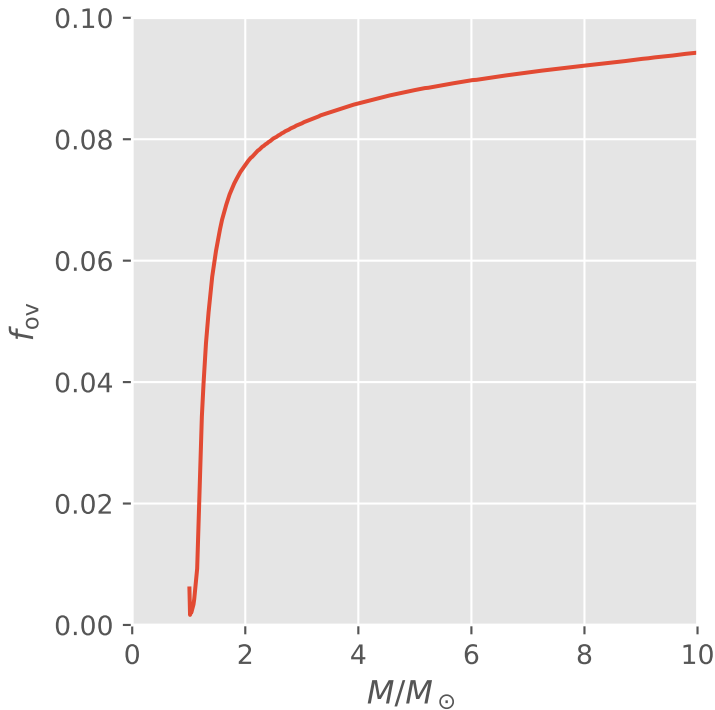


Figure 4.9: The convective overshoot parameter f_{ov} is shown as a function of stellar mass, computed with equation (4.58). The input stellar models were the same as those in Figure 4.8.

As a check of these calculations, Fig. 4.10 shows the spatial dependence of both the circulation diffusivity and the convective overshoot diffusivity for the three stellar models considered for Fig. 4.5. The latter was calculated with the exponential parametrisation and $f_{ov} = 0.09$, which is representative from Fig. 4.9. Note that, in each case, the crossover occurs roughly one scale-height from the edge of the convective core, in keeping with our matching to the exponential parametrisation. This both confirms the results of equation (4.58) and Fig. 4.9 and demonstrates the nature of the matching procedure we have used to infer f_{ov} .

4.10 Implementation in Stellar Models

While we have not yet implemented these enhanced circulation currents in stellar models, there are a variety of ways in which this could be done. As a rough approximation one could set the convective overshoot parameters according to equations (4.54) and (4.58). This is only an approximation because the circulation currents exhibit a different spatial dependence from that of convective overshooting, but it is straightforward to do.

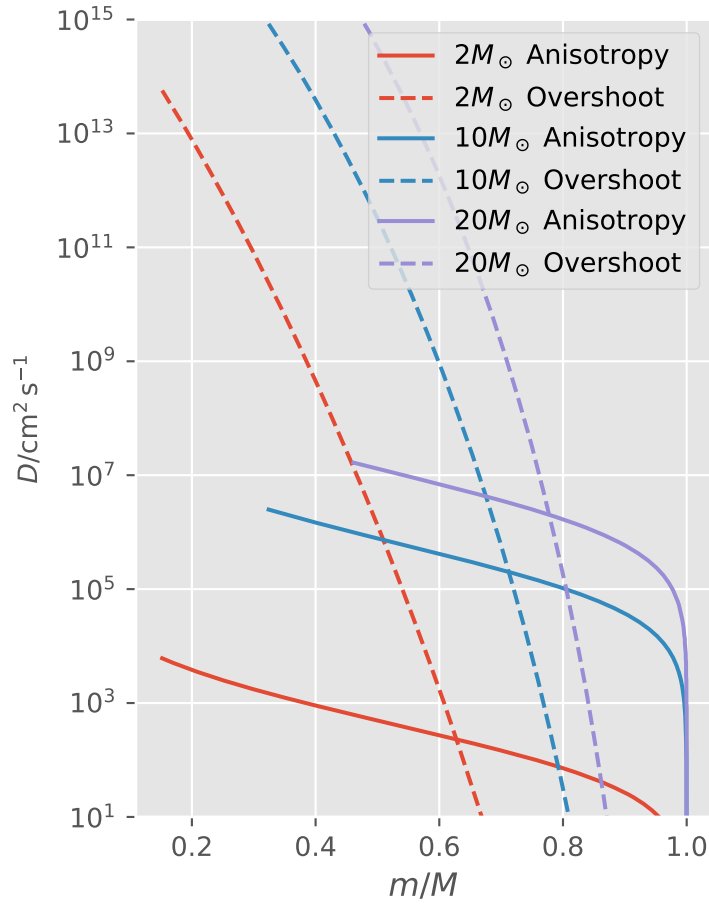


Figure 4.10: The effective circulation chemical diffusivity $D = \hbar u_r / 30$ and convective overshoot diffusivity are shown as functions of mass fraction m/M for three stellar models on the main sequence with masses of $2M_{\odot}$, $10M_{\odot}$ and $20M_{\odot}$. The circulation diffusivity was calculated with $\beta = 3/2$ and only includes that owing to convective anisotropy and not the Eddington–Sweet mechanism. The overshoot diffusivity was modelled with an exponential with $f_{\text{ov}} = 0.09$. These calculations were assuming rigid rotation and a surface velocity of $u_{\text{rot}} = 30 \text{ km s}^{-1}$.

A more complete accounting of this mechanism would require tracking the parameter α' in convection zones and α in radiative zones. This may be done either by directly computing these parameters according to the prescriptions in section 4.4 or by expanding the basic equations of stellar structure to incorporate the first several spherical harmonics. Of particular importance are the harmonics in the heat flux F as well as those in density. In addition a turbulence closure model⁵⁷ is needed to calculate \mathbf{D} in the convection zone, because this mechanism ultimately relies on convective anisotropy.

⁵⁷ such as that presented in Chapter 2

4.11 Interpretation

There are two further matters which are worth emphasizing. First, none of what we argue here is in contradiction of the Eddington–Sweet circulation calculations: we are simply extending them to account for convective anisotropy, incorporating its effects on stellar structure. Secondly, the origin of the velocity field we posit lies in turbulence and so the objection that an inviscid fluid cannot support such circulation currents is not applicable. This last point, particularly in the context of work of Busse (1981), has become something of an interpretational question because the Eddington–Sweet time is also the time-scale over which baroclinic transients decay⁵⁸. This leads to the suggestion that the resulting circulation is actually just a transient phenomenon.

⁵⁸ Osaki 1982

There are two ways in which this transient argument fails in the context of anisotropic convection. The first is that the turbulent transport of heat is not guaranteed to restore the star to an equilibrium and so the circulation time may be better understood as a transient turnover time. As we have shown in Chapter 2, turbulent transport coefficients depend non-linearly on several variables and gradients. There appears to be no proof that the net effect is to equilibrate the system. So there is no reason to suspect that the anisotropy which drives heat transport away from equilibrium decays at any point. It would be highly surprising if a phenomenon with so many degrees of freedom and based on inherent instabilities in fluid transport processes proved itself linearly stable. Also, despite the success of mixing length theories, turbulence supports long-range correlations. Thus the convection zone can have large-scale turbulent structures which manifest as a circulation current. So convection may pump baroclinic instabilities and cause mixing indefinitely. This pumping effect can pervade radiative zones just as well as convective zones, even though its origin lies in the latter.

Furthermore there are no angular momentum barriers to the circulation we are proposing and this is a key difference from the original Eddington–Sweet phenomenon. In convection zones, when $\Omega < |N|$, the circulation velocity is less than the convective speed and hence is slower than the maximum which would be permitted by turbulent angular momentum transport. In radiative zones we have argued that shear turbulence suffices to satisfy the momentum balance required by the circulation. Thus, our results are consistent with angular momentum conservation and rely on motions of orders which are already allowed in convection cells. When $\Omega > |N|$ the situation becomes more complicated but the same basic effect is likely to occur. Furthermore, even if there were no turbulence allowing this process, it could occur and give rise to an angular momentum flux. Similarly, even though radiative zones are stably stratified, a flow along the pressure gradient may occur if there is a driving heat accumulation because this can establish a new equilibrium position for fluid parcels and draw on the stratification to propel them upward under the effect of buoyancy.

However there may be magnetic barriers to mixing. There is strong differential rotation near the solar tachocline so it seems likely that there are also strong toroidal magnetic fields present in this region. These fields may work to inhibit transverse motion. At the same time though they serve to increase the turbulent anisotropy, which may partially act to counter this inhibiting effect. The net effect of magnetic fields in determining the solar meridional flow cannot be too significant because the predicted meridional velocities match observations even in the tachocline. This suggests that our non-magnetic scaling analysis may suffice, though we cannot say for certain that magnetic fields are generally irrelevant.

Thus we arrive at the conclusion that such circulations are physical and do not decay, even over long time-scales. This strong conclusion relies on the aforementioned properties of the convection zone and turbulence and does not straightforwardly extend to all drivers of circulation in radiative zones.

4.12 *Discussion and Outlook*

We have demonstrated that the meridional flow rate in the radiative zones of massive rotating stars in many cases is set by anisotropy in the central convection zone. This enhances mixing in massive stars as well as core-envelope angular momentum coupling in all stars with a radiative zone overlying a convection zone. These effects may aid in the formation of massive binary black hole pairs ⁵⁹ through enhanced mixing at long periods.

⁵⁹ Marchant, Pablo et al. 2016

More generally, such mixing would lead to stronger core-envelope mixing thus leading to massive stars growing larger burnt-out cores and living longer owing to mixing of fuel into the core. This mechanism mimics convective overshooting, and we have argued that it suffices to explain the anomalous overshoot distances which have been inferred from observations. In addition, such baroclinicity-driven mixing is likely to occur in stars with outer convection zones and inner radiative zones, though with more limited effect. This represents a fundamentally new phenomenon in stellar mixing and we expect it to have wide-reaching consequences for stellar evolution.

5 *Tidal heating of Hot Jupiters*

There is grandeur in this view of life...
from so simple a beginning endless forms
most beautiful and most wonderful have
been, and are being, evolved.

Charles Darwin

Abstract

We study the interaction between stellar irradiation and tidal heating in gaseous planets with short orbital periods. We show that many tidal models provide thermal feedback, producing interior radiative zones and leading to enhanced g-mode dissipation with a wide spectrum of resonances. These resonances are tuned by the thermal feedback, and so represent a novel form of thermomechanical feedback, coupling vibrational modes to the very slow thermal evolution of the planet. Stellar irradiation traps the heat produced by these modes at depth with high efficiency, leading to entropy increase in the central convective region, as well as expansion of the planet's radius sufficient to match observed swelling. We find that thermally driven winds play an essential role in this process by making the thermal structure of the atmosphere spherically symmetric within a few scale heights of the photosphere. We characterise the relationship between the swelling factor, the orbital period and the host star and determine the timescale for swelling. We show that these g-modes suffice to produce bloating on the order of the radius of the planet over Gyr timescales when combined with significant insolation and we provide analytic relations for the relative magnitudes of tidal heating and insolation.

5.1 Introduction

In recent data from Kepler and ground-based followups there is evidence for a large population of hot Jupiters which are substantially inflated relative to their degenerate radii ¹. The radii and periods of known members of this population as well as of the broader Jupiter-sized population are shown in Fig. 5.1 ². There is an apparent split in the observed population around periods of 10 d, such that planets with longer periods are generally not inflated while those with shorter periods are often substantially inflated. Importantly, planets at or above $2R_J$ must be inflated relative to their degenerate radii, otherwise their implied masses would make them stars ^{3,4}. In order to achieve this level of expansion, the central convection zone must be heated considerably relative to what would be expected as a result of the residual heat of formation ⁵, and there is evidence of planets re-inflating after cooling down ⁶. Complicating this is the thermodynamic requirement that heat flows only from hot to cold, not in the reverse fashion. This, combined with the expectation that temperature increases towards the core of the planet, means that any change in temperature at depth must be due to heat generated at or deeper than the point of interest.

¹ Hellier et al. 2012; Weiss et al. 2013; Hartman et al. 2012

² Rein 2012

³ Stevenson 1991

⁴ Jupiter has approximately the maximum radius for an unheated gas giant.

⁵ Lopez & Fortney 2016

⁶ Hartman et al. 2016

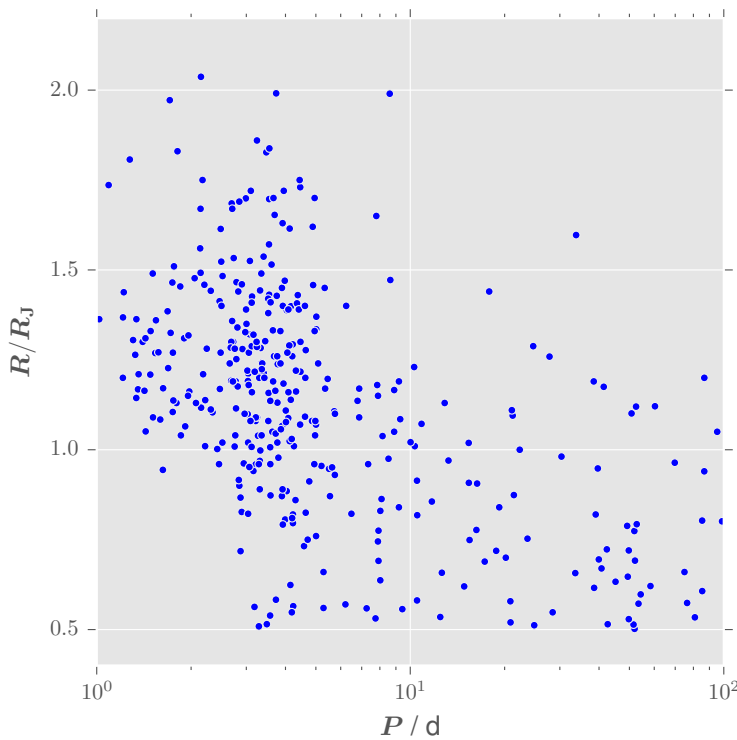


Figure 5.1: Known population of short-period planets with radii near that of Jupiter.

A variety of mechanisms have been suggested to generate deep heating,

with ohmic processes (Batygin, Stevenson & Bodenheimer, 2011; Spiegel & Burrows, 2013) and tidal dissipation⁷ among the more popular models. Because heat cannot flow from the surface of the planet into its core, the stellar flux is often neglected. However, somewhat surprisingly, the observed radii correlate strongly with the incident stellar flux, so that this flux may play a role in the inflation process⁸. Confounding this analysis is the fact that stellar flux is not independent of orbital period. So a theory of hot Jupiter inflation must handle the distinct effects of orbital period and incident flux, particularly when dealing with tidal heating.

⁷ Socrates 2013; Miller et al. 2009

⁸ Lopez & Fortney 2016

We investigate the effects of stellar flux on the structure of an internally heated hot Jupiter, making few assumptions about the nature or profile of the heating and considering the effects of wind redistribution. We show that the stellar flux acts to modulate the rate at which heat escapes from the planet. We then investigate the feedback that this heating produces on the thermal structure of the planet and show that a wide variety of realistic heating profiles gives rise to interior radiative zones. These zones migrate within the planet on thermal timescales, giving a broad and dynamically tuned spectrum of g-mode resonances which dissipate heat tidally in the planet. We then show that these modes suffice to produce the observed bloating. Finally we predict the relation between stellar flux, orbital period and planetary radius.

The new thermomechanical feedback mechanism we propose, shown schematically in Fig. 5.2, underscores the importance of considering planets as dynamical objects with complex behaviours coupling wildly different timescales. Vibrational effects with periods ranging from seconds to days can have a tremendous impact on thermal evolution over millions of years, and that thermal evolution in turn feeds back into the vibrational modes, creating a dynamically tuned spectrum which can ultimately determine the large-scale structure of the planet.

5.2 Isotropic Planetary Structure

We discuss the structure of a planet isotropically illuminated by flux F_e from its host star. Fig. 5.3 shows the orbital configuration of the planet-star system and Fig. 5.4 shows the thermodynamic structure of the planet with the relevant variables defined schematically. For the deep interior of the planet we adopt the analytic brown dwarf structure of Stevenson

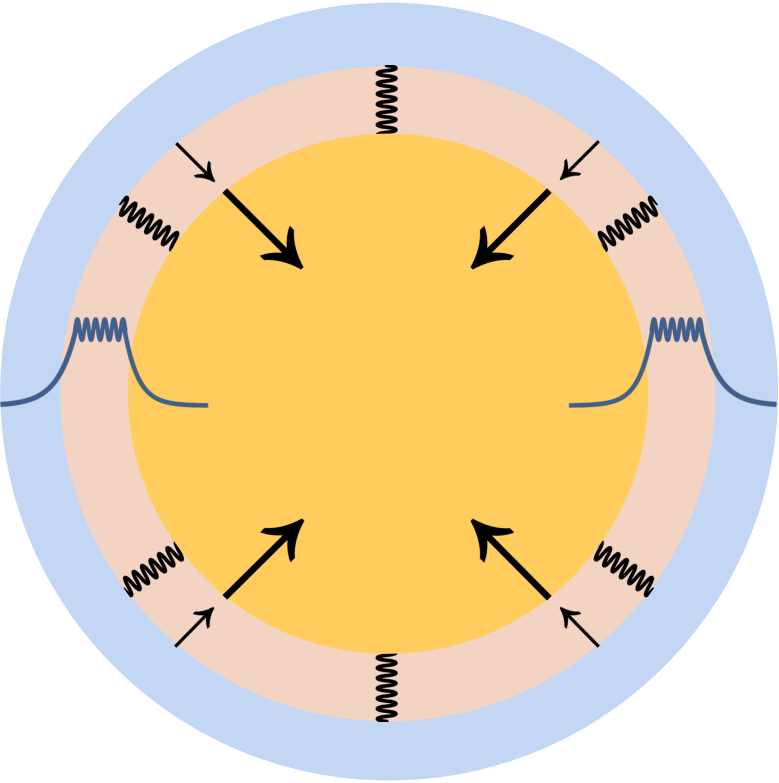


Figure 5.2: Schematic of the proposed thermomechanical feedback mechanism. The upper convective layer (blue), radiative layer (beige), and inner convective layer (yellow) are shown as concentric shells. The boundaries of the radiative layer are moving inward at different rates, allowing the zone to resize. Profiles of g-modes (dark blue) are shown along the equator and schematically depicted at other latitudes.

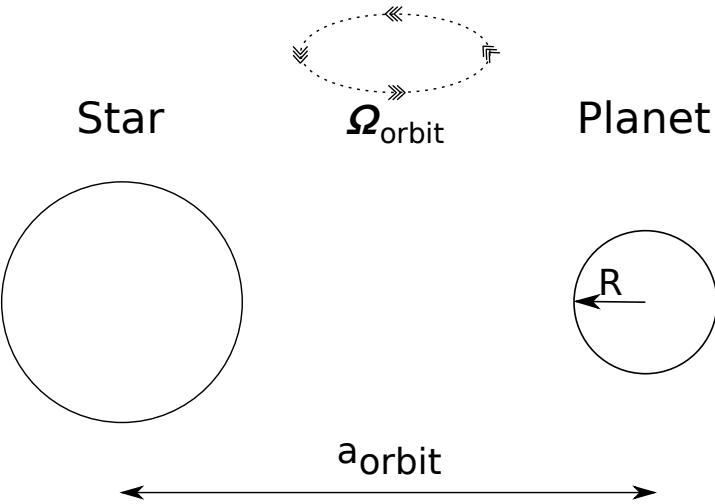


Figure 5.3: Orbital configuration of the planet and its host star.

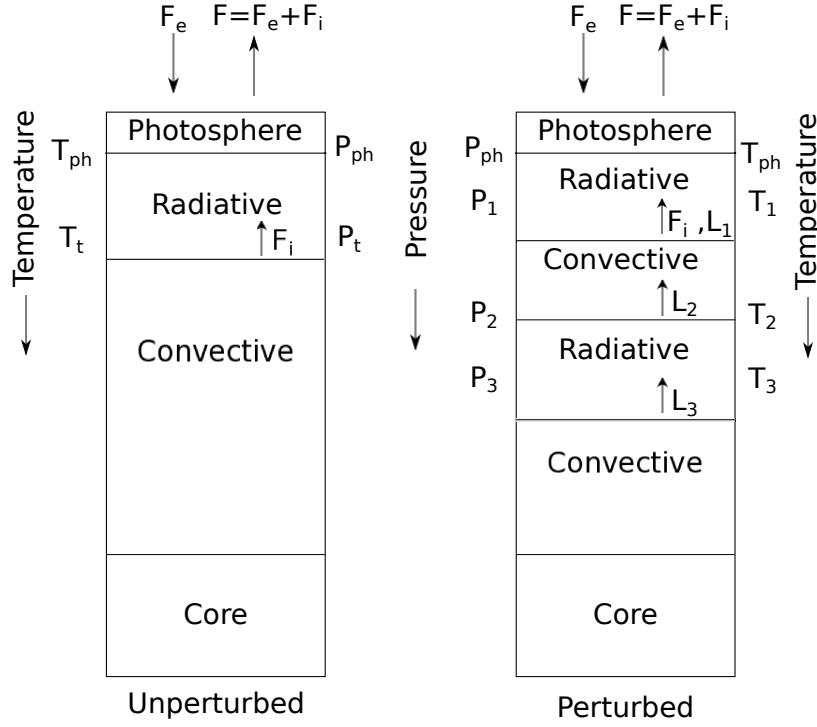


Figure 5.4: Thermodynamic structure of the planet. The unperturbed structure is shown on the left, while the heated (perturbed) structure is shown on the right.

(1991):

$$\psi \equiv \frac{k_B T}{E_F} = 8 \times 10^{-6} \mu_e^{2/3} \left(\frac{\rho}{\text{g cm}^{-3}} \right)^{-2/3} \left(\frac{T}{\text{K}} \right), \quad (5.1)$$

$$R_0 = 2.8 \times 10^9 \text{ cm} \left(\frac{M}{M_\odot} \right)^{-1/3} \mu_e^{-5/3},$$

$$r = R_0 \left(1 + \psi + \frac{\psi^2}{1 + \psi} \right), \quad (5.2)$$

$$p = 10^{13} \text{ erg cm}^{-3} \mu_e^{-5/3} \left(\frac{\rho}{\text{g cm}^{-3}} \right)^{5/3} \left(\frac{r}{R_0} \right), \quad (5.3)$$

and

$$\nabla_a \equiv \left. \frac{\partial \ln T}{\partial \ln p} \right|_s = \frac{2}{5},$$

where ψ is the electron degeneracy parameter, R_0 is the degenerate radius, r is the radial coordinate, E_F is the Fermi energy, M is the mass of the planet and ∇_a is the adiabatic temperature gradient⁹. These relations effectively parametrise a $\gamma = 5/3$ adiabatic atmosphere, accounting for electron degeneracy at high pressures. We assume solar composition in this paper, so that the mean molecular weight of electrons $\mu_e \approx 1.15$. In addition, we take R to be the radius of the planet. For convenience, we

⁹ This prescription is most suitable for objects above ten times the mass of Jupiter. Nearer to the mass of Jupiter it somewhat over-predicts radii by as much as a factor of three. There are known corrections which account for this, as discussed by [Stevenson \(1991\)](#), but these unnecessarily complicate our analysis so we neglect them. In our later expressions the net result of these corrections is to change \mathcal{R} , defined later on, for lower-mass objects by a factor of several, but none of our conclusions are altered by this.

define the parameters

$$\mathcal{R} \equiv R/R_0, \quad (5.4)$$

and

$$\mathcal{M} \equiv M/M_J,$$

where $M_J = 1.838 \times 10^{30} \text{ g}$ is the mass of Jupiter. We expect the gas line opacity to dominate in hot atmospheres, so we use this as fiducial and define ¹⁰

$$\kappa_0 \equiv 10^{-2} \text{ cm}^2 \text{ g}^{-1}.$$

¹⁰ Stevenson 1991

We connect the top of the convection zone to the photosphere with a radiative zone at transition pressure p_t . The photospheric temperature is given by

$$T_{\text{ph}} = \left(\frac{F}{\sigma} \right)^{1/4},$$

where F is the total flux leaving the planet's atmosphere and σ is the Stefan-Boltzmann constant. This flux may be divided into two components, as

$$F = F_i + F_e,$$

where F_i is the heat arriving from the planet's interior and F_e is the heat arriving from the host star. When F_e is large relative to the flux which would escape through the planet's natural cooling the photospheric temperature is determined entirely by F_e , such that

$$T_{\text{ph}} = \left(\frac{F_e}{\sigma} \right)^{1/4}. \quad (5.5)$$

The escaping flux F_i from the planet's core is just the flux which escapes from the convection zone. This may be generated by gravitational contraction, radioactive decay or by a decrease in the interior entropy; here we generally assume the last of these to be the dominant source of interior flux.

The radiative gradient is given by

$$\nabla_r = \frac{3\kappa p L}{64\pi G M \sigma T^4},$$

where L is the luminosity driving the gradient. At the convective-radiative boundary we have

$$\nabla_a = \nabla_r = \frac{3\kappa p_t L_i}{64\pi G M \sigma T_t^4}, \quad (5.6)$$

where

$$L_i = 4\pi R^2 F_i.$$

If we take κ to be a power law in both p and T of the form

$$\kappa = \kappa_0 T^a p^b$$

then

$$\nabla_a = \frac{3\kappa_0 p_t^{1+b} L_i}{64\pi G M \sigma T_t^{4-a}}.$$

Above the transition we have

$$\nabla_r = \nabla_a \left(\frac{p}{p_t} \right)^{1+b} \left(\frac{T}{T_t} \right)^{a-4} = \frac{d \ln T}{d \ln p}.$$

Integrating from the photosphere to the transition yields

$$1 - \left(\frac{T_{\text{ph}}}{T_t} \right)^{4-a} = \frac{4-a}{1+b} \nabla_a \left(1 - \left(\frac{p_{\text{ph}}}{p_t} \right)^{1+b} \right).$$

The photosphere pressure is generally much lower than the transition pressure so

$$\frac{T_{\text{ph}}}{T_t} = \left(1 - \frac{4-a}{1+b} \nabla_a \right)^{\frac{1}{4-a}},$$

which has a solution if and only if

$$1 - \frac{4-a}{1+b} \nabla_a \geq 0. \quad (5.7)$$

If $b > -1$ and $a > 4$ or $b < -1$ and $a < 4$ or $b > \frac{3-2a}{5}$ and $a < 4$ this is satisfied. There are other conditions under which it is satisfied, but these are the most relevant common cases. The exponents are generally of order unity and the result is raised to a small power so $T_{\text{ph}} \approx T_t$. This agrees with other analyses¹¹, which have found that in Jupiter-like planets, $T_{\text{ph}} < T_t < 1.5 T_{\text{ph}}$. The precise temperature ratio depends on the nature of the opacity function, so we simply take $T_t = 2^{1/4} T_{\text{ph}}$ (the Eddington closed grey body) as representative. If this holds and the flux from the star is dominant then

$$F_i = \frac{16\sigma g \nabla_a T_t^4}{3\kappa p_t} = \left(\frac{32g \nabla_a}{3\kappa p_t} \right) F_e. \quad (5.8)$$

Eliminating μ_e between equations 5.1 and 5.3, we may write p_t in terms of T_t at $r \approx R$ and R_0 , such that

$$p_t = 10^{13} \text{ erg cm}^{-3} \left(\frac{R}{R_0} \right) \left(\frac{T_t}{\text{K}} \right)^{5/2} \left(\frac{\psi}{8 \times 10^{-6}} \right)^{-5/2}. \quad (5.9)$$

¹¹ Ginzburg & Sari 2015

From equation (5.2) and the definition of R_0 (equation (5.4)) we find

$$\begin{aligned}\psi &= \frac{1}{4} \left(\frac{R}{R_0} - 2 + \sqrt{\left(\frac{R}{R_0} \right)^2 + 4 \left(\frac{R}{R_0} \right) - 4} \right) \\ &= \frac{1}{4} \left(\mathcal{R} - 2 + \sqrt{\mathcal{R}^2 + 4\mathcal{R} - 4} \right),\end{aligned}$$

where we have taken the positive root because $\psi > 0$ and $R > R_0$. Note that this is always of order unity, so to good approximation the majority of the variation in p_t comes from the R and T_t dependence in equation (5.9).

If the convective-radiative transition occurs at a shallow point in the atmosphere the corresponding column density is just

$$\Sigma_t \approx \frac{p_t}{g} = 4 \times 10^9 \text{ g cm}^{-2} \mathcal{R}^3 \mathcal{M}^{-5/3} \left(\frac{T_t}{K} \right)^{5/2} \left(\frac{\psi}{8 \times 10^{-4}} \right)^{-5/2},$$

again with $\mathcal{M} = M/M_J$. Eliminating T_t in favour of F_e and using $T_\odot = 5777\text{K}$ we find

$$\Sigma_t \approx 2 \times 10^6 \text{ g cm}^{-2} \mathcal{R}^3 \mathcal{M}^{-5/3} \left(\frac{F_e}{F_\odot} \right)^{5/8} \psi^{-5/2}.$$

Inserting this result into equation (5.8) we obtain

$$\frac{F_i}{F_e} = \frac{32g\nabla_a}{3\kappa p_t} = 2 \times 10^{-4} \mathcal{M}^{5/3} \left(\frac{F_e}{F_\odot} \right)^{-5/8} \left(\frac{\kappa}{\kappa_0} \right)^{-1} \frac{\psi^{5/2}}{\mathcal{R}^3}.$$

As one final manipulation, we wish to put our equations in terms of the stellar luminosity and orbital radius. The stellar luminosity is related to the external flux F_e by

$$4\pi R^2 F_e = \frac{\pi R^2 L_\star}{4\pi a_{\text{orbit}}^2}, \quad (5.10)$$

where L is the stellar luminosity, a_{orbit} is the orbital radius of the planet. The factor of πR^2 on the right-hand side is just the cross-section of the planet as seen from the star, while the factor of $4\pi R^2$ on the left-hand side reflects the definition of F_e as an average over the surface of the planet. So

$$F_e = \frac{L}{16\pi a_{\text{orbit}}^2}.$$

Comparing with the Sun we find

$$\frac{F_e}{F_\odot} = \frac{1}{4} \left(\frac{L_\star}{L_\odot} \right) \left(\frac{a_{\text{orbit}}}{R_\odot} \right)^{-2}. \quad (5.11)$$

Thus

$$\frac{F_i}{F_e} = 5 \times 10^{-4} \mathcal{M}^{5/3} \left(\frac{L_\star}{L_\odot} \right)^{-5/8} \left(\frac{a_{\text{orbit}}}{R_\odot} \right)^{5/4} \left(\frac{\kappa}{\kappa_0} \right)^{-1} \frac{\psi^{5/2}}{\mathcal{R}^3}. \quad (5.12)$$

Importantly, the exponent on the luminosity is greater than -1 . This means that while the ratio of escaping to incident flux decreases with increasing stellar flux, the total escaping flux increases. This conclusion is dependent primarily on how strongly the ratio T_t/T_{ph} varies with F_e , which in turn depends on the form of the opacity. In particular, it does not generally hold at extremely high temperatures where the gas line opacity ceases to dominate and Kramers-like rules take over. For brown dwarfs and hot Jupiters, however, this variation is small and should not pose a problem. It is also useful to compute the transition column density

$$\Sigma_\tau \approx \frac{P_t}{g} = 8 \times 10^5 \text{ g cm}^{-2} \mathcal{R}^3 \mathcal{M}^{-5/3} \left(\frac{L_\star}{L_\odot} \right)^{5/8} \left(\frac{a_{\text{orbit}}}{R_\odot} \right)^{-5/4} \psi^{-5/2}. \quad (5.13)$$

This is small enough that the shallow approximation is not bad.

5.3 Angular Temperature Distribution

The planets under consideration are generally highly insolated. This can lead to significant temperature differences between the day and night sides, particularly if the planet is tidally locked. In this section we show that winds suffice to make the thermal structure of the atmosphere spherically symmetric at depth even when there is a large temperature difference at the photosphere¹². This allows us to treat the structure of the planet as spherically symmetric where tidal effects are most prominent.

Consider a wind driven from one side of the planet to the other along isobars with characteristic velocity¹³ \mathbf{v} . Suppose further that the character of this wind changes in the vertical direction over distances of order the pressure scale height h and that it changes in the horizontal direction over distances of order the planet's radius. The specific force due to shear in the vertical direction is

$$\mathbf{F}_v = \nu_v \frac{\partial \mathbf{v}}{\partial r},$$

where ν_v is the viscosity for a circumferential flow shearing in the vertical direction. The corresponding power dissipated is

$$\mathcal{P}_v = \frac{\partial \mathbf{v}}{\partial r} \cdot \mathbf{F}_v = \nu_v \left(\frac{\partial \mathbf{v}}{\partial r} \right)^2.$$

¹² This result is derived from simplified arguments by [Jermyn \(2015\)](#).

¹³ When this wind is azimuthal it is a manifestation of differential rotation.

Likewise, the force due to shear in the horizontal direction is

$$\mathbf{F}_h = \nu_h \frac{\partial \mathbf{v}}{\partial \xi},$$

where ν_h is the viscosity for a circumferential flow shearing in the other circumferential direction and ξ is a coordinate along the flow. The corresponding power dissipated is

$$\mathcal{P}_h = \frac{\partial \mathbf{v}}{\partial \xi} \cdot \mathbf{F}_h = \nu_h \left(\frac{\partial v}{\partial \xi} \right)^2.$$

The total power dissipated is then

$$\mathcal{P} = \mathcal{P}_v + \mathcal{P}_h \approx v^2 \left[\frac{\nu_v}{h^2} + \frac{\nu_h}{r^2} \right],$$

where we have approximated the velocity derivatives with the velocity magnitude and the relevant scale heights, the pressure scale height h in the vertical direction and the radius r in the horizontal. We have also simplified the viscosity from a rank-4 tensor to two scalars, so this relation ought only to be interpreted as an order of magnitude of the power.

To determine v , we now match this power to the work which the wind may extract as a heat engine. We are interested in cases where the temperature difference between the two sides is large so the efficiency of the heat engine is of order unity even if diffusive losses make it irreversible. We may neglect diffusive losses because we have taken the microscopic thermal diffusivity to be small on the relevant scales. So we may write the specific rate of work as

$$\mathcal{W} = c_p \mathbf{v} \cdot \nabla T \approx c_p v \frac{\Delta T}{\pi r},$$

where equation (1.19) gives

$$c_p = \frac{5}{2} \left(\frac{k_B}{\mu m_p} \right)$$

for a monatomic ideal gas. This is simply the specific heat which is transported from one side of the planet to the other. In our case

$$\Delta T \equiv T_{\text{day}} - T_{\text{night}}$$

and

$$T \equiv \frac{1}{2} (T_{\text{day}} + T_{\text{night}}),$$

so T refers to the average temperature while ΔT refers to the temperature difference. By definition, $\Delta T/T \leq 2$. In the most extreme case this gives

$$\mathcal{W} \approx c_p v \frac{\Delta T}{\pi r} \approx \frac{c_p T v}{\pi r} \left(\frac{\Delta T}{T} \right) \approx \frac{5c_s^2 v}{2\gamma \pi r},$$

where as usual

$$c_s = \sqrt{\frac{\gamma k_B T}{\mu m_p}}$$

is the adiabatic sound speed. Equating the rate of work and power gives

$$c_s^2 = \frac{2\gamma}{5} \pi r v \left[\frac{\nu_v}{h^2} + \frac{\nu_h}{r^2} \right]. \quad (5.14)$$

To proceed further we must examine the forms of ν_v and ν_h . The nature of the viscosity differs between stably stratified and buoyantly unstable zones, so we must determine which of these are relevant and treat them separately.

We begin with radiative zones. In a stably stratified region the two viscosities differ because of Richardson stabilisation¹⁴, an effect which limits the scale of turbulence in the vertical direction by means of a buoyant restoring force (Galperin, Sukoriansky & Anderson, 2007). A straightforward prescription for the viscosities in this context is

$$\begin{aligned} \nu_h &\approx \nu r \\ \nu_v &\approx v^2 \left(\frac{\alpha + \nu_h}{gh(\nabla_a - \nabla)} \right), \end{aligned} \quad (5.15)$$

where α is the microscopic thermal diffusivity¹⁵. Generally we expect α to be small compared to ν_h because horizontal radiative transfer is inefficient., so we may neglect α and write

$$\nu_v = v^2 \left(\frac{\nu_h}{gh(\nabla_a - \nabla)} \right) = \frac{v^3 r}{gh(\nabla_a - \nabla)}.$$

By the Schwarzschild criterion $\nabla < \nabla_a$ in a stably stratified zone¹⁶. In general we expect radiative transport to be efficient far from the zone boundaries, so we take $\nabla \ll \nabla_a$ in most of such a zone. Using this we write

$$\nu_v = \frac{v^3 r}{gh \nabla_a}.$$

Now making use of equation (3.19) we find

$$gh = \frac{g p}{g \rho} = \frac{p}{\rho} = \gamma^{-1} c_s^2, \quad (5.16)$$

¹⁴ See Chapter 2 for more discussion on this effect.

¹⁵ Mathis et al. 2004

¹⁶ Böhm-Vitense 1958

hence

$$\nu_v = \frac{v^3 r \gamma}{c_s^2 \nabla_a}. \quad (5.17)$$

Inserting equations (5.15) and (5.17) into equation (5.14) gives

$$c_s^2 = \frac{2\gamma}{5} \pi r v \left[\frac{v^3 r \gamma}{c_s^2 h^2 \nabla_a} + \frac{v}{r} \right].$$

This may be rearranged to

$$\frac{5}{2\pi\gamma} = \frac{\gamma}{\nabla_a} \left(\frac{v}{c_s} \right)^4 \left(\frac{r}{h} \right)^2 + \left(\frac{v}{c_s} \right)^2.$$

Solving gives

$$\left(\frac{v}{c_s} \right)^2 = \frac{\nabla_a h^2}{2\gamma r^2} \left[-1 \pm \sqrt{1 + \frac{10r^2}{\pi \nabla_a h^2}} \right].$$

The positive branch is the one of interest, because we have implicitly taken $v > 0$ in writing it as a magnitude. In the upper regions of the planet's atmosphere $r \gg h$ so

$$\frac{v}{c_s} \approx \frac{h}{r} \sqrt{\frac{5}{2\pi\gamma}}.$$

Using equation (5.16) the rate at which heat is transported may be written as

$$\varepsilon = \mathcal{W} \approx \frac{5c_s^2 v}{2\pi\gamma r} \approx \frac{c_s^3 h}{r^2} \left(\frac{5}{2\pi\gamma} \right)^{3/2} \approx \frac{\gamma c_s^5}{gr^2} \left(\frac{5}{2\pi\gamma} \right)^{3/2}.$$

The region of interest is shallow so $gr^2 \approx GM$ and

$$\varepsilon \approx \frac{\gamma c_s^5}{GM} \left(\frac{5}{2\pi\gamma} \right)^{3/2}.$$

The depth, as measured by column density Σ_i , over which the winds make the flux distribution spherically symmetric is

$$\Sigma_i = \frac{F_e}{\varepsilon} \approx \frac{GM\sigma T_{\text{ph}}^4}{\gamma c_s^5} \left(\frac{2\pi\gamma}{5} \right)^{3/2}.$$

Evaluating the sound speed at the photosphere gives

$$\Sigma_i \approx 3 \times 10^3 \text{ g cm}^{-2} \mathcal{M} \left(\frac{T}{10^3 \text{ K}} \right)^{3/2},$$

where m_p is the proton mass. For comparison, the photosphere is at a depth of

$$\Sigma_{\text{ph}} \approx \kappa^{-1} = 10^2 \text{ g cm}^{-2} \left(\frac{\kappa}{\kappa_0} \right)^{-1}.$$

Thus the temperature distribution becomes spherically symmetric in a region deeper than the photosphere but shallower than the convective

transition. So we need not worry about the viscosity in convection zones.

This remains valid as long as the planet rotates slowly relative to v/R , such that the characteristic scale of circumferential motion remains R and is not reduced by Coriolis effects. At short periods, where this condition is most in danger, the anisotropy is very large, such that $v \approx hc_s/r$, and the surface temperature should be quite high because of insolation, such that $c_s \approx 3 \times 10^5 \text{ cm s}^{-1}$. In this regime, the rotational period of a Jupiter-radius planet must be at least 30 d with $h/r \approx 10^{-2}$ or 3 d with $l/r \approx 10^{-1}$ for the Coriolis effect to be negligible. Even at the shortest known periods of just under a day, the correction term is not too great and does not alter the conclusion that the temperature distribution becomes spherical above the convection zone, so we continue to use this approximation with the knowledge that it becomes worse as the period diminishes.

5.4 Heated Thermal Structure

In this section we work on timescales long compared to the adjustment of radiative or convective zones to thermal perturbations but short compared to the characteristic thermal timescale of the planet. This is the instantaneous equilibrium approximation¹⁷. This separation of scales exists because the thermal timescale of the planet is set by the thermal content of the core, whereas the radiative and convection regions of interest are shallow zones with much less mass and at much lower temperatures.

The equations governing the luminosity of the planet as a function of mass coordinate are

$$\begin{aligned} \frac{\partial L}{\partial m} &= \epsilon(m) - c_p \frac{\partial s}{\partial t}, \\ L(0) &= 0 \end{aligned} \quad (5.18)$$

and

$$L(M) = L_i,$$

where $\epsilon(m)$ is the specific energy generation by tides, radioactive decay and ohmic processes and the mass coordinate m corresponds to the spherical shell containing mass m . Note that mechanical expansion and contraction can generate energy, but in this coordinate system that generation provides no net contribution because it does not alter the specific entropy.

Thermodynamic consistency imposes the condition that heat travels from hot regions to cool ones. Assuming that T increases towards the

¹⁷ Despite its name, this is still a fundamentally non-equilibrium system.

core of the planet, this means that $L(m) \geq 0$ everywhere. In a convective atmosphere the thermal gradient is almost independent of the luminosity. This follows because the luminosity is determined by the superadiabaticity of the thermal gradient, rather than by the gradient. When convection is efficient, the convective zone is nearly isentropic so ¹⁸ $L \propto (\nabla - \nabla_a)^{3/2}$ and the atmosphere achieves significant scaling of luminosity with only small changes to ∇ . As a result, the conditions on L cannot generally be satisfied. This means that radiative zones are generically needed as interfaces between convective regions. More formally, we work in the limit of perfectly efficient convection, such that

$$T(p)p^{-\nabla_a} = \text{const.}$$

We also make the assumption that the convective turnover time for any region of interest is much shorter than the time-scale over which thermal quantities change, such that convection may be assumed to enforce an instantaneous adiabatic law.

Now suppose that we perturb a planet by injecting luminosity ΔL somewhere below the radiative-convective boundary. For $\Delta L \ll L_i$, we may solve equation (5.18) by simply reducing the luminosity escaping from deeper regions of the planet. That is, L_i goes unchanged but the luminosity in regions deeper than the injection depth is reduced by ΔL . In the limit of very efficient convection (or large opacity), this adjustment holds until $\Delta L \approx L_i$. For $\Delta L > L_i$ the adjustment still occurs, with the deep luminosity falling to the radiative luminosity at the adiabatic gradient, the minimum needed to maintain convection. The difference is that in this case there is an excess of luminosity reaching the convective-radiative transition and this must be accounted for. At the boundary we must have

$$\nabla_a = \nabla_r = \frac{3\kappa p_t L_i}{64\pi G M \sigma T_t^4}, \quad (5.19)$$

which must remain satisfied when we perturb L_i so

$$\Delta \ln p_t - 4\Delta \ln T_t + \Delta \ln \kappa + \Delta \ln L_i = 0. \quad (5.20)$$

If the transition temperature is similar to the photospheric temperature and if the radius does not change substantially owing to the perturbation $\Delta \ln L = \Delta \ln(L_i + L_e) = 4\Delta \ln T_t$. Because $F_e \gg F_i$ and L_e is fixed

$$4\Delta \ln T_t \approx \frac{\Delta L_i}{L_e} \ll 1.$$

¹⁸ Kippenhahn & Weigert 1990

So we may neglect the change in T_t and find

$$\Delta \ln p_t + \Delta \ln \kappa + \Delta \ln L_i = 0. \quad (5.21)$$

We generally expect that, at fixed temperature, κ rises as p rises. As a result, p_t must fall to satisfy this relation, so either the entropy of the central adiabat must rise or the adiabatic law must be broken somewhere in the planet. The central entropy cannot rise unless either heat is being added at the core or the photosphere is hotter than the core, because heat cannot be forced to move up the temperature gradient. Neither of these are generally the case so the adiabatic law must be broken. As a result the planet must form an interior radiative zone.

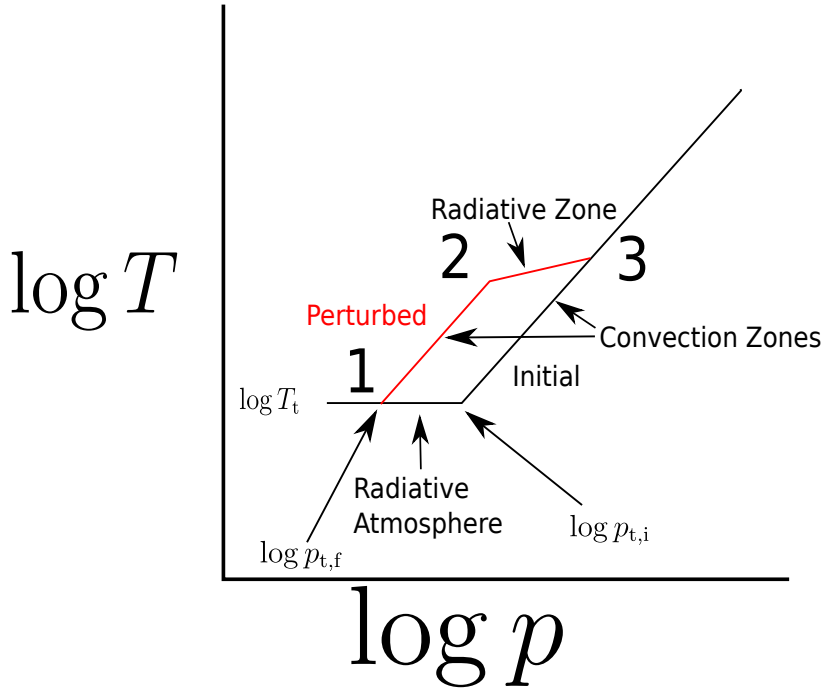


Figure 5.5: Perturbed (red) and unperturbed (black) pressure-temperature profiles.

To characterise these radiative zones, let p_1 be the transition pressure between the surface radiative zone and the new convection zone, p_2 the transition pressure between this zone and the interior radiative zone and p_3 the transition pressure between this zone and the central adiabat. The perturbed and unperturbed pressure-temperature structures are shown in Fig. 5.5. Let T_j , m_j , κ_j and L_j be the corresponding temperature, mass coordinate, opacity and luminosity at each transition. The new convection zone is adiabatic, so

$$\frac{T_1^{1/\nabla_a}}{p_1} = \frac{T_2^{1/\nabla_a}}{p_2}.$$

Assuming that $m \approx M$, the condition (5.19) for transition between radiative

and convective zones gives

$$p_1 \kappa_1 L_1 T_1^{-4} = p_2 \kappa_2 L_2 T_2^{-4} = p_3 \kappa_3 L_3 T_3^{-4}.$$

Finally, recalling that the central adiabat is fixed and that the new adiabat contains a point at the fixed temperature T_t , we find

$$\frac{T_2^{1/\nabla_a}}{p_2} = \frac{T_3^{1/\nabla_a}}{p_3} \left(\frac{p_{t,i}}{p_{t,f}} \right), \quad (5.22)$$

where the subscripts i and f refer to the initial unperturbed and final perturbed system respectively. Equation (5.22) thus expresses the entropy difference between the two adiabats. Note that with these subscript definitions,

$$L_{i,f} \equiv L_1. \quad (5.23)$$

Again with $\kappa \propto T^a p^b$ we may write equations (5.20) – (5.23) as a system of linear equations in the logarithms of temperature and pressure. Solving this system yields

$$\ln \frac{T_1}{T_2} = \frac{\nabla_a}{w} \ln \frac{L_1}{L_2}, \quad (5.24)$$

$$\ln \frac{T_2}{T_3} = \frac{\nabla_a}{w} \ln \frac{L_{i,f} L_2}{L_{i,i} L_3}, \quad (5.25)$$

$$\ln \frac{p_1}{p_2} = \frac{1}{w} \ln \frac{L_1}{L_2}, \quad (5.26)$$

and

$$\ln \frac{p_2}{p_3} = \frac{1}{w} \ln \frac{L_{i,f} L_2}{L_{i,i} L_3} + \frac{1}{1+b} \ln \frac{L_{i,f}}{L_{i,i}}, \quad (5.27)$$

where

$$w \equiv (4-a)\nabla_a - (1+b).$$

The transition temperature $T_1 \equiv T_t$ is known from the unperturbed state so with equations (5.24) and (5.25) we may determine the remaining temperatures. Likewise the unperturbed transition pressure $p_{t,i}$ is known from the unperturbed state. The perturbed transition pressure p_1 is related to the unperturbed by equation (5.21) so, with equations (5.26) and (5.27) we may determine the remaining pressures.

In equilibrium, the luminosities are related by

$$L_1 = L_2 + \int_{m_2}^{m_1} \epsilon(m) dm$$

and

$$L_2 = L_3 + \int_{m_3}^{m_2} \epsilon(m) dm.$$

With these we can compute the luminosity ratios. A consequence of equation (5.26) is that the new convective zone is maintained by heat generation in between p_1 and p_2 , or equivalently between m_1 and m_2 , because this is what allows for $L_1 \neq L_2$.

The minimum luminosity required for convection may be calculated from equation (5.19) as

$$L_{\min} = L_i \frac{\nabla_a}{\nabla_r}.$$

Both sides of this equation are functions of pressure. We generally expect that ∇_r rises quickly towards the interior of the planet as convection becomes more efficient so L_{\min} is a small fraction of L_i . This is actually guaranteed by equation (5.7) so we expect that L_{\min} is suppressed relative to L_i by a power-law in p and may calculate

$$L_3 = \int_0^{m_3} \epsilon(m) dm + L_i \frac{\nabla_a}{\nabla_r(p_{\text{inject}})}, \quad (5.28)$$

where p_{inject} is the pressure inside which minimal luminosity is injected.

5.5 Expansion

The expansion associated with changing the temperature profile of the planet is given by

$$\Delta V = \int_0^M \Delta(\rho^{-1}) dm. \quad (5.29)$$

In the limit where $\Delta R/R$ is small, $\Delta p/p$ is small at fixed m , so

$$\Delta(\rho^{-1}) \approx \left. \frac{\partial T}{\partial \rho} \right|_p \Delta(T^{-1}) \approx \rho^{-1} \frac{\Delta T}{T} \approx \rho^{-1} \Delta \ln T.$$

Substituting this into equation (5.29) we find

$$\Delta V \approx \int_0^M \rho^{-1} \Delta \ln T dm \approx \int_0^R 4\pi r^2 \Delta \ln T dr,$$

where the coordinate r refers to the unheated system. The integration proceeds up to R as an approximation, once more in the limit where $\Delta R/R$ is small. When this is the case and when the majority of the heating occurs near the surface at $r \approx R$ this may be approximated by

$$\Delta R \approx \int_{R-\delta R}^R \Delta \ln T dr. \quad (5.30)$$

Now we may approximate $\Delta \ln T$ as $\ln(T_2/T_1)$. The pressure depth over which this approximation (rather than $\Delta \ln T \approx 0$) is valid is $\Delta \ln p \approx \ln(p_1/p_{t,i})$. This corresponds to a physical depth of $h \ln(p_1/p_{t,i})$, because h is the characteristic scale of the thermal properties of the planet and hence sets the scale of the radiative zone which forms. So we may approximate equation (5.30) in terms of the heating parameters by

$$\Delta R \approx h \ln \frac{p_1}{p_{t,i}} \ln \frac{T_2}{T_1}.$$

With equation (5.21) we find

$$\Delta R = -\frac{h \nabla_a}{(1+b)w} \ln \frac{L_{i,f}}{L_{i,i}} \ln \frac{L_1}{L_2}.$$

For very deep zones, the relevant scale height is that near the base of the zone rather than the top, because the majority of the contribution to the integral comes from this region. This may be taken into account by noting that the scale height at the base of the radiative zone is given by equation (3.19) as

$$h = \frac{k_B T_3}{\mu m_p g}. \quad (5.31)$$

Inserting equation (5.24) and equation (5.25) we have

$$h = \frac{k_B T_1}{\mu m_p g} \left(\frac{L_{i,f}^2}{L_{i,i} L_3} \right)^{-\frac{\nabla_a}{w}}.$$

Making use of $T_1 \approx T_{ph}$, equations (5.5) and (5.10) give us

$$\begin{aligned} h &= \frac{k_B}{\mu m_p g} \left(\frac{L_\star}{4\pi\sigma a_{\text{orbit}}^2} \right)^{1/4} \left(\frac{L_{i,f}^2}{L_{i,i} L_3} \right)^{-\frac{\nabla_a}{w}} \\ &\approx 0.2 R_J \left(\frac{L_\star}{L_\odot} \right)^{\frac{1}{4}} \left(\frac{M_\star}{M_\odot} \right)^{-\frac{1}{6}} \left(\frac{\tau_{\text{orbit}}}{10 \text{d}} \right)^{-\frac{4}{3}} \\ &\quad \times \left(\frac{M}{M_J} \right)^{-1} \left(\frac{R}{R_J} \right)^2 \left(\frac{L_{i,f}^2}{L_{i,i} L_3} \right)^{-\frac{\nabla_a}{w}}, \end{aligned} \quad (5.32)$$

where τ is the orbital period. The expansion is therefore

$$\begin{aligned} \Delta R &\approx \frac{0.2 R_J \nabla_a}{(1+b)w} \left(\frac{L_\star}{L_\odot} \right)^{1/4} \left(\frac{M_\star}{M_\odot} \right)^{-1/6} \left(\frac{\tau_{\text{orbit}}}{10 \text{d}} \right)^{-4/3} \left(\frac{M}{M_J} \right)^{-1} \\ &\quad \times \left(\frac{R}{R_J} \right)^2 \left(\frac{L_{i,f}^2}{L_{i,i} L_3} \right)^{-\frac{\nabla_a}{w}} \ln \frac{L_{i,f}}{L_{i,i}} \ln \frac{L_2}{L_1}. \end{aligned} \quad (5.33)$$

A factor of a few from the luminosity term is therefore sufficient to substantially inflate the planet at short orbital periods.

5.6 *G-Modes*

The existence of internal radiative zones raises the possibility that g-modes may contribute to tidal heating. This is particularly interesting because, if g-mode dissipation is the dominant form of tidal heating ϵ is actually a function of the thermal structure of the planet. That is because g-modes predominantly resonate in radiative zones. What this amounts to is a form of feedback between the thermal and mechanical structures of the planet.

5.6.1 *Dynamical Tide*

In principle there are two sources of dynamical tides, namely gravitational and thermal. We expect that thermal tides do not couple to the g-modes considered here. There are two reasons for this. First, the thermal tide is significant only in the upper layers of the atmosphere where insolation is significant. In particular, the tide damps as ¹⁹ $e^{-\kappa\Sigma}$. The internal radiative zone begins at a comparable column density to the unperturbed radiative-convective transition. Equation (5.13) gives $\kappa_0\Sigma_t \approx 5 \times 10^2$, so the damping is on the order of $\exp(-5 \times 10^2)$, which suffices to make this effect negligible. Secondly, the thermal tide relies on timescale for redistributing heat being large relative to the orbital time. We have shown that the temperature distribution becomes spherical very near the photosphere and well above the convection zone, even for a tidally locked planet. This means that it will not reach even the upper convection zone. As a result we restrict our analysis to gravitational tides.

¹⁹ Arras & Socrates 2010

We take the Cowling approximation, so that the self-gravity of the tidal bulge is neglected ²⁰. We further take displacements to be small enough that the non-linear term in the Navier-Stokes equation may be neglected. Due to their frequencies being small relative to the acoustic frequency, g-modes may be treated them in the anelastic limit in which

²⁰ Savonije & Papaloizou 1983

$$\nabla \cdot (\rho \mathbf{u}) = 0,$$

where ρ is the unperturbed density field and \mathbf{u} is the mode velocity. This treatment may be accomplished done by separating the perturbing tidal potential into a hydrostatic equilibrium tide and a dynamical tide ²¹. The associated radial displacements ξ^{eq} and ξ^{dyn} obey the relations ²²

²¹ Zahn 1975

²² Goodman & Dickson 1998

$$\xi^{\text{eq}} = -\frac{\delta\Phi}{d\Phi/dr} \quad (5.34)$$

and

$$\begin{aligned} \frac{\partial^2}{\partial r^2}(r^2 \xi^{\text{dyn}}) + \frac{\partial}{\partial r} \left(\frac{d \ln \rho}{dr} r^2 \xi^{\text{dyn}} \right) + l(l+1) \left(\frac{N^2}{\omega^2} - 1 \right) \xi^{\text{dyn}} \\ = l(l+1) \xi^{\text{eq}} - \frac{\partial^2}{\partial r^2} (r^2 \xi^{\text{eq}}), \end{aligned} \quad (5.35)$$

where l is the latitudinal quantum number, ω is the frequency, Φ is the unperturbed planetary gravitational potential, $\delta\Phi$ is the perturbing tidal potential due to the star and N is the Brunt-Väisälä frequency, with N^2 positive in the radiative zone and negative in the surrounding convective regions. To analyse this equation we first solve the homogeneous version, with the right hand side set to zero, and then compute the overlap between the resulting modes and the forcing term given by the right-hand side.

5.6.2 Mode Profile

The homogeneous part of equation (5.35) is

$$\frac{\partial^2}{\partial r^2}(r^2 \xi^{\text{dyn}}) + \frac{\partial}{\partial r} \left(\frac{d \ln \rho}{dr} r^2 \xi^{\text{dyn}} \right) + l(l+1) \left(\frac{N^2}{\omega^2} - 1 \right) \xi^{\text{dyn}} = 0.$$

Defining

$$\xi \equiv r^2 \xi^{\text{dyn}}$$

we find

$$\frac{\partial^2 \xi}{\partial r^2} + \frac{\partial}{\partial r} \left(\frac{d \ln \rho}{dr} \xi \right) + \frac{l(l+1)}{r^2} \left(\frac{N^2}{\omega^2} - 1 \right) \xi = 0. \quad (5.36)$$

We now wish to perform a change of variables which will eliminate the first order derivative of ξ . To do this, we note that

$$\frac{\partial^2}{\partial r^2} = \left(\frac{\partial y}{\partial r} \right)^2 \frac{\partial^2}{\partial y^2} + \frac{\partial^2 y}{\partial r^2} \frac{\partial}{\partial y}.$$

This may be written as

$$\frac{\partial^2}{\partial r^2} = \left(\frac{\partial y}{\partial r} \right)^2 \frac{\partial^2}{\partial y^2} + \frac{\partial r}{\partial y} \frac{\partial^2 y}{\partial r^2} \frac{\partial}{\partial r}.$$

Using this, we pick

$$y = \int \rho^{-1} dr,$$

which gives

$$\frac{\partial^2}{\partial r^2} = \rho^{-2} \frac{\partial^2}{\partial y^2} - \frac{d \ln \rho}{dr} \frac{\partial}{\partial r}.$$

With this substitution, equation (5.36) becomes

$$\rho^{-2} \frac{\partial^2 \xi}{\partial y^2} + \frac{d^2 \ln \rho}{dr^2} \xi + \frac{l(l+1)}{r^2} \left(\frac{N^2}{\omega^2} - 1 \right) \xi = 0. \quad (5.37)$$

Qualitatively we expect N to peak near the centre of the radiative zone and fall to zero at the edges. To fit this, we pick a quadratic form in our new coordinate y , such that

$$N^2 = N_0^2 \left(1 - \left(\frac{y - y_0}{\delta y} \right)^2 \right),$$

where r_0 is the radial coordinate of the centre of the radiative zone and $2\delta y$ is the width of the zone in y . This form is useful because it will enable us to case equation (5.37) in the form of a quantum harmonic oscillator, which has known solutions with convenient properties. Defining

$$\chi \equiv \frac{N_0}{\omega}$$

and

$$x \equiv \frac{y - y_0}{\delta y},$$

the differential equation equation (5.37) becomes

$$\frac{1}{\rho^2 \delta y^2} \frac{\partial^2 \xi}{\partial x^2} + \frac{d^2 \ln \rho}{dr^2} \xi + \frac{l(l+1)}{r^2} (\chi^2 - x^2 \chi^2 - 1) \xi = 0.$$

We now define

$$q \equiv 1 - \frac{d^2 \ln \rho}{dr^2} \frac{r^2}{l(l+1)},$$

such that

$$\frac{\rho^2}{\delta y^2} \frac{\partial^2 \xi}{\partial x^2} + \frac{l(l+1)}{r^2} (\chi^2 - x^2 \chi^2 - q) \xi = 0. \quad (5.38)$$

Note that q is positive and large because

$$-r^2 \frac{d^2 \ln \rho}{dr^2} \approx \frac{r^2}{h^2} \gg 1.$$

This follows because ρ has characteristic scale h and because $h \ll r$ except near the core of the planet.

It is now worth noting that the physical width of the zone in r is

$$l_r \approx \rho \delta y.$$

This holds because for a thin zone with $l_r \lesssim h$, ρ does not change too much across it²³. In thick zones there would be deviations from this which

²³ This does not mean that we may neglect derivatives of ρ where they appear explicitly in our equations. Such instances depend on the context in which such derivatives occur. Hence, for instance, we cannot neglect the second derivative of ρ in computing q .

we neglect. Along similar lines we treat q and r as constant over the zone because the former varies with radial scale h and the latter with radial scale r , both of which are of order or larger than l_r .

For convenience we now define

$$\beta \equiv l(l+1) \left(\frac{l_r}{r} \right)^2.$$

Because we treat r as approximately constant over the zone this is constant as well. With this, equation (5.38) becomes

$$\frac{\partial^2 \xi}{\partial x^2} + \beta (\chi^2 - x^2 \chi^2 - q) \xi = 0.$$

This may also be written as

$$(\chi^2 - q) \xi = \left(\chi^2 x^2 - \beta^{-1} \frac{\partial^2}{\partial x^2} \right) \xi$$

which is the same as the equation for a quantum harmonic oscillator with energy $\chi^2 - q$, mass $-\hbar^2 \beta / 2$, and zero-point energy $\chi / \sqrt{\beta}$. Because we have argued that β and q are approximately constant over the radiative zone this identification may be used to compute the eigenvalues and associated eigenfunctions. It follows that the eigenvalues are quantised in the form

$$\chi^2 - q = \frac{2\chi}{\sqrt{\beta}} \left(\frac{1}{2} + n \right), n = 0, 1, 2, \dots$$

The sign of χ does not enter into equation (5.37) so we may take whichever branch of the solutions to this equation that we choose. Taking the positive we see that

$$\chi_n = \frac{1 + 2n + \sqrt{1 + 4(\beta q + n + n^2)}}{2\sqrt{\beta}}, n = 0, 1, 2, \dots$$

These correspond to periods and frequencies of

$$T_n = 2\pi \frac{1 + 2n + \sqrt{1 + 4(\beta q + n + n^2)}}{2N_0 \sqrt{\beta}}, n = 0, 1, 2, \dots$$

and

$$\omega_n = \frac{2N_0 \sqrt{\beta}}{1 + 2n + \sqrt{1 + 4(\beta q + n + n^2)}}, n = 0, 1, 2, \dots \quad (5.39)$$

The radial profiles of the solutions are the product of an exponential with

an Hermite polynomial. For $l = 2$, the dominant tidal mode, these are

$$\begin{aligned} \psi_{n,m}(r, \theta, \phi) \approx & \frac{\sqrt{2\chi_n\sqrt{\beta}}}{\sqrt{2^n n! r^3 \sqrt{\pi}}} e^{-2\chi_n\sqrt{\beta}x^2/2} \\ & \times H_n\left(x\sqrt{2\chi_n\sqrt{\beta}}\right) Y_{2m}(\theta, \phi), \end{aligned}$$

where Y_{lm} are the spherical harmonics, $n \in \{0, 1, 2, \dots\}$ and $m \in \{-2, -1, 0, 1, 2\}$.

The modes are normalised so that

$$\int_{\text{all space}} d^3\mathbf{r} |\psi_{n,m}|^2 = 1,$$

and we take ρ and r as constants throughout the radiative zone to compute this normalisation. This is consistent with approximations we make elsewhere.

5.6.3 Overlap Integral

In order to compute the tidal forcing $F_{n,m}(\omega)$, we must say something about the origin of the tidal potential. There are two potential sources, rotational asynchronisation and orbital eccentricity. In the former, the tidal forcing occurs at a frequency $\omega_{\text{rotation}} - \Omega_{\text{orbit}}$, while in the latter it occurs at a frequency of Ω_{orbit} . In both cases, working in the frame corotating with the planet's orbit,

$$\delta\Phi \propto \frac{GM_{\star}r^2}{a_{\text{orbit}}^3},$$

and further involves a sum of $l = 2$ spherical harmonics. Beyond this the two cases differ significantly because the eccentricity case has $\delta\Phi \propto e$ while the asynchronous case has no such factor. To capture both cases, we write

$$\delta\Phi = \Pi \frac{GM_{\star}r^2}{a_{\text{orbit}}^3} \sum_{m'} Y_{2m'}(\theta, \phi) k_{m'} \cos(\omega t - \phi_{m'}),$$

where $\phi_{m'}$ are phase factors, the factors $k_{m'}$ capture the magnitudes of the various harmonics and sum in quadrature to unity and Π is a dimensionless factor of order unity in the asynchronous case and of order e in the eccentric case. From this form and equation (5.34) we may write the equilibrium tide as

$$\xi^{\text{eq}} = \Pi \frac{M_{\star}r^4}{ma_{\text{orbit}}^3} \sum_{m'} Y_{2m'}(\theta, \phi) k_{m'} \cos(\omega t - \phi_{m'}).$$

The driving term associated with this equilibrium tide is the right-hand side of equation (5.35), given by

$$d(\xi) = l(l+1)\xi^{\text{eq}} - \frac{\partial^2}{\partial r^2}(r^2\xi^{\text{eq}}) = -24\xi^{\text{eq}}.$$

In computing the overlap of this with the eigenmodes of the homogeneous equation, we may treat factors of r as constant, because the radiative zone ought to be thin on the scale of the planetary radius. As a result, the projection is

$$\begin{aligned} \langle \psi_{2,m'} | d \rangle &= -24 \int \psi_{2,m'}(\mathbf{r}) \xi^{\text{eq}}(\mathbf{r}) d^3\mathbf{r} \\ &\approx -24\pi \frac{M_\star r^6}{ma_{\text{orbit}}^3} k_{m'} \int_{-l_r}^{l_r} \psi_{2,m'}(r') dr' \\ &= -24\pi \frac{M_\star r^6 l_r}{ma_{\text{orbit}}^3} k_{m'} \int_{-\infty}^{\infty} \psi_{2,m'}(x) dx \\ &= -24\pi \frac{M_\star r^{9/2} l_r s_n}{ma_{\text{orbit}}^3 \sqrt{2^n n!} \sqrt{\pi}} k_{m'} \int_{-\infty}^{\infty} e^{-s_n^2 x^2 / 2} H_n(s_n x) dx \\ &= -24\pi \frac{M_\star r^{9/2} l_r}{ma_{\text{orbit}}^3 \sqrt{2^n n!} \sqrt{\pi}} k_{m'} \int_{-\infty}^{\infty} e^{-w^2 / 2} H_n(w) dw, \end{aligned}$$

where we have centred the integral on r_0 , the radial coordinate corresponding to y_0 , and defined

$$s_n \equiv \sqrt{2\chi_n} \sqrt{\beta}.$$

We have also extended the integration bounds to infinity to make the computation easier because the exponential suppression in x makes the precise bounds irrelevant. Note that changing variables from r' to x is formally quite complicated, though in the approximation where ρ changes little over the course of the zone it just produces a prefactor of l_r .

The integral may now be evaluated with the generating function of the Hermite polynomials,

$$e^{2wt - t^2} = \sum_{n=0}^{\infty} H_n(w) \frac{t^n}{n!},$$

so

$$\begin{aligned} \int_{-\infty}^{\infty} e^{-w^2/2} H_n(w) dw &= \frac{d^n}{dt^n} \int_{-\infty}^{\infty} e^{2wt-t^2-w^2/2} dw \Big|_{t=0} \\ &= \sqrt{2\pi} \frac{d^n}{dt^n} (e^{t^2}) \Big|_{t=0} \\ &= \frac{n! \sqrt{2\pi}}{2\Gamma(1 + \frac{n}{2})} (1 + (-1)^n). \end{aligned}$$

As a result,

$$\langle \psi_{2,m'} | d \rangle \approx -24\Pi \frac{M_\star r^{9/2} l_r \pi^{1/4}}{ma_{\text{orbit}}^3 \Gamma(1 + \frac{n}{2})} k_{m'} \sqrt{\frac{n!}{2^{n-1}}}, \quad (5.40)$$

for even n and vanishes for odd n . There is complete degeneracy in both the dissipation and oscillation over m' , so we may form a linear combination of spherical harmonics which precisely matches the forcing term. This amounts to summing the right hand side of equation (5.40) in quadrature over m' and taking the square root, which gives

$$\langle \psi_2 | d \rangle \approx 24\Pi \frac{M_\star r^{9/2} l_r \pi^{1/4}}{ma_{\text{orbit}}^3 \Gamma(1 + \frac{n}{2})} \sqrt{\frac{n!}{2^{n-1}}}. \quad (5.41)$$

This expression gives the amplitude of the resonance. From this stage we take it as given that $l = 2$ and drop the label on ψ .

5.6.4 Dissipation

The square of the displacement, which is proportional to the dissipation, has maxima at a distance of order $\pm a$ from the centre of the radiative zone so, even if the dampening were uniform, we would expect the dissipation to be greatest near the edges of the zone. In practice, convective turbulence increases the dissipation just outside the zone and this assertion is even stronger. To evaluate the strength of this effect we turn to various linear dissipation mechanisms. Both radiative and viscous damping are potentially relevant. For each of these we may calculate a quality factor Q , giving the number of undriven cycles required for an e -fold reduction in strength. These combine as

$$Q = \frac{1}{\frac{1}{Q_{\text{rad}}} + \frac{1}{Q_{\text{turb}}}}.$$

We begin with radiative damping at finite opacity. The quality factor of mode n is of order ²⁴

$$Q_n \approx \omega_n \tau_n \approx \frac{3}{4\pi} \left(\frac{\omega_n \lambda_n}{c} \right) \left(\frac{p}{aT^4} \right) (\kappa \rho \lambda_n),$$

²⁴ Press 1986

where c is the speed of light and τ_n , ω_n and λ_n are the lifetime, frequency and wavelength corresponding to mode n . The wavelength is given by

$$\lambda_n \approx \frac{2l_r}{n+1}$$

which just comes from the fact that mode n has $n+1$ nodes over the zone width of $2l_r$. Thus

$$Q_n \approx \frac{3}{4\pi} \left(\frac{p}{aT^4} \right) \frac{4\omega_n \kappa \rho l_r^2}{c(n+1)^2}.$$

Let

$$m_z \equiv 2l_r \rho,$$

an approximate zone mass. We find

$$Q_n \approx \frac{3}{4\pi} \left(\frac{p}{aT^4} \right) \frac{2\omega_n m_z \kappa l_r}{c(n+1)^2}.$$

From equation (5.31) we know that the scale height h is proportional to T , so

$$\left(\frac{h}{r} \right)^4 \left(\frac{p}{aT^4} \right) \approx \frac{p k_B^4}{m_p^4 g^4 r^4 a}.$$

We are interested in regions which are sufficiently shallow so that g is nearly constant and so

$$p \approx \frac{g(M-m)}{4\pi r^2},$$

and

$$\begin{aligned} \left(\frac{h}{r} \right)^4 \left(\frac{p}{aT^4} \right) &\approx \left(\frac{k_B^4}{a m_p^4} \right) \left(\frac{M-m}{4\pi r^6 g^3} \right) \\ &= \left(\frac{k_B^4}{4\pi a G^3 m_p^4} \right) \frac{M-m}{m^3} \approx 4.6 \times 10^5 M_J^2 (M-m) m^{-3} \end{aligned}$$

so that

$$Q_n \approx 1.1 \times 10^5 \left(1 - \frac{m}{M} \right) \mathcal{M}^{-2} \left(\frac{M}{m} \right)^3 \frac{2\omega_n m_z \kappa l_r}{c(n+1)^2} \left(\frac{r}{h} \right)^4. \quad (5.42)$$

The radiative zone is stably stratified so we expect turbulent damping to be limited to the evanescent part of the mode which leaks into the neighbouring convective zones. The Navier-Stokes equation with a simple viscosity term is

$$\frac{\partial \mathbf{v}}{\partial t} + \mathbf{v} \cdot \nabla \mathbf{v} = \mathbf{g} - \frac{\nabla p}{\rho} + \nu \nabla^2 \mathbf{v}.$$

We now neglect the non-linear term because we are interested in understanding the linear growth and decay of modes and expect the absolute

velocities involved to be small. Without the nonlinear term

$$\frac{\partial \mathbf{v}}{\partial t} = \mathbf{g} - \frac{\nabla p}{\rho} + \nu \nabla^2 \mathbf{v}.$$

The balance between gravity and the pressure gradient is what gives us g-modes, so we may write the balance as

$$\frac{\partial \mathbf{v}}{\partial t} = \omega_n \mathbf{v} + \nu \nabla^2 \mathbf{v}.$$

Now let

$$\mathbf{v}' \equiv e^{i\omega_n t} \mathbf{v}$$

so that

$$\frac{\partial \mathbf{v}'}{\partial t} = \nu \nabla^2 \mathbf{v}'.$$

The kinetic energy density

$$K = \frac{1}{2} \mathbf{v}^* \cdot \mathbf{v} = \frac{1}{2} \mathbf{v}'^* \cdot \mathbf{v}',$$

where \mathbf{v}^* is the complex conjugate of \mathbf{v} , and evolves as

$$\partial_t K = \frac{1}{2} \nu \mathbf{v}'^* \cdot \nabla^2 \mathbf{v}' + \frac{1}{2} \nu \mathbf{v}' \cdot \nabla^{\dagger 2} \mathbf{v}'^*,$$

where ∇^\dagger is the adjunct gradient operator. When the spatial derivatives are greatest in the radial direction the Laplacian just produces a factor of $(2\pi/\lambda_n)^2$ so

$$\partial_t K = \left(\frac{2\pi}{\lambda_n} \right)^2 \nu K.$$

Integrating this equation over the whole planet we find

$$\begin{aligned} \frac{d}{dt} \int_0^M K dm &= \int_0^M \frac{\partial K}{\partial t} dm \\ &= \int_0^M \left(\frac{2\pi}{\lambda_n} \right)^2 \nu K dm \\ &= \left(\frac{2\pi}{\lambda_n} \right)^2 \int_0^M \nu K dm. \end{aligned}$$

The viscosity ν is only significant in the convection zones on either side of the radiative zone, where turbulent viscosity dominates. The kinetic energy density K is only significant inside the radiative zone and within a few wavelengths of the zone edges on either side. The damping integral is dominated by the region in which neither is small, so

$$\frac{d}{dt} \int_0^M K dm \approx \left(\frac{2\pi}{\lambda_n} \right)^2 \frac{\lambda_n}{l_r + \lambda_n} \nu \int_{\text{Radiative Zone}} K dm,$$

where ν is evaluated in the convecting regions and $2(l_r + \lambda_n)$ is roughly the radial extent of the region where the kinetic energy density is significant.

Similarly

$$\int_{\text{Radiative Zone}} K dm \approx m_z K,$$

where K on the right hand side is the average kinetic energy density in the zone. Then

$$\frac{d}{dt}(m_z K) \approx \left(\frac{2\pi}{\lambda_n}\right)^2 \frac{\lambda_n}{l_r} \nu m_z K.$$

Because m_z is constant we find that

$$\frac{d \ln K}{dt} \approx \left(\frac{2\pi}{\lambda_n}\right)^2 \frac{\lambda_n}{l_r} \nu$$

and the damping timescale is

$$\tau_{\text{turb}} = \frac{\lambda_n l_r}{4\pi^2 \nu}$$

with related quality factor

$$Q_n \approx \omega_n \tau_{\text{turb}} = \frac{\omega_n \lambda_n l_r}{4\pi^2 \nu}.$$

The turbulent diffusivity is of order $\nu_c h$ when the convective turnover is on a timescale shorter than the forcing frequency ω . It is ω rather than ω_n that matters here because the oscillation physically takes place at the driving frequency, not the mode period. The relevant turbulent frequency for motion over length-scale l_t is

$$\omega_{\text{turb}}(l_t) = \frac{v_c(l_t)}{l_t}.$$

Taking v_c to be given by a Kolmogorov spectrum, we find

$$\omega_{\text{turb}}(l_t) = \frac{v_c(h)}{h} \left(\frac{l_t}{h}\right)^{-2/3}.$$

It follows that the relevant diffusive motions are on a scale

$$\frac{l_t}{h} = \min \left[1, \left(\frac{v_c(h)}{h\omega} \right)^{3/2} \right]$$

and corresponding diffusivity is

$$\nu = v_c h \min \left[1, \left(\frac{v_c(h)}{h\omega} \right)^2 \right].$$

This is just the result of Goldreich & Keeley (1977) and yields a quality

factor

$$Q_n \approx \frac{\omega_n \lambda_n l_r}{4\pi^2 v_c h} \max \left[1, \left(\frac{v_c(h)}{h\omega} \right)^{-2} \right].$$

High-frequency driving leads to a high quality factor and Q_n scales as ω_n^2 because $\lambda_n \propto \omega_n$. This is a weaker scaling than the radiative Q , which goes as $\omega_n^3 \propto (n+1)^{-3}$. Thus at large n the convective mechanism dominates.

We are often interested in the lowest n because this mode is the least suppressed by overlap factors. The convective flux of interest is generally F_i , which equation (5.12) shows is on the order of $10^{-5} F_e$. The external flux is typically about $10^{-2} F_\odot$, so the relevant convective flux is on the order of $5 \times 10^3 \text{ erg cm}^{-2} \text{ s}^{-1}$. For a density of $10^{-1} \text{ g cm}^{-3}$ the convection speed is then

$$v_c \approx \left(\frac{F_i}{\rho} \right)^{1/3} \approx 30 \text{ cm s}^{-1}.$$

So for a scale height of 10^9 cm , $v_c/h \approx 3 \times 10^{-8} \text{ Hz}$. We show later that we are interested in frequencies on the order of 10^{-6} Hz . This means that the factor $[h\omega/v_c(h)]^2$ accounting for the eddy time is of order 10^5 , so the convective quality factor is $Q_1 \approx 300$. By comparison, the fiducial radiative quality factor with the same assumptions is $Q_1 \approx 1$. Thus we expect radiative damping to dominate by a reasonable margin unless the fluxes involved are many orders of magnitude larger or the frequencies are several orders of magnitude smaller.

5.6.5 Boundaries

We have shown that, when g-modes dominate the dissipation, ε is significant primarily near the edges of the radiative zone. It is also straightforward to show that the dissipation is spherically symmetric because the squared mode profiles are even. So ε is an even function, the integral of which is dominated by the regions just outside the zone boundaries. Suppose that the total luminosity produced by tides is L_t and that a fraction f of this is produced inside the radiative zone. In steady-state

$$L_2 - L_3 = f L_t$$

and

$$L_1 - L_2 = \frac{1}{2}(1-f)L_t.$$

Using equation (5.28) we find

$$L_3 = L_i \frac{\nabla_a}{\nabla_r(p_{\text{inject}})} + \frac{1}{2}(1-f)L_t.$$

If the heating is large relative to L_i and f is small then we expect

$$L_3 \approx \frac{1}{2}(1-f)L_t \quad (5.43)$$

so

$$\frac{L_1}{L_2} \approx 2 \quad (5.44)$$

and

$$\frac{L_2}{L_3} \approx 1. \quad (5.45)$$

Using equations (5.24) through (5.27) we find

$$\begin{aligned} \ln \frac{T_1}{T_2} &= \frac{\nabla_a}{w} \ln 2, \\ \ln \frac{T_2}{T_3} &= \frac{\nabla_a}{w} \ln \frac{L_t}{L_{i,i}}, \\ \ln \frac{p_1}{p_2} &= \frac{1}{w} \ln 2 \end{aligned}$$

and

$$\ln \frac{p_2}{p_3} = \left(\frac{1}{w} + \frac{1}{1+b} \right) \ln \frac{L_t}{L_{i,i}}.$$

With equations (5.43) and (5.44) equation (5.33) yields

$$\begin{aligned} \frac{\Delta R}{R_j} &\approx -0.1 \frac{\nabla_a}{(1+b)(w)} \left(\frac{L_\star}{L_\odot} \right)^{1/4} \left(\frac{M_\star}{M_\odot} \right)^{-1/6} \left(\frac{\tau_{\text{orbit}}}{10\text{d}} \right)^{-4/3} \\ &\times \left(\frac{M}{M_j} \right)^{-1} \left(\frac{R}{R_j} \right)^2 \left(\frac{2L_{i,f}}{L_{i,i}} \right)^{\frac{-\nabla_a}{w}} \ln \frac{L_{i,f}}{L_{i,i}}. \end{aligned} \quad (5.46)$$

Recall from equation (5.39) that the resonant frequencies are

$$\begin{aligned} \omega_n &= \frac{2N_0\sqrt{\beta}}{1+2n+\sqrt{1+4(\beta q+n+n^2)}} \\ &= \frac{2N_0\sqrt{\beta}}{(1+2n)\left(1+\sqrt{1+\frac{4\beta q}{(1+2n)^2}}\right)} \\ &= \frac{2N_0\sqrt{\beta}}{(1+2n)\left(1+\sqrt{1+\frac{4(l_r/h)^2}{(1+2n)^2}}\right)}. \end{aligned}$$

The right hand side has two characteristic regimes, one in which l_r/h is large and one in which it is small or of order unity. In the former case, $\omega_n \propto h$, while in the latter $\omega_n \propto l_r$. Both h and l_r increase with p_3/p_2 , so the resonant frequency goes up as the zone width increases. This means

that the resonance shifts up in frequency as the luminosity increases. That is,

$$\frac{d\omega_0}{dL_\tau} > 0.$$

So an increase in luminosity tends to tune the system towards resonance if it is being driven above resonance and pushes it away from resonance otherwise. The net result is that there is thermomechanical feedback which tends to bias systems towards resonance, particularly when their resonant frequency is below the driving frequency.

5.6.6 Power Production

Each mode may be treated as a separate damped and forced harmonic oscillator. Let ξ_n be the amplitude for mode n . Then

$$\omega_n^2 \xi_n + \frac{\omega_n}{Q_n} \dot{\xi}_n + \ddot{\xi}_n = \omega^2 \langle \psi | d \rangle e^{i\omega t}.$$

We may solve this differential equation in steady-state and fix the reference phase to find

$$\xi_n = \frac{\omega^2 \langle \psi | d \rangle e^{i\omega t}}{\omega_n^2 - \omega^2 + i\omega_n \omega Q_n^{-1}}.$$

The power dissipated is

$$\begin{aligned} \mathcal{P}_n &= \rho \Re \left(\dot{\xi}_n^* e^{i\omega t} \omega^2 \langle \psi | d \rangle \right) \\ &= \rho \Re \left(-i \dot{\xi}_n^* e^{i\omega t} \right) \omega^3 \langle \psi | d \rangle \\ &= \rho \Im \left(\xi_n^* e^{i\omega t} \right) \omega^3 \langle \psi | d \rangle \\ &= \rho \Im \left(\frac{1}{\omega_n^2 - \omega^2 - i\omega_n \omega Q_n^{-1}} \right) \omega^5 |\langle \psi | d \rangle|^2 \\ &= \frac{\omega_n \omega Q_n^{-1}}{(\omega_n^2 - \omega^2)^2 + (\omega_n \omega Q_n^{-1})^2} \rho \omega^5 |\langle \psi | d \rangle|^2. \end{aligned}$$

With equation (5.41) this becomes

$$\begin{aligned} \mathcal{P}_n &= \frac{\omega_n \omega^6 Q_n^{-1}}{(\omega_n^2 - \omega^2)^2 + (\omega_n \omega Q_n^{-1})^2} q \\ &= \frac{\omega^3}{Q_n \omega_n^{-1} \omega \left(\frac{\omega_n^2}{\omega^2} - 1 \right)^2 + \omega^{-1} \omega_n Q_n^{-1}} q, \end{aligned}$$

where

$$q \equiv 576 \Pi^2 \rho \frac{M_\star^2 r^9 l_r^2 \pi^{1/2}}{m^2 a_{\text{orbit}}^6} \left(\frac{n!}{2^{n-1} \Gamma(1 + \frac{n}{2})^2} \right).$$

If the tides are driven by the rotational energy of the planet then ω is the planet's rotation frequency. In many cases however the tides are driven by either orbital eccentricity, in which case the forcing frequency

is just the orbital frequency ²⁵. In this more generally interesting case, the driving frequency is

²⁵ Arras & Socrates 2010

$$\omega = \Omega_{\text{orbit}} = \frac{2\pi}{\tau_{\text{orbit}}} \approx 7 \times 10^{-6} \text{ Hz} \left(\frac{\tau_{\text{orbit}}}{10 \text{ d}} \right)^{-1}.$$

To compare, the highest resonant frequency occurs when $n = 0$ and is

$$\omega_0 = \frac{2N_0\sqrt{\beta}}{1 + \sqrt{1 + 4\beta q}},$$

equation (5.39). Because $\beta q \approx 1$,

$$\omega_0 \approx \frac{N_0\sqrt{\beta}}{1 + \sqrt{5}} \approx \frac{N_0 l_r}{R},$$

for $l = 2$. Now N_0 is the peak Brunt-Väisälä frequency in the radiative zone where the temperature gradient is substantially subadiabatic, so

$$N_0^2 \approx \nabla_a \frac{g}{h}.$$

This gives

$$\omega_0 \approx \frac{l_r \sqrt{\nabla_a}}{R} \sqrt{\frac{g}{h}}.$$

Now $l_r \approx h \ln(p_1/p_{t,i})$ so

$$\begin{aligned} \omega_0 &\approx \sqrt{\nabla_a} \ln \frac{p_1}{p_{t,i}} \sqrt{\frac{gh}{R^2}} \\ &= \frac{1}{\sqrt{Y}} \left(\frac{c_s}{R} \right) \ln \frac{p_1}{p_{t,i}} \\ &\approx 2 \times 10^{-5} \text{ Hz} \left(\frac{T}{1 \times 10^3 \text{ K}} \right)^{1/2} \left(\frac{R}{R_J} \right)^{-1} \ln \frac{p_1}{p_{t,i}}. \end{aligned}$$

This is quite close to the orbital frequency so we expect that resonances are not uncommon. Note also that it is somewhat greater than the orbital frequency, so there will generally be modes with frequencies lower than the orbital frequency which are pulled upward towards it by thermomechanical feedback.

The precise shape and spacing of the resonances depends on our ansatz for the Brunt-Väisälä frequency in the radiative zone and so it is not useful to make predictions which depend on our chosen form. If we instead average over resonances, we note that the forcing integral falls exponentially in n while the resonances fall off as a power law in n so that the $n = 0$ resonance always dominates on average. Individual systems far from the $n = 0$ resonance may exhibit significant dissipation by virtue of sitting directly on a higher resonance but we expect this to be rare. So we

assume that ω and ω_n are of the same order and write the net power

$$\begin{aligned}\mathcal{P} &= \sum_i \mathcal{P}_i \\ &\approx \mathcal{P}_0 \\ &\approx 2 \times 10^3 Q_0^{-1} \Pi^2 \rho \frac{\Omega_{\text{orbit}}^3 M_{\star}^2 r^9 l_r^2}{m^2 a_{\text{orbit}}^6} \left(\frac{\omega_0}{\Omega_{\text{orbit}}} \right).\end{aligned}$$

This may be converted to a flux as

$$F_t = \frac{\mathcal{P}}{4\pi r^2} \approx 2 \times 10^2 Q_0^{-1} \Pi^2 \rho \frac{\Omega_{\text{orbit}}^3 M_{\star}^2 r^7 l_r^2}{m^2 a_{\text{orbit}}^6} \left(\frac{\omega_0}{\Omega_{\text{orbit}}} \right).$$

5.7 Equilibrium Radius

To first order, suppose that $l_r \approx h$. The tidal flux is then given by

$$F_t \approx 2 \times 10^2 Q_0^{-1} \Pi^2 \rho \frac{\Omega_{\text{orbit}}^3 M_{\star}^2 r^7 h^2}{m^2 a_{\text{orbit}}^6} \left(\frac{\omega_0}{\Omega_{\text{orbit}}} \right).$$

Inserting equation (5.42) yields

$$F_t \approx 2 \times 10^{-3} \Pi^2 \rho \frac{\Omega_{\text{orbit}}^3 m M^2 r^3 h^5 M_{\star}^2 c}{2\omega_0 m_z \kappa M^3 a_{\text{orbit}}^6} \left(\frac{\omega_0}{\Omega_{\text{orbit}}} \right) \left(1 - \frac{m}{M} \right)^{-1}.$$

If the radiative zone is shallow but dominates the mass above its base then $m \approx M$. In addition,

$$M - m \approx 4\pi r^2 \rho l_r \approx 4\pi r^2 \rho h$$

so

$$\begin{aligned}F_t &\approx 2 \times 10^{-3} \Pi^2 \rho \frac{r^3 h^5 \Omega_{\text{orbit}}^2 M \pi^{1/2} c}{8\pi r^2 \rho^2 h^2 \kappa a_{\text{orbit}}^6} \left(\frac{M_{\star}}{M_J} \right)^2 \\ &\approx 2 \times 10^3 \Pi^2 \rho \frac{r h^5 \Omega_{\text{orbit}}^2 M c}{8\pi (\rho h)^2 \kappa a_{\text{orbit}}^6} \left(\frac{M_{\star}}{M_{\odot}} \right)^2.\end{aligned}$$

Noting that

$$\Sigma_t \approx h\rho$$

we find

$$F_t \approx 8 \times 10^1 \Pi^2 \frac{r h^4 \Omega_{\text{orbit}}^2 M c}{\Sigma_t \kappa a_{\text{orbit}}^6} \left(\frac{M_{\star}}{M_{\odot}} \right)^2.$$

Recalling equation (5.13) and neglecting the logarithmic correction to Σ_t owing to the motion of the zone boundary we write

$$F_t \approx 5 \times 10^{-5} F_\odot \Pi^2 \left(\frac{\tau_{\text{orbit}}}{10 \text{ d}} \right)^{-\frac{31}{6}} \left(\frac{M_\star}{M_\odot} \right)^{\frac{5}{12}} \left(\frac{R_0}{R_j} \right) \\ \times \mathcal{R}^{-2} \mathcal{M}^{8/3} \left(\frac{L_\star}{L_\odot} \right)^{-\frac{5}{8}} \psi^{\frac{5}{2}} \left(\frac{\kappa}{\kappa_0} \right)^{-1} \left(\frac{h}{r} \right)^4. \quad (5.47)$$

With the fiducial values and $h \approx 0.2r$ this flux produces an expansion at a rate

$$\frac{dR}{dt} \approx \frac{F_t}{\rho c_p T} \approx \frac{F}{p_t} \approx 3 \times 10^{-5} \text{ cm s}^{-1} \Pi^2,$$

which is sufficient to produce expansion of order R_j over million-year timescales.

As discussed in section 5.5 the expansion eventually increases the escaping flux to match the generated flux, so the expansion does not continue forever. The relevant dimensionless parameter for this equilibrium is the ratio F_t to $F_{i,i}$, which is the unperturbed F_i . Recall from equation (5.12) that

$$F_i \approx 5 \times 10^{-4} F_\odot \mathcal{M}^{5/3} \left(\frac{L_\star}{L_\odot} \right)^{-5/8} \left(\frac{a_{\text{orbit}}}{R_\odot} \right)^{5/4} \left(\frac{\kappa}{\kappa_0} \right)^{-1} \frac{\psi^{5/2}}{\mathcal{R}^3}.$$

Inserting equation (5.11) yields

$$F_i \approx 1.6 \times 10^{-4} F_\odot \mathcal{M}^{5/3} \left(\frac{L_\star}{L_\odot} \right)^{3/8} \left(\frac{a_{\text{orbit}}}{R_\odot} \right)^{-3/4} \left(\frac{\kappa}{\kappa_0} \right)^{-1} \frac{\psi^{5/2}}{\mathcal{R}^3} \\ \approx 3 \times 10^{-6} F_\odot \mathcal{M}^{5/3} \left(\frac{L_\star}{L_\odot} \right)^{3/8} \left(\frac{\tau_{\text{orbit}}}{10 \text{ d}} \right)^{-1/2} \\ \times \left(\frac{M_\star}{M_\odot} \right)^{-1/4} \left(\frac{\kappa}{\kappa_0} \right)^{-1} \frac{\psi^{5/2}}{\mathcal{R}^3}.$$

Thus

$$\frac{2F_t}{F_{i,i}} \approx 3 \times 10^7 \Pi^2 \mathcal{M} \mathcal{R}^{-2} \left(\frac{L_\star}{L_\odot} \right)^{-1} \left(\frac{R_0}{R_j} \right) \\ \times \left(\frac{\tau_{\text{orbit}}}{10 \text{ d}} \right)^{-14/3} \left(\frac{M_\star}{M_\odot} \right)^{2/3} \left(\frac{h}{R} \right)^4.$$

Inserting equation (5.32) we get

$$\frac{2F_t}{F_{i,i}} \approx 5 \times 10^4 \Pi^2 \mathcal{M}^{-3} \mathcal{R}^2 \left(\frac{R_0}{R_j} \right)^5 \left(\frac{\tau_{\text{orbit}}}{10 \text{ d}} \right)^{-10} \left(\frac{L_{i,f}^2}{L_{i,i} L_3} \right)^{\frac{-7v_a}{w}}.$$

If the expansion is small then the luminosity ratios may be replaced by flux ratios. If tidal heating is significant, the perturbed flux escaping from the

interior of the planet $F_{i,f} \approx F_t$, so

$$\frac{2F_t}{F_{i,i}} \approx 5 \times 10^4 \Pi^2 \mathcal{M}^{-3} \mathcal{R}^2 \left(\frac{R_0}{R_j} \right)^5 \left(\frac{\tau_{\text{orbit}}}{10 \text{ d}} \right)^{-10} \left(\frac{F_{i,f}^2}{F_{i,i} F_3} \right)^{\frac{-7\nabla_a}{w}}.$$

Using equations (5.44) and (5.45) we find

$$\frac{2F_t}{F_{i,i}} \approx 5 \times 10^4 \Pi^2 \mathcal{M}^{-3} \mathcal{R}^2 \left(\frac{R_0}{R_j} \right)^5 \left(\frac{\tau_{\text{orbit}}}{10 \text{ d}} \right)^{-10} \left(\frac{2F_{i,t}}{F_{i,i}} \right)^{\frac{-7\nabla_a}{w}}. \quad (5.48)$$

Note that R and \mathcal{R} must be the equilibrium radii here, not pre-expansion radii. Note that the absolute magnitude of the opacity does not enter our final expression. This cancellation is due to the assumption of efficient convection.

The quantity

$$f \equiv -\frac{7\nabla_a}{w}$$

is of key importance to the nature of the solution. If $f < 1$ then the solution is stable, meaning that a system initially perturbed away from this equilibrium solution returns to it over time. What this means physically is that an increase in the generated flux increases the temperature at the base of the radiative zone enough that the flux which escapes increases by more, leading to a negative feedback loop. If $f > 1$ then the solution is unstable, meaning that an increase in the generated flux increases the temperature in the radiative zone by less than what is required to allow that additional flux to escape, leading to a positive feedback loop. If a system has $f > 1$ then either the initial perturbation has the radiative zone deep enough that the runaway process keeps increasing the flux until some of our assumptions break down or the initial perturbation has the radiative zone shallow enough that the runaway process prevents it from migrating inward causing it to stay where it initially forms. If the prefactor on the right side of equation (5.48) exceeds unity then the unstable branch is always the relevant one because the initial perturbation must yield a ratio of at least unity in order to cause a radiative zone to form. If the prefactor is less than one then any radiative zone formed simply stays where the initial perturbation produces it.

Despite the uncertainties in the precise numbers involved, our results are fairly robust because the right-hand side of equation (5.48) scales as $\tau_{\text{orbit}}^{-10}$, and this scaling only becomes stronger once f is taken into account. For orbital periods shorter than of about 10 d, with some uncertainty, the flux generated may exceed the flux escaping from the centre of the planet.

When the tidal flux dominates the expansion is given by equation (5.46) and may be approximated by

$$\frac{\Delta R}{R_J} \approx 0.1 \frac{\nabla_a}{(1+b)(w)} \left(\frac{L_\star}{L_\odot} \right)^{1/4} \left(\frac{M_\star}{M_\odot} \right)^{-1/6} \left(\frac{\tau_{\text{orbit}}}{10\text{d}} \right)^{-4/3} \\ \times \left(\frac{M}{M_J} \right)^{-1} \left(\frac{R}{R_J} \right)^2 \left(\frac{2F_{i,f}}{F_{i,i}} \right)^{\frac{-\nabla_a}{w}} \ln \frac{F_{i,f}}{F_{i,i}}.$$

Neglecting the logarithmic dependence, this may be combined with equation (5.48) to give

$$\frac{\Delta R}{R_J} \approx 0.1 \frac{\nabla_a}{(1+b)(w)} \left(\frac{L_\star}{L_\odot} \right)^{1/4} \left(\frac{M_\star}{M_\odot} \right)^{-1/6} \left(\frac{\tau_{\text{orbit}}}{10\text{d}} \right)^{-\left(\frac{4}{3} + \frac{10f}{7(1-f)}\right)} \\ \times \left(\frac{M}{M_J} \right)^{-1} \left(\frac{R}{R_J} \right)^2 \left(5 \times 10^4 \Pi^2 \mathcal{M}^{-3} \mathcal{R}^2 \left(\frac{R_0}{R_J} \right)^5 \right)^{\frac{f}{7(1-f)}}.$$

Even though the dependence on the flux ratio is small, the ratio itself can be quite large, particularly at smaller periods. Many cases, such as $a = 0, b = 2$ or $a = 1, b = 1$, have $f > 1$ and so orbital periods of order $30 \text{ d} \Pi^{1/5}$ suffice to cause expansion of order R_0 . It is difficult to say more because many of our approximations break down at this point. If $f < 1$, as can be achieved for example with $a = 4, b = 2$, $\Delta R/R \propto \tau_{\text{orbit}}^{-64/3}$, orbital periods of order $20 \text{ d} \Pi^{3/16}$ suffice to produce unit expansion. This is consistent with most of the known cases of highly inflated Jupiter-mass planets, assuming $\Pi \approx e \approx 0.1$. For low-mass planets, the lower surface gravity makes larger expansion more feasible. This has been recently observed ²⁶. Stronger claims are difficult to make analytically because the dependence of the flux ratio on the specifics of the opacity are quite severe and the detailed compositions of the atmospheres of exoplanets at intermediate depths remain largely unknown. Precision studies of this thermomechanical feedback will likely require numerical tools in all but the simplest cases.

At sufficiently low masses, large flux ratios become impossible to attain given the factor of \mathcal{M}^{-3} in equation (5.48). At this point further expansion is impossible. Likewise at large enough radii the central adiabat disappears so that much of this analysis becomes invalid. We do not expect this to be a limiting factor, however. At short periods Roche lobe overflow becomes a substantial barrier. Substantial changes in the opacity may also occur, particularly if the Kramer regime becomes relevant, and this may invalidate much of the analysis too. In addition at large radii the neglected factors of R in converting from luminosities to fluxes become relevant and these act to limit the expansion.

²⁶ Bakos et al. 2016

5.8 Energetic Timescales

If the tides are eccentricity-driven, it is important to consider the timescale over which the orbit circularises. It suffices to the level of accuracy of interest to note that the energy which may be extracted from an orbit of eccentricity $e < 1$ is of order $e^2 v_{\text{orbit}}^2 M$. The circularisation timescale is therefore

$$\tau_{\text{circ}} \approx \frac{e^2 v_{\text{orbit}}^2 M}{\mathcal{P}} \approx \left(\frac{\tau_{\text{orbit}}}{10\text{d}} \right)^{5/2} 2 \times 10^{12} \text{ yr},$$

where we have taken $\Pi \approx e$ and used our fiducial values for all parameters other than h/r , which we have taken to be 0.2. From this it is clear that most systems of interest can be eccentricity-driven for billion-year timescales, even if they require shorter periods than the fiducial.

If the tides are driven by the planet's rotation they generally have many orders of magnitude less energy to draw from, and so are not sustained on the timescales of interest. They may still produce bloating, but not for long enough to be easily observable.

5.9 Comparison

For comparison with other mechanisms it is useful to compute the Love number associated with these g-modes. The Love number is defined in terms of the power and perturbing tidal potential as

$$\mathfrak{I}[k_l^m(\omega)] = \frac{8\pi G \mathcal{P}}{(2l+1)r|\delta\Phi|^2\omega}$$

²⁷. Summing in quadrature over all m and using $l = 2$ and equation (5.47) we find

²⁷ Ogilvie 2014

$$\begin{aligned} \mathfrak{I}(k) &\approx 3 \times 10^{-6} \left(\frac{\tau_{\text{orbit}}}{10\text{d}} \right)^{-17/6} \left(\frac{M_{\star}}{M_{\odot}} \right)^{-11/12} \\ &\times \mathcal{R}^{-3} \mathcal{M}^{8/3} \left(\frac{L_{\star}}{L_{\odot}} \right)^{-5/8} \psi^{5/2} \left(\frac{\kappa}{\kappa_0} \right)^{-1} \left(\frac{h}{0.2r} \right)^4. \end{aligned}$$

For comparison, inertial waves result in a frequency-averaged value of

$$\begin{aligned} \mathfrak{I}(k) &\approx 5 \frac{R^3 \Omega^2}{GM} \left(\frac{R_c}{R} \right)^5 \\ &\approx 8 \times 10^{-9} \left(\frac{M}{M_J} \right)^{-1} \left(\frac{R}{R_J} \right)^3 \left(\frac{\tau_{\text{orbit}}}{10\text{d}} \right)^{-2} \left(\frac{R_c}{0.1R} \right)^5 \end{aligned}$$

²⁸, where R_c is the core radius. Likewise viscoelastic dissipation in a solid core potentially yields $\mathfrak{I}(k) \approx 10^{-6}$, scaling with the elastic properties of the core ²⁹ and once more averaging over frequency. These mechanisms

²⁸ Ogilvie 2013

²⁹ Remus et al. 2012; Guenel et al. 2014

are therefore of comparable order, depending on precisely which fiducial value is chosen. The reason the g-mode mechanism inflates planets more readily despite having comparable or somewhat less power dissipation is that it heats primarily near the surface where the radius is more easily perturbed.

5.10 *Discussion and Outlook*

We have characterised the response of heavily insulated Jupiter-like planets to tidal heating for a wide range of tidal heating models. A necessary condition for significant bloating of these planets is deep heating. We find that tidal heating, either directly through tide–core interactions or indirectly through resonance-sensitive migration of radiative zones induced by g-modes, is of the right order of magnitude to induce the observed bloating if it is sufficiently deep. We have further shown that nearly every tidal heating model results in deep heating so long as the atmosphere is sufficiently irradiated. This explains the observation of substantially bloated hot Jupiters with a physically reasonable orbital period cutoff for such effects. The migration of interior radiative zones provides a natural explanation for the matching of tidal frequency with orbital frequency despite the observed wide range of orbital frequencies of hot Jupiters.

This entire analysis hinges on there being a luminosity perturbation to start. This luminosity then produces a self-sustaining interior radiative zone which dissipates substantially more heat. The initial perturbation may come from non-linear instabilities and so may provide an indirect probe of these effects. It may also come from planetary migration. If a planet migrates inward and if opacity falls as a result, the incident flux can temporarily force the creation of a radiative zone while the convection zone adjusts to the reduced flux it must carry. The g-mode hysteresis described in this paper may then prevent the zone from disappearing, even if its location shifts to better match resonance. Inflated planets may therefore carry a record of their migration histories.

Finally, the thermomechanical feedback mechanism we propose highlights the importance of considering dynamical effects across many timescales. Feedback is possible both from short timescales to long, as in tidal heating, and from long timescales to short, as in the dynamical tuning of g-modes. By their very nature couplings across so many scales are difficult to track down and so there may be many more which have yet to be discovered.

6 *Stellar Photospheric Abundances as a Probe of Disks and Planets*

And why that cerulean color? The blue comes partly from the sea, partly from the sky... We can explain the wan blueness of this little world because we know it well... the only home we've ever known.

Carl Sagan

Abstract

The composition of planets varies wildly. This is thought to be a result of chemical processing in protoplanetary disks. Despite significant advances, observing the chemistry of these and other circumstellar disks remains a challenge. We present a new probe of disk chemistry, appropriate whenever the central star accretes from the disk. Our theoretical framework (CAM) relates the photospheric composition of the central star to its bulk composition and the chemistry of the accreting material. This allows the abundance pattern of the circumstellar material to be calculated from measured stellar abundances, photospheric temperatures and rotation rates. Our method especially useful in B to mid-F type stars, which have radiative envelopes and hence less bulk-photosphere mixing. We apply it to several such stars, including ones hosting protoplanetary disk, debris disks, and even evaporating planets. We also discuss a potential explanation for the λ Boö phenomenon which arises naturally from this analysis.

6.1 Introduction

Accretion onto a star can have many origins. It may come from a protoplanetary disk, in which case its chemistry may be influenced by the formation of young planets. It may come from a debris disk or an evaporating planet, in which case its chemistry is almost entirely dictated by the aftermath of planetary formation and evolution. It may even come from the interstellar medium or earlier ejecta from the star itself. In each of these cases the elemental composition of the accreting material is a tracer of interesting chemical processes occurring around the star. Unfortunately this is difficult to investigate directly, particularly for solids¹, elements of low abundance, or elements whose major carrier species do not have easily observable energy transitions.

λ Boötis objects provide a classic example of accretion-contaminated stars. These are early-type² stars with photospheres that are depleted in refractory elements³ by a factor of up to a few hundred⁴. The depletion specifically in refractory elements is crucial to this phenomenon⁵ and suggests that the λ Boö anomaly occurs because the star preferentially accretes gas over dust^{6,7}. In particular many such stars, with varying levels of depletion, are well-explained by one protoplanetary disk mechanism which excludes dust from the inner disk before it gets close enough to sublimate and accrete⁸. Many if not all λ Boö stars are, then, lighthouses of ongoing, recent, or extensive accretion of material with a gas-to-dust ratio different from the canonical⁹ $\Delta_{g/d} = 100$. While λ Boö stars are of interest to us, we consider more generally any main-sequence star accreting from a circumstellar material reservoir, including protoplanetary and debris disk hosts as well as stars with evaporating or disrupted planets.

We present the Contamination by Accretion Method¹⁰, which provides a theoretical means for relating the photospheric composition of an accreting star to the composition of circumstellar material¹¹. This method incorporates analytic descriptions of the main mixing mechanisms in stars¹², including rotational, shear, thermohaline, and convective mixing as well as molecular diffusion. We neglect gravitational settling because this is important primarily for white dwarf systems which we do not consider here (Paquette et al., 1986; Koester, 2009). The key observable we predict is the stellar photospheric composition, $(X/H)_{\text{obs}}$. This is a mixture of the stellar bulk composition, which we assume is a known reference value such as solar¹³, and the accreted material. The origin of the accreting material does not matter for our purposes, though of particular interest are systems

¹ This is because solid grains tend to have smaller radiative cross-sections than the equivalent amount of gaseous material.

² mid-F to B

³ These are those with a condensation temperature $T_c > 300$ K, constituting inter- and circumstellar dust.

⁴ For reference these are roughly 2% (Gray & Corbally, 1998) of stars in the relevant spectral classes. In principle a similar phenomenon could occur in earlier spectral types (e.g. earlier than B8), but the lack of metal lines in such objects precludes their characterisation in practice.

⁵ Other types of chemically peculiar early-type stars, such as Ap and Am, can be produced by mechanisms intrinsic to the star (Michaud, 1970) and do not show this correlation of abundances with condensation temperature.

⁶ Venn & Lambert 1990

⁷ Gas is composed of volatile elements, which are those with $T_c < 300$ K, while dust is composed of refractories.

⁸ Kama et al. 2015

⁹ This is the mass ratio of gas to dust in the Galactic interstellar medium as well as that for a solar-composition mixture cooled to a few hundred kelvin. See e.g. Snow & Witt (1996).

¹⁰ CAM

¹¹ A similar method has been developed for white dwarf systems. See e.g. Fontaine & Michaud (1979). The mixing physics there is considerably different from that in protostars and main-sequence stars, particularly in that gravitational settling is often the dominant form of mixing, so little of that methodology is relevant to this work.

¹² We again exclude compact stellar remnants.

¹³ Asplund et al. 2009

in which the material originates in a circumstellar disk an outflowing planetary atmosphere, or indeed an entire disrupted planet. These scenarios typically yield accretion rates from 10^{-14} to $10^{-7} M_{\odot} \text{ yr}^{-1}$, and may have abundance patterns very different from, or identical to, the bulk of the star. Measuring the composition of the accreted mass fraction provides a new view on planet-forming and planetary material, complementary to observations explicitly targeting the circumstellar component.

For a given stellar mass, rotation rate, and mass accretion rate, we show how to calculate the mass fraction, f_{ph} , of freshly accreted¹⁴ material in the photosphere. We then derive the composition of the recently accreted materials from this mass fraction. Even if the accretion rate is not known our method constrains a combination of that and the composition of accreting material, which is still useful in many cases. We then discuss how to apply CAM to stars hosting protoplanetary and debris disks, and evaporating planets, and discuss specific examples. The method works best on stars with masses of at least $1.4 M_{\odot}$ because they have radiative envelopes, as shown in Fig. 6.1, such that accreted material is mixed down via slow non-convective processes¹⁵. For extremely high accretion rates, our method is also applicable to lower-mass stars where convection rapidly mixes accreted material with the bulk.

¹⁴ as opposed to stellar bulk

¹⁵ Charbonneau 1991; Charbonneau & Michaud 1991; Turcotte & Charbonneau 1993; Turcotte 2002

6.2 Theory

6.2.1 Overview

The picture we consider is one of a star accreting material at a steady rate \dot{M} from a circumstellar disc. If their compositions are different, the accreting material modifies the composition of the star as it accumulates. If the composition of the accreting material is constant during a given time period then to describe the radial composition profile as a function of time it suffices to track the fraction f of material at each point in the star which comes from accretion.

To make this task more straightforward we assume that the composition of the star is uniform along surfaces of constant column density¹⁶ Σ . This is equivalent to assuming that material which is accreted spreads out uniformly around the star in the angular direction on a timescale which is small compared to the vertical mixing time¹⁷. The reason to prefer column density over other measures is that it is a Lagrangian coordinate and so naturally incorporates the boundary conditions set by accretion.

The quantity we are after then is $f(\Sigma, t)$, where t is the time since

¹⁶ These surfaces coincide with isobars in the case where the gravitational acceleration is uniform.

¹⁷ This is not precisely true, but it should suffice for the level of precision available in both theory and observations. This is the case for two reasons. First, the mixing time increases rapidly with depth, so in most of the star it is the case that the vertical mixing time is long compared with the horizontal one. Secondly, the observable quantities of interest are, to leading order, linear in the amount of accreted material, and so if there is an angular distribution what is observed is an average over the star, which is precisely what this assumption provides.

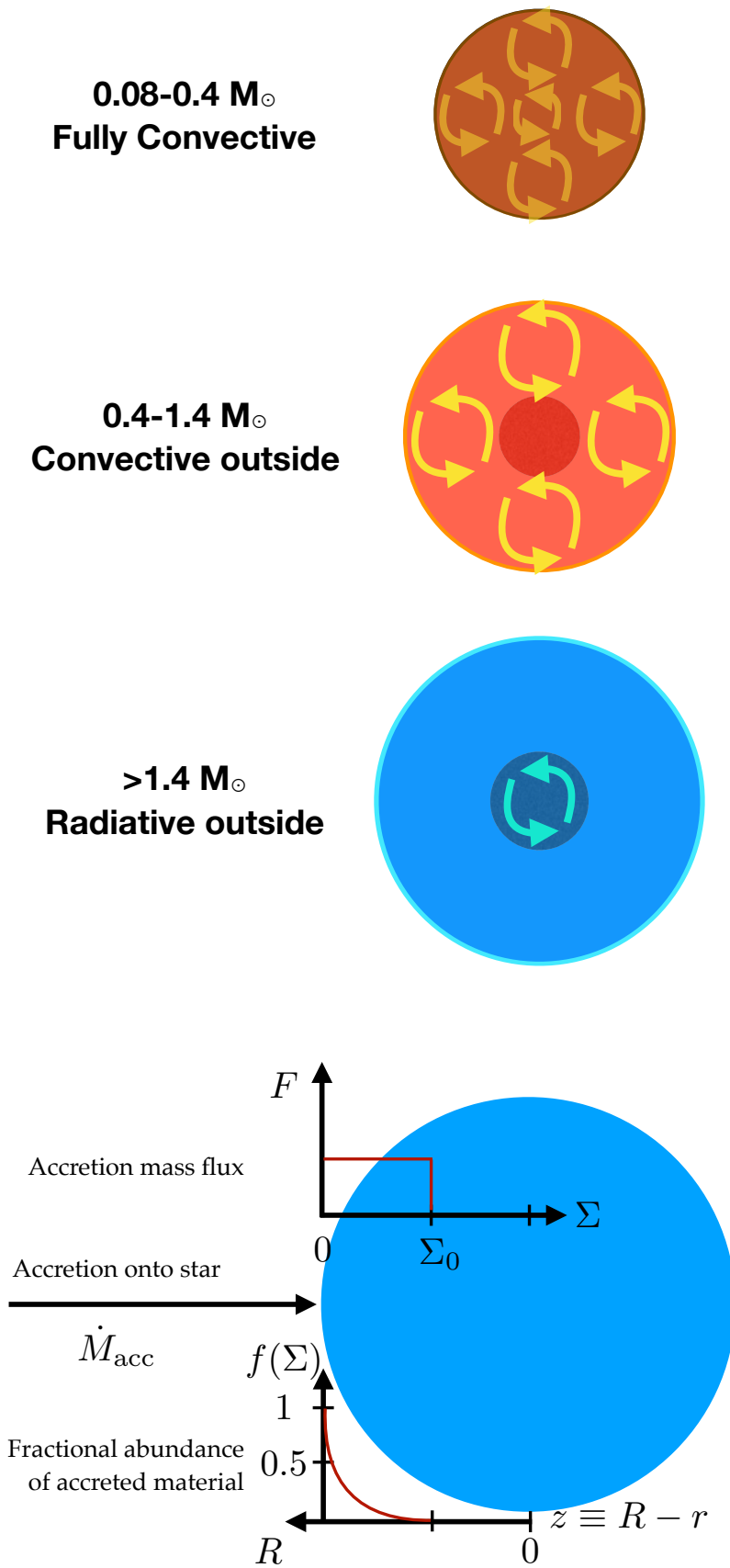


Figure 6.1: The internal structure of low-mass ($M < 0.4M_{\odot}$), intermediate-mass ($0.4M_{\odot} < M < 1.4M_{\odot}$) and high-mass ($M > 1.4M_{\odot}$) stars are shown schematically with a focus on their mixing properties. Low-mass stars are fully convective, intermediate-mass ones like the Sun develop an outer convective layer, and high-mass ones lose this layer.

Figure 6.2: Illustration of the accretion contamination model provided by Mihkel Kama. The radial coordinate z runs inside-out, opposite to r and the surface density Σ . The radial profile of f , the local fraction of accreted material, is given by Eq. 6.21.

the accretion began. As a further simplification we define $r(\Sigma)$ to be the mean radius associated with the corresponding surface of constant Σ . This allows us to work interchangeably with r and Σ without needing to impose spherical symmetry, which would disallow several mixing processes considered in Section 6.4. The model setup is visualized in Fig. 6.2.

With these assumptions, the accreted material diffuses through the star according to

$$\frac{Df}{Dt} = -\frac{1}{\rho} \frac{\partial F}{\partial z}, \quad (6.1)$$

where ρ is the density and

$$z \equiv R - r,$$

where R is the surface radius of the star. Here¹⁸

$$F = \rho D \frac{\partial f}{\partial z} \quad (6.2)$$

is the flux of accreted material and D is the spatially-varying effective diffusivity due to a variety of processes, including microscopic diffusivity, rotational mixing, convection and thermohaline mixing.

Because material is accreting the total derivative left-hand side of equation (6.1) is written according to equation (1.13) as

$$\frac{Df}{Dt} = \frac{\partial f}{\partial t} + \frac{\partial z}{\partial t} \frac{\partial f}{\partial z},$$

where the partial derivative of z is taken at constant Σ . This may equivalently be written as

$$\frac{Df}{Dt} = \frac{\partial f}{\partial t} + \frac{\partial \Sigma}{\partial t} \frac{\partial f}{\partial \Sigma}, \quad (6.3)$$

where the partial derivative of Σ is taken at constant z . Defining

$$\dot{\Sigma} \equiv \frac{\partial \Sigma}{\partial t}$$

and inserting equation (6.3) into equation (6.1) we find

$$\frac{\partial f}{\partial t} + \dot{\Sigma} \frac{\partial f}{\partial \Sigma} = -\frac{1}{\rho} \frac{\partial F}{\partial z}.$$

Now using the definition of the column density we see that

$$\frac{\partial \Sigma}{\partial z} = \rho$$

so

$$\frac{\partial f}{\partial t} + \dot{\Sigma} \frac{\partial f}{\partial \Sigma} = -\frac{\partial F}{\partial \Sigma}.$$

¹⁸ Note that ρ appears multiplying D rather than f because the diffusion in this case takes place in mass coordinates, rather than spatial ones. Equivalently note that if we consider it to be ρf that diffuses then we must account for the Boltzmann factor which maintains the background density gradient. This factor cancels the term $f \partial_z \rho$, leaving only $\rho \partial_z f$.

Using equation (6.2) to eliminate the $\partial f / \partial \Sigma$ we find

$$\frac{\partial f}{\partial t} - \dot{\Sigma} \frac{F}{\rho^2 D} = -\frac{\partial F}{\partial \Sigma}, \quad (6.4)$$

where ρ is the density and $\dot{\Sigma} \equiv \partial \Sigma / \partial t|_z$ is the column density accretion rate, given in terms of the mass accretion rate by

$$\dot{\Sigma} = \frac{\dot{M}}{4\pi R^2}.$$

As noted by Charbonneau (1991), a full treatment of this system requires solving an unwieldy initial value problem. In the case where the accreting material makes up a small fraction of the star the geometry is particularly straightforward; there is a single source at the stellar surface and its interior is limitless for the purposes of the accretion¹⁹. It is possible then to approximate the mixing as the above authors and later Turcotte (2002) did by a one-zone model, in which one tracks material entering and leaving a specific region of interest. As we will find, however, the diffusivity and density change quite rapidly with depth and so this is not sufficient for our purposes. Rather we will retain the spatial degree of freedom and make a somewhat less restrictive set of assumptions.

We begin by treating the system as being in instantaneous equilibrium so that

$$\frac{\partial f}{\partial t} \ll \left| \dot{\Sigma} \frac{F}{\rho^2 D} \right|, \left| \frac{\partial F}{\partial \Sigma} \right|.$$

This is motivated by the fact that in many cases the dominant effect of equation (6.4) is to transport material without changing f locally. This is obviously only an approximation but as we shall show it holds quite well in the systems of interest. With this approximation, equation (6.4) becomes

$$\dot{\Sigma} \frac{F}{\rho^2 D} = \frac{\partial F}{\partial \Sigma},$$

which is solved by

$$F = A \dot{\Sigma} e^{\alpha \Sigma},$$

where A is a constant of integration,

$$\alpha(\Sigma_{\text{ref}}, \Sigma) \equiv \int_{\Sigma_{\text{ref}}}^{\Sigma} \frac{d\Sigma'}{\rho^2 D} \quad (6.5)$$

and Σ_{ref} is an arbitrary reference depth. Note that we assume that the thermal and pressure structure of the system is decoupled from the mixing fraction, such that this is time-independent. Inserting this into equa-

¹⁹ Even in heavily accreting protoplanetary disks, $M_{\star} / \dot{M}_{\text{acc}} \sim 10^7$ years. Typical disk lifetimes are somewhat shorter than this, of order 10^5 yr, so the total mass which may be accreted is only a small fraction of the mass of the star.

tion (6.2) gives

$$\frac{\partial f}{\partial \Sigma} = -\frac{A\dot{\Sigma}}{\rho^2 D} e^{\alpha\dot{\Sigma}} = -A\dot{\Sigma} \frac{d\alpha}{d\Sigma} e^{\alpha\dot{\Sigma}}.$$

Integrating yields

$$\int_0^\Sigma \frac{d\alpha}{d\Sigma} e^{\alpha\dot{\Sigma}} d\Sigma = \frac{1}{\dot{\Sigma}} \left[e^{\alpha(\Sigma_{\text{ref}}, \Sigma)\dot{\Sigma}} - e^{\alpha(\Sigma_{\text{ref}}, 0)\dot{\Sigma}} \right]$$

and hence

$$f(\Sigma) = f(0) - A \left[e^{\alpha(\Sigma)\dot{\Sigma}} - e^{\alpha(0)\dot{\Sigma}} \right],$$

where we have dropped the reference column density argument for clarity.

The material at $\Sigma = 0$ is what was just accreted, so $f(0) = 1$, hence

$$f(\Sigma) = 1 - A \left[e^{\alpha(\Sigma)\dot{\Sigma}} - e^{\alpha(0)\dot{\Sigma}} \right]. \quad (6.6)$$

Equation (6.6) hides a complication, namely that there is nothing preventing f from becoming negative at some Σ . Indeed the integrand is monotonically increasing and F_0 is positive by definition, so this is a distinct possibility. To prevent this the integration must halt at the depth Σ_0 at which $f(\Sigma_0) = 0$, for here the instantaneous equilibrium approximation is clearly incorrect. This depth parametrises the extent to which material has mixed into the star. For $\Sigma > \Sigma_0$ we let $f(\Sigma) \approx 0$, as the solution must be monotonic in depth and yet cannot become negative.

The cutoff depth may be used to eliminate A . With this, equation (6.6) becomes

$$f(\Sigma) = 1 - \frac{e^{\alpha(\Sigma)\dot{\Sigma}} - e^{\alpha(0)\dot{\Sigma}}}{e^{\alpha(\Sigma_0)\dot{\Sigma}} - e^{\alpha(0)\dot{\Sigma}}}. \quad (6.7)$$

This defines a family of solutions, one for each possible value of Σ_0 . We can relate these solutions to the time evolution by means of mass conservation. Let the total accreted column density be

$$\Sigma_{\text{acc}} \approx \int_0^t \frac{\dot{M}_{\text{acc}}}{4\pi r^2} dt,$$

where this is approximate because we have neglected the variation in r with depth. This column density must equal the integrated column density of accreted material, so

$$\Sigma_{\text{acc}} = \int_0^t \dot{\Sigma} dt \approx \int_0^{\Sigma_0} f(\Sigma) d\Sigma. \quad (6.8)$$

This defines Σ_{acc} as a function of Σ_0 . Because this is a monotonic relation it may be inverted to define Σ_0 as a function of Σ_{acc} and to thereby define f as a function of time.

6.3 Mixing Depth

In this section we are searching for a solution to equation (6.8), so

$$\Sigma_{\text{acc}} = \int_0^{\Sigma_0} f(\Sigma) d\Sigma.$$

Inserting equation (6.7) we find

$$\Sigma_{\text{acc}} = \int_0^{\Sigma_0} 1 - \frac{e^{\dot{\Sigma}\alpha(\Sigma)} - e^{\dot{\Sigma}\alpha(0)}}{e^{\dot{\Sigma}\alpha(\Sigma_0)} - e^{\dot{\Sigma}\alpha(0)}} d\Sigma.$$

For notational convenience let

$$\gamma(\Sigma) \equiv \alpha(\Sigma)\dot{\Sigma}. \quad (6.9)$$

Then

$$\Sigma_{\text{acc}} = \int_0^{\Sigma_0} 1 - \frac{e^{\gamma(\Sigma)} - e^{\gamma(0)}}{e^{\gamma(\Sigma_0)} - e^{\gamma(0)}} d\Sigma.$$

Differentiating with respect to Σ_0 yields

$$\begin{aligned} \frac{d\Sigma_{\text{acc}}}{d\Sigma_0} &= \frac{d}{d\Sigma_0} \int_0^{\Sigma_0} 1 - \frac{e^{\gamma(\Sigma)} - e^{\gamma(0)}}{e^{\gamma(\Sigma_0)} - e^{\gamma(0)}} d\Sigma \\ &= \int_0^{\Sigma_0} \frac{d}{d\Sigma_0} \left[1 - \frac{e^{\gamma(\Sigma)} - e^{\gamma(0)}}{e^{\gamma(\Sigma_0)} - e^{\gamma(0)}} \right] d\Sigma, \end{aligned}$$

where we have made use of the fact that the integrand vanishes at Σ_0 .

Evaluating the derivative inside the integral we find

$$\begin{aligned} \frac{d\Sigma_{\text{acc}}}{d\Sigma_0} &= - \int_0^{\Sigma_0} \frac{d}{d\Sigma_0} \left[\frac{e^{\gamma(\Sigma)} - e^{\gamma(0)}}{e^{\gamma(\Sigma_0)} - e^{\gamma(0)}} \right] d\Sigma \\ &= \int_0^{\Sigma_0} \frac{d\gamma(\Sigma_0)}{d\Sigma_0} \frac{e^{\gamma(\Sigma_0)}}{e^{\gamma(\Sigma_0)} - e^{\gamma(0)}} \left[\frac{e^{\gamma(\Sigma)} - e^{\gamma(0)}}{e^{\gamma(\Sigma_0)} - e^{\gamma(0)}} \right] d\Sigma. \end{aligned}$$

Noting that the first two factors inside the integral do not depend on Σ we may commute them with the integral to find

$$\begin{aligned} \frac{d\Sigma_{\text{acc}}}{d\Sigma_0} &= \frac{d\gamma(\Sigma_0)}{d\Sigma_0} \frac{e^{\gamma(\Sigma_0)}}{e^{\gamma(\Sigma_0)} - e^{\gamma(0)}} \int_0^{\Sigma_0} \frac{e^{\gamma(\Sigma)} - e^{\gamma(0)}}{e^{\gamma(\Sigma_0)} - e^{\gamma(0)}} d\Sigma \\ &= \frac{d\gamma(\Sigma_0)}{d\Sigma_0} \frac{e^{\gamma(\Sigma_0)}}{e^{\gamma(\Sigma_0)} - e^{\gamma(0)}} [\Sigma_0 - \Sigma_{\text{acc}}] \\ &= \frac{d\gamma(\Sigma_0)}{d\Sigma_0} \frac{1}{1 - e^{\gamma(0) - \gamma(\Sigma_0)}} [\Sigma_0 - \Sigma_{\text{acc}}]. \end{aligned}$$

Because ρ and D are positive quantities, α is monotonic and hence either asymptotes to a finite value or else diverges. Because $\dot{\Sigma}$ is also positive, γ does the same. In the event that γ diverges we may set $e^{\gamma(0) - \gamma(\Sigma_0)}$ to zero. Likewise we will argue later that under all cases of interest where γ

asymptotes, it does so to a value much greater than $\gamma(0)$, and so we may make the same approximation. Thus we write in both cases

$$\frac{d\Sigma_{\text{acc}}}{d\Sigma_0} \approx \frac{d\gamma(\Sigma_0)}{d\Sigma_0} [\Sigma_0 - \Sigma_{\text{acc}}],$$

which may also be written as

$$\frac{d\Sigma_{\text{acc}}}{d\Sigma_0} \approx \left. \frac{d\gamma}{d\Sigma} \right|_{\Sigma_0} [\Sigma_0 - \Sigma_{\text{acc}}]. \quad (6.10)$$

From this we see that it is not the asymptotic behaviour of γ that we care about, but rather that of

$$\frac{d\gamma}{d\Sigma} = \frac{\dot{\Sigma}}{\rho^2 D}.$$

Noting that ρ is monotonic in Σ , and taking D to be monotonic in ρ , we find that this either goes to zero, diverges, or approaches a non-zero finite asymptote.

In the event that $d\gamma/d\Sigma \rightarrow \infty$ as $\Sigma \rightarrow \infty$, the solution to equation (6.10) asymptotically approach a scenario in which

$$\Sigma_0 - \Sigma_{\text{acc}} \approx \left. \frac{d\Sigma}{d\gamma} \right|_{\Sigma_0} \rightarrow 0.$$

This is because the prefactor of Σ_{acc} on the right-hand side of equation (6.10) is negative and so causes the solution to damp towards this point. Thus in this situation

$$\Sigma_{\text{acc}} \approx \Sigma_0 \quad (6.11)$$

and

$$f(\Sigma < \Sigma_0) \approx 1. \quad (6.12)$$

Indeed this solution holds approximately even when $d\gamma/d\Sigma$ tends to a non-zero finite asymptote, because in that case the solution tends to

$$\Sigma_{\text{acc}} = \Sigma_0 - \left. \frac{d\Sigma}{d\gamma} \right|_{\Sigma_0} \approx \Sigma_0,$$

again with $f(\Sigma < \Sigma_0) \approx 1$.

In the opposite limit, where $d\gamma/d\Sigma \rightarrow 0$ as $\Sigma \rightarrow \infty$, Σ_0 increases much more rapidly than Σ_{acc} . Equation (6.10) may then be approximated as

$$\frac{d\Sigma_{\text{acc}}}{d\Sigma_0} \approx \left. \frac{d\gamma}{d\Sigma} \right|_{\Sigma_0} \Sigma_0. \quad (6.13)$$

This yields a lower bound on Σ_{acc} of

$$\Sigma_{\text{acc}} > \frac{1}{2} \frac{d\gamma}{d\Sigma} \Big|_{\Sigma_0} \Sigma_0^2,$$

where we have simply used the derivative evaluated at Σ_0 , which is the minimum value it takes over the interval from 0 to Σ_0 .

To derive more than a lower bound we need to know more about the structure of γ . Under the assumptions of hydrostatic equilibrium and spherical symmetry,

$$\frac{dp}{dr} = -\rho g.$$

Inserting the ideal gas law as per equation (1.1) we find

$$\frac{d}{dr} \left[\rho T \frac{k_B}{\mu m_p} \right] = -\rho g,$$

where μ is the mean molecular weight. In the outer regions of the star T , g and μ are approximately constant²⁰ so

$$\frac{d \ln \rho}{dr} = -\frac{\mu m_p g}{k_B T}.$$

As such we let

$$h \equiv \frac{k_B T}{\mu g}$$

be the scale height for *both* pressure and density and write

$$\rho = \rho_0 \exp(z/h),$$

which yields

$$\Sigma = \int_{-\infty}^z \rho dz' = h\rho = h\rho_0 e^{-z/h}. \quad (6.14)$$

Combining this with equations (6.5) and (6.9) we find

$$\frac{d\gamma}{d\Sigma} = \frac{\dot{\Sigma}}{\rho^2 D} = \frac{h^2}{D} \frac{\dot{\Sigma}}{\Sigma^2}.$$

As a result equation (6.13) may be written as

$$\frac{d\Sigma_{\text{acc}}}{d\Sigma_0} = \frac{h^2}{D} \frac{\dot{\Sigma}}{\Sigma_0}. \quad (6.15)$$

In all of the cases discussed in Section 6.4, D is a power-law in Σ of the form²¹

$$D = D_0 \Sigma^\beta. \quad (6.16)$$

²⁰ See Paczyński (1969) for a more detailed discussion of these approximations.

²¹ The combined diffusivity is a sum of the diffusivities of all applicable processes. This is generally not a power-law but is well-approximated by one in most cases because one process is usually dominant over all others. Even should this approximation fail the power-law approximation is primarily a convenience rather than a limit essential to the calculation.

Note that the asymptotic behaviour of $dy/d\Sigma$ changes at $\beta = -2$, and below this point the limit in which it diverges is applicable. Thus taking $\beta > -2$ and inserting this into equation (6.15) we find

$$\frac{d\Sigma_{\text{acc}}}{d\Sigma_0} = \frac{h^2}{D_0} \dot{\Sigma} \Sigma^{-1-\beta}.$$

Integrating and using $\Sigma_{\text{acc}}(\Sigma_0 = 0) = 0$ yields

$$\begin{aligned} \Sigma_{\text{acc}} &= \frac{h^2 \dot{\Sigma} \Sigma_0^{-\beta}}{(-\beta) D_0} \\ &= \frac{h^2 \dot{\Sigma}}{|\beta| D(\Sigma_0)}, \end{aligned} \quad (6.17)$$

so long as $\beta < 0$.

The resulting profile for f depends on depth. Assuming that $\gamma - \gamma(\Sigma_0) \ll 1$ and neglecting $e^{\gamma(0)}$ as discussed, we find that

$$f(\Sigma) \approx \gamma(\Sigma_0) - \gamma. \quad (6.18)$$

At shallower depths $f \approx 1$. Thus we may write

$$f(\Sigma) \approx \min(1, \gamma(\Sigma_0) - \gamma).$$

In the event that D is a power-law we can evaluate γ to find

$$f(\Sigma) \approx \min\left(1, \frac{h^2 \dot{\Sigma}}{\Sigma D(\Sigma)} - \frac{h^2 \dot{\Sigma}}{\Sigma_0 D(\Sigma_0)}\right),$$

where we have let $\Sigma_0 \rightarrow \infty$ and dropped multiplicative factors depending only on β . Note that for $-1 < \beta < 0$, $\gamma(\Sigma_0)$ and hence $(\Sigma_0 D(\Sigma_0))^{-1}$ vanishes asymptotically and so at long times we may neglect this term and find the time-independent result that

$$f(\Sigma) \approx \min\left(1, \frac{h^2 \dot{\Sigma}}{\Sigma D(\Sigma)}\right).$$

For $-2 < \beta \leq -1$, $\gamma(\Sigma_0)$ grows without bound even though its derivative asymptotes to zero. In this case there is still a time-dependence to the profile even at long times. When $\beta = -1$, a case which is both physically relevant and mathematically convenient,

$$f(\Sigma, t) \approx 1 - \left(\frac{\Sigma}{\Sigma_0}\right)^{h^2 \dot{\Sigma}/D_0}$$

and

$$\Sigma_{\text{acc}} = \frac{h^2 \dot{\Sigma}}{D_0} \Sigma_0,$$

hence

$$\Sigma_0 = \frac{D_0}{h^2} t.$$

Letting

$$t_{\text{mix}}(\Sigma) \equiv \frac{h^2}{D_0} \Sigma$$

we find

$$f(\Sigma, t) \approx 1 - \left(\frac{t_{\text{mix}}(\Sigma)}{t} \right)^{h^2 \dot{\Sigma} / D_0},$$

which in a series expansion yields

$$f(\Sigma, t) \approx \frac{h^2 \dot{\Sigma}}{D_0} \ln \frac{t}{t_{\text{mix}}} = \frac{h^2 \dot{\Sigma}}{D(\Sigma) \Sigma} \ln \frac{t}{t_{\text{mix}}}. \quad (6.19)$$

This form is valid so long as it yields $f < 1$, at which point the appropriate approximation is $f = 1$. For further decreases in β the time-dependence becomes stronger, but in all cases we have considered thus far we find a number well-approximated by

$$f(\Sigma) \approx \min \left(1, \frac{h^2 \dot{\Sigma}}{\Sigma D(\Sigma)} \right),$$

which is at most wrong by logarithmic factors in time.

The only case not yet considered is $\beta > 0$, in which $d\gamma/d\Sigma$ goes to zero rapidly as $\Sigma \rightarrow \infty$. In this limit material is brought so rapidly into the star that it is no longer valid to treat the centre as being infinitely far away from the surface. That is, the interior boundary condition matters in this limit. This does not occur in any of the physical cases considered, and so we need not consider it further.

In all cases note that we have found $\Sigma_0 > \Sigma_{\text{acc}}$, which must be the case because $f \leq 1$ everywhere. As a result, however, once we have waited a long time relative to the time required to accrete material corresponding to some depth Σ , we can be assured that Σ_0 exceeds this depth. This justifies our assumption that Σ_0 is large relative to photospheric depths, as even $10^{-15} M_{\odot} \text{ yr}^{-1}$ accreted for 30yr suffices to produce Σ_{acc} well in excess of the typical photospheric depths of 0.1 g cm^{-2} .

Finally, earlier in this section we claimed that the asymptotic value of $\gamma(\Sigma_0) - \gamma(0)$ is, in the cases of interest, generically large when finite. We now justify this claim. First suppose that D is a power-law in Σ as in equation (6.16). When $\beta > -1$, $\gamma(0) \rightarrow -\infty$ while $\gamma(\Sigma_0) \rightarrow$ goes to a constant as $\Sigma_0 \rightarrow \infty$, so $\gamma(\Sigma_0) - \gamma(0) \rightarrow \infty$. When $\beta < -1$, $\gamma(0)$ is finite but $\gamma(\Sigma_0) \propto \Sigma_0^{-1-\beta} \rightarrow \infty$, so once more $\gamma(\Sigma_0) - \gamma(0) \rightarrow \infty$. This covers all mixing mechanisms we have considered in this paper. Note that even

if we regularise the integrals which have $\beta > -1$ ²², the regularisation point must be shallower than the photosphere²³, where the densities are extremely small, and so γ still ought to vary substantially. As a result we expect that γ may be taken to have a large dynamic range between the point at which material enters the system and the deepest regions.

Suppose though that we are interested in a case where this argument fails, as there are pathological cases in which it does, such as the limit of vanishing $\dot{\Sigma}$ with a regularised integral. We would then have $\gamma(0)$ close to the asymptotic value of $\gamma(\Sigma_0)$. Then expanding equation (6.7) we find

$$f \approx \frac{\gamma(\Sigma_0) - \gamma(\Sigma)}{\gamma(\Sigma_0) - \gamma(0)},$$

which is enhanced relative to equation (6.21) by a factor of $(\gamma(\Sigma_0) - \gamma(0))^{-1}$. This means that we ought to infer Σ_0 be smaller by the same factor for a fixed accreted mass, and also means that the profile of f near the surface becomes independent of $\dot{\Sigma}$, which only enters multiplicatively in γ . This is physically what happens when the accretion rate is low and the dynamic diffusivity increases rapidly inwards, as then material is then whisked away on a timescale which is much faster than the rate at which it accumulates, so the diffusivity at the point where it arrives is the limiting factor. This scenario is somewhat artificial, in that all mechanisms we have examined lack the regularising cutoff and hence do not exhibit such behaviour, but it is useful to keep in mind in the event that such a cutoff becomes physically interesting. This usually occurs at higher accretion rates, where the radial velocity is significant, but there could be cases we have not considered in which it becomes relevant.

In summary, there are two relevant limits: either $d\alpha/d\Sigma$ asymptotes to zero as $\Sigma \rightarrow \infty$ or it does not. In the former case we find that

$$t \approx \frac{h^2}{D(\Sigma_0)} \quad (6.20)$$

(see equation 6.11). where h is evaluated at Σ_0 . This may be interpreted physically as the material diffusing to the column density at which the diffusion timescale matches the accretion time, which is a generic feature of diffusion problems with a localised source and dynamic diffusivity increasing away from the source. The associated material fraction is well-approximated by

$$f(\Sigma) \approx \min \left(1, \frac{h^2 \dot{\Sigma}}{D\Sigma} \right). \quad (6.21)$$

While the case where $d\alpha/d\Sigma$ remains non-zero does not arise physically with any of the transport processes we consider here²⁴, it is still worth

²² This would be accomplished by cutting off the integration at some shallow point, which could be physically motivated if the accretion has a significant radial component or otherwise mixes immediately to some non-trivial depth.

²³ Otherwise there is no point in the calculation because the observed f will be unity.

²⁴ See Section 6.4.

examining for completeness. In this case we find (see equation (6.17)) that

$$\Sigma_{\text{acc}} \approx \Sigma_0, \quad (6.22)$$

with

$$f(\Sigma) \approx 1.$$

This is because the dynamic diffusivity is decreasing inward, and so material just piles up at the surface. At the interface between the two cases there is more complex behaviour (e.g. when α diverges slowly), but the qualitative picture is well-captured by equations (6.20) and (6.22).

6.3.1 Steady State

To validate the assumption that mixing processes may be treated as being in a quasi-steady state (i.e. an instantaneous equilibrium) we differentiate equations (6.12) and (6.18) in time. The former is trivial, and yields zero everywhere except near Σ_0 , where the steady-state approximation must break regardless because this is the location of the diffusion front. The latter is nearly zero when $f \approx 1$ and elsewhere yields

$$\frac{df}{dt} = \frac{d\gamma(\Sigma_0)}{dt},$$

where we have used the fact that only Σ_0 depends on time to evaluate this derivative. Now

$$\begin{aligned} \frac{d\gamma(\Sigma_0)}{dt} &= \left. \frac{d\gamma}{d\Sigma} \right|_{\Sigma_0} \frac{d\Sigma_0}{dt} \\ &= \left. \frac{d\gamma}{d\Sigma} \right|_{\Sigma_0} \frac{d\Sigma_0}{d\Sigma_{\text{acc}}} \frac{d\Sigma_{\text{acc}}}{dt} \\ &= \dot{\Sigma} \left. \frac{d\gamma}{d\Sigma} \right|_{\Sigma_0} \frac{d\Sigma_0}{d\Sigma_{\text{acc}}}. \end{aligned}$$

Inserting equation (6.10) we find

$$\frac{d\gamma(\Sigma_0)}{dt} \approx \frac{\dot{\Sigma}}{\Sigma_0 - \Sigma_{\text{acc}}}.$$

We are working in the limit where $d\gamma/d\Sigma \rightarrow 0$, so $\Sigma_0 \gg \Sigma_{\text{acc}}$, and hence

$$\frac{df}{dt} = \frac{d\gamma(\Sigma_0)}{dt} \approx \frac{\dot{\Sigma}}{\Sigma_0}.$$

In order to neglect this it must be smaller than the term $dF/d\Sigma$ on the right-hand side of equation (6.4). In other words, we need the dimensionless

ratio

$$\lambda \equiv \frac{df/dt}{dF/d\Sigma}$$

to be small. Evaluating this yields

$$\begin{aligned} \lambda &= \left(\frac{\dot{\Sigma}}{\Sigma_0} \right) \left(\frac{dF}{d\Sigma} \right)^{-1} \\ &= \left(\frac{\dot{\Sigma}}{\Sigma_0} \right) \left(\frac{d}{d\Sigma} \left[-\rho^2 D \frac{\partial f}{\partial \Sigma} \right] \right)^{-1} \\ &\approx \left(\frac{\dot{\Sigma}}{\Sigma_0} \right) \left(\frac{d}{d\Sigma} \left[\rho^2 D \frac{d\gamma}{d\Sigma} e^{\gamma-\gamma(\Sigma_0)} \right] \right)^{-1} \\ &= \left(\frac{\dot{\Sigma}}{\Sigma_0} \right) \left(\frac{d}{d\Sigma} \left[\dot{\Sigma} e^{\gamma-\gamma(\Sigma_0)} \right] \right)^{-1} \\ &= \left(\frac{\dot{\Sigma}}{\Sigma_0} \right) \left(\dot{\Sigma} \frac{d\gamma}{d\Sigma} e^{\gamma-\gamma(\Sigma_0)} \right)^{-1} \\ &= \left(\frac{\dot{\Sigma}}{\Sigma_0} \right) \left(\frac{\dot{\Sigma}^2}{\rho^2 D} e^{\gamma-\gamma(\Sigma_0)} \right)^{-1} \\ &= \left(\frac{\rho^2 D}{\dot{\Sigma} \Sigma_0} \right) \left(e^{\gamma-\gamma(\Sigma_0)} \right)^{-1}. \end{aligned}$$

Noting that $e^{\gamma-\gamma(\Sigma_0)} \approx 1$ in this regime, we find

$$\begin{aligned} \lambda &\approx \frac{\rho^2 D}{\dot{\Sigma} \Sigma_0} \\ &\approx \frac{\Sigma^2 D}{h^2 \dot{\Sigma} \Sigma_0}, \end{aligned}$$

where we have made use of equation (6.14) in the last line. Combining this with equation (6.17) we find

$$\lambda \approx |\beta|^{-1} \frac{\Sigma^2}{\Sigma_{\text{acc}} \Sigma_0} \approx \frac{\Sigma^2}{\Sigma_{\text{acc}} \Sigma_0},$$

where we have dropped β because it is of order unity. Thus λ is small in the regime where

$$\Sigma \ll \sqrt{\Sigma_0 \Sigma_{\text{acc}}}.$$

This is as expected: the approximation is a good one certainly up to Σ_{acc} and for much of the region beyond that, but breaks down as we approach Σ_0 , which is the location of the diffusion front.

In summary, the region near the surface of the star is the one of most interest, and in all cases considered above we have found that for $\Sigma \ll \Sigma_{\text{acc}}$ the quasi-steady state approximation holds as desired.

6.3.2 Time Dependence

If the accretion suddenly halts the system continues to mix, but now $\dot{\Sigma} = 0$ and the boundary condition on $f(0)$ is replaced with a condition on the surface flux, namely that

$$F(0) = 0,$$

subject to the equation

$$\frac{\partial f}{\partial t} = -\frac{\partial F}{\partial \Sigma}.$$

Once more taking the instantaneous equilibrium approximation we find that F is a constant, in this case zero, such that

$$\frac{\partial f}{\partial \Sigma} = 0,$$

and hence f is a constant as well. The boundary between the region in which the old solution applies and that in which the new one applies sits at the depth Σ_b , such that

$$f(\Sigma_b)_- = f(\Sigma_b)_+, \quad (6.23)$$

where the subscripts $-$ and $+$ refer respectively to the region at greater depth than Σ_b and that at shallower depth. Along with conservation of mass this yields a time evolution relation, namely that the amount of accreted material in the region which has adapted to the new surface condition is

$$\Sigma_{\text{acc}+} = \int_0^{\Sigma_b} f(\Sigma) d\Sigma = \Sigma_{\text{acc}} - \int_0^t F(\Sigma_b)_- dt, \quad (6.24)$$

where time is now measured since the accretion ended. This gives

$$f(\Sigma < \Sigma_b) = 1 - \frac{1}{\Sigma_{\text{acc}}} \int_0^t F(\Sigma_b)_- dt, \quad (6.25)$$

As we only ever find ourselves in the case given by equation (6.21), we combine this with equation (6.23) to find that at depths for which $\dot{\Sigma} h^2 / D(\Sigma_b) \Sigma_b < 1$,

$$\frac{\dot{\Sigma} h^2}{D(\Sigma_b) \Sigma_b} = 1 - \frac{1}{\Sigma_{\text{acc}}} \int_0^t F(\Sigma_b)_- dt,$$

where $\dot{\Sigma}$ is the accretion rate prior to it halting. Assuming that $\rho \propto h$ and that D obeys a power-law in Σ we find

$$\Sigma_b \approx \Sigma_{\text{acc}} \frac{h^2}{D(\Sigma_b)(t_{\text{acc}} - t)},$$

where t_{acc} is the time over which the system accreted. Letting $\Sigma_b = \Sigma_0$

and using equation (6.20) we find

$$\Sigma_b \approx \Sigma_{\text{acc}} \frac{t_{\text{acc}}}{t_{\text{acc}} - t}. \quad (6.26)$$

Thus we see that the timescale over which the photospheric composition returns to its pre-accretion state is essentially the timescale over which the accretion occurred in the first place. This behaviour may be seen in Fig. 6.3, which shows the evolution of the accreted fraction with time for three stars which differ only in the behaviour of the diffusivity. More specifically, we have taken

$$D = D_0 \Sigma^\beta,$$

and varied β between the three stars. What is shown is the solution to equations (6.7), (6.20), (6.23), (6.24), and (6.25). In both cases accretion is turned on at $t = 0$ and off at $t = 10^2$. In the first case, with $\beta = -0.5 > -1$, the star rapidly mixes material to increasing depths, and when the accretion is turned off the material disperses into the star in a timescale comparable to the accretion time. In the second case, with $\beta = -1$, the marginal²⁵ scaling of f with time that we found previously is apparent. Finally in the second case, with $\beta = -1.5 < -1$, the diffusion front progresses much more slowly. In each case when the accretion is turned off the surface rapidly relaxes to match the peak accreted fraction, which it then tracks as the material slowly disperses. In particular, the phenomenology is precisely what we have described in equation (6.26), with the timescale for dispersal is being set by the depth to which the material had reached, which in turn is set by the timescale over which material was accreted. The notable exception to this is if D_0 changes after the accretion halts, in which case the new timescale is

$$t' = t \frac{D_0}{D'_0}. \quad (6.27)$$

²⁵ e.g. logarithmic in the small- f regime

6.4 Mixing Processes

In the stars of interest there are five basic mixing processes which could play a role:

1. Molecular Diffusion
2. Rotational Mixing
3. Shear Mixing
4. Thermohaline mixing

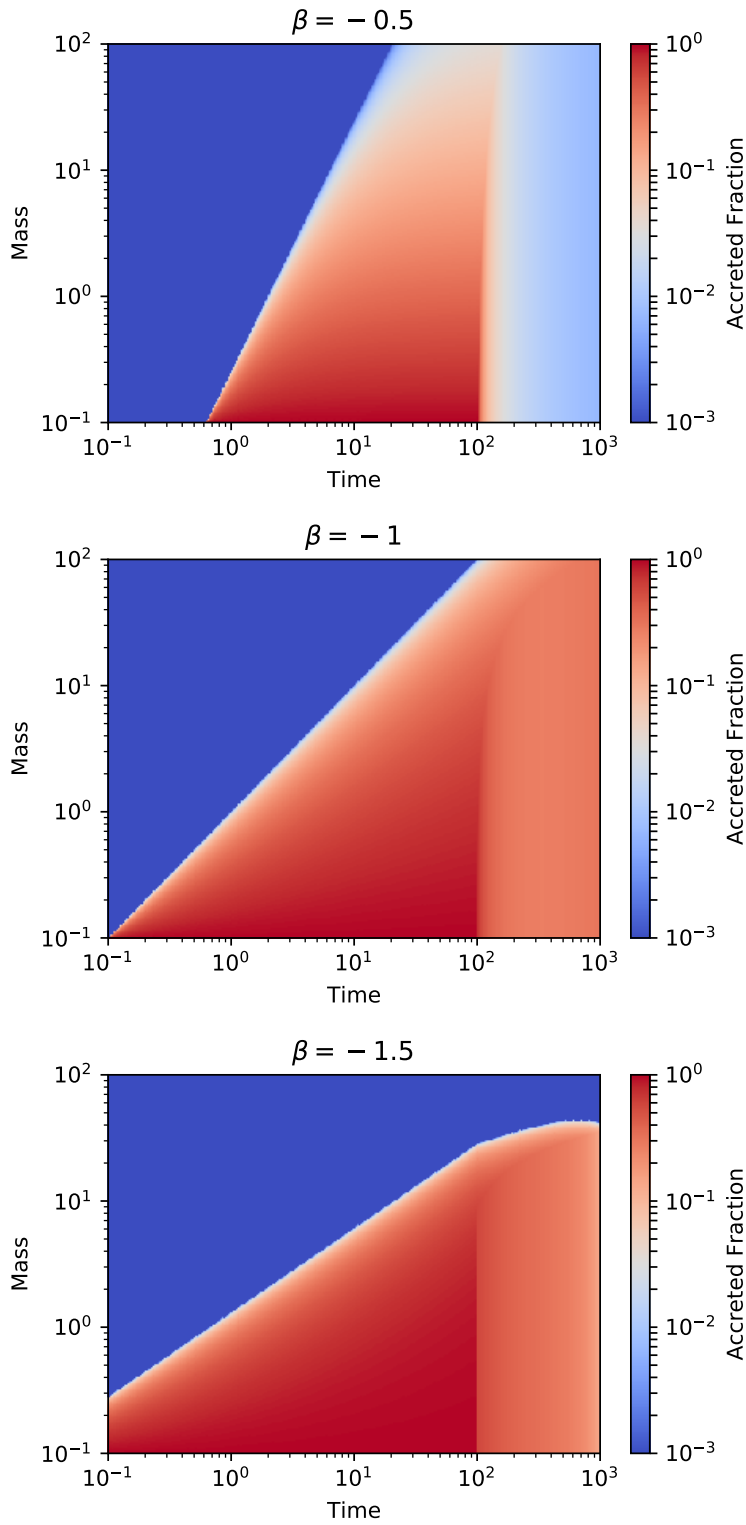


Figure 6.3: The accreted fraction f is shown as a function of mass coordinate, defined to be zero at the surface, and time for three stars with different power-law diffusivities ($\beta = -0.5$, $\beta = -1$, and $\beta = -1.5$ respectively from top to bottom). These models were computed using the instantaneous equilibrium assumption for both $\Sigma < \Sigma_b$ and $\Sigma > \Sigma_b$. In both cases the units are arbitrary, and were chosen such that $h = D_0 = 1$ and $\dot{\Sigma} = 0.1$. Accretion begins at time $t = 0$ and ends at $t = 10^2$. In both cases the timescale for mixing away from the surface after accretion ends is set by the depth to which the material had reached, which in turn is set by the timescale over which material was accreted.

5. Convection

In all but the last of these we assume the fluid to be stably stratified, as convection dominates all of these processes when it occurs. We neglect gravitational settling because, as we shall show, the time-scales over which the above processes act are of order hours to days whereas those for gravitational settling are of order months to years even in white dwarf atmospheres ²⁶.

²⁶ Fontaine & Michaud 1979

To first order these effects contribute additively to the diffusivity, and so each may be considered independent of the others. In this section we examine each of these in turn. We then compare their relative magnitudes as a function of the stellar parameters and discuss the extent to which they ought to contribute to mixing in accreting A-type stars.

6.4.1 Molecular Diffusion

Molecular diffusion, also known as microscopic diffusion, is the process whereby random thermal motions of particles in a fluid mix material within the fluid. We discussed this in Section 1.4.1, where we used the expression

$$D \approx 5.2 \times 10^{-15} (\ln \Lambda)^{-1} \left(\frac{T}{\text{K}} \right)^{5/2} \left(\frac{\rho}{\text{g/cm}^3} \right)^{-1} \text{ cm}^2 \text{ s}^{-1} \quad (6.28)$$

²⁷, where

²⁷ Spitzer 1956

$$\ln \Lambda = \begin{cases} -17.4 + 1.5 \ln T - 0.5 \ln \rho & T < 1.1 \times 10^5 \text{ K} \\ -12.7 + \ln T - 0.5 \ln \rho & T > 1.1 \times 10^5 \text{ K} \end{cases}$$

and T and ρ are measured in C.G.S.K. units when they appear in a logarithm. For simplicity we take $\ln \Lambda = -10$ and ignore both thermal and magnetic corrections to this factor. Inserting this into equation (6.28) and rescaling with a representative temperature and density we find

$$D \approx 5 \times 10^{-5} \left(\frac{T}{10^4 \text{ K}} \right)^{5/2} \left(\frac{\rho}{0.1 \text{ g/cm}^3} \right)^{-1} \text{ cm}^2 \text{ s}^{-1}.$$

When this mode of mixing dominates the diffusivity is a power-law with $\beta = -1$ (see Appendix 6.3).

6.4.2 Rotational Mixing

Rotational mixing is a result of the Eddington-Sweet circulation. Because we are primarily interested in phenomenon in the surface layers of radiative stars²⁸ and because the effects discussed in Chapter 4 decay rapidly towards the surface of the star we neglect these and just retain the standard

²⁸ This is never the dominant process in convective stars.

Eddington–Sweet circulation. While this manifests as a meridional flow, near the surface it has radial scale z and velocity

$$u \approx \left(\frac{F_\star}{p} \right) \frac{\Omega^2 R}{g}$$

²⁹, where Ω is the angular velocity, F_\star is the heat flux and p is the pressure. The radial velocity is offset from this by a factor of h/R , so the effective radial diffusivity is

$$D \approx u_r h \approx h \left(\frac{h}{R} \right) \left(\frac{F_\star}{p} \right) \frac{\Omega^2 R}{g} = \left(\frac{z}{R^2} \right) \left(\frac{F_\star}{p} \right) \frac{u_{\text{rot}}^2}{g}, \quad (6.29)$$

where u_{rot} is the rotation speed at the surface, which is typically of order tens to hundreds of kilometres per second. This prescription is quite similar to that found by [Chaboyer & Zahn \(1992\)](#) in a more detailed analysis.

Equation (6.29) gives rise to $\beta = -1$. The abundances are thus enhanced over what we expect for $\beta > -1$ by a factor of ³⁰ $\ln(D_0 t / h^2)$, and so varies logarithmically in time rather than asymptoting to a fixed value. For the purposes of our calculations below we neglect this logarithmic factor, but simply note that it could cause the real abundances to exceed those that we predict by a factor of several when this is the dominant mixing mechanism.

²⁹ [Eddington 1929](#)

³⁰ See equation (6.19) and the preceding discussion.

6.4.3 Shear Mixing

Shear mixing is due to differential rotation or other shears present in the star. Non-rotational shears may come from meridional circulations, but in that case they cannot produce more mixing than the circulation itself because they have the same fundamental length- and time-scales as the circulation ³¹. Thus we need only consider shears due to differential rotation.

³¹ [Maeder 2009](#)

There are two main sources of differential rotation in these systems, namely the angular momentum brought to the surface of the star by the infalling material and the long-term buildup of angular momentum due to meridional circulations. While in systems with very strong accretion the former may be severe, in most cases the accretion magnetically truncates outside the star ³². When this occurs the infalling material is brought into corotation and so does not create a surface shear. Rather the angular momentum is transported via the magnetic field, which may spread it through a large volume of the star. As such we neglect the shears due to accreting material.

³² [Littlefair 2014](#)

Along similar lines, the long-term buildup of angular momentum is expected to be quite large in some cases ³³, but astereoseismic measure-

³³ [Zahn 1992](#); [Meynet & Maeder 2000](#); [Lau et al. 2011](#)

ments appear to run counter to this prediction ³⁴. There have also been suggestions that more exotic angular momentum transport mechanisms are at work near the surfaces of stars (see e.g. [Kumar et al., 1999](#)). Given the uncertainties involved in this physics we neglect this effect in our analysis, but note that it could change our results should there be strong shears in the stars of interest.

³⁴ [Cantiello et al. 2014](#); [Keen et al. 2015](#); [Deheuvels et al. 2015](#); [Eggenberger et al. 2017](#)

6.4.4 Thermohaline Mixing

When the accreting material is metal-poor mixing due to an unstable molecular weight gradient ought not to occur. This is because such a situation leads to a stable molecular weight gradient, which is the opposite of what is needed for the molecular gradient mixing mechanism. One might worry that a stable weight gradient would hinder other mixing mechanisms, but this effect should not be significant. While the effect of accreting metal-poor material on the spectrum of the star may be profound, its impact on the molecular weight gradient is small, especially if the ratio of hydrogen to helium in the accreting material matches that in the star. As such we are justified in neglecting all effects associated with molecular weight gradients for such scenarios.

By contrast when the accreting material is metal-rich relative to the star it causes an unstable molecular weight gradient. This may either be a diffusively unstable gradient, resulting in convection, or one unstable to double-diffusive processes, resulting in semi-convection or fingering. The former occurs when ³⁵

³⁵ [Traxler et al. 2011](#)

$$\frac{d \ln \mu}{d \ln p} < \frac{d \ln T}{d \ln p} - \frac{\gamma - 1}{\gamma},$$

where as usual γ is the adiabatic index and μ is the molecular weight. In radiative zones the right-hand side is negative and of order a few tenths. Hence a large molecular weight gradient is required, particularly if it is to be sustained over a significant region of the star, and so even if it occurs we expect the region over which it does to be small enough that its effects may be neglected³⁶. By contrast the doubly-diffusive instability merely requires that ³⁷

³⁶ This may fail if the accretion rate is high enough, but in such cases we shall generally find that the entire photosphere is replaced by accreted material.

³⁷ [Traxler et al. 2011](#)

$$\frac{d \ln \mu}{d \ln p} < 0. \quad (6.30)$$

This is a much weaker condition which is readily realised, so we shall focus on it to the exclusion of μ -induced convection.

The result of a gradient satisfying equation (6.30) is turbulence with an

effective diffusivity of the form

$$D \approx CK \left| \frac{d \ln \mu}{d \ln p} \right|$$

³⁸, where μ is the molecular weight, $C \approx 10^3$ is a constant³⁹ and

$$K = \frac{4acT^3}{3\rho^2\kappa c_p}.$$

Using

$$\frac{df}{dz} = \frac{F_0}{\rho D}$$

we find that

$$\begin{aligned} \frac{d \ln \mu}{d \ln p} &= \frac{d}{d \ln p} \ln [\mu_\star(1-f) + f\mu_{\text{acc}}] \\ &= \frac{\mu_{\text{acc}} - \mu_\star}{\mu_\star(1-f) + f\mu_{\text{acc}}} \frac{df}{d \ln p} \\ &= \frac{\mu_{\text{acc}} - \mu_\star}{\mu_\star(1-f) + f\mu_{\text{acc}}} h \frac{df}{dz} \\ &= \frac{\mu_{\text{acc}} - \mu_\star}{\mu_\star(1-f) + f\mu_{\text{acc}}} \frac{hF_0}{\rho D}. \end{aligned}$$

Thus

$$D \approx \sqrt{\frac{hF_0CK}{\rho} \left| \frac{\mu_{\text{acc}} - \mu_\star}{\mu_\star(1-f) + f\mu_{\text{acc}}} \right|}. \quad (6.31)$$

This scales like $\rho^{-3/2}$, so $\beta = -3/2$ and hence the dynamic diffusivity actually decreases with depth. As a result this mechanism is rapid in the photosphere and becomes slow deeper down. As in the case of rotational mixing, because $\beta \leq -1$ there is a logarithmic enhancement in abundances as a function of time which we neglect for the purposes of our abundance calculations because it is generally small.

Because this mechanism depends on f and F_0 in principle it should be incorporated by solving the differential equations defining F and Σ anew. Instead of this we simply solve equation (6.12) consistently with equation (6.31). This amounts to making a local calculation of the mixing near the photosphere. Because the photospheric abundance is primarily set by mixing processes near the photosphere this ought to be a good approximation, even if its naive extrapolation into the interior is more problematic.

In the opposite case, in which a star accretes material which is much lighter than the bulk composition, the material gradient acts to suppress certain kinds of turbulent mixing, most notably convection. However surface convection zones are somewhat superadiabatic, so we are justified

³⁸ Ulrich 1972

³⁹ It is worth noting that there is considerable uncertainty in the constant C . Reported values inferred from observations include 658 (Charbonnel & Zahn, 2007), 667 (Charbonnel & Lagarde, 2010) and approximately unity (Kippenhahn et al., 1980). Numerical as well as more theoretically-motivated studies show similar disagreement, with values including 2 (Cantiello & Langer, 2010), of order 10 (Traxler et al., 2011), 658 (Ulrich, 1972) and 1294 (Brown et al., 2013). Some of this variation is owing to differences in the precise conventions used to define C , including different means of accounting for the microscopic thermal and material diffusivities (Brown et al., 2013). This may explain discrepancies of factors of several between studies. Nevertheless, comparative studies which standardise around consistent definitions indeed find considerable disagreement in the literature (Traxler et al., 2011). We use $C = 10^3$ for this study because it provides good agreement with observations, but this remains a significant source of uncertainty.

in generally ignoring this effect.

6.4.5 Convective Mixing

Convection transports heat by means of bulk turbulent mixing of material. As usual we approximate the associated diffusivity via Mixing Length Theory as

$$D \approx h v_c \quad (6.32)$$

⁴⁰, where h is as defined in equation (3.19) and v_c is the convection speed. When convection is efficient (i.e. nearly adiabatic) the latter may be approximated as

⁴⁰ Böhm-Vitense 1958

$$v_c \approx \left(\frac{F_\star}{\rho} \right)^{1/3} \quad (6.33)$$

⁴¹, where F_\star is the heat flux. At the photosphere proper this is not a good approximation, as a significant fraction of the flux there is carried by radiation, but below this point the approximation typically becomes very good⁴². Furthermore because there may be other dynamical processes which mix material at the photosphere itself as the accreting material hits the star we suspect that this approximation does not result in our neglecting an important bottleneck to mixing.

⁴¹ Böhm-Vitense 1992

⁴² The error in this approximation falls exponentially in optical depth at low depths before hitting a (typically low) floor set by the radiative diffusivity.

Combining equations (6.32) and (6.33) we find

$$D \approx h \left(\frac{F_\star}{\rho} \right)^{1/3}.$$

This may also be written as

$$D \approx h c_s \left(\frac{F_\star}{\rho c_s^3} \right)^{1/3}.$$

Noting that $p \approx \rho c_s^2$ we find that

$$D \approx h c_s \left(\frac{F_\star}{p c_s} \right)^{1/3}.$$

We are interested in the diffusivity at the photosphere, which is given by equation (6.36) as

$$p \approx g \kappa^{-1},$$

so

$$D \approx h c_s \left(\frac{F_\star \kappa}{g c_s} \right)^{1/3}.$$

The sound speed is proportional to $T^{1/2}$, the scale height to T/g , and the flux to T^4 , so neglecting the effects of molecular weight variations

$$D \approx h_{\odot} c_{s,\odot} \left(\frac{F_{\odot} \kappa_{\odot}}{g_{\odot} c_{s,\odot}} \right)^{1/3} \left(\frac{T}{T_{\odot}} \right)^{8/3} \left(\frac{g}{g_{\odot}} \right)^{-4/3} \left(\frac{\kappa}{\kappa_{\odot}} \right)^{1/3}.$$

Making use of $L \propto M^{3.5}$ and ⁴³ $R \propto M$ we find that $T^4 \propto M^{3/2}$ and hence $T^{8/3} \propto M$. Similarly we find that $g \propto M^{-1}$, and hence

⁴³ Böhm-Vitense 1992

$$D \approx h_{\odot} c_{s,\odot} \left(\frac{F_{\odot} \kappa_{\odot}}{g_{\odot} c_{s,\odot}} \right)^{1/3} \left(\frac{M}{M_{\odot}} \right)^{7/3} \left(\frac{\kappa}{\kappa_{\odot}} \right)^{1/3}.$$

Using $\kappa_{\odot} \approx 10 \text{ cm}^2/\text{g}$ we find

$$D \approx 7 \times 10^{13} \text{ cm}^2 \text{ g}^{-1} \left(\frac{M}{M_{\odot}} \right)^{7/3} \left(\frac{\kappa}{10 \text{ cm}^2 \text{ g}^{-1}} \right)^{1/3}. \quad (6.34)$$

6.5 Application to observations

Sources of accretion onto stars include protoplanetary disks, debris disks, and evaporating or tidally disrupted planets or planetesimals. Intermediate-mass stars develop radiative envelopes fairly quickly, either on the Henyey track or immediately off the Hayashi track ⁴⁴. This allows the CAM framework to be applied to very young, disk-hosting early-type stars as well as main-sequence ones. Using known stellar parameters and the equations presented in the previous sections, one can calculate the fraction f_{ph} of accreted material in the stellar photosphere as a function of time and determine its composition. We detail the required equations and discuss various source types below.

⁴⁴ Palla 2012

We denote the observed fractional abundance of element X in the stellar photosphere with $(X/H)_{\text{obs}}$, and use analogous notation for the reference stellar composition⁴⁵ and recently accreted material⁴⁶. The normalization with hydrogen (H) is arbitrary and just the most common convention. The fraction of accreted material $f(r)$ is not a directly-observable quantity. Rather, what is observed is the composition of the photosphere, $(X/H)_{\text{obs}}$. For a given element X measured by a transition at wavelength λ , the inferred composition is

⁴⁵ “bulk”

⁴⁶ “acc”

$$\left(\frac{X}{H} \right)_{\text{obs}} = \frac{\int_0^R \rho e^{-\tau_{\lambda}(z)} \left[f(z) \left(\frac{X}{H} \right)_{\text{acc}} + (1 - f(z)) \left(\frac{X}{H} \right)_{\text{bulk}} \right] dz}{\int_0^R \rho e^{-\tau_{\lambda}(z)} dz},$$

where, $\tau_{\lambda}(z)$ is the optical depth at z for light of wavelength λ , $(X/H)_{\text{acc}}$ is the concentration of X in the accreted material, and $(X/H)_{\text{bulk}}$ is the

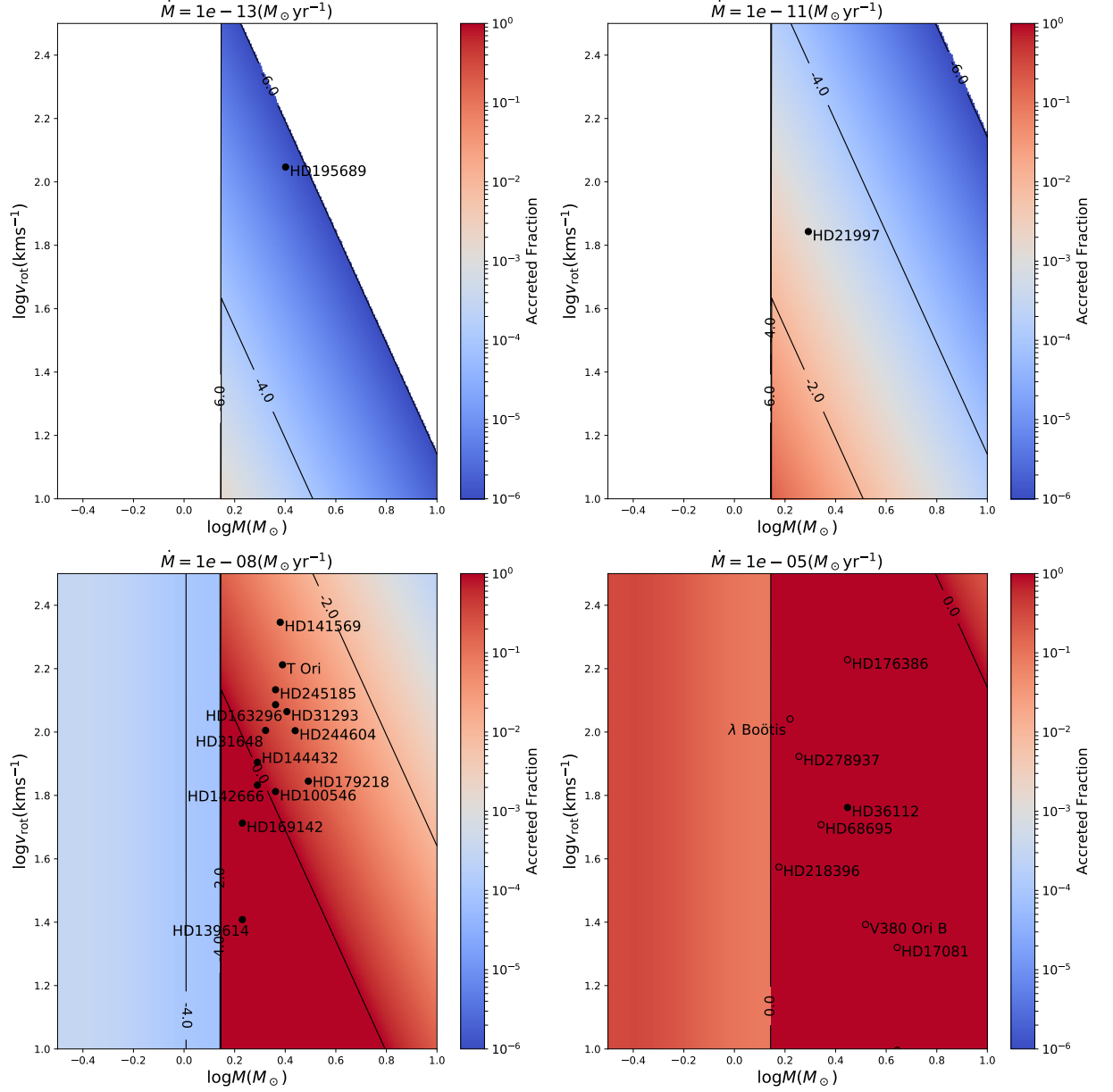


Figure 6.4: The photospheric abundance of accreted material is shown in colour for main sequence stars as a function of stellar mass (horizontal) and rotation speed (vertical). Four accretion rates are shown: $10^{-13} M_{\odot}/\text{yr}$ (top-left), $10^{-11} M_{\odot}/\text{yr}$ (top-right), $10^{-8} M_{\odot}/\text{yr}$ (bottom-left) and $10^{-5} M_{\odot}/\text{yr}$ (bottom-right). Each star is placed on the panel which most closely matches its measured or predicted accretion rate. Stars with no such data are placed on the bottom-right panel and shown with open circles. Contours correspond to factor of 100 increments. Regions with $f < 10^{-6}$ are shown in white. Note the sudden change around $1.4 M_{\odot}$, corresponding to the onset of a surface convection zone which greatly enhances photospheric mixing. The accretion rate for HD 245815 is due to Donehue & Brittain (2011).

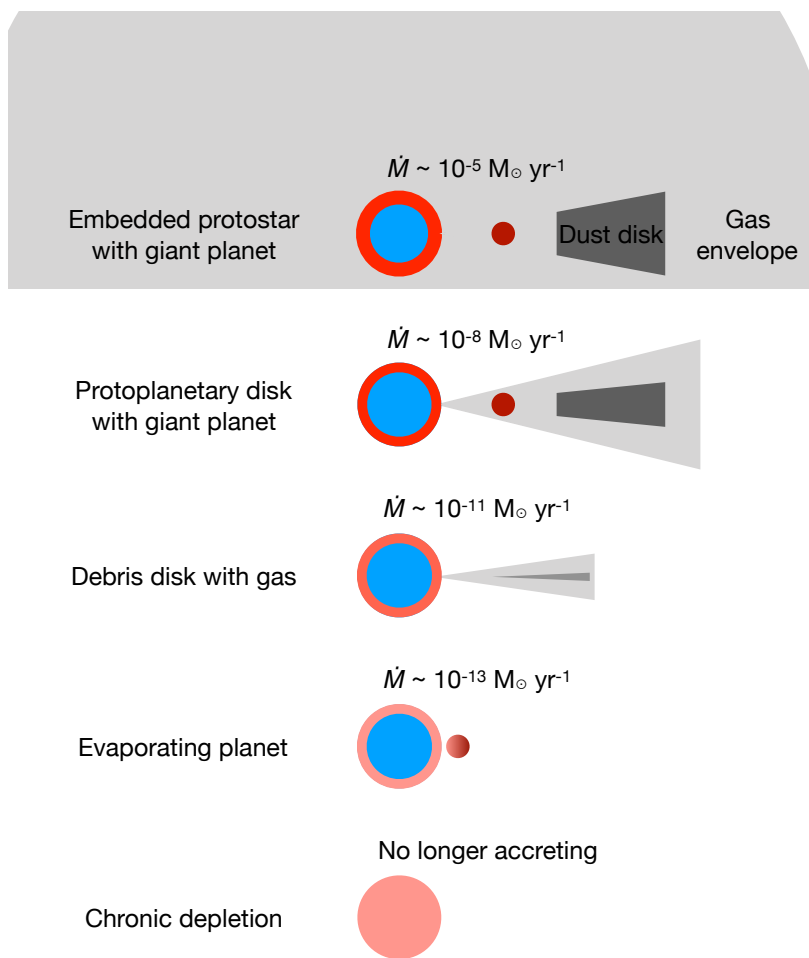


Figure 6.5: Evolutionary phases where an early-type star may display surface abundance anomalies due to ongoing or recent accretion. Red material on the star indicates accreted material, while blue indicates primordial composition. Planet-induced radial dust depletion can provide selective accretion in the disk phase. Chronic depletion refers to hypothetical signatures which remain for $\gtrsim 100$ Myr after accretion ceases. This figure was provided by Mihkel Kama.

concentration of X in the stellar material. That is, the composition which is measured is a transmittance-weighted average over the star.

A reasonable approximation to this average is to identify the depth z_{ph} of the photosphere for a given spectral feature. This depth is given by the implicit equation

$$\tau_{\lambda}(z_{\text{ph}}) = \int_{-\infty}^{z_{\text{ph}}} \kappa_{\lambda}(\rho(z), p(z)) \rho dz \approx 1, \quad (6.35)$$

where $\kappa_{\lambda}(\rho, p)$ is the opacity of material at pressure p and density ρ at wavelength λ . This expression in turn may be approximated as

$$\begin{aligned} \tau_{\lambda}(z_{\text{ph}}) &= \int_{-\infty}^{z_{\text{ph}}} \kappa_{\lambda}(\rho(z), p(z)) \rho dz \\ &\approx \int_0^{\Sigma(z_{\text{ph}})} \kappa_{\lambda}(\rho(z), p(z)) d\Sigma \\ &\approx \int_0^{p(z_{\text{ph}})} \kappa_{\lambda}(\rho(z), p(z)) g^{-1} dp \\ &\approx \kappa_{\lambda}(\rho_{\text{ph}}, p_{\text{ph}}) p_{\text{ph}} g^{-1}, \end{aligned}$$

where we have made use of $d\Sigma = \rho dz$ and $p \approx \Sigma g^{-1}$ near the photosphere. As T is nearly constant throughout the photosphere, the equation of state determines ρ from p and so equation (6.35) may be written simply as

$$\kappa_{\lambda}(p_{\text{ph}}) p_{\text{ph}} g^{-1} \approx 1.$$

To leading order the dependence on λ may be dropped and κ may be approximated by the Rosseland mean opacity, resulting in

$$\kappa(p_{\text{ph}}) p_{\text{ph}} g^{-1} \approx 1. \quad (6.36)$$

The solution to this equation yields a photospheric pressure, which may be converted to a depth using the equation of hydrostatic equilibrium $dp = -\rho g dz$. The photospheric fraction f_{ph} is then given by equation (6.21), which may be approximated as

$$f_{\text{ph}} \approx \min\left(1, \frac{\dot{M} h}{4\pi R^2 \rho_{\text{ph}} D_{\text{ph}}}\right).$$

Note that we have used the form for cases in which $\rho^2 D$ increases with depth, as this is the only one relevant for the mixing mechanisms considered in the previous section. A further approximation makes use of $h \ll R$ to write

$$M_{\text{ph}} \approx 4\pi R^2 h \rho_{\text{ph}},$$

where M_{ph} is the mass of the photosphere, which typically varies from $10^{-12}M_{\odot}$ for Sun-like stars to $10^{-10}M_{\odot}$ in more massive stars. As such,

$$f_{\text{ph}} \approx \min\left(1, \frac{\dot{M}}{M_{\text{ph}}} \left(\frac{h^2}{D_{\text{ph}}}\right)\right). \quad (6.37)$$

For context h is typically of order 10^7 cm and D_{ph} varies between $10^2 \text{ cm}^2 \text{ s}^{-1}$ when molecular diffusion dominates and $10^{14} \text{ cm}^2 \text{ s}^{-1}$ for stars with surface convection zones. Finally, this fraction is related to the observed abundance of element X by the relation

$$\left(\frac{\text{X}}{\text{H}}\right)_{\text{obs}} = f_{\text{ph}} \left(\frac{\text{X}}{\text{H}}\right)_{\text{acc}} + (1 - f_{\text{ph}}) \left(\frac{\text{X}}{\text{H}}\right)_{\text{bulk}}. \quad (6.38)$$

The accreted fraction of the photosphere asymptotes rapidly to a constant except in the case where rotational mixing dominates, in which case there is a logarithmic correction in time. Fig. 6.4 shows the fractional abundance of accreted material in the photosphere, neglecting the logarithmic correction, for main sequence stars as a function of mass and rotation speed for accretion rates $\dot{M}_{\text{acc}} = 10^{-5}$, 10^{-8} , 10^{-11} , and $10^{-13} M_{\odot}/\text{yr}$. These rates represent accretion from the envelope of a protostar, a protoplanetary disk, a gas-rich debris disk, and an evaporating planet, respectively. Various evolutionary stages where a star may show surface abundance anomalies due to accretion are shown along with the relevant order-of-magnitude accretion rate in Fig. 6.5. We also include chronic (long-lived) depletion, which may occur if the total mass fraction accreted from material with an abundance anomaly is sufficient that a residual signature remains even after complete mixing, or if the mixing happens on a long timescale ($t_{\text{mix}} \gtrsim 100 \text{ Myr}$).

The abundance of X in the mass reservoir providing the accretion is

$$\left(\frac{\text{X}}{\text{H}}\right)_{\text{acc}} = \frac{1}{f} \left(\frac{\text{X}}{\text{H}}\right)_{\text{obs}} - \frac{1-f}{f} \left(\frac{\text{X}}{\text{H}}\right)_{\text{bulk}} \quad (6.39)$$

Aside from calculating f , we need to assume a reference point for the bulk stellar abundances. Reasonable choices include the composition of the Sun⁴⁷ or an average of nearby early-type stars⁴⁸. In the current work, we favour the former for accuracy and precision, but the latter choice may be a better reference because it was obtained using spectroscopic methods nearly identical to those used in studies of protoplanetary disk hosting early-type stars (e.g. Acke & Waelkens, 2004; Folsom et al., 2012) and in our own ongoing observational efforts.

We now consider four source types where we can obtain new insight

⁴⁷ Lodders 2003; Asplund et al. 2009

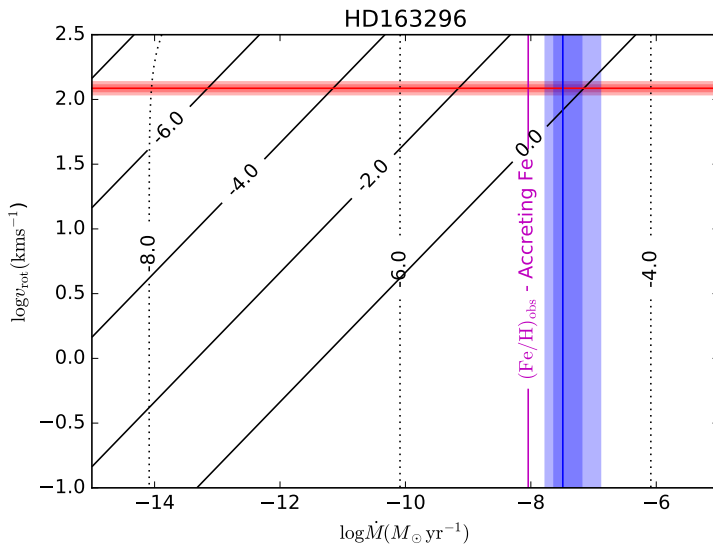
⁴⁸ Fossati et al. 2011; Martin et al. 2017

on the accreting material:

1. Protoplanetary disks (e.g. HD 163296, HD 100546)
2. Debris disks (e.g. HD 141569 A, HD 21997)
3. Evaporating planets (e.g. HD 195689/KELT-9)
4. λ Boötis stars

We accompany each of the example stars with a figure; Figs. 6.6, 6.7, 6.8, 6.9, and 6.10 respectively. Input and calculated parameter values are summarized in Table 6.1. The figures show the newly accreted photospheric mass fraction, f_{ph} , calculated from Eq. 6.37⁴⁹. As a comparison with this theoretical calculation, f_{ph} can also be estimated from observations using the measured stellar rotation rate, v_{rot} , and the measured or predicted accretion rate⁵⁰, \dot{M}_{acc} . Observed v_{rot} values are shown for each star, while \dot{M}_{acc} is either observational, or predicted from models or theory.

Where available, e.g. for HD 100546 (Fig. 6.7), the observed $(\text{Fe}/\text{H})_{\text{obs}}$ is used to calculate a lower limit⁵¹ on f_{ph} , which corresponds to the fraction of the photosphere that needs to be replaced with pure H in order to decrease (Fe/H) to the observed level. If $(\text{Fe}/\text{H})_{\text{obs}}$ is super-solar, e.g. for HD 163296, we obtain instead an upper limit⁵² on f_{ph} under the assumption that the accretion flow contains only Fe. An analogous reasoning would apply to any other element, here we use iron because it is easy to determine and indicative of a depletion of dust from the accreted material. Specific elemental signatures may be different in specific cases, depending on the origin of the accreted material.



⁴⁹ solid black lines

⁵⁰ intersection of red horizontal and blue vertical lines

⁵¹ purple diagonal line

⁵² purple vertical line

Figure 6.6: HD 163296 hosts a full protoplanetary disk. We show the theoretical accreted photospheric mass fraction f_{ph} from accreting hydrogen-rich material (solid black lines) or accreting pure Fe (dotted), f_{ph} from the observed accretion and rotation rate (intersection of horizontal red and vertical blue bars, to be compared with the solid black lines), and an upper limit from the observed super-solar (Fe/H) of the star (vertical purple line, to be compared with the dotted black lines). The $\pm\sigma$ and $\pm 2\sigma$ contours for $\log v_{\text{rot}}$ are shown in red while those for $\log \dot{M}_{\text{acc}}$ are shown in blue.

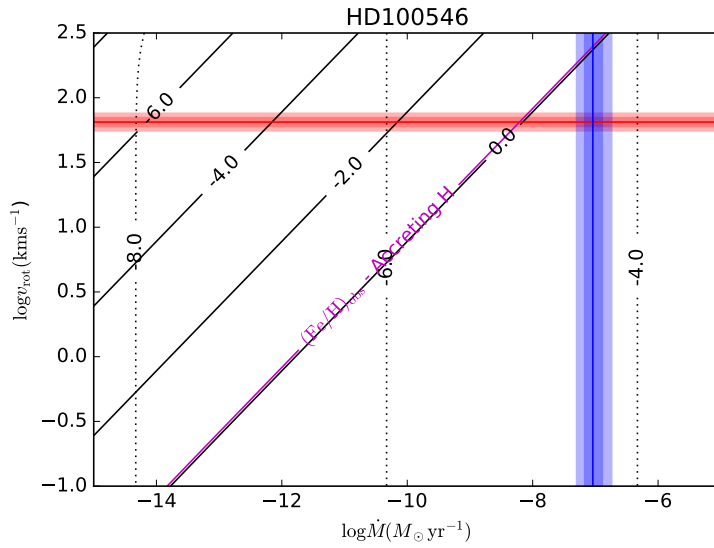


Figure 6.7: HD 100546 hosts a transitional protoplanetary disk. We show the theoretical accreted photospheric mass fraction f_{ph} from accreting hydrogen-rich material (solid black lines) or accreting pure Fe (dotted, not relevant in this source), f_{ph} from the observed accretion and rotation rate (intersection of horizontal red and vertical blue bars, to be compared with the solid black lines), and a lower limit from the observed low (Fe/H) of the star (diagonal purple line, to be compared with the solid black lines and the red and blue bars). The $\pm\sigma$ and $\pm 2\sigma$ contours for $\log v_{\text{rot}}$ are shown in red while those for $\log \dot{M}_{\text{acc}}$ are shown in blue.

| Star | Type | $\log(\frac{\text{Fe}}{\text{H}})_{\text{obs}}$ | v_{rot} (km s^{-1}) | Age (Myr) | \dot{M}_{acc} ($M_{\odot} \text{ yr}^{-1}$) | $\log t_{\text{ph}}$ (s) | $\log f$ (Pred.) | $\log f$ (Pred. Heavy) |
|-----------|--|---|--|------------------------|---|-----------------------------|---------------------|---------------------------|
| HD 163296 | A3 | $-4.39^{+0.15}_{-0.15}$ | 122.0 ± 3.0 | $7.56^{+2.17}_{-2.17}$ | $-7.49^{+0.3}_{-0.14}$ | 3.9 | -0.33 | -4.70 |
| HD 100546 | Ao | $-5.67^{+0.08}_{-0.08}$ | 64.9 ± 2.2 | $7.02^{+1.49}_{-1.49}$ | $-7.04^{+0.15}_{-0.13}$ | 3.5 | +0.00 | -4.45 |
| HD 141569 | B9.5 | $-5.25^{+0.32}_{-0.32}$ | 222.0 ± 7.0 | $9.0^{+4.5}_{-4.5}$ | $-7.65^{+0.47}_{-0.33}$ | 3.7 | -0.92 | -4.76 |
| HD 21997 | A3 | -4.47* | 69.7* | 30.0 | -10.4^{\dagger} | 4.3 | -2.40 | -5.98 |
| HD 195689 | Ao | $-4.53^{+0.20}_{-0.20}$ | 111.4 ± 1.3 | 300.0 | $-13.0^{+2.0\dagger}_{-2.0}$ | 3.6 | -5.98 | -7.52 |
| Star | Notes | | | | | | | |
| HD 163296 | Folsom et al. (2012); Fairlamb et al. (2015) | | | | | | | |
| HD 100546 | Folsom et al. (2012); Fairlamb et al. (2015); Kama et al. (2016) | | | | | | | |
| HD 141569 | Folsom et al. (2012); Fairlamb et al. (2015) | | | | | | | |
| HD 21997 | Vigan et al. (2012); Kral et al. (2016, 2017); Netopil (2017); Kral (2017) | | | | | | | |
| HD 195689 | Gaudi et al. (2017) | | | | | | | |

Table 6.1: Stars chosen to demonstrate the application of CAM to study the composition of accreting material. t_{ph} is h^2/D evaluated at the photosphere. The predicted $\log f$ was calculated using equation (6.21), with molecular weight gradients incorporated in the heavy case on the assumption of Fe accretion. * – $(\text{Fe}/\text{H})_{\text{obs}}$ for HD 21997 was determined photometrically and no errorbar was reported. Likewise no errorbar was reported for v_{rot} for this star. \dagger – Accretion rates predicted from models. References are shown in the lower half of the table.

6.5.1 Protoplanetary disks

Because our method allows us to link the chemistry of the photospheres of early-type stars to that of their circumstellar material it is particularly powerful when applied to protoplanetary disk hosts. In particular there are three immediate applications which can likely be achieved with existing data. First, we can measure the mass ratio of gas to dust in these systems by determining how refractory-depleted, or enhanced, the accreting material is relative to the bulk of the star. Secondly, we can determine the fraction of each element locked in dust and other refractory particles by determining the variation of this depletion across different species. Finally in the subset of these stars which are young and still accreting at high rates we can determine whether or not they have developed a radiative envelope⁵³. We now discuss each of these in turn.

1. Gas-to-dust mass ratio in the inner disk:

For young⁵⁴ early-type stars there is a known correlation between the presence of dust-depleted gaps in protoplanetary disks and a depletion of refractory elements in the stellar photosphere⁵⁵. If the photosphere is entirely replaced by accreted material this depletion corresponds to $\Delta_{\text{g/d}}$ values as high as⁵⁶ 1000. Applying our formalism we can compute f_{ph} and find that it is somewhat less than one in several systems. As a result we expect to find some $\Delta_{\text{g/d}}$ values much larger than before. This is in better agreement with the dust depletions directly determined from spatially resolved continuum observations⁵⁷.

For instance HD 163296⁵⁸ and HD 100546⁵⁹ host a full and a transitional disk and we predict $f_{\text{ph,HD 163296}} = 0.47$ and $f_{\text{ph,HD 100546}} =$

⁵³ Early-type stars are expected to be convective initially before becoming radiative as they move onto the main-sequence.

⁵⁴ 1–10 Myr old

⁵⁵ Kama et al. 2015

⁵⁶ Kama et al. 2015

⁵⁷ e.g. van der Marel et al. (2015, 2016), though that data is limited by the fact that the gas surface density is measured indirectly via CO

⁵⁸ Fig. 6.6

⁵⁹ Fig. 6.7

1.0 respectively. These high theoretical⁶⁰ $f_{\text{ph,HD 163296}} = 0.47$ and $f_{\text{ph,HD 100546}} = 1.0$ confirm that the photospheric abundance pattern closely follows the abundance pattern of the accreting material. For the latter the calculations in Kama et al. (2015) are correct, while that study underestimates the gas-to-dust ratio of the former by a factor of $(0.47)^{-1} \approx 2$.

A peculiarity of HD 163296 is that it is actually enhanced in several refractory elements relative to solar⁶¹. This means that either its bulk composition differs from the solar reference or else $(\text{Fe}/\text{H})_{\text{acc}} \gtrsim (\text{Fe}/\text{H})_{\odot}$. The former is possible but it would be odd for the system to be enhanced specifically in refractory elements through a means other than accretion. The latter therefore seems more likely, and implies that the relevant features to examine in Fig. 6.6 are the theoretical f_{ph} from pure-Fe accretion⁶² and the upper limit on f_{ph} from the observed photospheric abundance $(\text{Fe}/\text{H})_{\text{obs}}$. An enhancement of refractories is consistent with disk models which suggest the disk material around HD 163296 is gas-poor⁶³. In other words, this system is preferentially accreting dust.

The analysis of HD 100546 is more straightforward because the observed abundance of refractory elements is low⁶⁴. Following our predictions for H-rich accretion in Fig. 6.7⁶⁵ and the observed rotation and accretion rate constraints⁶⁶ gives $f_{\text{ph}} = 1.0$ and $(\text{Fe}/\text{H})_{\text{acc}} = (\text{Fe}/\text{H})_{\text{obs}}$. The observed iron abundance is a factor of 10 below solar and so gives $\Delta_{\text{g/d}} = 1000$, consistent with the structure of the inner dust cavity in gas-dust disk models⁶⁷.

2. The refractory vs volatile fraction of elements:

As we have discussed, the most refractory elements⁶⁸ are typically depleted by a factor of several in the photospheres of stars with a transitional disk⁶⁹. Equation (6.39) allows us to infer the abundances of these elements in the accretion stream from those in the photosphere. We have argued that the accretion stream is depleted because it preferentially contains gas rather than dust. Hence its composition is reflective of the fraction of each species which is in dust versus the gas phase. By comparing the depletion factors of different elements we expect to be able to determine these fractions both for various species and for various kinds of disks, which may perform different kinds of chemical processing and thereby result in different refractory fractions.

Preliminary data indicate that this approach is viable. Transitional disks have extended radial zones where the surface density of large particles is reduced by up to several orders of magnitude. Furthermore

⁶⁰ See Table 6.1.

⁶¹ Folsom et al. 2012

⁶² dotted black lines

⁶³ $\Delta_{\text{g/d}} \approx 20$, Boneberg et al. (2016)

⁶⁴ For instance $(\text{Fe}/\text{H})_{\text{obs}} = -5.67$ (Kama et al., 2016), well below solar.

⁶⁵ solid black lines

⁶⁶ red and blue bars

⁶⁷ Bruderer et al. 2012; Kama et al. 2016

⁶⁸ i.e. those with the greatest condensation temperature

⁶⁹ Kama et al. 2015

while the most volatile elements, such as C and O, have similar photospheric abundances for all disk-hosting early-type stars regardless of the disk structure ⁷⁰, elements of intermediate sublimation temperature may be sensitive to the structure of the disk and the kinds of chemical processing it performs. One such element which we shall address in the future is sulfur, which is predominantly refractory in primitive solar system meteorites, but whose refractory fraction in protoplanetary disks has not yet been observationally determined.

⁷⁰ Kama et al. 2015

3. Identification of convective envelopes:

A tantalising possibility is that it may be possible to probe the evolution of young early-type stars. It is usually possible to measure the photospheric abundances ⁷¹ of *and* accretion rates onto these stars ⁷². When the accreting material has a composition significantly different from the bulk stellar material these two pieces of information suffice to constrain the diffusivity in the outer portions of the star. This is important in stars with masses above $1.4M_{\odot}$ which are expected to be fully convective when young and become radiative in their outer layers as they move on to the main-sequence. Because the development of a radiative zone entails a dramatic reduction in diffusivity near the photosphere the change to a radiative envelope ought to be detectable even in highly uncertain measurements. Hence it may be possible to place strong constraints on the ages of certain stars, which is otherwise quite difficult to do ⁷³.

⁷¹ Acke & Waelkens 2004; Folsom et al. 2012

⁷² Mendigutía et al. 2011; Fairlamb et al. 2015

To understand this quantitatively, recall that the fraction of accreted material in the photosphere is given by equation (6.37) as

⁷³ Tout et al. 1999; Soderblom et al. 2014

$$f_{\text{ph}} \approx \frac{\dot{M}}{M_{\text{ph}}} \left(\frac{h^2}{D_{\text{ph}}} \right).$$

For a species where the stellar and accreted material have very different abundances this fraction is readily measured and closely related to any depletion/enhancement by equation (6.38). Inserting equation (6.34) we find

$$f_{\text{ph}} \approx 10s \frac{\dot{M}}{M_{\text{ph}}} \left(\frac{M}{M_{\odot}} \right)^{5/12} \left(\frac{\kappa}{10\text{cm}^2\text{g}^{-1}} \right)^{-1/3}. \quad (6.40)$$

The upshot of this being so much less than any of the mechanisms active in radiative stars is that it provides a robust means of determining which stars have formed their radiative envelopes and which ones are still fully convective.

If f_{ph} can be measured or bounded and is found to be much greater

than Eq. (6.40) suggests – such as would be inferred if a significant depletion of refractories is found – mixing must be much less efficient than convection and so the upper regions of the star must be radiative. Similarly if f_{ph} is found to be consistent with this equation then this strongly suggests a convection zone. Central to the determination either way is that the accreting material must be known to have a different composition from the bulk stellar material. This could be inferred from observations of the accretion disk. For example a disk might be seen to have dust depletion in its inner regions. If such a disk were seen around a star with a high abundance of refractory elements that would be good evidence that the recent accretion contained a significant dust component and hence was very different from the stellar bulk in composition.

The power of this test in the face of the typically order of magnitude uncertainty in the accretion rates and up to a factor of two in abundances comes from the massive difference in mixing efficiency between radiative mechanisms and bulk turbulent convection.

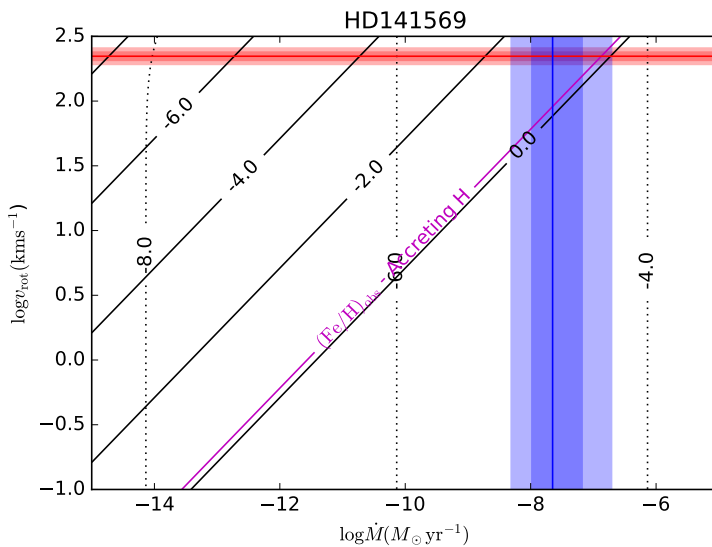


Figure 6.8: HD 141569 hosts a hybrid disk. We show the theoretical accreted photospheric mass fraction f_{ph} from accreting hydrogen-rich material (solid black lines) or accreting pure Fe (dotted, not relevant in this source), f_{ph} from the observed accretion and rotation rate (intersection of horizontal red and vertical blue bars, to be compared with the solid black lines), and a lower limit from the observed low (Fe/H) of the star (diagonal purple line, to be compared with the solid black lines and the red and blue bars). The $\pm\sigma$ and $\pm 2\sigma$ contours for $\log v_{\text{rot}}$ are shown in red while those for $\log \dot{M}_{\text{acc}}$ are shown in blue.

6.5.2 Debris disks

Debris disks are generally depleted in gas, characterised by a gas-to-dust mass ratio $\Delta_{\text{g/d}} \lesssim 1$. Because of this the dust dynamics are decoupled from those of the gas. Recently it has been found that large amounts of carbon and oxygen can be present in these disks in the gas phase, either in the form of CO molecules, or neutral or ionized C or O atoms. Such disks

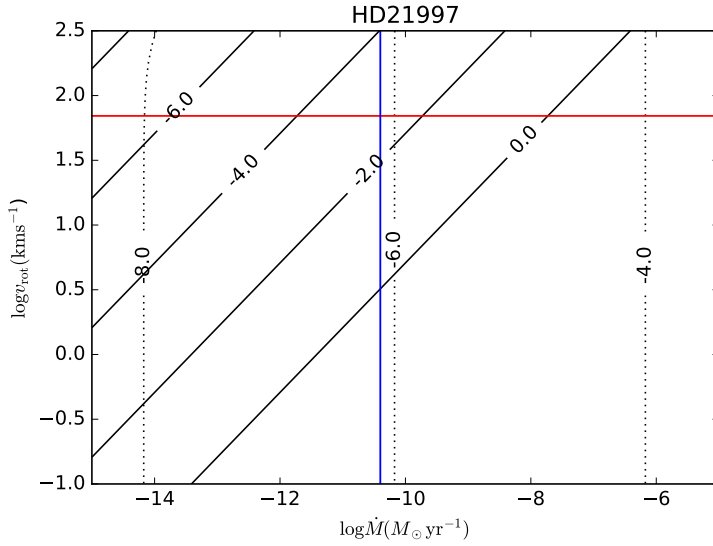


Figure 6.9: HD 21997 hosts a hybrid disk. The high v_{rot} , and the accretion rate predicted by the Kral et al. (2016, 2017) model, $\dot{M}_{\text{acc}} \sim 10^{-11} M_{\odot} \text{ yr}^{-1}$, yields $f_{\text{ph}} = 4 \times 10^{-3}$. We show the theoretical accreted photospheric mass fraction f_{ph} from accreting hydrogen-rich material (solid black lines) or accreting pure Fe (dotted), f_{ph} from the model-predicted accretion and observed rotation rate (intersection of horizontal red and vertical blue bars). Note that no uncertainties are given for v_{rot} because none were reported from observations, and likewise none are given for \dot{M}_{acc} because none were given in the predicted rates. If the accreted material is largely C and O, the stellar photospheric abundances of these elements may be dominated by outgassed debris disk material.

with gas are found around early-type⁷⁴ stars and fall into two categories, namely gas-poor and gas-rich⁷⁵. In the gas-poor disks the C and O gas mass can be explained with outgassing of CO and H₂O from exocomets, such as β Pic, HD 181327, and Fomalhaut. By contrast the gas-rich debris disks⁷⁶ such as HD 141569 A and HD 21997 may be primordial, gas-rich disks in a late stage of dissipation⁷⁷. For our purposes a key difference between the two types is that the hybrid disks are likely still dominated by H₂, while in the outgassing disks C, O, and H are likely comparable in number density because the hydrogen comes from H₂O photodissociation and the C/O ratio is not far from unity.

Models of exocometary gas production and viscous disk evolution predict the accretion rate of C- and O-rich gas onto the host star to be in the range of 10^{-13} to $10^{-11} M_{\odot} \text{ yr}^{-1}$ ⁷⁸. Using these and observed rates where available we can calculate the fraction f_{ph} of the photosphere composed of accreted material. For instance HD 141569 A hosts a hybrid disk and is observed to be heavily accreting. As shown in Fig. 6.8 we predict $f_{\text{ph}} = 0.12$ despite this star being a rapid rotator⁷⁹. In comparison, the observed photospheric iron abundance gives a lower limit of $f_{\text{obs}} \geq 0.9$. Because the errorbars on \dot{M}_{acc} are so large⁸⁰, the theoretical and observationally constrained f are consistent and suggest that a large fraction of the photosphere is composed of freshly accreted, refractory-poor material. This implies that the bulk of the measured accretion is indeed composed of hydrogen and other volatile elements, indicating that at least the inner disk is relatively gas-rich. This conclusion is supported by the fact that a large-scale CO gas disk has been resolved with ALMA⁸¹.

⁷⁴ A, F

⁷⁵ Both poor and rich are relative terms, because all debris disks are gas-poor relative to, say, protostellar or protoplanetary disks.

⁷⁶ i.e. “hybrid” disks

⁷⁷ Moór et al. 2011; Péricaud et al. 2017; Marino et al. 2016; Kral et al. 2017; Hughes et al. 2017; Matrà et al. 2017a,b; Moór et al. 2017

⁷⁸ Kral et al. (2016, 2017) and private communication

⁷⁹ At such velocities rotational mixing dominates and is expected to be very effective.

⁸⁰ The error in our prediction of f_{ph} is dominated by that in the accretion rate because that is much less certain than any of the other system parameters.

⁸¹ Flaherty et al. 2016; White et al. 2016

By contrast the hybrid-disk system HD 21997 has no reported detection of accretion onto the star. Unfortunately a precise, spectroscopic $(\text{Fe}/\text{H})_{\text{obs}}$ was not immediately available from the literature. We use an \dot{M}_{acc} value from the Kral et al. (2016) model to obtain $f_{\text{ph}} = 4 \times 10^{-3}$, shown in Fig. 6.9,. The disk in this system is thought to be gas-rich, with a large amount of primordial hydrogen remaining. The photospheric abundances of the star offer a way to distinguish such a primordial origin of the gas from the cometary outgassing scenario. In the latter case the volatile elements C and O would be accreted in large quantities with barely any hydrogen, while in the primordial case the accretion would be hydrogen-dominated. Hence measuring the stellar C and O abundances may differentiate between the two scenarios. Because we expect the accreted mass fraction of this system to be quite small this test may prove challenging, but it may prove viable should a similar system be found with either slower rotation or faster accretion.

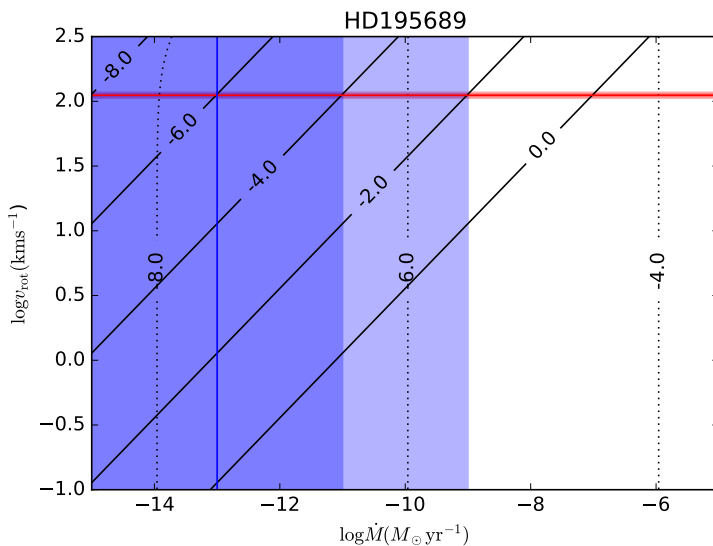


Figure 6.10: HD 195689 hosts the hottest known Hot Jupiter, with $T_{\text{eq}} = 4600 \text{ K}$ (KELT-9b, Gaudi et al., 2017). We show the theoretical accreted photospheric mass fraction f_{ph} from accreting hydrogen-rich material (solid black lines) or accreting pure Fe (dotted), and f_{ph} from the model-predicted accretion and observed rotation rate (intersection of horizontal red and vertical blue bars). The $\pm\sigma$ and $\pm 2\sigma$ contours for $\log v_{\text{rot}}$ are shown in red while those for $\log(\dot{M}_{\text{acc}})$ are shown in blue.

6.5.3 Evaporating or disrupted planets

The environment near a star poses several dangers to planets. First, heavy ultra-violet⁸² irradiation can gradually cause the planet to evaporate. Secondly, at sufficiently close distances the planet may undergo Roche lobe overflow or, depending on the circumstances, more violent tidal disruption. In either case some or most of the planetary material will accrete onto the star, where it may potentially be observed as photospheric contamination. This possibility was first suggested by Jura (2015) for early-type stars as a way to explain why stars without any apparent circumstellar mass reservoir

⁸² UV

display the λ Boö abundance anomaly.

Some fraction of the UV flux onto a planet is turned into heat and dissipated radiatively along with the bulk of the incident stellar flux. The rest serves to drive a wind which escapes the planet ⁸³. At high UV flux⁸⁴ the mass-loss rate is given by

$$\dot{M}_{\text{UV}} \approx 4 \times 10^{12} \left(\frac{F_{\text{UV}}}{F_0} \right)^{1/2} \left[\frac{\text{g}}{\text{s}} \right]. \quad (6.41)$$

The best candidate for this mechanism found thus far is HD 195689b⁸⁵. Using Eq. 6.41 and adopting $L_{\text{UV}} \approx 10^{-3} L_{\odot}$ for the UV-luminosity of the host star, we find $\dot{M}_{\text{UV}} = 5.7 \times 10^{12} \text{ g s}^{-1}$ or $10^{-13} M_{\odot} \text{ yr}^{-1}$. In Fig. 6.10 we show the photospheric mass fraction of accreted material for this accretion rate with an assumed relative uncertainty of 10^2 in both directions. Taking the mean over $\log \dot{M}$, we find $f_{\text{ph}} = 10^{-6}$. For the highest potential planetary evaporation rate, $\dot{M}_{\text{acc}} = 10^{-11} M_{\odot} \text{ yr}^{-1}$, we find $f_{\text{ph}} \approx 3 \times 10^{-5}$. If the accreting material is similar to solar in composition this is too-small a signal to detect with current instruments. On the other hand if the material is very different from solar it may lead to a detectable enhancement in the stellar photospheric abundances of certain elements.

HD 195689b⁸⁶ and HD 185603b⁸⁷ are the only Hot Jupiter planets known to-date to orbit main sequence A0 stars ⁸⁸. As the *KELT* and *MASCARA* programs continue more such heavily irradiated exoplanets will likely be found. Applying our method to their host stars may provide new information on the mass loss rate and elemental abundance ratios of such planets. In particular, it may be feasible to obtain a completely independent measurement of the C/O ratio in the atmosphere of giant planets⁸⁹.

Earth-like or Super-Earth planets can also undergo disruption or evaporation. Such accretion may produce a detectable signal despite the relatively small amount of mass involved because the accreted material would consist mostly of refractory elements, which generally less abundant than volatiles in stars. For instance accreting a $1 M_{\oplus}$ planet over 1 Myr yields an average accretion rate $\dot{M}_{\text{acc}} = 10^{-12} M_{\odot} \text{ yr}^{-1}$. This could produce a factor of several relative enhancement of the abundances of some refractory elements, and such a signature would remain visible in the photosphere for 0.1 to 1 Myr.

It is important to emphasise that we are talking about accretion of material onto the surface of a star and its subsequent mixing into the bulk, rather than a purely bulk effect. The latter has been studied in various contexts but generally produces somewhat smaller signals because the bulk

⁸³ Murray-Clay et al. 2009

⁸⁴ $F_{\text{UV}} > F_0$, where $F_0 = 450 \text{ erg cm}^{-2} \text{ s}^{-1}$

⁸⁵ Also known as KELT-9b, this was the first planet found around a B9/A0 star (Gaudi et al., 2017).

⁸⁶ i.e. MASCARA-2b

⁸⁷ i.e. KELT-20b

⁸⁸ Talens, G. J. J. et al. 2018; Lund et al. 2017

⁸⁹ The C/O ratio is noteworthy as a potential tracer of planetary migration. This is because its distribution in protoplanetary disks is heavily influenced by the condensation properties of a variety of ices which freeze out of the gas at different distances from the host star. The inflation mechanism discussed in Chapter 5 predicts that hot Jupiters which form in regions where tidal heating is important are more likely to be inflated than those which formed further out because the former are more likely to form and maintain interior radiative zones. Hence better measurements of the C/O ratio may serve as a test of that mechanism.

of the star heavily dilutes the planetary material. For instance it has been suggested that elemental abundances in solar-like stars with planets are modified by a large fraction of refractories being locked in rocky planets or by the accretion of entire giant planets ⁹⁰. Other studies suggest a relation between the overall metallicity of the system and the masses of its planets ⁹¹. Our method, by contrast, focuses on a snapshot in time of the composition of material currently or recently (≤ 1 Myr) lost from a planet and accreted onto its host star.

6.5.4 λ Boötis Stars

As discussed previously, roughly $\sim 2\%$ of B to mid-F type stars exhibit significant photospheric depletion of refractory elements ⁹². This is known as the λ Boö phenomenon. A natural explanation for this abundance pattern is that it arises in stars which accrete material which has been processed in a disk. This processing can separate volatiles from refractories, so that if the accreting material is mainly formed of gas it is depleted in refractories and transfers that signature to the star.

The challenge for an explanation based on current disk accretion is that only some stars with the λ Boö phenomenon are found to have disks. These tend to be young ⁹³ stars with protoplanetary disks, but the phenomenon has been observed in stars as old as 1 Gyr, which is on the order of their main-sequence lifetimes ⁹⁴. Some older systems have been found to host debris disks ⁹⁵, but the fraction of confirmed debris disks was found to be statistically indistinguishable from that in non- λ Boö sources ⁹⁶. Hence if the phenomenon in old systems is a result of accretion from a disk then additional considerations are needed to explain why only some stars with disks are refractory-depleted.

Among protoplanetary disk hosts the λ Boö phenomenon is most often seen in stars of types B to mid-F ⁹⁷. Despite this the refractory element depletion does not correlate with stellar age ⁹⁸. This suggests two important conclusions. First, most young λ Boö stars can indeed be explained by temporary selective accretion of gas rather than dust ⁹⁹, rather than by some longer-term process. Indeed it has been shown that in young stars the λ Boö phenomenon is a result of the star hosting a dust-depleted “transitional” disk ¹⁰⁰. Secondly, a small fraction of λ Boö stars appear to survive to old age with a long-lasting or chronic depletion. A possible explanation is that the transitional disk phase for such λ Boö stars was early and long-lasting enough for the dust-poor material to compose a significant fraction of the total mass of the star.

⁹⁰ e.g. Meléndez et al. (2009); Ramírez et al. (2009); Wilson et al. (2018).

⁹¹ Buchhave et al. 2014

⁹² Paunzen & Gray 1997; Paunzen et al. 2001; Paunzen 2001; Murphy et al. 2015

⁹³ ~ 0.1 to 10 Myr

⁹⁴ Murphy & Paunzen 2017

⁹⁵ Draper et al. 2016

⁹⁶ Gray et al. 2017

⁹⁷ In this window $\gtrsim 30$ per-cent exhibit refractory depletion (Folsom et al., 2012).

⁹⁸ Iliev & Barzova 1995

⁹⁹ Venn & Lambert 1990

¹⁰⁰ Kama et al. 2015

Two alternative explanations emerge in the context of this work. First, it is possible that the transitional disk phase lasted for a substantial fraction of the age of the star but did not result in the accretion of a substantial fraction of its mass. In that case the accretion signatures would still be apparent in its photosphere according to equation (6.26) even though the accretion might have ceased long ago. Secondly, and potentially in better agreement with the fraction of stars observed to have such accretion, it is possible that the transitional disk phase was both short relative to the age of the star and provided comparatively little material, but that the diffusivity in the star fell significantly towards the end of the accretion period. In that case equation (6.27) indicates that the time over which the accreted material should be observable in the photosphere ought to be enhanced by a factor of $D_{\text{old}}/D_{\text{new}}$.

Under this second story, long-term accretion results in material mixing to significant depths, as Σ_0 may become quite large. At such depths the dominant mechanism for mixing would be rotational mixing¹⁰¹. If the star magnetically breaks¹⁰² from a rotation rate of Ω_{old} to one of Ω_{new} towards the end of the accretion period then the timescale over which the accreted material ought to be observable is of order

$$t_{\text{obs}} \approx t_{\text{acc}} \left(\frac{\Omega_{\text{old}}}{\Omega_{\text{new}}} \right)^2.$$

This possibility is particularly interesting because during the accretion process the disk may transfer significant quantities of angular momentum to the star, even bringing it to near breakup with relatively modest amounts of material¹⁰³, and so it is quite natural for the star to spin up during the transitional disk phase and spins down shortly afterwards. If the spin-down occurs on the same time-scale as the accretion or faster and if the spin-down is significant then the historical accretion could remain observable for considerably longer than would otherwise be expected. This is likely not long enough for the prototypical λ Boö but with either a somewhat longer accretion phase or a more severe spin-down may explain at least some of the observed systems.

6.6 Discussion and Outlook

We have presented a new means for relating the observed photospheric composition of a star to its bulk composition and that of the accreting material. This is done via equations (6.37), (6.38), and (6.39). Where the stellar parameters and the accretion rate are observationally constrained,

¹⁰¹ e.g. meridional flows

¹⁰² When the star is young it could well have both winds and a fossil magnetic field.

¹⁰³ On the order of $0.05M_{\odot}$ (Matrozi et al., 2017) would suffice.

we find very good agreement between the observed photospheric composition and our theoretical predictions. For instance we predict that the photospheres of HD 163296, HD 100546, and HD 141569 A are primarily composed of accreted material. This is confirmed for the first by its slightly super-solar $(\text{Fe}/\text{H})_{\text{obs}}$, which is consistent with its accretion from a somewhat gas-poor disk. The latter two have dust-poor disks with radial gaps, so we predict that the accreting material ought to have sub-solar $(\text{Fe}/\text{H})_{\text{obs}}$ and indeed this is what is seen from their photospheres.

In systems with less data we can make predictions but cannot test them without further information. We predict that HD 21997, which hosts a debris disk, and HD 195689¹⁰⁴, which is thought to host an evaporating hot Jupiter, should exhibit mild photospheric contamination from these sources. The signal we predict for these systems is quite small, but debris disks and planets often have chemistries very different from solar and so may yield detectable signals in spite of this.

¹⁰⁴ KELT-9

Our method also enables more robust statistical inferences to be drawn for many systems. In particular, preliminary work suggests that it allows us to refine estimates of the mass ratio of gas to dust and the refractory fractions of different elements. Furthermore by providing accretion rate estimates in systems for which this is not measured our method enables us to probe accretion physics in a much wider array of systems, which may enable broader studies of circumstellar disk structure and composition in the future.

7 *Conclusions*

When we try to pick out anything by
itself we find that it is bound fast by a
thousand invisible cords that cannot be
broken, to everything in the Universe.

John Muir

Stars and planets exhibit rich behaviours which emerge from a vast array of scales. The scattering of individual photons has as much consequence for their evolution as do the tendencies of turbulence and the glacially-slow burning of light elements into nuclear ash. In this dissertation I have built up from small scales to large and in so doing constructed effective descriptions of the relevant physics for several examples. This was done out of necessity, but also makes each phenomenon feel ordinary and detached from its origins. I now wish to climb back down the ladder of scales, not for any practical purpose but simply to better appreciate the *distance* between the fundamental rules and infinitesimal constituents and the variety of phenomena they produce.

In Chapter 3 I investigated the differential rotation of convecting stars and planets. This phenomenon may be seen in sunspots moving at different rates, or inferred from the subtle harmonies of asteroseismology. In either case the effect is at a large scale, but has its origin on much smaller scales.

Convecting bodies lie poised on the edge of an instability. With even a slightly shallower entropy gradient they would largely be still, their particles moving randomly and slowly diffusing over the eons. This is not the case. Matter heats more rapidly than it can cool via radiation, so it expands and rises. Cooler material contracts and falls in its place. This provides a mechanical shortcut to transport heat.

When such objects rotate slowly, the mechanical shortcut does more than carry heat. Because angular momentum is conserved, rising material finds itself rotating more slowly than the surrounding medium and pushes against it¹. The same occurs for falling material but in reverse. In this way

¹ This is just the Coriolis effect.

rotating convection develops a directional preference, which causes it to pump momentum.

Countering this pump is the mixing convection entails. Turbulence is messy and chaotic and cannot be so cleanly separated into rising and falling plumes. Hence there is mixing, which serves to equalise momenta and counter shears². This balances the pumping, and in that balance the body is sheared in proportion to the rotation.

It is worth noting that the phenomenon which pumps momentum is fundamentally dissimilar from that which works to counter shears. The latter is purely local³, while the former has a global element to it because it depends on the relation between angular momentum and linear velocity. The structure that emerges is therefore a compromise between the local and the global.

A similar result arises when these bodies rotate quickly, except that here inertia⁴ becomes more important than momentum mixing. The inertial term arises because as a fluid element participates in the rotation it turns, and this turning requires changing its angular momentum about its centre. As a result it is really a global effect, tied to the radius of the planet and the overall rotation. The reason this term is more important than momentum mixing in this limit is that it scales proportional to the angular momentum without bound while the latter cannot exceed the scale of the underlying turbulence. This results in a new balance, with relative shear decaying as inertia grows ever more important.

A further consequence of rapid rotation is that convection is suppressed. This is because a rising fluid element is rapidly pushed aside by its more rapidly moving neighbours. When the fluid is ionized magnetism offers an escape; energy may be transported more readily by magnetic fields⁵, which are not subject to the same constraints as the fluid itself. The result is even slower convection and even less shear.

Stepping further down in scale, the unimaginably numerous particles which make up stars and planets neither know nor care about angular momentum. Their existence, at least over short time-scales, is largely unaltered by convection or turbulence or rotation or shear. These large-scale phenomena change the behaviour of any one particle only on average, and then only by a tiny amount relative to its thermal motion. Yet as I showed in Chapter 4 such small changes set the lifetime of many stars. There through a similar set of arguments I found that rotation and the pumping of heat in the cores of massive stars conspire to set their envelopes in motion. Local convective motions in the core determine the thermal

² Such mixing is the source of the turbulent viscosity.

³ Local in this context means that it is determined without reference to the large-scale structure of the body, for instance by considering only structures smaller than a scale height h .

⁴ i.e. the Taylor-Proudman term $\boldsymbol{\omega} \cdot \nabla(\Omega R)$

⁵ More formally super-equipartition fields allow the energy transported to significantly exceed the kinetic energy in the flow.

structure of the envelope and hence the motion of nuclei all across the star. Over millions of years some of these nuclei which would not otherwise have entered the core do so and fuse, thereby sustaining the star for longer than it would otherwise have lasted. In this way the whole star is affected by the workings of seemingly isolated phenomena in a few small regions.

Turning to planets, in Chapter 5 I investigated Jupiter-like bodies orbiting very near to their host stars. Over billions of years these planets cool⁶, which gradually reduces the average energy of their constituent particles and causes them to shrink⁷. Before they were observed, therefore, the expectation was that only a small fraction, namely those which had not yet had time to cool, should be particularly large. It was therefore surprising and fascinating when so many were observed to be dramatically inflated.

The question of how this inflation comes about is fundamentally not about energy. The incident stellar flux is often well in excess of what is required to inflate a planet. Rather the question is about *free energy*, or equivalently entropy. The difficulty is that the incident stellar flux cannot directly cause inflation because it is at a much lower temperature than the bulk of the planet⁸. It follows that the inflation must be a result of heat being generated inside the planet at or below the depths which are inflated.

One way to generate heat within a planet is through viscous dissipation. This process acts at the aptly named dissipative scale⁹ λ by virtue of molecular diffusion turning structured motion into random thermal motion. However, were it only this effect acting, the dissipation could not matter because molecular diffusion is only effective over very short length-scales. Hence turbulence must play a role, folding large-scale shears over themselves repeatedly until their energy reaches a length-scale at which diffusion can act¹⁰.

So turbulence combined with diffusion may generate heat from shears, but this begs the question: from whence does the shear come? Tides present one option. Because one side of the planet is further from its host star than the other they experience different gravitational fields. The difference is very slight, but suffices to periodically push and pull at material in the planet as it proceeds in its orbit. This excites waves which, under the right circumstances¹¹, resonate and grow. Such waves produce sufficient shearing that the planet heats and inflates, in some cases by a factor of several. Furthermore these waves influence the thermal structure of the planet so as to maintain the conditions which allow them to resonate.

⁶ Interestingly the rate of cooling is set by the opacity of the outer layers of the planet. In this way the details of photon scattering in a medium in a small region dictate the long-term evolution of the entire planet.

⁷ This is a consequence of the virial theorem.

⁸ This is a direct consequence of the second law of thermodynamics, which itself is remarkable because the stellar flux is energy which is accessible to the constituents of the planet and it is purely the statistics of their motion which preclude its use.

⁹ See Chapter 1.

¹⁰ In this way turbulence is like a conveyor belt, carrying energy from the scales at which it originates to those at which it may be processed into heat.

¹¹ e.g. in the presence of a radiative zone

Hence waves with periods of hours interact with turbulent and diffusive processes to tune the planet over billions of years to be more receptive to their kind, and in doing so cause it to inflate. This phenomenon spans not only scales of space and time but also different kinds of motion, including random¹², structured¹³ and turbulent.

The final scenario I have investigated is of a somewhat different sort. In Chapter 6 I developed a connection between the chemistry of nascent stellar systems and mixing on the surfaces of young stars. This connection does not influence the lifetimes or structure or evolution of these systems in any significant manner. Rather it influences what we can learn from them. By accumulating in a thin layer near the surface of a star a very small amount accreting material influences its light¹⁴ much more strongly than if it mixed efficiently. In this way these stars become beacons which amplify the signal of the chemistry that surrounds them.

These examples serve to illustrate that stars and planets are laboratories of unusual and complex physics¹⁵, and are potentially home to many more such strange phenomena. A theme which appears again and again is that the characteristic scale on which a phenomenon acts may be dramatically altered by feedback and interactions. This presents a challenge, but also means that the resulting behaviours are incredibly rich and subtle. The complexity of these bodies is that which makes them numinous.

¹² i.e. thermal

¹³ e.g. waves

¹⁴ specifically the spectrum of its light

¹⁵ This was put well by Sterl Phinney, who once told me that “The wonderful thing about astronomy is that you can pick your favourite physics and find where in the Universe it happens.”

Acknowledgements

A great deal has happened since I signed on, flew out and began in a place that, while ancient in every sense of the word, was very new to me. The beginning was difficult, and that is why it meant so much that my supervisor, Chris Tout^{1,2}, was so welcoming. It is a sincere pleasure to be able to thank him for this and for the steadfast advocacy and guidance and kind encouragement which made this endeavour possible. I am also truly grateful to Anna Żytkow³ and Sterl Phinney⁴ for a great deal of mentoring, stimulating conversations and friendship.

The joy in science for me is in searching for connections over all scales, from particles to proteins to antennae and the Universe itself. Prineha Narang⁵, Ravishankar Sundararaman⁶, Alex Rasmussen⁷ and Milo Lin⁸ all encouraged and supported me in this when we were at Caltech and that support has not wavered. I know how special an opportunity they have given me.

While science was the motive, this journey has been about much more. Jeff Holzgrafe⁹, Nick Ader¹⁰, Katherine McDaniel¹¹, Jules Ebert¹² and Dillon Dong¹³ were there to share in the experience of being American in Her Majesty's United Kingdom. Jesse Salomon¹⁴ and Nicholas Schiefer¹⁵ kept me in touch with my Caltech roots. Alex Rasmussen¹⁶, Sid Ghandi¹⁷ and Douglas Boubert¹⁸ shared in the *experience* of doing science, of the fears and doubts as well as the joys and triumphs. It has been incredibly uplifting to be among such thoughtful and introspective people.

None of this would have been possible without the UK Marshall Commission, which supported me financially and in my travels through the UK. In addition the Institute of Astronomy at Cambridge, the Association of Marshall Scholars and the Hertz Foundation supported my travel to several intensely engaging workshops and conferences. Pierre Lesaffre^{19,20} hosted me at ENS in Paris and Kumar Chitre^{21,22} hosted me at CEBS in Mumbai and both are good friends, generous and warm: the ideal company for thinking and talking through the mysteries of our Sun.

Finally I want to thank my family. My grandmother Ray²³ makes visits a pleasure, and tells me how much it would have meant to my grandfather Robert²⁴ to see where I've gone. My siblings Eva²⁵, Mike²⁶ and Marie²⁷ make a real effort to meet up when I find myself on their side of the pond and seeing them really means a great deal to me. And of course Mom^{28,29} and Dad^{30,31} have now twice supported my adventures in immeasurable ways despite the distance.

I am grateful to you all.

¹ "Indeed this could be very interesting."

² "I can find you a gown if you don't have one yet... I'll sign you in as my guest."

³ "What do you think? Does it work?"

⁴ "... more sartorially sophisticated than myself..."

⁵ "Go save the world!"

⁶ "The details matter."

⁷ "A par-a-fermion, you mean a boson?!"

⁸ "I think we're getting there."

⁹ "It's a house boat."

¹⁰ "All I'm saying is that it might be more complicated than that."

¹¹ "What thoughts have you been thinking?"

¹² "Lobster robots!"

¹³ "Bunnies!"

¹⁴ "Go to bed frosh!"

¹⁵ "Ah yes the most reasonable plan."

¹⁶ "Nobody could be that tall!"

¹⁷ "Would you say that's at a low thermodynamic temperature?"

¹⁸ "Boardgames? Boardgames!"

¹⁹ "I think that doesn't quite work..."

²⁰ "Don't count the coins, I'll get lunch."

²¹ "Let me show you something we did some years ago."

²² "I'll take you to our favourite fish restaurant."

²³ "You're just the same as always!"

²⁴ "Die mense word slim."

²⁵ "We could make that."

²⁶ "... paint over the sky..."

²⁷ "Pyjamas!"

²⁸ "I think there's a relation there..."

²⁹ "Well this is civilised."

³⁰ "Let's go for a walk."

³¹ "We can watch the sun rise."

Bibliography

- Abbott B. P., et al., 2016, *Phys. Rev. Lett.*, 116, 061102
- Acke B., Waelkens C., 2004, *Astronomy and Astrophysics*, 427, 1009
- Anderson P. W., 1972, *Science*, 177, 393
- Antia H. M., private communication, 2016
- Antia H. M., Basu S., 2001, *The Astrophysical Journal* L, 559, L67
- Antia H. M., Basu S., Chitre S. M., 2008, *The Astrophysical Journal*, 681, 680
- Arras P., Socrates A., 2010, *The Astrophysical Journal*, 714, 1
- Ashcroft N., Mermin N., 1976, *Solid State Physics*. Saunders College, Philadelphia
- Ashkenazi S., Steinberg V., 1999, *Physical Review Letters*, 83, 4760
- Asplund M., Grevesse N., Sauval A. J., Scott P., 2009, *Annual Review of Astronomy and Astrophysics*, 47, 481
- Augustson K. C., Brun A. S., Toomre J., 2011, in Brummell N. H., Brun A. S., Miesch M. S., Ponty Y., eds, *IAU Symposium Vol. 271, Astrophysical Dynamics: From Stars to Galaxies*. pp 361–362 ([arXiv:1011.1016](#)), [doi:10.1017/S1743921311017790](#)
- Augustson K. C., Brun A. S., Toomre J., 2013, *The Astrophysical Journal*, 777, 153
- Augustson K., Mathis S., Brun A. S., 2016a, in 19th Cambridge Workshop on Cool Stars, Stellar Systems, and the Sun (CS19). p. 152, [doi:10.5281/zenodo.237251](#)
- Augustson K. C., Brun A. S., Toomre J., 2016b, *The Astrophysical Journal*, 829, 92
- Aurnou J., Heimpel M., Wicht J., 2007, *Icarus*, 190, 110
- Bahng J., Schwarzschild M., 1961, *The Astrophysical Journal*, 134, 312
- Bakos G. Á., et al., 2016, HAT-P-47b AND HAT-P-48b: Two Low Density Sub-Saturn-Mass Transiting Planets on the Edge of the Period–Mass Desert ([arXiv:1606.04556](#))
- Balbus S. A., Hawley J. F., 1991, *The Astrophysical Journal*, 376, 214
- Balbus S. A., Schaan E., 2012, *Monthly Notices of the Royal Astronomical Society*, 426, 1546
- Balbus S. A., Latter H., Weiss N., 2012, *Monthly Notices of the Royal Astronomical Society*, 420, 2457
- Batygin K., Stevenson D. J., Bodenheimer P. H., 2011, *The Astrophysical Journal*, 738, 1
- Becquerel H., 1896, *Comptes Rendus*, 122, 420

- Benzi R., Tripiccion R., Massaioli F., Succi S., Ciliberto S., 1994, *EPL (Europhysics Letters)*, 25, 341
- Berntsen J., Espelid T. O., Genz A., 1991, *ACM Trans. Math. Softw.*, 17, 437
- Böhm-Vitense E., 1958, *Zeitschrift für Astrophysik*, 46, 108
- Böhm-Vitense E., 1992, *Introduction to stellar astrophysics. Volume 3. Stellar structure and evolution..* Cambridge University Press
- Bonanno A., Fröhlich H.-E., Karoff C., Lund M. N., Corsaro E., Frasca A., 2014, *Astronomy and Astrophysics*, 569, A113
- Boneberg D. M., Panić O., Haworth T. J., Clarke C. J., Min M., 2016, *Monthly Notices of the Royal Astronomical Society*, 461, 385
- Brown B., Browning M., Brun A., Miesch M., Toomre J., 2007, *Astronomische Nachrichten*, 328, 1002
- Brown J. M., Garaud P., Stellmach S., 2013, *The Astrophysical Journal*, 768, 34
- Browning M. K., Brun A. S., Toomre J., 2003, in *American Astronomical Society Meeting Abstracts*. p. 1342
- Bruderer S., van Dishoeck E. F., Doty S. D., Herczeg G. J., 2012, *Astronomy and Astrophysics*, 541, A91
- Brun A. S., Palacios A., 2009, *The Astrophysical Journal*, 702, 1078
- Brun A. S., Rempel M., 2009, *Space Science Reviews*, 144, 151
- Brun A. S., Toomre J., 2002, *The Astrophysical Journal*, 570, 865
- Brun A. S., Browning M. K., Toomre J., 2005, *The Astrophysical Journal*, 629, 461
- Brun A. S., Antia H. M., Chitre S. M., 2010, *Astronomy and Astrophysics*, 510, A33
- Brun A. S., et al., 2017, *The Astrophysical Journal*, 836, 192
- Buchhave L. A., et al., 2014, *Nature*, 509, 593
- Burbidge E. M., Burbidge G. R., Fowler W. A., Hoyle F., 1957, *Reviews of Modern Physics*, 29, 547
- Busse F. H., 1981, *Geophysical and Astrophysical Fluid Dynamics*, 17, 215
- Cabrera B., 1982, *Physical Review Letters*, 48, 1378
- Caccin B., Donati-Falchi A., Falciani R., 1976, *Solar Physics*, 46, 29
- Caleo A., Balbus S. A., 2016, *Monthly Notices of the Royal Astronomical Society*, 457, 1711
- Caleo A., Balbus S. A., Potter W. J., 2015, *Monthly Notices of the Royal Astronomical Society*, 448, 2077
- Cantiello M., Langer N., 2010, *Astronomy and Astrophysics*, 521, A9
- Cantiello M., Mankovich C., Bildsten L., Christensen-Dalsgaard J., Paxton B., 2014, *The Astrophysical Journal*, 788, 93
- Canuto V. M., 1994, *The Astrophysical Journal*, 428, 729
- Canuto V. M., 1997, *The Astrophysical Journal*, 482, 827
- Canuto V. M., Hartke G. J., 1986, *Astronomy and Astrophysics*, 168, 89
- Canuto V. M., Cheng Y., Howard A. M., Esau I. N., 2008, *Journal of Atmospheric Sciences*, 65, 2437

- Carati D., 1990, *Phys. Rev. A*, 41, 3129
- Chaboyer B., Zahn J.-P., 1992, *Astronomy and Astrophysics*, 253, 173
- Chadwick J., 1932, *Proceedings of the Royal Society of London Series A*, 136, 692
- Chan K. L., 2001, *The Astrophysical Journal*, 548, 1102
- Chandrasekhar S., 1931, *Monthly Notices of the Royal Astronomical Society*, 91, 456
- Chandrasekhar S., 1960, *Proceedings of the National Academy of Science*, 46, 253
- Chandrasekhar S., 1961, *Hydrodynamic and hydromagnetic stability*. Dover Publications
- Chaplin W. J., Houdek G., Elsworth Y., Gough D. O., Isaak G. R., New R., 2005, *Monthly Notices of the Royal Astronomical Society*, 360, 859
- Charbonneau P., 1991, *The Astrophysical Journal*, 372, L33
- Charbonneau P., Michaud G., 1991, *The Astrophysical Journal*, 370, 693
- Charbonnel C., Lagarde N., 2010, *Astronomy and Astrophysics*, 522, A10
- Charbonnel C., Zahn J.-P., 2007, *Astronomy and Astrophysics*, 467, L15
- Christensen U. R., Aubert J., 2006, *Geophysical Journal International*, 166, 97
- Christensen-Dalsgaard J., Schou J., 1988, in Rolfe E. J., ed., *ESA Special Publication Vol. 286, Seismology of the Sun and Sun-Like Stars*.
- Christensen U. R., Holzwarth V., Reiners A., 2009, *Nature*, 457, 167
- Claret A., Torres G., 2017, *The Astrophysical Journal*, 849, 18
- Coriolis M. G., 1835, *Memoire*
- Courant R., Friedrichs K., Lewy H., 1929, *Mathematische Annalen*, 100, 32
- Cowling T. G., 1933, *Monthly Notices of the Royal Astronomical Society*, 94, 39
- Cowling T. G., 1951, *The Astrophysical Journal*, 114, 272
- Danilov S., Gurarie D., 2002, *Phys. Rev. E*, 65, 067301
- Deheuvels S., et al., 2012, *The Astrophysical Journal*, 756, 19
- Deheuvels S., Ballot J., Beck P. G., Mosser B., Østensen R., García R. A., Goupil M. J., 2015, *Astronomy and Astrophysics*, 580, A96
- Deissler R. G., 1986, *The Physics of Fluids*, 29, 1453
- Demircan O., Kahraman G., 1991, *Astrophysics & Space Science*, 181, 313
- Di Mauro M. P., Dziembowski W. A., Paternó L., 1998, in Korzennik S., ed., *ESA Special Publication Vol. 418, Structure and Dynamics of the Interior of the Sun and Sun-like Stars*. p. 759
- Dirac 1931, *Proceedings of the Royal Society of London A: Mathematical, Physical and Engineering Sciences*, 133, 60
- Dobrowolny M., Mangeney A., Veltri P., 1980, *Phys. Rev. Lett.*, 45, 144

- Donati J.-F., et al., 2008, *Monthly Notices of the Royal Astronomical Society*, 390, 545
- Donehew B., Brittain S., 2011, *The Astrophysical Journal*, 141, 46
- Draper Z. H., Matthews B. C., Kennedy G. M., Wyatt M. C., Venn K. A., Sibthorpe B., 2016, *Monthly Notices of the Royal Astronomical Society*, 456, 459
- Eddington A. S., 1917, *The Observatory*, 40, 290
- Eddington A. S., 1918, *The Astrophysical Journal*, 48, 205
- Eddington A. S., 1929, *Monthly Notices of the Royal Astronomical Society*, 90, 54
- Eggenberger P., et al., 2017, *Astronomy and Astrophysics*, 599, A18
- Eggleton P. P., 1971, *Monthly Notices of the Royal Astronomical Society*, 151, 351
- Eggleton P. P., Yakut K., 2017, *Monthly Notices of the Royal Astronomical Society*, 468, 3533
- Eggleton P. P., Fitchett M. J., Tout C. A., 1989, *The Astrophysical Journal*, 347, 998
- Einstein A., 1905, *Annalen der Physik*, 322, 549
- Fairlamb J. R., Oudmajer R. D., Mendigutía I., Ilee J. D., van den Ancker M. E., 2015, *Monthly Notices of the Royal Astronomical Society*, 453, 976
- Farmer R., Fields C. E., Timmes F. X., 2015, *The Astrophysical Journal*, 807, 184
- Ferguson J. W., Alexander D. R., Allard F., Barman T., Bodnarik J. G., Hauschildt P. H., Heffner-Wong A., Tamanai A., 2005, *The Astrophysical Journal*, 623, 585
- Feynman R. P., 1964, *Feynman lectures on physics. Volume 2: Mainly electromagnetism and matter*. Addison-Wesley, http://www.feynmanlectures.caltech.edu/II_toc.html
- Fick A., 1855, *Annalen der Physik*, 170, 59
- Fisher M. E., 1974, *Rev. Mod. Phys.*, 46, 597
- Flaherty K. M., et al., 2016, *The Astrophysical Journal*, 818, 97
- Folsom C. P., Bagnulo S., Wade G. A., Alecian E., Landstreet J. D., Marsden S. C., Waite I. A., 2012, *Monthly Notices of the Royal Astronomical Society*, 422, 2072
- Fontaine G., Michaud G., 1979, *The Astrophysical Journal*, 231, 826
- Fossati L., Folsom C. P., Bagnulo S., Grunhut J. H., Kochukhov O., Landstreet J. D., Paladini C., Wade G. A., 2011, *Monthly Notices of the Royal Astronomical Society*, 413, 1132
- Frasca A., Fröhlich H.-E., Bonanno A., Catanzaro G., Biazzo K., Molenda-Żakowicz J., 2011, *Astronomy and Astrophysics*, 532, A81
- Fuller J., Lecoanet D., Cantiello M., Brown B., 2014, *The Astrophysical Journal*, 796, 17
- Galperin B., Sukoriansky S., Huang H.-P., 2001, *Physics of Fluids*, 13, 1545
- Galperin B., Sukoriansky S., Anderson P. S., 2007, *Atmospheric Science Letters*, 8, 65
- Garaud P., Acevedo Arreguin L., 2009, *The Astrophysical Journal*, 704, 1
- Garaud P., Bodenheimer P., 2010, *The Astrophysical Journal*, 719, 313

- Garaud P., Brummell N. H., 2008, *The Astrophysical Journal*, 674, 498
- Garaud P., Ogilvie G. I., Miller N., Stellmach S., 2010, *Monthly Notices of the Royal Astronomical Society*, 407, 2451
- Garaud P., Gagnier D., Verhoeven J., 2017, *The Astrophysical Journal*, 837, 133
- Gastine T., Wicht J., Aurnou J. M., 2013, *Icarus*, 225, 156
- Gastine T., Yadav R. K., Morin J., Reiners A., Wicht J., 2014, *Monthly Notices of the Royal Astronomical Society*, 438, L76
- Gaudi B. S., et al., 2017, *Nature*, 546, 514
- Genz A., Malik A., 1980, *Journal of Computational and Applied Mathematics*, 6, 295
- Gilman P. A., 1977, *Geophysical and Astrophysical Fluid Dynamics*, 8, 93
- Gilman P. A., 1979, *The Astrophysical Journal*, 231, 284
- Ginzburg S., Sari R., 2015, *The Astrophysical Journal*, 803, 111
- Goldreich P., Keeley D. A., 1977, *The Astrophysical Journal*, 211, 934
- Goldreich P., Sridhar S., 1995, *The Astrophysical Journal*, 438, 763
- Goldstein S., 1969, *Annual Review of Fluid Mechanics*, 1, 1
- Goodman J., Dickson E. S., 1998, *The Astrophysical Journal*, 507, 938
- Gough D., 1977, in Spiegel E. A., Zahn J.-P., eds, *Lecture Notes in Physics*, Berlin Springer Verlag Vol. 71, Problems of Stellar Convection. pp 15–56, doi:10.1007/3-540-08532-7_31
- Gough D. O., 1978, in *Proceedings of the Workshop on Solar Rotation*. p. 337
- Gough D. O., 2012, *ISRN Astronomy and Astrophysics*, 2012, 987275
- Gough D. O., 2017, *Solar Physics*, 292, 70
- Gough D. O., McIntyre M. E., 1998, *Nature*, 394, 755
- Gough D. O., Thompson M. J., 1991, *The inversion problem*. University of Arizona Press, pp 519–561
- Gray R. O., Corbally C. J., 1998, *The Astrophysical Journal*, 116, 2530
- Gray R. O., Riggs Q. S., Koen C., Murphy S. J., Newsome I. M., Corbally C. J., Cheng K.-P., Neff J. E., 2017, *The Astrophysical Journal*, 154, 31
- Guenel M., Mathis S., Remus F., 2014, *Astronomy and Astrophysics*, 566, L9
- Guennebaud G., Jacob B., et al., 2010, *Eigen v3*, <http://eigen.tuxfamily.org>, <http://eigen.tuxfamily.org>
- Guerrero G., Smolarkiewicz P. K., Kosovichev A. G., Mansour N. N., 2013, *The Astrophysical Journal*, 779, 176
- Guillot T., Stevenson D. J., Hubbard W. B., Saumon D., 2004, *The Interior of Jupiter*. Cambridge University Press, pp 35–57, <http://resolver.caltech.edu/CaltechAUTHORS:20130702-131227525>
- Guillot T., et al., 2018, *Nature*, 555, 227
- Hansen C. J., Kawaler S. D., 1994, *Stellar Interiors. Physical Principles, Structure, and Evolution*. Springer-Verlag

- Hartman J. D., et al., 2012, *The Astronomical Journal*, 144, 139
- Hartman J. D., et al., 2016, *The Astronomical Journal*, 152, 182
- Hellier C., et al., 2012, *Monthly Notices of the Royal Astronomical Society*, 426, 739
- Herwig F., Bloeker T., Schoenberner D., El Eid M., 1997, *Astronomy and Astrophysics*, 324, L81
- Holloway M. G., Bethe H. A., 1940, *Physical Review*, 57, 747
- Hotta H., Rempel M., Yokoyama T., 2015, *The Astrophysical Journal*, 803, 42
- Hough S. S., 1897, *Philosophical Transactions of the Royal Society of London Series A*, 189, 201
- Hoyle F., Fowler W. A., 1973, *Nature*, 241, 384
- Hughes A. M., et al., 2017, *The Astrophysical Journal*, 839, 86
- Hunter J. D., 2007, *Computing in Science Engineering*, 9, 90
- Iglesias C. A., Rogers F. J., 1996, *The Astrophysical Journal*, 464, 943
- Ilgner M., Nelson R. P., 2006, *Astronomy and Astrophysics*, 445, 205
- Iliev I. K., Barzova I. S., 1995, *Astronomy and Astrophysics*, 302, 735
- Inc. W. R., 2016, *Mathematica*, Version 11.0.0.0
- Ingersoll A. P., Pollard D., 1982, *Icarus*, 52, 62
- Isserlis L., 1918, *Biometrika*, 12, 134
- Jeans J. H., 1902, *Philosophical Transactions of the Royal Society of London Series A*, 199, 1
- Jeans J. H., 1917, *Monthly Notices of the Royal Astronomical Society*, 78, 28
- Jeans J. H., 1926, *Monthly Notices of the Royal Astronomical Society*, 86, 328
- Jermyn A. S., 2015, *The Atmospheric Dynamics of Pulsar Companions*. California Institute of Technology, <http://resolver.caltech.edu/CaltechTHESIS:06112015-211414622>
- Jermyn A. S., Kama M., 2018, *Monthly Notices of the Royal Astronomical Society*, 476, 4418
- Jermyn A. S., Tout C. A., Ogilvie G. I., 2017, *Monthly Notices of the Royal Astronomical Society*, 469, 1768
- Jermyn A. S., Lesaffre P., Tout C. A., Chitre S. M., 2018, *Monthly Notices of the Royal Astronomical Society*, 476, 646
- Jura M., 2015, *The Astrophysical Journal*, 150, 166
- Kama M., Folsom C. P., Pinilla P., 2015, *Astronomy and Astrophysics*, 582, L10
- Kama M., et al., 2016, *Astronomy and Astrophysics*, 592, A83
- Käpylä P., 2011, *Astronomische Nachrichten*, 332, 43
- Käpylä P. J., Korpi M. J., Tuominen I., 2004, *Astronomy and Astrophysics*, 422, 793
- Käpylä P. J., Mantere M. J., Guerrero G., Brandenburg A., Chatterjee P., 2011, *Astronomy and Astrophysics*, 531, A162
- Kardar M., 2006, *Statistical Physics of Particles*. Cambridge University Press

- Kaspi Y., Flierl G. R., Showman A. P., 2009, *Icarus*, 202, 525
- Kaspi Y., et al., 2018, *Nature*, 555, 223
- Keen M. A., Bedding T. R., Murphy S. J., Schmid V. S., Aerts C., Tkachenko A., Ouazzani R.-M., Kurtz D. W., 2015, *Monthly Notices of the Royal Astronomical Society*, 454, 1792
- Kichatinov L. L., 1986, *Geophysical and Astrophysical Fluid Dynamics*, 35, 93
- Kichatinov L. L., 1987, *Geophysical and Astrophysical Fluid Dynamics*, 38, 273
- Kichatinov L. L., Rudiger G., 1993, *Astronomy and Astrophysics*, 276, 96
- Killworth P. D., 1980, *Dynamics of Atmospheres and Oceans*, 4, 143
- King A. R., Pringle J. E., Livio M., 2007, *Monthly Notices of the Royal Astronomical Society*, 376, 1740
- Kippenhahn R., 1963, *The Astrophysical Journal*, 137, 664
- Kippenhahn R., Weigert A., 1990, *Stellar Structure and Evolution*. Springer-Verlag, Berlin
- Kippenhahn R., Ruschenplatt G., Thomas H.-C., 1980, *Astronomy and Astrophysics*, 91, 175
- Kirk R. L., Stevenson D. J., 1987, *The Astrophysical Journal*, 316, 836
- Kissin Y., Thompson C., 2015, *The Astrophysical Journal*, 808, 35
- Kitchatinov L. L., 2013, in Kosovichev A. G., de Gouveia Dal Pino E., Yan Y., eds, *IAU Symposium Vol. 294, Solar and Astrophysical Dynamos and Magnetic Activity*. pp 399–410 ([arXiv:1210.7041](https://arxiv.org/abs/1210.7041)), [doi:10.1017/S1743921313002834](https://doi.org/10.1017/S1743921313002834)
- Kitchatinov L. L., Ruediger G., 1995, *Astronomy and Astrophysics*, 299, 446
- Kitchatinov L. L., Pipin V. V., Ruediger G., 1994, *Astronomische Nachrichten*, 315, 157
- Klion H., Quataert E., 2017, *Monthly Notices of the Royal Astronomical Society: Letters*, 464, L16
- Koester D., 2009, *Astronomy and Astrophysics*, 498, 517
- Kolmogorov A., 1941a, *Akademiia Nauk SSR Doklady*, 30, 301
- Kolmogorov A. N., 1941b, *Akademiia Nauk SSR Doklady*, 32, 16
- Kral Q., private communication, 2017
- Kral Q., Wyatt M., Carswell R. F., Pringle J. E., Matrà L., Juhász A., 2016, *Monthly Notices of the Royal Astronomical Society*, 461, 845
- Kral Q., Matrà L., Wyatt M. C., Kennedy G. M., 2017, *Monthly Notices of the Royal Astronomical Society*, 469, 521
- Kramers H. A., 1923, *The London, Edinburgh, and Dublin Philosophical Magazine and Journal of Science*, 46, 836
- Küker M., Rüdiger G., 2005, *Astronomy and Astrophysics*, 433, 1023
- Kulenthirarajah L., Garaud P., 2018, preprint, ([arXiv:1803.11530](https://arxiv.org/abs/1803.11530))
- Kumar P., Talon S., Zahn J.-P., 1999, *The Astrophysical Journal*, 520, 859
- Landau L. D., Lifshitz E. M., 1959, *Fluid mechanics*. Addison-Wesley

- Lattimer J. M., 2012, *Annual Review of Nuclear and Particle Science*, 62, 485
- Lau H. H. B., Potter A. T., Tout C. A., 2011, *Monthly Notices of the Royal Astronomical Society*, 415, 959
- Lauder B., Spalding D., 1974, *Computer Methods in Applied Mechanics and Engineering*, 3, 269
- Lebovitz N. R., 1965, *The Astrophysical Journal*, 142, 1257
- Lecoanet D., Quataert E., 2013, *Monthly Notices of the Royal Astronomical Society*, 430, 2363
- Lecoanet D., Zweibel E. G., Townsend R. H. D., Huang Y.-M., 2010, *The Astrophysical Journal*, 712, 1116
- Lee D., 2013, *Journal of Computational Physics*, 243, 269
- Lesaffre P., Balbus S. A., Latter H., 2009, *Monthly Notices of the Royal Astronomical Society*, 396, 779
- Lesaffre P., Chitre S. M., Potter A. T., Tout C. A., 2013, *Monthly Notices of the Royal Astronomical Society*, 431, 2200
- Li L., Han Z., Zhang F., 2004, *Monthly Notices of the Royal Astronomical Society*, 351, 137
- Littlefair S. P., 2014, in Petit P., Jardine M., Spruit H. C., eds, *IAU Symposium Vol. 302, Magnetic Fields throughout Stellar Evolution*. pp 91–99, doi:10.1017/S1743921314001793
- Liu J., Goldreich P. M., Stevenson D. J., 2008, *Icarus*, 196, 653
- Lodders K., 2003, *The Astrophysical Journal*, 591, 1220
- Lohse D., Xia K.-Q., 2010, *Annual Review Of Fluid Mechanics*, 42, 335
- Lopez E. D., Fortney J. J., 2016, *The Astrophysical Journal*, 818, 4
- Lund M. B., et al., 2017, *The Astrophysical Journal*, 154, 194
- Luschgy H., PagÀls G., 2008, *Electron. Commun. Probab.*, 13, 422
- Mabuchi J., Masada Y., Kageyama A., 2015, *The Astrophysical Journal*, 806, 10
- Maeder A., 1995, *Astronomy and Astrophysics*, 299, 84
- Maeder A., 1997, *Astronomy and Astrophysics*, 321, 134
- Maeder A., 2009, *Physics, Formation and Evolution of Rotating Stars*. Springer Science & Business Media, doi:10.1007/978-3-540-76949-1
- Maeder A., Zahn J.-P., 1998, *Astronomy and Astrophysics*, 334, 1000
- Marchant, Pablo Langer, Norbert Podsiadlowski, Philipp Tauris, Thomas M. Moriya, Takashi J. 2016, *Astronomy and Astrophysics*, 588, A50
- Marino S., et al., 2016, *Monthly Notices of the Royal Astronomical Society*, 460, 2933
- Martin A. J., Stiff M. J., Fossati L., Bagnulo S., Scalia C., Leone F., Smalley B., 2017, *Monthly Notices of the Royal Astronomical Society*, 466, 613
- Mathis S., Palacios A., Zahn J.-P., 2004, *Astronomy and Astrophysics*, 425, 243
- Matrà L., et al., 2017a, *Monthly Notices of the Royal Astronomical Society*, 464, 1415
- Matrà L., et al., 2017b, *The Astrophysical Journal*, 842, 9

- Matrozis E., Abate C., Stancliffe R. J., 2017, *Astronomy and Astrophysics*, 606, A137
- Matt S., Do Cao O., Brown B., Brun A., 2011, *Astronomische Nachrichten*, 332, 897
- McKinney J. C., Tchekhovskoy A., Sadowski A., Narayan R., 2014, *Monthly Notices of the Royal Astronomical Society*, 441, 3177
- Meléndez J., Asplund M., Gustafsson B., Yong D., 2009, *The Astrophysical Journal*, 704, L66
- Mendigutía I., Calvet N., Montesinos B., Mora A., Muzerolle J., Eiroa C., Oudmaijer R. D., Merín B., 2011, *Astronomy and Astrophysics*, 535, A99
- Menou K., Balbus S. A., Spruit H. C., 2004, *The Astrophysical Journal*, 607, 564
- Mermin N. D., Wagner H., 1966, *Physical Review Letters*, 17, 1133
- Meynet G., Maeder A., 2000, *Astronomy and Astrophysics*, 361, 101
- Michaud G., 1970, *The Astrophysical Journal*, 160, 641
- Miesch M. S., Toomre J., 2009, *Annual Review of Fluid Mechanics*, 41, 317
- Miesch M. S., Brun A. S., Toomre J., 2006, *The Astrophysical Journal*, 641, 618
- Miller N., Fortney J. J., Jackson B., 2009, *The Astrophysical Journal*, 702, 1413
- Moór A., et al., 2011, *The Astrophysical Journal*, 740, L7
- Moór A., et al., 2017, *The Astrophysical Journal*, 849, 123
- Moravveji E., Townsend R. H. D., Aerts C., Mathis S., 2016, *The Astrophysical Journal*, 823, 130
- Moreno-Insertis F., Spruit H. C., 1989, *The Astrophysical Journal*, 342, 1158
- Murphy S. J., Paunzen E., 2017, *Monthly Notices of the Royal Astronomical Society*, 466, 546
- Murphy G. C., Pessah M. E., 2015, *The Astrophysical Journal*, 802, 139
- Murphy S. J., et al., 2015, *Publications of the Astronomical Society of Australia*, 32, e036
- Murray-Clay R. A., Chiang E. I., Murray N., 2009, *The Astrophysical Journal*, 693, 23
- Netopil M., 2017, *Monthly Notices of the Royal Astronomical Society*, 469, 3042
- Newton I., 1687, *Philosophiae naturalis principia mathematica*. J. Societatis Regiae ac Typis J. Streater, <https://books.google.co.uk/books?id=-dVKAQAIAAJ>
- Nielsen M. B., Schunker H., Gizon L., Schou J., Ball W. H., 2017, *Astronomy and Astrophysics*, 603, A6
- Ogilvie G. I., 2013, *Monthly Notices of the Royal Astronomical Society*, 429, 613
- Ogilvie G. I., 2014, *Annual Reviews of Astronomy and Astrophysics*, 52, 171
- Osaki Y., 1982, *Publications of the Astronomical Society of Japan*, 34, 257
- Paczyński B., 1969, *Acta Astronomica*, 19, 1
- Palla F., 2012, *AIP Conference Proceedings*, 1480, 22
- Paquette C., Pelletier C., Fontaine G., Michaud G., 1986, *The Astrophysical Journal Supplement Series*, 61, 197
- Parker E. N., 1955, *The Astrophysical Journal*, 122, 293

- Paunzen E., 2001, *Astronomy and Astrophysics*, 373, 633
- Paunzen E., Gray R. O., 1997, *Astronomy and Astrophysics*, 126, 407
- Paunzen E., Duffee B., Heiter U., Kuschnig R., Weiss W. W., 2001, *Astronomy and Astrophysics*, 373, 625
- Paxton B., Bildsten L., Dotter A., Herwig F., Lesaffre P., Timmes F., 2011, *The Astrophysical Journal*, 192, 3
- Paxton B., et al., 2015, *The Astrophysical Journal, Supplement*, 220, 15
- Péicaud J., Di Folco E., Dutrey A., Guilloteau S., Piétu V., 2017, *Astronomy and Astrophysics*, 600, A62
- Pessah M. E., Goodman J., 2009, *The Astrophysical Journal, Letters*, 698, L72
- Pessah M. E., Chan C.-K., Psaltis D., 2006, *Monthly Notices of the Royal Astronomical Society*, 372, 183
- Pessah M. E., Chan C.-K., Psaltis D., 2008, *Monthly Notices of the Royal Astronomical Society*, 383, 683
- Planck M., 1914, The theory of heat radiation. P. Blakiston's Son & Co : Philadelphia, <https://archive.org/details/theoryofheatradi00planrich>
- Pols O. R., Tout C. A., Eggleton P. P., Han Z., 1995, *Monthly Notices of the Royal Astronomical Society*, 274, 964
- Prat, V. Guilet, J. Viallet, M. Müller, E. 2016, *A&A*, 592, A59
- Prather M. J., Demarque P., 1974, *The Astrophysical Journal*, 193, 109
- Press W. H., 1986, in Sturrock P. A., Holzer T. E., Mihalas D. M., Ulrich R. K., eds, , Vol. 1, Physics of the Sun. Reidel Publishing Company, Dordrecht, Holland, Chapt. 4, pp 77–94
- Procaccia I., Zeitak R., 1989, *Physical Review Letters*, 62, 2128
- Quentin L. G., Tout C. A., 2018, *Monthly Notices of the Royal Astronomical Society*,
- Rajaguru S. P., Antia H. M., 2015, *The Astrophysical Journal*, 813, 114
- Ramírez I., Meléndez J., Asplund M., 2009, *Astronomy and Astrophysics*, 508, L17
- Rast M. P., Ortiz A., Meisner R. W., 2008, *The Astrophysical Journal*, 673, 1209
- Rein H., 2012, A proposal for community driven and decentralized astronomical databases and the Open Exoplanet Catalogue ([arXiv:1211.7121](https://arxiv.org/abs/1211.7121))
- Reiners A., Schmitt J. H. M. M., 2003, *Astronomy and Astrophysics*, 412, 813
- Remus F., Mathis S., Zahn J.-P., Lainey V., 2012, *Astronomy and Astrophysics*, 541, A165
- Rhines P., 1973, *Boundary-Layer Meteorology*, 4, 345
- Ribas I., Jordi C., Giménez Á., 2000, *Monthly Notices of the Royal Astronomical Society*, 318, L55
- Richardson L. F., 1922, *Quarterly Journal of the Royal Meteorological Society*, 48, 282
- Roberts P. H., Glatzmaier G. A., 2000, *Reviews of Modern Physics*, 72, 1081
- Rogers T. M., 2015, *The Astrophysical Journal Letters*, 815, L30
- Rogers F. J., Swenson F. J., Iglesias C. A., 1996, *The Astrophysical Journal*, 456, 902
- Roxburgh I. W., 1991, Differential Rotation of Fully Convective Pre-Main Sequence Stars. Springer Netherlands, Dordrecht, pp 83–88, doi:10.1007/978-94-011-3580-1_7

- Rüdiger G., Egorov P., Ziegler U., 2005a, *Astronomische Nachrichten*, 326, 315
- Rüdiger G., Egorov P., Kitchatinov L. L., Küker M., 2005b, *Astronomy and Astrophysics*, 431, 345
- Ruediger G., 1989, Differential rotation and stellar convection. Sun and the solar stars. Taylor & Francis
- Rutherford E., 1919, *The London, Edinburgh, and Dublin Philosophical Magazine and Journal of Science*, 37, 571
- Salvesen G., Simon J. B., Armitage P. J., Begelman M. C., 2016, *Monthly Notices of the Royal Astronomical Society*, 457, 857
- Saslaw W. C., Schwarzschild M., 1965, *The Astrophysical Journal*, 142, 1468
- Savonije G. J., Papaloizou J. C. B., 1983, *Monthly Notices of the Royal Astronomical Society*, 203, 581
- Schmid C., 2011, *American Journal of Physics*, 79, 536
- Schou J., et al., 1998, *The Astrophysical Journal*, 505, 390
- Schroder K.-P., Pols O. R., Eggleton P. P., 1997, *Monthly Notices of the Royal Astronomical Society*, 285, 696
- Schunker H., Schou J., Ball W. H., Nielsen M. B., Gizon L., 2016, *Astronomy and Astrophysics*, 586, A79
- Seiff A., et al., 1998, *Journal of Geophysical Research*, 103, 22857
- Shaviv N. J., 2001, *The Astrophysical Journal*, 549, 1093
- Shaviv N. J., 2005, in Humphreys R., Stanek K., eds, *Astronomical Society of the Pacific Conference Series Vol. 332, The Fate of the Most Massive Stars*. p. 183
- Showman A. P., Kaspi Y., Flierl G. R., 2011, *Icarus*, 211, 1258
- Smolec R., Houdek G., Gough D., 2011, in Brummell N. H., Brun A. S., Miesch M. S., Ponty Y., eds, *IAU Symposium Vol. 271, Astrophysical Dynamics: From Stars to Galaxies*. pp 397–398 ([arXiv:1011.3813](https://arxiv.org/abs/1011.3813)), [doi:10.1017/S1743921311017972](https://doi.org/10.1017/S1743921311017972)
- Snow T. P., Witt A. N., 1996, *The Astrophysical Journal*, 468, L65
- Socrates A., 2013, preprint ([arXiv:1304.4121](https://arxiv.org/abs/1304.4121))
- Soderblom D. R., Hillenbrand L. A., Jeffries R. D., Mamajek E. E., Naylor T., 2014, *Protostars and Planets VI*, pp 219–241
- Soderlund K. M., Heimpel M. H., King E. M., Aurnou J. M., 2013, *Icarus*, 224, 97
- Spiegel D. S., Burrows A., 2013, *The Astrophysical Journal*, 772, 76
- Spitzer L., 1956, *Physics of Fully Ionized Gases*. Interscience Publishers
- Sreenivasan B., Jones C. A., 2006, *Geophysical Journal International*, 164, 467
- Sridhar S., Goldreich P., 1994, *The Astrophysical Journal*, 432, 612
- Stancliffe R. J., Fossati L., Passy J.-C., Schneider F. R. N., 2015, *Astronomy and Astrophysics*, 575, A117
- Starling R. L. C., Siemiginowska A., Uttley P., Soria R., 2004, *Monthly Notices of the Royal Astronomical Society*, 347, 67
- Stevenson D. J., 1982, *Geophysical and Astrophysical Fluid Dynamics*, 21, 113

- Stevenson D. J., 1991, *Annual Reviews of Astronomy and Astrophysics*, 29, 163
- Stewartson K., 1966, *Journal of Fluid Mechanics*, 26, 131–144
- Stokes G. G., 1851, *Transactions of the Cambridge Philosophical Society*, 9, 8
- Sukoriansky S., Dikovskaya N., Galperin B., 2006, *Journal of the Atmospheric Sciences*, 64
- Sun Z., Schubert G., 1995, *Physics of Fluids*, 7, 2686
- Sweet P. A., 1950, *Monthly Notices of the Royal Astronomical Society*, 110, 548
- Talens, G. J. J. et al., 2018, *Astronomy and Astrophysics*, 612, A57
- Teplitskaya R. B., Ozhogina O. A., Pipin V. V., 2015, *Astronomy Letters*, 41, 848
- Thompson M. J., Christensen-Dalsgaard J., Miesch M. S., Toomre J., 2003, *Annual Review of Astronomy and Astrophysics*, 41, 599
- Thomson W., 1871, *The London, Edinburgh, and Dublin Philosophical Magazine and Journal of Science*, 42, 362
- Timmes F. X., Swesty F. D., 2000, *The Astrophysical Journal Supplement Series*, 126, 501
- Tout C. A., Livio M., Bonnell I. A., 1999, *Monthly Notices of the Royal Astronomical Society*, 310, 360
- Traxler A., Garaud P., Stellmach S., 2011, *The Astrophysical Journal*, 728, L29
- Tuominen I., Ruediger G., 1989, *Astronomy and Astrophysics*, 217, 217
- Tuominen I., Brandenburg A., Moss D., Rieutord M., 1994, *Astronomy and Astrophysics*, 284, 259
- Turcotte S., 2002, *The Astrophysical Journal*, 573, L129
- Turcotte S., Charbonneau P., 1993, *The Astrophysical Journal*, 413, 376
- Ulrich R. K., 1972, *The Astrophysical Journal*, 172, 165
- Unno W., 1957, *The Astrophysical Journal*, 126, 259
- Venn K. A., Lambert D. L., 1990, *The Astrophysical Journal*, 363, 234
- Verhoeven J., Stellmach S., 2014, *Icarus*, 237, 143
- Vigan A., et al., 2012, *Astronomy and Astrophysics*, 544, A9
- Wagoner R. V., Fowler W. A., Hoyle F., 1967, *The Astrophysical Journal*, 148, 3
- Weiss L. M., et al., 2013, *The Astrophysical Journal*, 768, 14
- White J. A., Boley A. C., Hughes A. M., Flaherty K. M., Ford E., Wilner D., Corder S., Payne M., 2016, *The Astrophysical Journal*, 829, 6
- Wick G. C., 1950, *Phys. Rev.*, 80, 268
- Wilson K. G., 1971, *Physical Review B*, 4, 3174
- Wilson R. F., et al., 2018, *The Astrophysical Journal*, 155, 68
- Winterberg F., 1968, *Zeitschrift Naturforschung Teil A*, 23, 1471
- Yakhot V., Orszag S. A., 1986, *Journal of Scientific Computing*, 1, 3

- Yakovlev D. G., Shalybkov D. A., 1991, *Astrophysics and Space Science*, 176, 171
- Zahn J.-P., 1975, *Astronomy and Astrophysics*, 41, 329
- Zahn J.-P., 1992, *Astronomy and Astrophysics*, 265, 115
- Zahn J.-P., 1993, "Space Sci. Rev.", 66, 285
- Zeipel H. v., 1924, *Monthly Notices of the Royal Astronomical Society*, 84, 665
- Zhou Y., McComb D. W., Vahala G., 1997, NASA Contractor Reports
- van der Marel N., van Dishoeck E. F., Bruderer S., Pérez L., Isella A., 2015, *Astronomy and Astrophysics*, 579, A106
- van der Marel N., van Dishoeck E. F., Bruderer S., Andrews S. M., Pontoppidan K. M., Herczeg G. J., van Kempen T., Miotello A., 2016, *Astronomy and Astrophysics*, 585, A58
- van der Walt S., Colbert S. C., Varoquaux G., 2011, *Computing in Science Engineering*, 13, 22
- von Helmholtz H., 1868, *Philos. Mag.*, 36